HELMHOLTZ
Centre for Environmental Research

Maria Balda

Colloidal activated carbon and Fe/C composites by hydrothermal carbonization and subsequent pyrolysis: mechanisms of formation, pollutant adsorption and reductive dechlorination

PHD DISSERTATION 4|2024
Helmholtz Centre for Environmental Research –UFZ
Department of Technical Biochemistry

ISSN 2941-3885

Colloidal activated carbon and Fe/C composites by hydrothermal carbonization and subsequent pyrolysis: mechanisms of formation, pollutant adsorption and reductive dechlorination

Von der Fakultät für Chemie und Mineralogie
der Universität Leipzig
genehmigte

DISSERTATION

zur Erlangung des akademischen Grades

DOCTOR RERUM NATURALIUM

(Dr. rer. nat.)

vorgelegt von

M. Sc. Maria Balda

geboren am 30.01.1994 in Freyung, Deutschland

Angenommen aufgrund der Gutachten von:

Prof. Dr. Frank-Dieter Kopinke
Assoc. Prof. PhD Anna Rigol Parera

Tag der Verleihung: 12.04.2024

This work was created from October 2018 to November 2023 at the Helmholtz Centre for Environmental Research in the Department of Environmental Engineering under the supervision of Dr. Anett Georgi, Dr. Katrin Mackenzie and Prof. Dr. Frank-Dieter Kopinke.

Bibliographic description

Maria Balda

Colloidal activated carbon and Fe/C composites by hydrothermal carbonization and subsequent pyrolysis: mechanisms of formation, pollutant adsorption and reductive dechlorination

Leipzig University, Doctoral Thesis

112 Pages, 53 Figures, 13 Tables, 296 References

Abstract

In this work, three colloidal material types were prepared by hydrothermal carbonization (HTC) and subsequent pyrolysis – two carbonaceous adsorbents and one reactive Fe/C composite. The process parameters were closely investigated and adjusted for generating particles with the desired textural and colloidal properties. The latter are essential for the planned application in *in-situ* groundwater remediation where stable suspensions are needed for injection into aquifers.

The two carbonaceous adsorbents were synthesized by HTC of sucrose with an optional subsequent pyrolysis step. The addition of the stabilizing agent carboxymethyl cellulose (CMC) during the HTC of sucrose optimized the mass yield of carbonaceous spheres (CS) with a narrow size distribution around 1 µm. Due to their hydrophilic surface and negative surface charges these 'raw' CS exhibit an extraordinary suspension stability which makes them suitable for *in-situ* groundwater remediation. Sorption coefficients of up to 10^5 L kg^{-1} were observed for hydrophobic substances such as phenanthrene in environmental concentrations.

The parameters for pyrolysis of the CS were investigated closely and suitable conditions were found in order to maintain the aqueous dispersibility of the activated CS (aCS) also after the pyrolysis step. Under all applied pyrolysis conditions, a low heating rate of about 1 K min^{-1} was crucial in order to minimize inter-particulate aggregation processes and to ensure sufficient dispersibility of the aCS in water. The defunctionalization in combination with tuning the mean pore diameter upon adding 3 vol.-% steam to the N_2-atmosphere during the pyrolysis led to high adsorption coefficients of up to $10^{6.5}$ L kg^{-1} even for the anionic contaminant perfluorooctanoic acid (PFOA) at an equilibrium concentration of 20 µg L^{-1} PFOA. However, the ageing of the aCS surface during storage over one month in water with abundant oxygen significantly impaired the adsorption of PFOA.

For the generation of a material that is sorptive as well as reactive, mechanically stable Fe/C composites with the desired colloidal properties were hydrothermally synthesized. In this process, ferrous gluconate proved as most promising precursor due to the complexation of Fe^{2+} by gluconate. It was shown that the morphology and speciation of the synthesized Fe/C composite enable reductive dechlorination of chloroform with specific activities (normalized to the concentration of zero-valent iron (ZVI) equivalents) that are comparable to nanoscale ZVI. X-ray diffraction (XRD) analyses revealed the presence of Fe_3C in addition to pristine Fe^0 in the crystalline phase of the composite. It is assumed that Fe_3C additionally generates reactive species (e^- and H^*) needed for the reductive dechlorination.

The synthesis process parameters derived in this work can be seen as a basis for future studies where mass yield and material properties can be optimized further according to specific classes of pollutants. Alternative substrates for the production of CS, *e.g.* derived from regional waste sources, can be explored within the developed scopes in order to improve the sustainability of the synthesis.

Bibliographische Beschreibung

Maria Balda

Kolloidale Aktivkohle und Eisen-Kohlenstoffkomposite durch hydrothermale Carbonisierung und Pyrolyse: Mechanismen der Partikelentstehung, Schadstoffadsorption und reduktiven Dechlorierung

Universität Leipzig, Dissertation

112 Seiten, 53 Abbildungen, 13 Tabellen, 296 Referenzen

Zusammenfassung

In dieser Arbeit wurden drei Arten von kolloidalen Materialien mittels hydrothermaler Carbonisierung (HTC) und Pyrolyse hergestellt und umfassend charakterisiert – zwei kohlenstoffbasierte Adsorbentien und ein Fe/C-Kompositmaterial. Die Prozessparameter wurden untersucht und angepasst, um Partikel mit den gewünschten Material- und Kolloideigenschaften zu erhalten. Letztere sind unerlässlich für die geplante Anwendung in *In-situ*-Sanierungsprozessen, bei denen stabile Partikelsuspensionen für die Injektion in Grundwasserleiter benötigt werden. Die zwei verschiedenen Kohlenstoffadsorbentien wurden durch HTC von Saccharose und einem optionalen Pyrolyseschritt synthetisiert. Die Zugabe von Carboxymethylcellulose (CMC) als Stabilisator während der HTC von Saccharose optimierte die Massenausbeute an sphärischen, braunkohleartigen Partikeln (*carbonaceous spheres*, CS) mit einer schmalen Größenverteilung um etwa 1 µm. Diese ‚rohen' CS wiesen aufgrund ihrer hydrophilen Oberfläche und negativen Oberflächenladungen eine außerordentliche Suspensionsstabilität auf, weshalb sie für die *In-situ*-Sanierung von Grundwasser geeignet sein könnten. Hohe Sorptionskoeffizienten von bis zu 10^5 l kg^{-1} wurden für hydrophobe Substanzen gefunden wie z.B. für Phenanthren in umweltrelevanten Konzentrationen.

Durch die Untersuchung der Pyrolysebedingungen der CS wurden geeignete Bedingungen gefunden, um die Dispergierbarkeit der aktivierten CS (aCS) in Wasser auch nach dem Pyrolyseschritt zu erhalten. Unter allen angewandten Pyrolysebedingungen war eine geringe Heizrate von ca. 1 K min^{-1} entscheidend, um eine ausreichende Dispergierbarkeit der aCS in Wasser zu gewährleisten. Die Zugabe von 3 Vol.-% Wasserdampf zur N_2-Atmosphäre führte zu einer ausgeprägten Defunktionalisierung der aCS-Oberfläche. In Kombination mit der Einstellung des mittleren Porendurchmessers konnten sogar für Perfluoroktansäureanionen (PFOA) hohe Adsorptionskoeffizienten von bis zu $10^{6,5}$ l kg^{-1} erreicht werden bei einer Gleichgewichtskonzentration von 20 µg l^{-1} PFOA. Jedoch verringerte sich durch die oxidative Alterung der aCS-Oberfläche nach einmonatiger Lagerung in sauerstoffhaltigem Wasser die Adsorptionsaffinität gegenüber PFOA signifikant.

Für die Herstellung von mechanisch stabilen Fe/C-Kompositen mit den gewünschten kolloidalen Eigenschaften erwies sich Eisen(II)-Gluconat als geeignet aufgrund der Komplexierung von Fe^{2+} durch Gluconat. Die Morphologie des synthetisierten Fe/C-Komposits ermöglichte die reduktive Dechlorierung von Chloroform mit ähnlich hohen spezifischen Aktivitäten (bezogen auf die Konzentration an nullwertigem Eisen) wie nanopartikuläres Fe^0. Die Charakterisierung mittels Röntgendiffraktion (XRD) zeigte, dass neben reinem Fe^0 auch Fe_3C in der kristallinen Phase des Komposits vorlag. Es wird angenommen, dass dieses zusätzlich reaktive Spezies (e^- und H^*) erzeugt, die für die reduktive Dechlorierung benötigt werden.

Die in dieser Arbeit entwickelten Parameter der Syntheseprozesse können als Grundlage für künftige Untersuchungen verstanden werden, bei denen sowohl die Massenausbeute als auch die Materialeigenschaften der Adsorbentien oder reaktiven Komposite je nach Schadstoffklassen und geplanter Anwendung angepasst werden können. Darüber hinaus können die Syntheseparameter für den Einsatz alternativer Substrate, z. B. regionale Reststoffe, angepasst werden, um die Nachhaltigkeit der Synthese weiter zu verbessern.

Outline

1 Introduction

The potential to constructively tackle the existing environmental challenges has never been as great as currently in the 21st century. Due to climate change as well as the ever-increasing global pollution, water and land/soil scarcity become increasingly relevant. The terrestrial cycle of matter is disrupted, on the one hand by the extraction of resources and on the other hand through the introduction of pollutants along and at the end of product value chains. Sustainable and closed-cycle approaches for the production of goods are not fundamental requirements but the implementation of a preferably sustainable way of production is rather dependent on cost factors. In order to tackle the existing challenges, it is not only necessary to convert the ways of energy extraction and production of goods but also to efficiently remediate polluted environmental compartments. During the production of materials for the remediation principles based on sustainablility should be applied *a priori* with respect to future production standards. In the case of groundwater remediation, activated carbon (AC) is often used as injectable adsorbent for the *in-situ* treatment of contaminants. The versatile and non-intrusive character of *in-situ* techniques make them feasible also at sites which are difficult to access. For very persistent substances such as poly- and perfluoroalkyl substances (PFAS), adsorptive *in-situ* treatment is often the only solution for damage control where quick action is called for in order to protect drinking water resources. However, most of the AC applied in Germany is imported and/or produced from bituminous coals which leave rather large carbon footprints. Therefore, a more sustainable alternative would be to generate the AC from renewable resources. For successful *in-situ* remediation, it must be taken into account that the (activated) carbon produced should have the desired particle sizes around 1 µm [3] so that the particles can be injected in the form of a suspension as quasi-liquid sorbent. However, also if the adsorbents are consequently generated from renewable resources, this remediation technique is only a medium-term solution as the pollutants can be leached from the adsorbents again after certain periods of time, depending on the pollutants and the given conditions [4]. Therefore, it would be more sustainable to not only generate an adsorbent but a reactive adsorbent with a preferably cheap synthesis from renewable resources. The used materials should be non-toxic nor release toxic substances into the soil and groundwater over time. For this purpose, carbon and iron have proven to be most suitable [5].

The motivation of this work is to contribute to the technology of environmental remediation as sustainably and as resource-efficient as possible. Therefore, we aim at the generation of a carbon-based adsorbent and a reactive composite material based on zero-valent iron (ZVI) and carbon. Both elements, carbon and iron, are major constituents of our natural environment. In order to synthesize the desired materials in a sustainable way, the production was based on hydrothermal carbonization (HTC) with a subsequent pyrolysis step.

2 Background

2.1 *In-situ* groundwater remediation

In-situ remediation techniques are non-intrusive alternatives to *ex-situ* groundwater remediation where groundwater or soil are lifted and remediated above ground. During *in-situ* treatments, the adsorbents and/or reagents are directly injected into the aquifer and bind or degrade pollutants at or close to the source of contamination [6]. One possibility for the degradation is the oxidation with soluble oxidants such as permanganate or radical precursors such as peroxydisulfate or hydrogen peroxide [7]. This so-called *in-situ* chemical oxidation (ISCO) is in principle able to mineralize most of the known organic pollutants. However, ISCO can significantly influence the bacterial communities in the aquifers. Based on the specific techniques additional requirements such as pH controlling are necessary in order to prevent detrimental effects on microbes [8]. Furthermore, when it comes to persistent pollutants, other substrates present under *in-situ* conditions, *e.g.* humic substances, can decrease the efficiency of ISCO [9]. Alternatives to ISCO are enhanced natural attenuation, adsorptive remediation or reductive degradation of pollutants. Natural attenuation basically means the passive remediation of pollutants by physical principles (*e.g.* dilution, ad-/absorption in the environment etc.) or biodegradation. Therefore, natural attenuation depends on many factors such as pH, concentration of various mineral ions, redox potentials of the soil minerals etc. which influence the sorptive removal and the chemical or microbial degradation. These processes can be enhanced by pH adjustments [10], the addition of electron donors/acceptors or nutrients to enhance biodegradation [11] or even the extraction, stimulation and re-injection of microorganisms (so-called bioaugmentation) [12]. However, the typically low concentrations of contaminants and their distribution along pollutant plumes makes efficient remediation approaches often difficult.

This can be resolved by using adsorptive *in-situ* technologies, where adsorbents are injected at contaminated sites to concentrate the contaminants in the adsorbent phase [13]. For the adsorptive remediation mostly AC is used due to versatility and cost efficiency [4, 13–15]. In particle-based remediation approaches the colloidal properties of the materials are crucial in order to ensure the ability for injection in quasi-liquid form [13, 16]. In order to obtain the desired colloidal properties, the used particles have to provide diameters of about 1 µm. For AC, the small particle size is typically generated top-down by wet-milling of commercial AC [17]. However, adsorptive approaches are only medium-term solutions as the contaminants remain and can be leached out of the adsorbents after saturation or after altering the adsorbent properties through ageing. The reductive degradation of pollutants is often achieved with particle-based reagents, for example zero-valent iron (ZVI) [18–20]. However, at sites with low contaminant concentrations, either the use of large quantities of ZVI or highly reactive nanoscale ZVI (nZVI) is necessary to achieve the desired remediation performance, which reduces cost-effectiveness [21]. Therefore, innovative technologies combine adsorptive and reductive techniques in ZVI/AC composite materials in order to enrich the pollutants in the adsorbent phase and degrade them with the added reductant [22, 23]. As mentioned above, colloidal AC is synthesized on the industrial scale by wet-milling of AC. For ZVI/AC composites, there is the possibility to combine this finely powdered AC with ZVI by wet-impregnation with Fe salts and subsequent carbothermal reduction [22]. This method holds the drawback that multiple steps with high energy demand precede the synthesis of the actual composite material. An alternative for the production of ZVI/AC at large scales is the milling of ZVI and AC together [24]. However, the milling procedure does not ensure a mechanically stable connection of the ZVI and AC particles in the resulting composite material. This would likely have implications during particle injection and sub-surface transport.

In contrast to the top-down synthesis methods, in this work, the described materials were generated with a bottom-up syntheses. HTC was chosen as a method with preferentially sustainable character.

2.2 Generation of micrometer-sized particles *via* HTC

2.2.1 Without additives – basic mechanisms

When aiming for a bottom-up synthesis of micrometer-sized carbonaceous particles, HTC is a suitable method. Dissolved carbohydrates naturally form perfectly spherical shapes upon carbonization as the forming hydrophobic carbonaceous phase tends to minimize the contact area with the aqueous medium [25]. In order to guide this process in a favorable direction, not only monosaccharides or easily hydrolysable polysaccharides are needed but also the particle growth mechanism has to be considered. Previously, a LaMer-like mechanism [26] was postulated where the dissolved intermediates, *e.g.* hydroxymethyl furfural (HMF), diffuse to the carbon surface and react with the reactive oxygen functional groups [27, 28]. Recently, Jung *et al.* investigated the mechanism more closely and found that growth likely proceeds *via* agglomeration and inter-particulate dehydration/polymerization of the carbonaceous nuclei [1]. This is typically an uncontrolled process which leads to carbonaceous spheres (CS) of various diameters (Figure 1 a). However, this growth process can be moderated when certain additives are present. It is assumed that these additives stabilize the formed nuclei and prevent uncontrolled agglomeration as illustrated in Figure 1 b. This might be why in literature, positive effects of polymers [29, 30], polyelectrolytes [2, 31, 32] or high concentrations of inorganic salts [33–36] have been observed for more even particle size distributions. All these additives most likely reduce the agglomeration tendency of the formed carbonaceous nuclei.

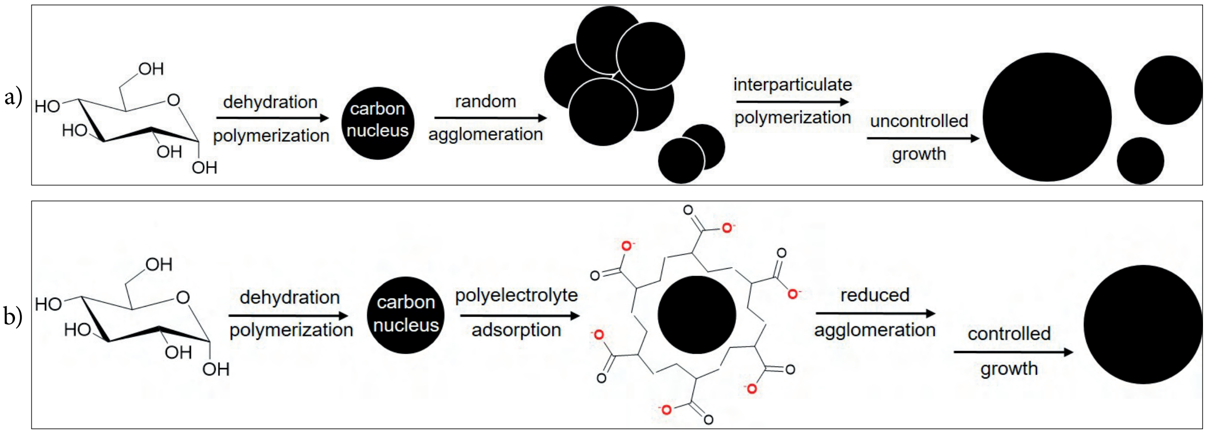

Figure 1 Suggested growth mechanisms during the HTC of glucose as model carbohydrate a) in the absence and b) in the presence of a polyelectrolyte (polyacrylate) as stabilizing agent. Schemes were developed based on the proposed mechanisms of a) [1] and b) [2].

2.2.2 With metal additives

Considering the bottom-up synthesis of iron-containing micrometer-sized carbonaceous particles *via* HTC, a secondary effect had to be put into account: metal ions influence the HTC process, more specifically they promote the dehydration and polymerization reactions [37] based on their (Lewis-)acidic properties [38]. Iron, for example, can promote the HTC due to a decrease in pH value and enhancing the agglomeration of the C precursors and/or carbonaceous nuclei [39]. While this effect can be beneficial for the generation of various carbonaceous products such as porous aerogels [38, 40], metal-containing nanocables and chain-like structures [41], the structural influence of metal ions is not favorable when aiming at very uniform and unisized particles [34]. For the generation of a colloidal metal-carbon composite *via* HTC, it is therefore crucial to select carbon and metal precursors, in this case iron, which interact in a beneficial way to form compact and dispersible particles where Fe and C are homogeneously distributed and combined in a mechanically stable manner. Previously, Fe/C composites were achieved by using iron-containing nanoparticles and soluble carbon precursors (*cf.* section 4.3, Table 1). Due to the rather hydrophilic properties of the metal oxide surface and the comparably hydrophobic properties of the forming carbonaceous phase, the deposition of the carbonaceous phase on the particles has to be forced. Typically, this was achieved by using relatively high concentrations of nanoparticles in dilute sugar solutions and pre-treatment with stirring the suspensions. Furthermore, the iron-containing nanoparticles were often freshly synthesized before use in HTC [42–44]. There were very few one-pot approaches starting from dissolved precursors (*cf.* 4.3, Table 2) and even fewer led to (presumably) dispersible particles with homogeneously distributed Fe and C within the resulting composite: Xuan *et al.* mixed glucose, $FeCl_3$ and urea to yield nanoparticles (100–200 nm) consisting of a carbon shell and a single crystalline Fe_3O_4 core [45]. Luo *et al.* achieved the synthesis of carbon-coated Fe_3O_4 particles through the HTC of $FeCl_3$ and sodium gluconate [46]. However, Luo *et al.* were the only group who actually showed the aqueous dispersibility of the synthesized material. Their approach was rather interesting because it suggests that a complexation of the iron ions by the carbon precursors apparently favors the formation of mechanically stable composites during the HTC process. The according formation mechanism is proposed in section 4.3, Figure 2.

2.2.3 Dispersibility and suspension stability

HTC of biomass has been used to prepare hydrochar for a broad scope of applications after further treatment such as physical or chemical activation. Their adsorption behavior towards different organic compounds [47–50] or heavy metals [48, 51–54] and also their electrical properties [55–57] have been investigated. However, the properties of hydrochar particles as colloids have not been comprehensively investigated so far. The dispersibility of synthesized CS [44, 58] and their suspension stability in aqueous media [28] are only mentioned in passing. Nonetheless, the dispersibility of the particles is a crucial property and can too easily be annihilated by choosing unfavorable conditions in the subsequent activation of HTC products by high-temperature pyrolysis. The only hint from literature regarding this issue was the very low heating rate applied by Wang *et al.* for pyrolysis of HTC-derived CS [59]. This led us to detailed investigations regarding the influence of the heating rate on the dispersibility of the final product (*cf.* section 4.2).

When the particles are homogeneously dispersed in suspension in a relatively stable manner, the sedimentation velocity is dependent on the particle radius and density according to Stokes' theory. As the 'raw' CS exhibit still rather high oxygen contents and a large amount of negatively charged surface groups, they are rather hydrophilic and not prone to agglomeration. The pyrolyzed/activated CS, however, provide a significantly decreased oxygen content and increased hydrophobicity. That is why they have to be stabilized in suspension, *e.g.* by polyelectrolytes, in order to prevent agglomeration and decelerate their sedimentation [60].

When the carbonaceous particles are combined with a metal fraction, the density of particles and consequently the sedimentation velocity is significantly increased [28].

Furthermore, as discussed in section 2.2.2, the dispersibility of the resulting particles can be influenced by the addition of metals during the HTC, based on the promoting effect and a subsequently favored inter-particle polymerization over intra-particle polymerization. The dispersibility of Fe/C composites generated *via* HTC is mentioned in some publications [42–44, 58, 61], however, it was never specifically characterized and no stability tests were performed. Only Luo *et al.* actually showed the dispersibility and mechanical stability by magnetic separation of the generated Fe_3O_4/C composite [46].

2.3 Material properties crucial for the adsorptive removal of pollutants

2.3.1 Porosity

The CS generated by HTC are lignite-like and therefore non-porous. Although, they exhibit a significant absorption potential regarding hydrophobic substances (*cf.* section 4.1) the generation of micropores allows the adsorptive removal of pollutants which can lead to more versatile applications as adsorbent. The introduction of pores already during the HTC process would be possible by adding various additives, such as alkaline and/or transition metal salts or particles [38, 62] or soft-templating with *e.g.* co-polymers [63]. However, this type of porosity-generation typically relies on the promotion of the HTC process with consequential increased inter-particle polymerization. This is counterproductive for the generation of individual and dispersible carbonaceous particles. Therefore, the hydrothermal synthesis of porous and dispersible individual particles can only be realized *via* hard-templating processes, *e.g.* with meso-porous silica beads [64]. In this case, the preceding hydrophobization and subsequent removal of the silica beads with ammonium hydrogen difluoride compromises the facile and sustainable character of the HTC process.

There is also the possibility to pyrolyze the hydrothermally formed carbonaceous particles which leads to a porous system by default. Pyrolysis processes consist of further dehydration ($T < 260$ °C), depolymerization (240 °C $< T <$ 300 °C) with subsequent formation of volatile "chars" and aromatization at $T > 400$ °C through Diels-Alder-type reactions which finally leads to the formation of a submicroscopic pore structure [65]. In order, to generate a more pronounced porous system, enhancement of the pyrolysis with various additives is necessary turning the pyrolysis to an activation process. Possible activating agents are "harsh" additives such as H_3PO_4, HNO_3, NaOH/KOH, $ZnCl_2$, K_2CO_3 or "mild" additives such as CO_2 or H_2O. Both strategies are combined with treatments at elevated temperatures of about 600–900 °C. While activation with K_2CO_3 and H_3PO_4 can lead to very high surface areas of up to 2600 m^2 g^{-1} [66, 67] and with KOH even up to 3320 m^2 g^{-1} [68], the initial structure of the material cannot be retained [56]. With addition of steam of CO_2, the achieved specific surface areas reported are not as high (up to 1300 m^2 g^{-1} as reported in [69], however, the spherical morphology of CS could be maintained [49].

During the pyrolysis and/or activation process, not only porosity is introduced but naturally also the oxygen content of the carbonaceous material is significantly decreased compared to the starting material. Depending on the pyrolysis/activation process this "de-functionalization" leads to a greater aromaticity and hydrophobicity of the carbonaceous material and subsequent higher affinity towards organic pollutants. However, it can also leave reactive centers behind which lead to increased surface reactivity that can enhance oxidation processes of the pyrogenic surface [70].

2.3.2 Surface functionalities and oxidative ageing

It is known from the literature that the surface of AC more or less slowly oxidizes after activation when exposed to air and/or water [71, 72]. It has been observed that this 'ageing' process can influence the adsorption properties of the carbonaceous material [17, 73]. However, when it comes to (pyro-)hydrochar and biochar, the number of literature studies that deal with the change of surface functional groups is scarce. Xiao *et al.* investigated the alteration of surface chemistry and pore size distribution of biochars exposed to oxygen at 400 °C [73]. Liu *et al.* looked into the oxidative ageing of hydrochar and biochar with H_2O_2 [74]. However, there are no studies of (pyro-)hydrochar/biochar ageing under ambient air conditions. Boutillara *et al.* monitored changes in surface composition and porosity of different AC samples during storage under 40 °C in 80 % relative humidity [75]. The observed changes due to oxidation suggest that it is crucial to monitor ageing of carbonaceous materials for specific applications. However, no data were found on the practical effects of the ageing of pyrogenic carbon surfaces in water. That is why, in this work, the ageing of de-functionalized activated CS and the according influence on the sorption affinity towards different contaminants was monitored in detail (*cf.* section 4.2).

2.4 Properties crucial for the reductive removal of pollutants

2.4.1 Mechanisms of reductive dechlorination with ZVI

In order to form particles that are able to not only adsorb but also reductively degrade pollutants, the combination of the carbonaceous phase with a reactive component is essential. As cheap, non-toxic reductant, ZVI (Fe^0) has been established in groundwater remediation for the last decades. The described mechanism of reductive dehalogenation reactions with ZVI typically involves electron and hydrogen or proton transfer (eqs. (5–7)) [76, 77]. ZVI naturally produces the required reactive species in anoxic aqueous media due to the anaerobic corrosion of Fe^0. Firstly, protons are reduced on the ZVI surface by Fe^0 (eq. (1)) to atomic hydrogen (H^*). H^* can then combine with another H^* into molecular hydrogen (eq. (2)) which is known as the Volmer-Tafel reaction pathway [78]. Alternatively, the Volmer-Heyrowski reaction can take place where H^* reacts with another molecule under simultaneous uptake of an electron. In the case of H_2O (eq. (3)) [78], additional hydrogen evolves whereas in the case of a chlorinated organic molecule such as chloroform (CF) this leads to reductive dechlorination, yielding products with a lower chlorination degree and chloride (eq. (4)).

$$2\,H^+ + Fe^0 \rightarrow 2\,H^* + Fe^{2+} \tag{1}$$
$$2\,H^* \rightarrow H_2 \tag{2}$$
$$H^* + H_2O + e^- \rightarrow H_2 + OH^- \tag{3}$$
$$H^* + CHCl_3 + e^- \rightarrow CH_2Cl_2 + Cl^- \tag{4}$$

Eq. (4) presents a sum reaction equation which actually involves a stepwise mechanism. In the case of aliphatic compounds such as CF, the first step likely is the dissociative electron transfer onto the chlorinated molecule producing a radical and a chloride ion (eq. (5)) [77]. The formed radical would then stabilize itself by taking up a hydrogen atom (eq. (6)) or a second electron and a proton (eq. (7)).

$$CHCl_3 + e^- \rightarrow {}^{\bullet}CHCl_2 + Cl^- \tag{5}$$
$${}^{\bullet}CHCl_2 + H^* \rightarrow CH_2Cl_2 \tag{6}$$
$${}^{\bullet}CHCl_2 + e^- + H^+ \rightarrow CH_2Cl_2 \tag{7}$$

As the standard potentials for the reductive dechlorination decrease with decreasing number of chlorine substituents in the molecule, the reactivity decreases as well [79, 80]. That is why CH_2Cl_2 is not prone to further (stepwise) dechlorination by ZVI. However, in the case of CF, the complete dechlorination to CH_4 is possible *via* a direct hydrodechlorination-like pathway involving the transfer of multiple electrons and hydrogen atoms [81]. Due to the participation of protons or hydrogen atoms in the reaction, the reaction proceeds faster and with more favorable selectivities when more hydrogen atoms are available in close vicinity. A higher concentration of H^* could simply be achieved by lowering the pH and thus increasing the concentrations of H^+ serving as educt for H^* [82, 83]. However, as this is mostly not feasible in environmental applications, a greater abundance of adsorbed H^* is often realized by modifying the ZVI either by sulfidation [84, 85] or by combining the ZVI with a metal providing hydrogenation activity and simultaneously enhancing ZVI corrosion by formation of local elements [79, 86–89]. The resulting change in reaction mechanism leads to hydrodechlorination reactions which not only proceed faster but also enable the degradation of more challenging pollutants, *e.g.* lesser chlorinated aromatics such as monochlorobenzene [90, 91]. In the bimetallic systems, the reactive species are generated on the ZVI surface and stabilized by chemisorption on the surface of the catalytically active metal. In the case of M/ZVI where M is a catalytically active metal, the transfer of H^*_{ZVI} to H^*_M may typically proceed *via* the formation of molecular H_2 and subsequent dissociative adsorption at the M surface [81]. However, there is in theory also the possibility that H^* can be directly transported from one material component to another.

2.4.2 Transfer of reactive species between different material components

The phenomenon that reactive species can be transferred from their source (typically described as 'initiator' or 'activator') to another component of the material where the generation of these species is not possible, is known as 'spillover' in heterogeneous catalysis [92–94]. Depending on the vicinity or distance of initiator and acceptor the spillover is characterized as primary or secondary transfer, respectively [92]. In heterogeneous catalysis, spillover was mechanistically investigated for H^* in various catalyst/support systems. In these systems, H^* is typically generated by dissociation of molecular hydrogen and chemisorption of the single H atoms on metals with hydrogenation activity such as Pt, Pd, Ni, Rh or Cu [92]. Afterwards, H^* is transported across catalyst supports, typically different metal oxides. The oxygen contained in these support materials can act as hydrogen acceptor. Different transport mechanisms were postulated throughout the years and it is likely that mechanisms differ depending on the catalyst supports. For reducible metal oxides (*e.g.* TiO_2, SiO_2), the transfer *via* protons and electrons was postulated [95, 96]. Thereby, the active hydrogen donates its electron to a reducible metal surface site and the remaining proton adds to a nearby oxygen surface group. Like this, the transfer can proceed from site to site over the surface until a reactant is met which irreversibly takes up the proton and electron. This mechanism explains why a promoting effect was often observed in the presence of H_2O (moisture) as proton movement over the surface might then be enhanced according to the Grotthuß mechanism [97].

Regarding a system consisting of ZVI on an AC support, it is reasonable that H^* spillover might proceed in similar ways. The binding of an H atom to graphitic structures is exothermic, where the binding energies are in the range of 60–190 kJ mol^{-1} [95]. These are smaller than the energy needed to stably maintain single H atoms (218 kJ mol^{-1}) which equals half of the binding energy of the H–H bond in molecular hydrogen [95]. Therefore, hydrogen spillover from catalytically active metals (*e.g.* Pd) onto graphitic structures might thermodynamically not be feasible. However, when it comes to ZVI/AC the active H^* on ZVI is not adsorbed as strongly. Therefore, it might be possible that short distance spillover to graphitic structures on the support occurs. However, graphitic structures are more predisposed to mediate electrons due to their electric conductivity [98] while the according protons might add to oxygen-containing surface groups exhibiting basic properties such as chromenes/pyrones [99, 100]. Furthermore, the transfer of a whole H atom to carboxylic groups, lactones or semiquinones which are typically found on carbonaceous materials is assumed to be thermodynamically feasible as the binding energies are close to the needed minimum value in order to maintain single H atoms [95].

Recent investigations on the transfer of reactive species in the ZVI/AC system involved the thorough characterization of the AC and identifying properties that are beneficial for enabling reductive dehalogenation reactions. It was assumed that the carbonaceous phase is able to transfer reactive species from the ZVI to the adsorbed pollutant when it is electrically conductive and/or provides certain (redox-active) oxygen-containing functionalities [98, 101–104]. Earlier findings showed that the transfer of reactive species from ZVI to AC was possible even when the two materials were not interconnected but only in ‘dynamic contact’ with each other as was proven by degradation of almost completely adsorbed trichloroethene (TCE). Further investigations illustrated the necessity for H^* (besides e^-) for the degradation reaction. This led to the conclusion that H^* spillover is not only theoretically but also practically possible on AC [101]. In successive studies, it was found that certain oxygen-functional groups cannot only enable but also promote reductive dechlorination reactions. Vogel *et al.* investigated this in terms of the reductive dechlorination of TCE with microscale ZVI in the presence of AC. It was observed that AC which had been in contact with ZVI was able to reduce TCE even after the ZVI was fully removed [102]. Temperature-programmed decomposition (TPD) analyses of the functional groups prior to and after the contact with ZVI suggested that quinoid structures might be reduced to phenolic groups when in contact with ZVI. Afterwards, they are re-oxidized while reducing the chlorinated pollutant, thus acting as redox mediators [102]. Previously, it had been shown that quinoid structures can act as redox mediators for some other reductive processes [103–105]. A scheme for the mechanism (in our case for the reduction of CF) is proposed in Figure 2.

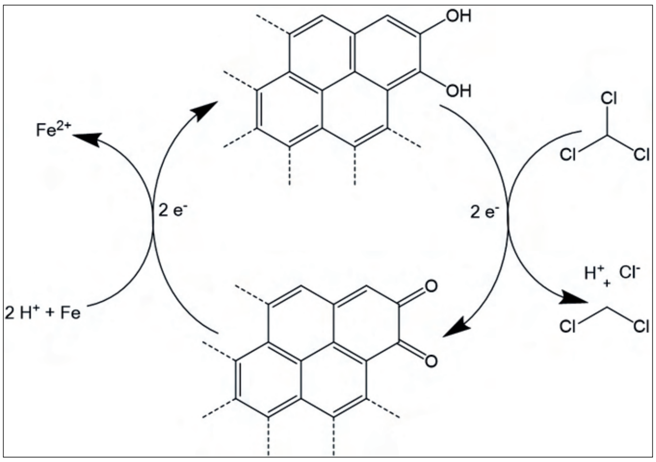

Figure 2 Schematic illustration regarding the possible involvement of the redox-active groups 1,2-hydroxybenzene/1,2-benzoquinone on a carbon surface regarding the reductive dechlorination of chloroform (adapted from [102]); dotted lines represent further connections to the aromatic carbon backbone which is depicted in a simplified way.

While the mechanistic interactions have been studied for ZVI/AC systems, studies on ZVI/hydrochar composites regarding the reductive dechlorination are still scarce [106, 107]. In contrast to the impregnation of 'mature' AC with ZVI precursors, combining ZVI precursors with 'raw' carbonaceous materials, *e.g.* biomass or hydrochar, might have a greater influence on the speciation of the material components during the carbothermal reduction. For example, it was recently observed that the HTC of pinewood and iron(III) nitrate with subsequent thermal treatment led to the formation of iron carbide species in addition to pristine ZVI [108, 109]. Furthermore, Meng *et al.* observed that the iron carbide also plays a role in the reductive dechlorination of trichloroethene (TCE) [109].

As described above, the addition of a catalytically active metal (M) to ZVI and creating a bimetallic system leads to a change in reaction mechanism towards hydrodechlorination. It is also possible to add M to ZVI when the latter is supported on a porous carbon material as it was demonstrated *e.g.* for Pd on ZVI/AC [110]. The influence of the carbonaceous support on the catalytic activity was investigated before [111–113]. It was observed that oxygen-containing functional groups such as carboxyl, anhydride and phenol groups increased Pd dispersion on the carbonaceous support materials leading to higher catalytic activities [114]. A similar effect was observed for Rh on reduced graphene oxide (RGO) [115]. Furthermore, these oxygen functional groups may enhance the transfer of H^* as described above. Simagina *et al.* reported comparable findings but explained it differently. As they observed the highest catalytic activity in the hydrodechlorination of chlorobenzene for Pd on an AC-support with a high ash content, in their case, the Pd dispersion was likely enhanced by the metal-oxide impurities (ashes) on the surface [112].

2.4.3 Influence of the composite morphology on the reactivity

In order to enable the reactivity of the ZVI within the composite material, certain particle morphologies are needed. The carbon and iron phase should be finely distributed as well as mechanically connected in order to ensure the fast transfer of reactive species. Regarding the planned application, also the transport of the complete composite material has to be ensured. Previously, it was observed that the incorporation of nZVI into a porous AC matrix reduced particle agglomeration and sedimentation tendencies in aqueous suspensions compared to pristine nZVI while preserving high reactivities for reductive dechlorination [22]. As nanoparticulate clusters of ZVI were deposited onto the AC matrix, this system can be described as AC-supported nZVI.

In contrast, during the bottom-up synthesis of an Fe/C composite *via* HTC, Fe_xO_y particles are likely formed at first and the precipitating carbonaceous phase deposits as coating on the solids under certain conditions. Previously, it was reported that during the coating of stainless-steel substrates in a stirred HTC process, a tar-like layer formed on the substrate prior to the coating with hydrochar [116]. If the coating of particles proceeds in a similar way, this might lead to a full coverage of the Fe-containing particles during the HTC process by this tar-like layer. Depending on the thickness of the carbon coating, two scenarios can be proposed after pyrolysis:

a) If the carbonaceous shell is too thick, a pore structure with spatially heterogeneously distributed pore diameters is formed where the pores in greater distance to ZVI might be too narrow to be accessible for H_2O (H^+) and/or CF (*cf.* Figure 3 a).
b) If Fe_xO_y is homogeneously distributed throughout the carbonaceous phase in sufficient concentrations, a continuous pore structure with homogeneously distributed and sufficiently large pore diameters is formed where ZVI is accessible for H_2O (H^+) and CF (*cf.* Figure 3 b).

As Fe_xO_y consumes C during carbothermal reduction, the formation of large micro- or mesopores in the vicinity of Fe is suspected. Considering the molecular and kinetic diameters of CO_2 and CO [117, 118], narrow micropores ($\leq$ 0.4 nm) can act as transport ways for the discharge of generated CO_x molecules. If the carbonaceous shell is too thick and the Fe core has no influence on the outer shell, a pore system with heterogeneously distributed pore sizes would be the consequence, *i.e.* pores in the outer shell with less than 0.4 nm in diameter. In this scenario a) reactive ZVI surfaces would not be accessible to CF which has a minimum molecular diameter of about 0.5 nm [117]. While H_2O molecules exhibit smaller minimum molecular diameters of 0.3 nm [117] they probably do not transition into the comparatively hydrophobic

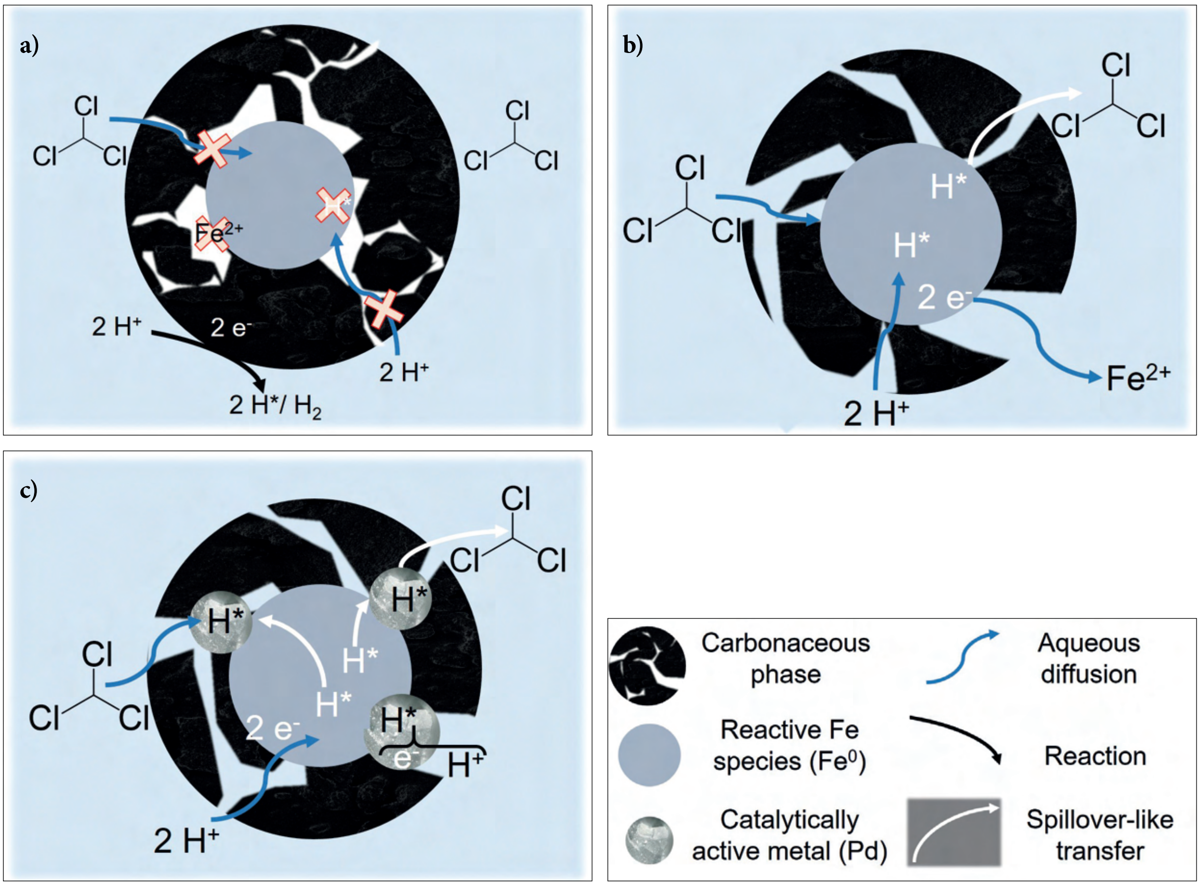

Figure 3 Simplified schemes for the possible pathways of generating/transferring reactive species on the synthesized Fe/C and Pd/Fe/C composite particles; a) ZVI coated with an insufficiently porous carbon layer where ZVI is not accessible; b) ZVI coated with a porous carbon layer where ZVI is accessible; c) accessible Fe/C composite after palladization.

pore space as single molecules while sacrificing hydrogen bonds. Protons could add to oxygen-functional groups in the vicinity of pore entries. However, it would be unlikely that they are transported further into the porous system when the pores are not filled with water [119, 120]. Electrons might be transferred from the ZVI to the material surface through the carbonaceous bulk and reduce protons according to the above described Volmer reactions (eqs. (1–2)). However, these reactions have a higher overpotential at the carbon surface compared to the ZVI surface [101]. Furthermore, it is not likely that Fe^{2+} is formed in the absence of water in the anaerobic system when no possible counter-ions such as (hydr-)oxide are present. Consequently, the transfer of reactants to and reactive species from the ZVI is inhibited (*cf.* Figure 3a). This might reduce reaction kinetics or even eliminate the reactivity under ambient conditions.

It is supposed that hydrothermal Fe/C composites with a core-shell structure only form a well-pronounced porous system with sufficiently large pore diameters according to scenario b) where Fe$_x$O$_y$ is homogeneously distributed and the carbonaceous coatings are not too thick. This would then enable the direct contact of the ZVI surface with water (H$^+$) and CF and the rapid transport of reactants and reactive species (*cf.* Figure 3 b). It is likely that this system functions similarly to the ZVI/AC systems described above, however, there is still the question if the carbonaceous phase exhibits suitable properties in order to transport the reactive species to the chlorinated pollutant (*e.g.* CF) or if the CF needs access to the reactive ZVI surface.

As discussed in section 2.4.2, also for the addition of a catalytically active metal, in this case Pd, the Fe/C morphology and speciation are important. Again, the interactions are described to some extent for Pd on AC or ZVI/AC, however, the speciation and morphology of a ZVI/C composite derived from one-pot HTC most likely is different from that of a (porous) carbon support loaded with Pd and/or ZVI NPs. In order to enable a facile palladization of the HTC-derived Fe/C according to the electrochemical series (eq. (8)), the ZVI again has to be accessible according to Figure 3 b).

$$Fe^0 + Pd^{2+} \rightarrow Fe^{2+} + Pd \quad (8)$$

Alternatively, the transport of e^- through the carbonaceous bulk and the reduction of Pd^{2+} on the AC surface and the subsequent reduction of H^+ on the Pd surface might be possible, however, the former might not proceed at ambient temperatures [121]. Nevertheless, it is expected that material characterization and reactivities of the composite give impressions about the accessibility of the ZVI. If the morphology of the Fe/C composite allows the palladization with a high dispersion of the formed Pd clusters, the Pd particles can take up H^* afterwards and induce the hydrodechlorination of CF with high activities and selectivities to methane.

3 Research questions

A bottom-up HTC process was chosen to synthesize colloidal carbonaceous particles, as soluble carbohydrates naturally form lignite-like spherical microparticles under HTC conditions. In order to generate these in the desired size range and simultaneously increase the yield, in previous studies typical stabilizing agents like hazardous and/or expensive polyelectrolytes or high salt concentrations were added to the HTC which compromise or even annihilate the sustainable character of the process. Consequently, alternative additives were sought which are not hazardous but functional as well as cheap. The second crucial aspect of the bottom-up synthesis is the preservation of the dispersibility of the formed individual particles. The latter is excellent directly after the developed HTC process, however, for the generation of porous carbon particles a pyrolysis or activation step is needed during which the dispersiblity can easily be eradicated. Therefore, the pyrolysis conditions were investigated closely in order to find suitable parameters for maintaining the dispersiblity of the product. In addition, the porous system and surface properties of the adsorbent should be tailored during the pyrolysis. The surface should preferentially be de-functionalized which has proven to be best for the adsorption of challenging organic pollutants such as PFOA [122]. However, especially de-functionalized surfaces are prone to 'ageing' due to oxidation processes in (humid) air and water under ambient conditions. To tackle these issues, the following three research questions were important for the bottom-up preparation of very fine (activated) carbon particles:

(I) How can the yield of microparticles in the desired size range be optimized without potentially hazardous additives during the HTC process?
(II) How can the high aqueous dispersibility of the microparticles be kept after pyrolysis?
(III) How can the porosity and surface characteristics of the AC be tailored to benefit the adsorption of certain pollutant classes?

When iron is added to the process, further aspects have to be considered for the generation of a reactive composite material. As described above, iron salts influence the HTC process which means the process parameters have to be adjusted accordingly in order to generate a similar particle size as in the process without Fe. Furthermore, the (composite) particles provide different morphologies depending on the initially used iron source. As mentioned above, the morphologies forming during the bottom-up synthesis of the Fe/C composite might not be favorable for enabling the generation of reactive species needed for reductive dechlorination reactions. Although not all classes of pollutants can be degraded reductively, we focused on the capability as reductant of the Fe/C within this work. The mechanisms of reductive dechlorination are well understood, however, the reactivity of colloidal composites synthesized with bottom-up HTC has not been investigated previously. Therefore, it was necessary to find out which composite morphologies as well as Fe and C speciations form during the one-pot bottom-up HTC and if they can be rendered active with respect to reductive dechlorination reactions. The reactivity of the composite materials was investigated by using CF as a model compound as it not only allows to measure reaction kinetics but also selectivities to chlorinated and non-chlorinated products. While ZVI and ZVI/C systems are able to dechlorinate aliphatic (and highly chlorinated aromatic) compounds, the selectivities might be poor and desirable products may not be formed within desired periods of time, *i.e.* the lifetime of ZVI in water. Furthermore, some chlorinated pollutants are simply not degradable with pristine ZVI as discussed in section 2.4.1. Therefore, it was also investigated if the palladization of the Fe/C composite would be sufficient to extend the spectrum of pollutants that can be degraded while shifting the selectivity towards lesser chlorinated and more hydrogenated products. The specific catalyst activities were compared with those of other typical Pd-containing catalysts. Consequently, the following research questions were posed:

(IV) Is it possible to generate a functional iron-carbon composite with the desired morphology within a one-pot synthesis based on HTC?
(V) Do the morphology and speciation of the composite after carbothermal reduction allow the reductive dechlorination of chlorinated hydrocarbons in water?
(VI) What is the gain in selectivity towards fully dechlorinated products achievable by palladization of the composite?

In order to answer these six questions, distinct working packages were conducted which led to two different carbonaceous adsorbent types and one reactive Fe/C composite. The results were published in the form of three individual manuscripts (*cf.* section 4).

In manuscript 1 (section 4.1), the bottom-up synthesis of uniform and dispersible CS was conducted *via* HTC of sucrose. By adding the stabilizing agent CMC, the yield of particles with a very narrow particle size distribution was optimized. As the CS already exhibited a significant sorption affinity regarding hydrophobic substances such as polycyclic aromatic hydrocarbons (PAHs), the sorption of various pollutants onto/into the CS matrix was investigated. Furthermore, the dispersibility and aqueous suspension stability were characterized in detail. The HTC of sucrose at 180 °C for 2 h presents a very low-threshold synthesis. Therefore, in some cases, the generated CS can be an alternative for the typically used AC which is produced at high temperatures.

In manuscript 2 (section 4.2), the uniform CS generated were activated with a mild steam-activation process. The process was designed in order to maintain the dispersibility of the aCS, generate high specific surface areas with a micropore system exactly fitting certain molecular diameters and simultaneously tuning the surface properties towards a low oxygen content. It was demonstrated that the micropore width could be adjusted by setting temperature and time of the activation in order to exactly fit the diameter of the elongated chain of PFOA. Furthermore, the surface ageing of the defunctionalized aCS surface in water and air under ambient conditions was closely monitored.

Manuscript 3 (section 4.3) deals with the one-pot bottom-up synthesis of a mechanically stable Fe/C composite *via* HTC. An extensive literature review revealed certain gaps regarding the synthesis of mechanically stable composites from dissolved precursors. This synthesis approach holds some challenges regarding the combination of Fe and C in a mechanically stable manner and the particle sizes/morphologies. After a precursor screening, ferrous gluconate was chosen as precursor for the HTC in order to profit from the complex formation between $Fe^{2+/3+}$ and gluconate. This ensured uniform particle morphologies, the homogeneous distribution of Fe and C and thus mechanical stability, however, it came at the expense of a significantly lower product mass yield. The particles were tested for reductive dechlorination after carbothermal reduction at 800 °C for 2 h under N_2 using CF as model substrate. The composites were palladized and the selectivities and specific catalyst activities of the synthesized Pd/Fe/C composite for the CF degradation were compared to other typical Pd-containing catalysts. In order to get an impression of the material speciations which might be involved in the reductive dechlorination reactions, characterization of the composites before and after the reductive dechlorination reactions with XPS and XRD was performed.

References

[1] D. Jung, M. Zimmermann, A. Kruse, *Hydrothermal carbonization of fructose: growth mechanism and kinetic model*, ACS Sustainable Chemistry & Engineering 6 (2018) 13877–13887.

[2] Y. Gong, L. Xie, H. Li, Y. Wang, *Sustainable and scalable production of monodisperse and highly uniform colloidal carbonaceous spheres using sodium polyacrylate as the dispersant*, Chemical Communications 50 (2014) 12633–12636.

[3] N. Tufenkji, M. Elimelech, *Correlation equation for predicting single-collector efficiency in physicochemical filtration in saturated porous media*, Environ. Sci. Technol. 38 (2004) 529–536.

[4] A. Georgi, A. Schierz, K. Mackenzie, F.-D. Kopinke, *Colloidal activated carbon for* in-situ *groundwater remediation – Transport characteristics and adsorption of organic compounds in water-saturated sediment columns*, Journal of Contaminant Hydrology 179 (2015) 76–88.

[5] S. Bleyl, F.-D. Kopinke, K. Mackenzie, *Carbo-Iron® – synthesis and stabilization of Fe^0-doped colloidal activated carbon for in situ groundwater treatment*, Chem. Eng. J. 191 (2012) 588–595.

[6] T. Zhang, G.V. Lowry, N.L. Capiro, J. Chen, W. Chen, Y. Chen, D.D. Dionysiou, D.W. Elliott, S. Ghoshal, T. Hofmann, H. Hsu-Kim, S. Liu, J. Ma, B. Pan, T. Phenrat, X. Qu, X. Quan, V. Saleh, P.J. Vikesland, Q. Wang, P. Westerhoff, M.S. Wong, T. Xia, B. Xing, B. Yan, L. Zhang, D. Zhou, P.J.J. Alvarez, In situ *remediation of subsurface contamination: opportunities and challenges for nanotechnology and advanced materials*, Environ. Sci.: Nano 6 (2019) 1283–1302.

[7] K.-H. Wei, J. Ma, B.-D. Xi, M.-D. Yu, J. Cui, B.-L. Chen, Y. Li, Q.-B. Gu, X.-S. He, *Recent progress on* in-situ *chemical oxidation for the remediation of petroleum contaminated soil and groundwater*, J. Hazard. Mater. 432 (2022) 128738.

[8] Y.-C. Chang, Y.-P. Peng, K.-F. Chen, T.-Y. Chen, C.-T. Tang, *The effect of different in situ chemical oxidation (ISCO) technologies on the survival of indigenous microbes and the remediation of petroleum hydrocarbon-contaminated soil*, PSEP 163 (2022) 105–115.

[9] T.A. Bruton, D.L. Sedlak, *Treatment of perfluoroalkyl acids by heat-activated persulfate under conditions representative of* in situ *chemical oxidation*, Chemosphere 206 (2018) 457–464.

[10] S. Hafeznezami, A.G. Zimmer-Faust, D. Jun, M.B. Rugh, H.L. Haro, A. Park, J. Suh, T. Najm, M.D. Reynolds, J.A. Davis, T. Parhizkar, J.A. Jay, *Remediation of groundwater contaminated with arsenic through enhanced natural attenuation: batch and column studies*, Water Res. 122 (2017) 545–556.

[11] R. Kolhatkar, M. Schnobrich, *Land application of sulfate salts for enhanced natural attenuation of benzene in groundwater: a case study*, GWMR 37 (2017) 43–57.

[12] K.M. Scow, K.A. Hicks, *Natural attenuation and enhanced bioremediation of organic contaminants in groundwater*, COBIOT 16 (2005) 246–253.

[13] M. Sørengard, B.K. D., L. Ahrens, *Stabilization of per- and polyfluoroalkyl substances (PFASs) with colloidal activated carbon (PlumeStop®) as a function of soil clay and organic matter content*, J. Environ. Manage. 249 (2019).

[14] G.R. Carey, R. McGregor, A.L. Pham, B. Sleep, S. Hakimabadi, *Evaluating the longevity of a PFAS* in situ *colloidal activated carbon remedy*, Remediation J. (29) (2019) 17–31.

[15] Intrapore, *Particle-based ground-water remediation*. https://intrapore.com/en/, accessed on 21.05.2022, 2022. https://intrapore.com/en/.

[16] P. Bardos, C. Merly, P. Kvapil, H.-P. Koschitzky, *Status of nanoremediation and its potential for future deployment: risk-benefit and benchmarking appraisals*, Remediation Journal 28 (2018) 43–56.

[17] H. Takaesu, H. Matsui, Y. Nishimura, T. Matsushita, N. Shirasaki, *Micro-milling super-fine powdered activated carbon decreases adsorption capacity by introducing oxygen/hydrogen-containing functional groups on carbon surface from water*, Water Res. 155 (2019) 66–75.

[18] K. Mackenzie, A. Georgi, *NZVI synthesis and characterization*, in: T. Phenrat, G.V. Lowry (Eds.), *Nanoscale zerovalent iron particles for environmental restoration*, Springer International Publishing AG, Basel, 2019, pp. 45–95.

[19] F. Obiri-Nyarko, S.J. Grajales-Mesa, G. Malina, *An overview of permeable reactive barriers for* in situ *sustainable groundwater remediation*, Chemosphere 111 (2014) 243–259.

[20] K. Pandey, S. Sharma, S. Saha, *Advances in design and synthesis of stabilized zero-valent iron nanoparticles for groundwater remediation*, J. Environ. Chem. Eng. 10 (2022) 107993.

[21] A. Pavelková, V. Stejskal, O. Vološčuková, J. Nosek, *Cost-effective remediation using microscale ZVI: comparison of commercially available products*, Ecol. Chem. Eng. S. 27 (2020) 211–224.

[22] K. Mackenzie, S. Bleyl, F.-D. Kopinke, H. Doose, J. Bruns, *Carbo-Iron as improvement of the nanoiron technology: from laboratory design to the field test*, Sci. Total Environm. 563–564 (2016) 641–648.

[23] M. Lawrinenko, Z. Wang, R. Horton, D. Mendivelso-Perez, E.A. Smith, T.E. Webster, D.A. Laird, J.H. van Leeuwen, *Macroporous carbon supported zerovalent iron for remediation of trichloroethylene*, ACS Sustainable Chemistry & Engineering 5 (2017) 1586–1593.

[24] W. Wang, B. Hu, C. Wang, Z. Liang, F. Cui, Z. Zhao, C. Yang, *Cr(VI) removal by micron-scale iron-carbon composite induced by ball milling: the role of activated carbon*, Chem. Eng. J. 389 (2020) 122633.

[25] B. Hu, K. Wang, L. Wu, S.-H. Yu, M. Antonietti, M.-M. Titirici, *Engineering carbon materials from the hyrothermal carbonization process of biomass*, Adv. Mater. 22 (2010) 813–828.

[26] V.K. LaMer, *Nucleation in phase transitions*, Ind. Eng. Chem. 44 (1952) 1270–1277.

[27] R. Li, A. Shahbazi, *A review of hydrothermal carbonization of carbohydrates for carbon spheres preparation*, Trends in Renewable Energy 1 (2015) 43–56.

[28] X. Sun, Y. Li, *Colloidal carbon spheres and their core/shell structures with noble-metal nanoparticles*, Angew. Chem. 116 (2004) 607–611.

[29] Y. Cheng, M. Yang, C. Fang, J. Chen, M. Bai, J. Su, *Controllable morphologies of carbon microspheres* via *green hydrothermal method using fructose and xylose*, Chemistry Letters 46 (2017) 1400–1402.

[30] J. Su, C. Fang, M. Yang, Y. Cheng, Z. Wang, Z. Huang, C. You, *A controllable soft-templating approach to synthesize mesoporous carbon microspheres derived from D-xylose* via *hydrothermal method*, Journals of Materials Science & Technology 38 (2020) 183–188.

[31] L. Xie, X. Li, J. Deng, Y. Gong, H. Wang, S. Mao, Y. Wang, *Sustainable and scalable synthesis of monodisperse carbon nanostructures and their derived superstructures*, Green Chemistry 20 (2018) 4596–4601.

[32] C. Tang, Z. Pingping, Y. Sun, L. Bai, *Size-tunable synthesis of mono-disperse wastewater-derived carbon spheres with polyacrylamide as a directing agent*, Micro Nano Lett. 10 (2015) 603–606.

[33] H. Yang, G. Wang, N. Ding, C. Yin, Y. Chen, *Size-controllable synthesis of carbon spheres with assistance of metal ions*, Synthetic Metals 214 (2016) 1–4.

[34] H. Zhao, X. Lu, Y. Wang, B. Sun, X. Wu, H. Lu, *Effects of additives on sucrose-derived activated carbon microspheres synthesized by hydrothermal carbonization*, Journal of Materials Science 52 (2017) 10787–10799.

[35] M. Liang, J. Wang, M. Zhao, J. Cai, M. Zhang, N. Deng, B. Wang, B. Li, K. Zhang, *Borax-assisted hydrothermal carbonization to fabricate monodisperse carbon spheres with high thermostability*, Materials Research Express 6 (2019).

[36] P. Liu, W. Cai, J. Wei, Z. Cai, M. Zhu, B. Han, Z. Yang, J. Chen, M. Jaroniec, *Ultrafast preparation of saccharide-derived carbon microspheres with excellent dispersibility* via *ammonium persulfate-assisted hydrothermal carbonization*, J. Mater. Chem. A 7 (2019) 18840–18845.

[37] X. Cui, M. Antonietti, S.-H. Yu, *Structural effects of iron oxide nanoparticles and iron ions on the hydrothermal carbonization of starch and rice carbohydrates*, Small (2006) 756–759.

[38] N. Fechler, S.-A. Wohlgemuth, P. Jäker, M. Antonietti, *Salt and sugar: direct synthesis of high surface area carbon materials at low temperatures via hydrothermal carbonization of glucose under hypersaline conditions*, J. Mater. Chem. A 1 (2013) 9418–9421.

[39] V. Saadattalab, X. Wang, A.E. Szego, N. Hedin, *Effects of metal ions, metal and metal oxide particles on the synthesis of hydrochars*, ACS Omega 5 (2020) 5601–5607.

[40] T.-P. Fellinger, R.J. White, M.M. Titirici, M. Antonietti, *Borax-mediated formation of carbon aerogels from glucose*, Adv. Funct. Mater. 22 (2012) 3254–3260.

[41] S.-H. Yu, X. Cui, L. L., K. Li, B. Yu, M. Antonietti, H. Cölfen, *From starch to metal/carbon hybrid nanostructures: hydrothermal metal-catalyzed carbonization*, Adv. Mater. 16 (2004) 1636–1640.

[42] X.-W. Wei, G.-X. Zhu, C.-J. Xia, Y. Ye, *A solution phase fabrication of magnetic nanoparticles encapsulated in carbon*, Nanotechnology 17 (2006) 4307–4311.

[43] S. Zhang, H. Niu, Z. Hu, Y. Cai, Y. Shi, *Preparation of carbon coated Fe_3O_4 nanoparticles and their application for solid-phase extraction of polycyclic aromatic hydrocarbons from environmental water samples*, Journal of Chromatography A 1217 (2010) 4757–4764.

[44] L. Bai, B. Mei, Q.-Z. Guo, Z.-G. Shi, Y.-Q. Feng, *Magnetic solid-phase extraction of hydrophobic analytes in environmental samples by a surface hydrophilic carbon-ferromagnetic nanocomposite*, Journal of Chromatography A 1217 (2010) 7331–7336.

[45] S. Xuan, L. Hao, W. Jiang, X. Gong, Y. Hu, Z. Chen, *A facile method to fabricate carbon-encapsulated* Fe_3O_4 *core/shell composites*, Nanotechnology 18 (2007).

[46] Z. Luo, H. Tang, L. Qu, T. Han, X. Wu, *A visible-light-driven solid state photo-Fenton reagent basedon magnetite/carboxylate-rich carbon spheres*, CrystEngComm 14 (2012) 5710–5713.

[47] S. Li, F. Liang, J. Wang, H. Zhang, S. Zhang, *Preparation of mono-dispersed carbonaceous spheres* via *a hydrothermal process*, Advanced Powder Technology 28 (2017) 2648–2657.

[48] Y. Liu, S. Ma, J. Chen, *A novel pyro-hydrochar* via *sequential carbonization of biomass waste: preparation, characterization and adsorption capacity*, Journal of Cleaner Production 176 (2018) 187–195.

[49] A.J. Romero-Anaya, M.A. Lillo-Ródenas, A. Linares-Solano, *Activation of a spherical carbon for toluene adsorption at low concentration*, Carbon 77 (2014) 616–626.

[50] P. Sun, K. Zhang, S. Shang, J. Song, D. Wang, *Sustainable production of activated carbon spheres from ethyl cellulose*, RSC Advances 6 (2016) 95656–95662.

[51] H. Cai, X. Lin, L. Tian, X. Luo, *One-step hydrothermal synthesis of carbonaceous spheres from glucose with an aluminum chloride catalyst and its adsorption characteristic for uranium(VI)*, Industrial & Engineering Chemistry Research 55 (2016) 9648–9656.

[52] Z.Z. Chowdhury, B. Krishnan, S. Sagadevan, R.F. Rafique, N.A.B. Hamizi, Y.A. Wahab, A.A. Khan, R.B. Johan, Y. Al-douri, S.N. Kazi, S.T. Shah, *Effect of temperature on the physical, electro-chemical and adsorption properties of carbon micro-spheres using hydrothermal carbonization process*, Nanomaterials 8 (2018) 597–616.

[53] X. Zhao, W. Li, S.-X. Liu, *Coupled soft-template/hydrothermal process synthesis of mesoporous carbon spheres from liquefied larch sawdust*, Materials Letters 107 (2013) 5–8.

[54] Z. Chen, L. Ma, S. Li, J. Geng, Q. Song, J. Liu, C. Wang, H. Wang, J. Li, Z. Qin, S. Li, *Simple approach to carboxyl-rich materials through low-temperature heat treatment of hydrothermal carbon in air*, Applied Surface Science 257 (2011) 8686–8691.

[55] X. Xia, L. Shi, H. Liu, L. Yang, Y. He, *A facile production of microporous carbon spheres and their electrochemical performance in EDLC*, Journal of Physics and Chemistry of Solids 73 (2012) 385–390.

[56] L. Mao, Y. Zhang, Y. Hu, K.H. Ho, Q. Ke, H. Liu, Z. Hu, D. Zhao, J. Wang, *Activation of sucrose-derived carbon spheres for high performance supercapacitor electrodes*, RSC Advances 5 (2015) 9307–9313.

[57] Y. Wang, R. Yang, M. Li, Z.J. Zhao, *Hydrothermal preparation of highly porous carbon spheres from hemp (*Cannabis sativa *L.) stem hemicellulose for use in energy-related applications*, Industrial Crops and Products 65 (2015) 216–226.

[58] J. Yang, J.-Y. Li, J.-Q. Qian, H.-Z. Lian, H.-Y. Chen, *Solid phase extraction of magnetic carbon doped* Fe_3O_4 *nanoparticles*, Journal of Chromatography A 1325 (2014) 8–15.

[59] Q. Wang, H. Li, L. Chen, X. Huang, *Monodispersed hard carbon spherules with uniform nanopores*, Carbon 39 (2001) 2211–2214.

[60] A. Philippe, G.E. Schaumann, *Interactions of dissolved organic matter with natural and engineered inorganic colloids – a review, Environ*. Sci. Technol. 48 (2014) 8946–8962.

[61] Z. Wang, H. Guo, Y. Yu, N. He, *Synthesis and characterization of a novel magnetic carrier with its composition of* Fe_3O_4*/carbon using hydrothermal reaction*, Journal of Magnetism and Magnetic Materials 302 (2006) 397–404.

[62] A. Jain, R. Balasubramanian, M.P. Srinivasan, *Hydrothermal conversion of biomass waste to activated carbon with high porosity: a review*, Chem. Eng. J. 283 (2016) 789–805.

[63] S. Kubo, J.R. White, K. Tauer, M.M. Titirici, *Flexible coral-like carbon nanoarchitectures* via *a dual block copolymer-latex templating approach*, Chemistry of Materials 25 (2013) 4781–4790.

[64] M.-M. Titirici, A. Thomas, M. Antonietti, *Replication and coating of silica templates by hydrothermal carbonization*, Adv. Funct. Mater. 17 (2007) 1010–1018.

[65] N.M. Osmond, *Activated carbon fibre adsorbent materials*, Adsorp. Sci. Technol. 18 (2000) 529–539.

[66] M. Kiliç, E. Apaydin-Varol, E.A. Pütün, *Preparation and surface characterization of activated carbons from* Euphorbia rigida *by chemical activation with* $ZnCl_2$, K_2CO_3, *NaOH and* H_3PO_4, Applied Surface Science 261 (2012) 247–254.

[67] A. Kumar, H.M. Jena, *Preparation and characterization of high surface area activated carbon from Fox nut (*Euryale ferox*) shell by chemical activation with H_3PO_4*, Results in Physics 6 (2016) 651–658.

[68] L. Ding, B. Zou, Y. Li, H. Liu, Z. Wang, Z. C., Y. Su, Y. Guo, *The production of hydrochar-based hierarchical porous carbons for use as electrochemical supercapacitor electrode materials*, Colloids and Surfaces: A: Physicochemical and Engineering Aspects 423 (2013) 104–111.

[69] G. Chegini, C. Briens, D. Pjontek, *Production and characterization of adsorbents from a hydrothermal char by pyrolysis, carbon dioxide and steam activation*, Biomass Conv. Bioref. (2022).

[70] J.J. Pignatello, W.A. Mitch, W. Xu, *Activity and reactivity of pyrogenic carbonaceous matter toward organic compounds*, Environ. Sci. Technol. 51 (2017) 8893–8908.

[71] J.C. Petit, Y. Bahaddi, *New insight on the chemical role of water vapour in the ageing of activated carbon*, Carbon 31 (1993) 821–825.

[72] J.A. Menéndez, J. Philips, B. Xia, L.R. Radovic, *On the modification and characterization of chemical surface properties of activated carbon: in the search of carbons with stable basic properties*, Langmuir 12 (1996) 4404–4410.

[73] F. Xiao, J.J. Pignatello, *Effects of post-pyrolysis air oxidation of biomass chars on adsorption of neutral and ionizable compounds*, Environ. Sci. Technol. 50 (2016) 6276–6283.

[74] Y. Liu, S.P. Sohi, F. Jing, J. Chen, *Oxidative ageing induces change in the functionality of biochar and hydrochar: mechanistic insights from sorption of atrazine*, Environ. Pollut. 249 (2019) 1002–1010.

[75] Y. Boutillara, L.F. Velasco, P. Lodewyckx, G. De Weireld, *Textural and functional modifications of activated carbons subjected to severe storing conditions*, Adsorption 24 (2018) 601–612.

[76] W.A. Arnold, A.L. Roberts, *Pathways and kinetics of chlorinated ethylene and chlorinated acetylene reaction with Fe^0 particles*, Environ. Sci. Technol. 34 (2000) 1794–1805.

[77] C.P. Andrieux, J.M. Saveant, K.B. Su, *Kinetics of dissociative electron-transfer – direct and mediated electrochemical reductive cleavage of the carbon halogen bond*, Journal of Physical Chemistry 90(16) (1986) 3815–3823.

[78] M.R. Gennero de Chialvo, A.C. Chialvo, *Hydrogen evolution reaction: analysis of the Volmer-Heyrovsky-Tafel mechanism with a generalized adsorption model*, Journal of Electroanalytical Chemistry 372 (1994) 209–223.

[79] X. Wang, C. Chen, Y. Chang, H. Liu, *Dechlorination of chlorinated methanes by Pd/Fe bimetallic nanoparticles*, J. Hazard. Mater. 161 (2009) 815–823.

[80] S. Liu, J.A. Otero, M. Martin-Martinez, D. Rodriguez-Franco, J.J. Rodriguez, L.M. Gómez-Sainero, *Understanding hydrodechlorination of chloromethanes. Past and future of the technology*, Catalysts 10 (2020) 1462–1500.

[81] T. Phenrat, T.S.T. Le, B. Naknakorn, G.V. Lowry, *Chemical reduction and oxidation of organic contaminants by nanoscale zerovalent iron*, in: T. Phenrat, G.V. Lowry (Eds.), *Nanoscale zerovalent iron particles for environmental restoration*, Springer International Publishing AG, Basel, 2019, pp. 97–155.

[82] L.J. Matheson, P.G. Tratnyek, *Reductive dehalogenation of chlorinated methanes by iron metal*, Environ. Sci. Technol. 28(12) (1994) 2045–2053.

[83] Y.Q. Liu, G.V. Lowry, *Effect of particle age (Fe^0 content) and solution pH on nZVI reactivity: H_2 evolution and TCE dechlorination*, Environ. Sci. Technol. 40(19) (2006) 6085–6090.

[84] L. Gong, J. Chen, Y. Hu, K. He, E.J. Bylaska, P.G. Tratnyek, F. He, *Degradation of chloroform by zerovalent iron: effect of mechanochemical sulfidation and nitridation on the kinetics and mechanism*, Environ. Sci. Technol. 57 (2023) 9811–9821.

[85] M. Vogel, A. Georgi, F.-D. Kopinke, K. Mackenzie, *Sulfidation of ZVI/AC composite leads to highly corrosion-resistant nanoremediation particles with extended life-time*, Sci. Total Environm. 665 (2019) 235–245.

[86] Y.H. Shih, Y.C. Chen, M.Y. Chen, Y.T. Tai, C.P. Tso, *Dechlorination of hexachlorobenzene by using nanoscale Fe and nanoscale Pd/Fe bimetallic particles*, Colloids and Surfaces a-Physicochemical and Engineering Aspects 332(2–3) (2009) 84–89.

[87] B.A. Asfaw, K. Sakaguchi-Söder, T. Schiedek, N. Michelsen, A. Bernstein, H. Siebner, C. Schüth, *Isotopic evidence ($\delta^{13}C$, $\delta^{37}Cl$, $\delta^{2}H$) for distinct transformation mechanisms of chloroform: catalyzed H_2-water system vs. zero-valent iron (ZVI)*, J. Environ. Chem. Eng. 11 (2023) 110005.

[88] G.V. Lowry, M. Reinhard, *Hydrodehalogenation of 1- to 3-carbon halogenated organic compounds in water using a palladium catalyst and hydrogen gas*, Environ. Sci. Technol. 33 (1999) 1905–1910.

[89] X. Chen, X.Y. Yao, C.N. Yu, X.M. Su, C.F. Shen, C. Chen, R.L. Huang, X.H. Xu, *Hydrodechlorination of polychlorinated biphenyls in contaminated soil from an e-waste recycling area, using nanoscale zerovalent iron and Pd/Fe bimetallic nanoparticles*, Environ. Sci. Pollut. 21(7) (2014) 5201–5210.

[90] Y. Han, W. Li, M. Zhang, K. Tao, *Catalytic dechlorination of monochlorobenzene with a new type of nanoscale Ni(B)/Fe(B) bimetallic catalytic reductant*, Chemosphere 72 (2008) 53–58.

[91] M. Balda, F.-D. Kopinke, *The role of nickel traces in fine chemicals for hydrodechlorination reactions with zero-valent iron*, Chem. Eng. J. 388 (2020) 124185.

[92] V.V. Rozanov, O.V. Krylov, *Hydrogen spillover in heterogeneous catalysis*, Russ. Chem. Rev. 66 (1997) 107–119.

[93] S. Khoobiar, *Particle to particle migration of hydrogen atoms on platinum-alumina catalysts from particle to neighboring particles*, Journal of Physical Chemistry 68 (1964) 411–412.

[94] W. Karim, C. Spreafico, A. Kleibert, J. Gobrecht, J. VandeVondele, Y. Ekinci, J.A. Van Bokhoven, *Catalyst support effects on hydrogen spillover*, Nature 541 (2017) 68–85.

[95] R. Prins, *Hydrogen spillover. Facts and fiction*, Chem. Rev. 112 (2012) 2714–2738.

[96] S.S.E. Collins, M. Cittadini, C. Pecharromán, A. Martucci, P. Mulvaney, *Hydrogen spillover between single gold nanorods and metal oxide supports: a surfaceplasmon spectroscopy study*, ACS Nano 9 (2015) 7846–7856.

[97] L.R. Merte, G. Peng, R. Bechstein, F. Rieboldt, C.A. Farberow, L.C. Grabow, W. Kudernatsch, S. Wendt, E. Lægsgaard, M. Mavrikakis, F. Besenbacher, *Water-mediated proton hopping on an iron oxide surface*, Science 336 (2012) 889–893.

[98] S.-Y. Oh, D.K. Cha, P.C. Chiu, *Graphite-mediated reduction of 2,4-dinitrotoluene with elemental iron*, Environ. Sci. Technol. 36 (2002) 2178–2184.

[99] J.L. Figueiredo, M.F.R. Pereira, M.M.A. Freitas, J.J.M. Órfao, *Characterization of active sites on carbon catalysts*, Industrial & Engineering Chemistry Research 46 (2007) 4110–4115.

[100] M.S. Shafeeyan, W.M.A.W. Daud, A. Houshmand, A. Shamiri, *A review on surface modification of activated carbon for carbon dioxide adsorption*, J. Anal. Appl. Pyrolysis 89 (2010) 143–151.

[101] F.-D. Kopinke, G. Speichert, K. Mackenzie, E. Hey-Hawkins, *Reductive dechlorination in water: interplay of sorption and reactivity*, Appl. Catal. B 181 (2016) 747–753.

[102] M. Vogel, F.-D. Kopinke, K. Mackenzie, *Acceleration of microiron-based dechlorination in water by contact with fibrous activated carbon*, Sci. Total Environm. 660 (2019) 1274–1282.

[103] H.J. Amezquita-Garcia, E. Razo-Flores, F.J. Cervantes, J.R. Rangel-Mendez, *Activated carbon fibers as redox mediators for the increased reduction of nitroaromatics*, Carbon 55 (2013) 276–284.

[104] F.P. Van der Zee, I.A.E. Bisschops, G. Lettinga, *Activated carbon as an electron acceptor and redox mediator during the anaerobic biotransformation of azo dyes*, Environ. Sci. Technol. 37 (2003) 402–408.

[105] K. Mackenzie, J. Battke, R. Koehler, F.-D. Kopinke, *Catalytic effects of activated carbon on hydrolysis reactions of chlorinated organic compounds: part 2. 1,1,2,2-Tetrachloroethane*, Appl. Catal. B 59 (2005) 171–179.

[106] J. Zhan, B. Sunkara, L. Le, V.T. John, J. He, G.L. McPherson, G. Piringer, Y. Lu, *Multifunctional colloidal particles for* in situ *remediation of chlorinated hydrocarbons*, Environ. Sci. Technol. 43 (2009) 8616–8621.

[107] Z.G. Liu, F. Zhang, S.K. Hoekman, T.T. Liu, C. Gai, N.N. Peng, *Homogeneously dispersed zerovalent iron nanoparticles supported on hydrochar-derived porous carbon: simple,* in situ *synthesis and use for dechlorination of PCBs*, ACS Sustainable Chemistry & Engineering 4(6) (2016) 3261–3267.

[108] C. Gai, F. Zhang, Q. Lang, T. Liu, N. Peng, Z. Liu, *Facile one-pot synthesis of iron nanoparticles immobilized into the porous hydrochar for catalytic decomposition of phenol*, Appl. Catal. B 204 (2017) 566–576.

[109] F. Meng, Z. Li, C. Lei, K. Yang, D. Lin, *Removal of trichloroethene by iron-based biochar from anaerobic water: key roles of Fe/C ratio and iron carbides*, Chem. Eng. J. 413 (2021) 127391.

[110] H. Choi, S. Agarwal, S.R. Al-Abed, *Adsorption and simultaneous dechlorination of PCBs on GAC/Fe/Pd: mechanistic aspects and reactive capping barrier concept*, Environ. Sci. Technol. 43(2) (2009) 488–493.

[111] J. Bedia, L.M. Gómez-Sainero, J.M. Grau, M. Busto, M. Martin-Martinez, J.J. Rodriguez, *Hydrodechlorination of dichloromethane with mono- and bimetallic Pd-Pt on sulfated and tungstated zirconia catalysts*, J. Catal. 294 (2012) 207–215.

[112] V.I. Simagina, O.V. Netskina, E.S. Tayban, O.V. Komova, E.D. Grayfer, E.D. Ischenko, E.M. Pazhetnov, *The effect of support properties on the activity of Pd/C catalysts in the liquid-phase HDC of chlorobenzene*, Appl. Catal. A: Gen. 379 (2010) 87–94.

[113] E.V. Golubina, E.S. Lokteva, V.V. Lunin, N.S. Telegina, A.Y. Stakheev, P. Tundo, *The role of Fe addition on the activity of Pd-containing catalysts in multiphase hydrodechlorination*, Appl. Catal. A: Gen. 302 (2006) 32–41.

[114] Y. Chen, X. Ding, W. Qiu, J. Song, J. Nan, G. Bai, S. Pang, *Effects of surface oxygen-containing groups of the flowerlike carbon nanosheets on palladium dispersion, catalytic activity and stability in hydrogenolytic debenzylation of tetraacetyldibenzylhexaazaisowurtzitane*, Catalysts 11 (2021) 441–458.

[115] Y. Ren, G. Fan, C. Wang, *Aqueous hydrodechlorination of 4-chlorophenol over an Rh/reduced graphene oxide synthesized by a facile one-pot solvothermal process under mild conditions*, J. Hazard. Mater. 274 (2014) 32–40.

[116] L.-M. Frenzel, U. Roland, F.-D. Kopinke, *Coating of solid substrates with carbon* via *hydrothermal carbonization*, Materials Letters (2020) submitted.

[117] C.E. Webster, R.S. Drago, M.C. Zerner, *Molecular dimensions for adsorptives*, J. Am. Chem. Soc. 120 (1998) 5509–5516.

[118] G. Aguilar-Armenta, M. Patiño-Iglesias, R. Leyva-Ramos, *Adsorption kinetic behaviour of pure CO_2, N_2 and CH_4 in natural clinoptilolite at different temperatures*, Adsorp. Sci. Technol. 21 (2002) 81–91.

[119] E.D. Raczyńska, J.-F. Gal, P.-C. Maria, M. Szeląg, *Proton transfer chemistry in the gas phase. Is a spontaneous 'neutralization' reaction a myth or a reality?*, Croat. Chem. Acta 82 (2009) 87–103.

[120] V.B. Delchev, H. Mikosch, *DFT study of the gas phase proton transfer in guanine assisted by water, methanol, and hydrogen peroxide*, J. Mol. Model. 12 (2006) 229–236.

[121] K. Karaoğlu, Z. Özçifçi, M. Çalişkan, T. Baran, H.T. Akçay, *Catalytic activity of palladium doped activated carbon from waste coffee on some environmental pollutants*, Mater. Chem. Phys. 15 (2022) 125857.

[122] N. Saeidi, F.-D. Kopinke, A. Georgi, *What is specific in adsorption of perfluoroalkyl acids on carbon materials?*, Chemosphere 273 (2021) 128520.

4 Results

4.1 Uniform and dispersible carbonaceous microspheres as quasi-liquid sorbent[1]

Maria Balda, Katrin Mackenzie, Frank-Dieter Kopinke, Anett Georgi

Department of Environmental Engineering, Helmholtz Centre for Environmental Research – UFZ, D-04318 Leipzig, Germany

Abstract: Functional colloidal carbon materials find various applications, including the remediation of contaminated water and soil in so-called particle-based *in-situ* remediation processes. In this study, uniform and highly dispersible micro-sized carbonaceous spheres (CS) were generated by hydrothermal carbonization (HTC) of sucrose in the presence of carboxymethyl cellulose (CMC) as environmentally friendly polyelectrolyte stabilizer. In order to ensure their optimal subsurface delivery and formation of a self-contained treatment zone, a narrow size distribution and low agglomeration tendency of the particles is desired. Therefore, the obtained CS were thoroughly characterized and optimized with respect to their colloidal properties which are a crucial factor for their application as quasi-liquid sorbent. The as-prepared uniform CS are readily dispersible into single particles in water, as confirmed by digital microscopy and form stable suspensions. Due to their perfectly spherical shape, particle sedimentation in aqueous suspensions is well predicted by Stokes' law. High sorption coefficients on the synthesized CS $K_{\mathrm{D,CS}}$ were determined for phenanthrene (up to log ($K_{\mathrm{D,CS}}$ / [L kg^{-1}]) = 5) and other hydrophobic groundwater contaminants. This confirms the application potential of the CS, which were prepared by an economic low-temperature process using sucrose as bio-based precursor, for generating *in-situ* sorption barriers for groundwater and soil remediation.

Keywords: Hydrothermal carbonization; uniform carbonaceous microspheres; dispersibility; CMC; sucrose; phenanthrene

---

[1] This article was published in Chemosphere, Vol. 307, Maria Balda, Katrin Mackenzie, Frank-Dieter Kopinke, Anett Georgi, *Uniform and dispersible carbonaceous microspheres as quasi-liquid sorbent*, 136079, © Elsevier (2022).

1 Introduction

As water scarcity is an emerging problem worldwide, it becomes increasingly important to ensure the quality of existing water sources such as groundwater. Remediation of groundwater contamination due to past and ongoing industrial and other activities remains a demanding and costly task which requires continuous development towards more sustainable and cost-efficient technologies. For *ex-situ* treatment techniques, the contaminated groundwater has to be pumped up and either remediated on-site or transported to the treatment facility. This is why off-site techniques are mostly expensive and energy-intensive. A possible alternative are *in-situ* remediation techniques where adsorbents and/or reagents are directly injected into the groundwater in order to bind or degrade pollutants directly at or close to the source of contamination [3]. These can either be dissolved chemicals such as permanganate, hydrogen peroxide or persulfate for *in-situ* chemical oxidation (ISCO) or particle-based adsorbents/reagents for the setting of permeable reactive barriers (PRBs) or retention zones within the aquifers.

The latter approach is termed particle-based *in-situ* remediation and makes use of colloidal materials which can be applied in quasi-liquid form to treat contaminations in the environment, forming stationary PRBs or zones in soils and aquifers by simple injection of adsorbent or reagent particles [4]. The most common nanoreagent is nanoscale zero-valent iron (NZVI) for contaminants which can be treated by reductive processes [5]. At the same time, carbonaceous materials play an important role as adsorbents and carriers of reactants, whereby activated carbon in colloidal form (ACC) is the most prominent example which is applied at technical scale in remediation [6–9]. ACC is typically obtained from conventional activated carbon produced from coal, coconut shell or wood precursors in a top-down process by milling to a particle size of about 1 µm [6, 10]. ACC is applied in order to stop further spreading of pollutants with the groundwater flow, to reduce exposure and keep contaminants at place for further remediation measures such as stimulated biodegradation [7, 11].

Hydrothermal carbonization (HTC) is an alternative process for preparing carbon materials, whereby carbohydrates are dehydrated and polymerized into a char-like product in water at temperatures above 100 °C and self-generated pressures [12]. On the one hand, HTC can be used to convert waste biomass into carbonaceous materials, so-called hydrochars, which can subsequently be activated [13] or used as solid fuel [14]. On the other hand, with the use of additives during the process, HTC also grants access to very specific carbon products such as hollow carbon spheres [15, 16], porous carbon spheres [17–19], metal-carbon core-shell composites [20–22] or highly spherical carbonaceous particles [23, 24]. Especially for synthesizing the latter, HTC is a rather elegant method because soluble carbohydrates such as mono, di- and easily hydrolyzable polysaccharides naturally carbonize into a spherical shape during the hydrothermal process [25]. Thus, HTC is able to produce colloidal particles directly in a low-temperature bottom-up approach whereas biochar formation from solid natural materials would require a high-temperature pyrolysis with subsequent milling steps. In addition, the HTC process results in a lignite-like carbon material which can expected to have already exploitable sorption properties for hydrophobic contaminants. Adsorbent synthesis *via* HTC therefore deserves closer investigation as an alternative to the energy-intensive and CO_2-releasing high-temperature processes related to biochar and activated carbon production. The proposed underlying mechanism in HTC consists of three major steps: intramolecular dehydration of the saccharide into (hydroxymethyl)furfural (HMF) derivatives, polymerization of the former leading to soluble polymers, and particle formation *via* further intermolecular dehydration and crosslinking of said polymers [26]. After reaching a critical supersaturation, nucleation occurs. Commonly, it was presumed that the formed nuclei grow according to the LaMer model [27] by diffusion of the dissolved intermediates, *e.g.* HMF, to the carbon surface and reaction with the reactive oxygen functional groups [20, 26]. However, it was recently shown by Jung *et al.* (2018) that the depletion of HMF is directly proportional to the formation of fresh hydrochar nuclei rather than particle growth [28]. Only when the hydrochar nuclei formation rate decreases and HMF is depleted, do the particles grow increasingly. This suggests that the particles grow *via* agglomeration and inter-particle polymerization/carbonization [28].

When aiming for the efficient generation of uniform micrometer-sized carbonaceous spheres (CS) for particle-based *in-situ* remediation, two contrary aspects have to be considered: increasing carbohydrate concentration, reaction temperature and reaction time each lead to a greater mass yield of hydrochar [23, 29]. However, simultaneously the CS become bigger, less uniform and less dispersible [28, 30].

The findings cited above on the inter-particle polymerization growth mechanism of HTC particles imply that efficient stabilization against agglomeration is a key factor for obtaining rather uniform particles instead of a wide size range of individual and aggregated particles.

There have been some studies of HTC with additives such as synthetic polymers/-electrolytes [19, 24] or even inorganic salts in large concentrations [31–33] in order to optimize the yield of uniform CS. However, the excessive use of salts or the addition of hazardous compounds compromise the sustainable character of the HTC process. Carboxymethyl cellulose (CMC) is known as a cheap, non-toxic and environmentally friendly stabilizing agent which is used in particle-based *in-situ* remediation to improve suspension stability and mobility of the particles during injections. It acts as particle dispersant by a combination of electrostatic and steric forces [5, 34]. However, despite of its benign properties, CMC has not yet been tested as polyelectrolyte additive in HTC processes. Its application might even appear counterintuitive as it is subject to hydrolysis and/or carbonization under harsh HTC conditions [35].

In terms of potential application of HTC-derived carbonaceous particles, previous studies focused extensively on their adsorption behavior towards heavy metals [36-39]. However, there is little data on the sorption of organic compounds [40]. The actual colloidal properties of the particles such as the dispersibility of the synthesized CS and their suspension stability in aqueous media are only mentioned in passing [20, 22] and have, to the best of our knowledge, not yet been studied in detail. The mentioned characteristics are linked to the surface charge of the particles as well as their size distribution and shape, and strongly determine their injectability and mobility regarding particle-based *in-situ* remediation [6]. Achieving sufficiently large transport distances before injected particles deposit on the aquifer sediment has been a major issue in developing technologies for particle-based *in-situ* remediation [41]. Simultaneously, the particles need to be precisely delivered to the target zone and their uncontrolled migration needs to be prevented [42]. Particle mobility in saturated porous media such as aquifer sediments is dependent on hydrological and hydrochemical parameters but first of all on particle size [43]. Uniform microparticles with a narrow size distribution are thus a pre-requisite for controlled placement of a reactive zone in the subsurface without the blockage of sediment pores [6, 44]. In addition, for particles with a density close to water, particle diameters in the range of 1 µm yield optimal mobility, facilitating a large radius of influence for each injection of the particle suspension [43].

Consequently, in this work, we aimed at the generation of readily dispersible CS with a narrow size distribution close to 1 µm by HTC of sucrose. For the first time, their colloidal properties were optimized through the addition of CMC as environmentally friendly stabilizer and careful adjustment of the HTC process parameters. Thus, our study helps to address the recently highlighted need for greener and more sustainable products and methods for particle-based *in-situ* remediation [45].

The applicability of CS for contaminant removal was thoroughly characterized using phenanthrene (PHE), a polycyclic aromatic hydrocarbon (PAH) frequently detected in oil-derived groundwater contaminations. The influence of pollutant properties on the sorption affinities of the synthesized material was investigated using a cocktail of different organic substances with saturated and unsaturated carbon backbones covering a wide range of hydrophobicity and differing in the number and location of chlorine substituents. The chosen pollutants were trichloroethylene (TCE), lindane (LIN), acenaphthene (ACE), hexachlorobenzene (HCB) and 2,3,4-trichlorobiphenyl (TCB). The combined colloid and adsorbent characteristics of the herein synthesized particles show promising application potential in the field of *in-situ* groundwater and soil remediation in case of contamination with hydrophobic compounds.

2 Materials and Methods

2.1 Chemicals

Commercially available sugar was used as starting material for HTC. CMC sodium salt with a molecular weight of about 90 kDa, a polymerization degree of 400, a substitution degree (by – CH_2COO^-) of 0.65–0.90 with a sodium content of approximately 8 wt.-% and a purity of 99.5 %, was purchased from Sigma-Aldrich. LIN, ACE, PHE (≥ 99.8 %) as well as per-deuterated PHE (98 atom-%) were also purchased from Sigma-Aldrich. Dichloromethane and chloroform (both gas-chromatography grade), potassium hydroxide (p.a.), potassium nitrate (p.a.) and calcium chloride di-hydrate (p.a.) were purchased from Merck. Potassium hydrogen phthalate, TCE, HCB and TCB were all in analytical grade and purchased from Riedel-de Haën.

2.2 Preparation of carbonaceous spheres *via* HTC

For the hydrothermal synthesis of uniform carbonaceous spheres, 0.25–0.75 M sucrose (85.6–256.7 g L^{-1}) dissolved in de-ionized water with 0.3–3 wt.-% of CMC (in relation to initial sucrose) was placed into a stainless steel autoclave with a glass insert. After closing, the autoclave was heated in an oven for 1 to 4 h at 170–200 °C. Comparative experiments were performed in the absence of CMC. The formed precipitate, called hydrochar or CS synonymously, was collected through centrifugation, washed once with de-ionized water and air-dried. The size distribution and aggregation states of CS were characterized by means of digital microscopy.

2.3 Sedimentation of CS in aqueous media

The dried CS were dispersed in aqueous media at concentrations of 1 and 10 g L^{-1} using an ultrasonic bath RK 100 SH Sonorex (Bandelin Electronic) with a power of 160 W and a frequency of 35 kHz. The native pH of the samples was measured and an aliquot was taken in order to observe the dispersion of the CS under the digital microscope. The suspensions were then allowed to stand without agitation for 18 h. In order to study the sedimentation of the particles, samples were taken with a syringe from 2 cm below the water surface at 0 h and at 18 h and analyzed using a total organic carbon (TOC) analyzer. The detailed experimental setup is described in the SI part. Furthermore, the sedimentation behavior in the presence of two different salts – KNO_3 and $CaCl_2$ – in two different pH ranges was investigated exemplarily on the basis of the CS sample synthesized with 0.5 M sucrose, 1 wt.-% CMC (in relation to sucrose) at 180 °C for 2 h (CS_1%). The relative TOC content of the samples taken after 18 h at 2 cm below suspension surface was used as a parameter for comparing the sedimentation behavior of various CS samples.

2.4 Batch sorption experiments

Sorption experiments with PHE were performed in batches with 0.05 g L^{-1} CS and initial PHE concentrations of 0.01–1.4 mg L^{-1} at (21 ± 1) °C. Batches with total PHE concentrations close to or above its water solubility were spiked step-wise in portions so that the concentration of PHE in the aqueous phase always remained below the solubility limit. The dried CS were first dispersed in a 1 g L^{-1} KNO_3 solution by 10 min of ultrasonication, then the appropriate amount of a stock solution of PHE in acetone was added to the mixture. The batches were shaken on a horizontal shaker with 200 rpm for at least 5 days. Kinetic experiments showed that sorption equilibrium was approached before that time, after approximately 48 h, as no significant change in the aqueous phase concentration of PHE was observed for prolonged contact times. In order to terminate the batch experiments, CS and liquid phase were separated by centrifugation at 4500 rpm for 5 min and the CS as well as the liquid phase were each extracted with chloroform containing 2.5 mg L^{-1} per-deuterated phenanthrene (PHE-D10) as internal standard. The CS were extracted twice with chloroform (mass ratio CS:solvent = 1:1300) in order to close mass balances. The extracts were analyzed by means of gas chromatography with coupled mass-spectrometry (GC-MS). The obtained thermodynamic data for the PHE sorption were fitted according to the Freundlich model using the software OriginPro 2018G (© 1991–2017 OriginLab Corporation). The batch experiment for measuring the single point sorption coefficients of other compounds (TCE, LIN, ACE, HCB and TCB) was conducted analogously in a combined batch with initial concentrations of 10 µg L^{-1} for each analyte. TCE was analyzed *via* GC-MS of the batch headspace. LIN, ACE, HCB and TCB were extracted analogously to PHE followed by GC-MS analysis of the extracts.

2.5 Analytical methods

Microscopic images were recorded with a VHX digital microscope (Keyence). Random samples of 100–150 particles were measured with the open-source software ImageJ 1.52a in order to determine the particle diameters for the dry CS samples. The measured values were processed with RStudio 1.4 (© 2009–2021 RStudio, PBC) in order to obtain the frequency distribution.

The SEM analyses were conducted with a Zeiss Merlin VP compact. The beam current was 250 pA and the electron landing energy added up to 10 kV.

Elemental (C, H) analysis of the CS samples was conducted with a TruSpec® CHN macro-analyzer (LECO). The oxygen content was derived by difference calculation.

The zeta potential was characterized with a Zetasizer Ultra (Malvern Panalytical). Samples were prepared by dispersing the CS in 10 mM KNO_3 at a concentration of 2 mg L^{-1}, and the pH was adjusted to 6 with 1 M KOH.

Temperature-programmed decomposition (TPD) was performed under Ar (50 mL min^{-1}) with a BELCAT-B chemisorption analyzer (BEL). The samples were pretreated at 50 °C for 30 min, heated to 1100 °C with 10 K min^{-1} and held for 30 min. Evolving CO and CO_2 were detected with an Infralyt analyzer (SAXON Junkalor).

The specific surface area (SSA) of the CS was determined with a Belsorp MINI (BEL Japan). Adsorption/desorption of N_2 was performed at -196 °C after pretreatment of the samples under vacuum at 100 °C overnight. The obtained data were evaluated according to the Brunauer-Emmet-Teller (BET) theory.

GC-MS analyses were carried out with a GCMS-QP2010 (Shimadzu). The column (DB-5ms, Agilent) had a length of 30 m, an inner diameter of 0.25 mm and a film thickness of 0.25 µm. For analysis of PHE, 1 µL of the chloroform extract was injected at 250 °C. The following temperature program was used: 60 °C (1 min), with 10 K min^{-1} to 230 °C and with 30 K min^{-1} to 290 °C (5 min). The column He flow rate was 1 mL min^{-1}. For the analysis of LIN, ACE, HCB and TCB, the chloroform extracts were injected at 200 °C with an initial column temperature of 100 °C (3 min) and heating with 15 K min^{-1} to 220 °C (2 min) at a He flow rate of 1.4 mL min^{-1}. TCE was analyzed prior to extraction *via* headspace sampling at an injection temperature of 200 °C and a column temperature of 60 °C with a He flow of 1 mL min^{-1}.

3 Results and Discussion

3.1 Effect of CMC on the morphology of the formed carbonaceous spheres

In order to demonstrate the major effect of the polyelectrolyte CMC during the HTC of sucrose, two different samples were generated: one in the absence (a: CS_0%) and another one in the presence of CMC (b,c: CS_1%). Figure 1 demonstrates the significant differences between the two CS samples. The particle size distribution of the sample synthesized from sucrose without CMC is broad and reaches from 1 to 10 µm.

In contrast, when sucrose was hydrothermally carbonized in the presence of CMC, smaller and uniform CS were formed with a very narrow size range from 0.8 to 1.5 µm (*cf.* Figure 1, Table 1). Their highly spherical shape was confirmed by SEM analysis (*cf.* Figure 1 c). The mean particle diameters for samples CS_0% and CS_1% were 1.9 µm and 1.1 µm respectively. As the solid yields of the two samples did not differ significantly (*cf.* Table 1), it can be concluded that the yield of CS in the desired size range of about 1 µm was significantly increased by addition of CMC.

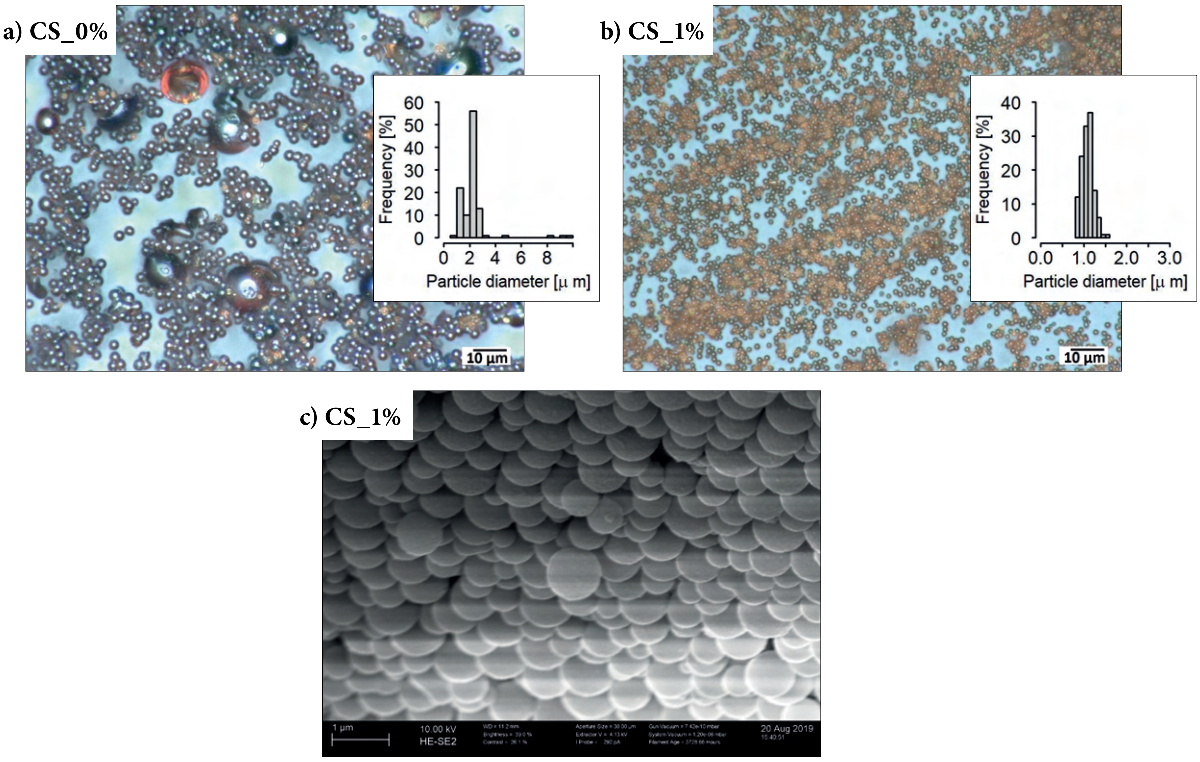

Figure 1 Digital microscopy a), b) and SEM analysis, c) of hydrochar prepared from 0.5 M sucrose a) without and b), c) with 1 wt.-% CMC (in relation to sucrose) at 180 °C for 2 h.

Based on the inter-particle polymerization growth mechanism proposed by Jung *et al.* (2018), one can hypothesize that the CMC adsorbs on freshly formed particles and prevents them from agglomerating and forming larger particles. As CMC is a macromolecular polyelectrolyte with a molecular mass of around 90 kDa, this effect can be ascribed to the enhanced electrostatic repulsion along with sterical hindrance, a so-called electrosteric stabilization effect [34]. Although CMC itself is a carbohydrate, it is obviously sufficiently stable under the applied HTC conditions to provide this stabilizing effect. Thus, it can be used as a cheap and environmentally friendly alternative to previously tested polymers such as *e.g.* poly(acrylamide) [46], which can release toxic acrylamide upon decomposition. In order to synthesize equivalently uniform CS in the absence of CMC, the reaction time had to be reduced to 1 h (see Figure S5 f); however, this was at the expense of a strongly reduced mass yield (only 17 % of the yield after 2 h, Tab 1).

In order to investigate more closely the formation of uniform CS by HTC of sucrose in the presence of CMC, a systematic study was performed whereby the reaction parameters were changed one-by-one and the mean particle diameter as well as the solid yield (defined as the mass of CS divided by the mass

Table 1 Particle diameter specifications derived from digital microscopy of the dry CS and the according solid yields generated by HTC of sucrose with varying reaction parameters (0–3 wt.-% CMC in relation to sucrose, 0.25–0.75 M sucrose, 1–4 h, 170–200 °C). Limiting upper diameters below which 10, 50 and 90 % of particles could be found (d_{10}, d_{50}, d_{90}) were calculated from random samples of 100–150 particles. Samples where the difference between d_{90} and d_{10} did not exceed 0.6 µm were considered 'uniform' (highlighted in **bold**).

Fixed parameters	Varied parameter	Sample name	Particle size distribution			Yield
			d_{10}	d_{50}	d_{90}	$Y = \frac{m_{CS}}{m_{sucrose}}$
			[µm]			[%]
0.5 M sucrose, 180 °C	**1 h**	**CS_0%1h**	**1.0**	**1.2**	**1.5**	**2.3±0.3**
	2 h	CS_0%	1.3	2.2	2.6	13.3±1.0
0.5 M sucrose, 180 °C, 2 h	0.3 % CMC	CS_0.3%	1.3	1.5	3.6	13.0±1.1
	0.5 % CMC	**CS_0.5%**	**1.2**	**1.4**	**1.5**	**13.9±0.7**
	1 % CMC	**CS_1%**	**0.9**	**1.1**	**1.3**	**13.7±1.1**
	2 % CMC	**CS_2%**	**1.2**	**1.4**	**1.6**	**12.1±0.3**
	3 % CMC	CS_3%	1.0	1.4	1.9	14.2±0.2
1 % CMC, 180 °C, 2 h	**0.25 M sucrose**	**CS_0.25M**	**0.6**	**0.9**	**1.1**	**7.0±0.3**
	0.5 M sucrose	**CS_0.5M**	**0.9**	**1.1**	**1.3**	**13.7±1.1**
	0.75 M sucrose	CS_0.75M	1.4	1.8	2.6	13.3±0.1
0.5 M sucrose, 1 % CMC, 180 °C	**1 h**	**CS_1h**	**0.9**	**1.1**	**1.2**	**1.7±0.3**
	2 h	**CS_2h**	**0.9**	**1.1**	**1.3**	**13.7±1.1**
	3 h	**CS_3h**	**1.1**	**1.3**	**1.6**	**21.0±0.6**
	4 h	CS_4h	1.4	1.9	2.4	23.9±1.7
0.5 M sucrose, 1 % CMC, 2 h	**170 °C**	**CS_170C**	**0.8**	**0.9**	**1.1**	**5.4±0.6**
	180 °C	**CS_180C**	**0.9**	**1.1**	**1.3**	**13.7±1.1**
	190 °C	**CS_190C**	**1.1**	**1.4**	**1.6**	**20.2±0.2**
	200 °C	**CS_200C**	**1.5**	**1.7**	**2.0**	**32.6±0.5**

of sucrose) was determined and summarized in Table 1. The particles were defined as 'uniform' when the difference between d_{10} and d_{90} did not exceed 0.6 µm. Please note the extensive material in the supporting information where Figures S3–S6 provide a visual impression. Uniform CS samples can be distinguished from the irregular ones at first sight under the digital microscope.

In Table 2 it is shown that CMC fractions of 0.5–2 wt.-% related to sucrose proved to be optimal for obtaining uniform CS. CMC concentrations of < 0.5 wt.-% are apparently not sufficient to affect the particle formation mechanism. However, also too high CMC concentrations do not have the desired effect. A similar observation was described by Tang *et al.* (2015) when using poly(acrylamide) as stabilizer – below or above an "ideal" concentration range, the particles had quite irregular shapes and sizes. This phenomenon was ascribed to the potential crosslinking of spherical particles when too much of the polymer was present [46].

Variation of sucrose concentration and reaction time showed that uniform CS could be obtained up to 0.5 M initial sucrose concentration and up to 3 h reaction time. It is worth mentioning that the effect of CMC could still be observed at a reaction temperature as high as 200 °C. This suggests that CMC was stable under these hydrothermal conditions and itself neither hydrolyzed nor carbonized significantly. This is consistent with previous studies where temperatures of 210 °C and higher were required in order to hydrothermally carbonize cellulose [35, 47, 48] or CMC [49]. Furthermore, the hydrolysis of cellulose under hydrothermal conditions occurs only at temperatures ≥ 220 °C, which is indicated by carbonization into microspheres without the retention of the original substrate morphology [29, 35, 47–49].

It can be assumed that the slow hydrolysis of CMC also becomes relevant at longer reaction times. This could explain why CMC was not effective at a reaction time of 4 h.

The elemental analysis of CS samples resulted in carbon contents of 62.6–65.8 wt.-%, hydrogen contents of 3.9–4.8 wt.-% and derived oxygen contents of 29.9–33.5 wt.-% (*cf.* Table S1). No large differences could be detected for any combination of samples, as the reaction conditions were only varied slightly. Nevertheless, certain expected trends can be seen in Table S1 as the C content increases and the O content decreases with increasing sucrose concentration, reaction time and temperature, due to enhanced dehydration of the hydrochars. The observed elemental contents and trends are in good agreement with previous literature studies on the HTC of saccharides [23].

3.2 Dispersibility of the CS and stability in aqueous media

The CS collected after HTC were washed with de-ionized water once and then dried. In order to investigate their actual dispersibility in aqueous media, they were suspended in de-ionized water and subjected to 10 min of ultrasonic treatment (US). Figure 2 shows the synthesized CS_1%, which are readily dispersed and appear mostly as single spheres when dispersed by US. Even at high concentrations, such as 10 g L^{-1} (see Figure 2 b), no larger agglomerates beyond 5 µm were found in the freshly prepared suspensions. An alternative dispersion method is the use of a high-speed homogenizer (*e.g.* UltraTurrax®) which is also applied at technical scale in the field [50]. For further information see Figure S14 in the SI. The fact that hydrothermally synthesized CS are well dispersible is due to their high density of functional groups and thus their hydrophilic surface. The dispersibility has been mentioned in a few studies where functional composites were synthesized *via* HTC [20, 51–54], but has rarely been actually investigated [55] and, to the best of our knowledge, never been actually demonstrated. We found that all CS synthesized within this study, which were considered 'uniform' based on the particle size distribution as determined by microscopy of the dry sample, could be dispersed into mostly single spheres *via* US (see Figure S9–S12) with a low tendency to agglomerate. On the contrary, CS samples which exhibited a broader particle size distribution for the dry sample were not dispersed into single spheres *via* US (*cf.* Figure S9 a, e, S10 c, S11 d). Therefore, it is deduced that, with proceeding HTC, not only the particle size distribution becomes broader but also the particles become more aggregated. This observation is in line with the proposed growth mechanism by Jung *et al.* (2018) which is based on inter-particle polymerization.

Sample CS_1% showed no significant agglomeration after 1 month storage as non-agitated aqueous suspension, even at a high particle concentration of 10 g L^{-1} (*cf.* Figure S6). This can be explained by means of the Derjaguin-Landau-Verwey-Overbeek (DLVO) theory which states that agglomeration is a function

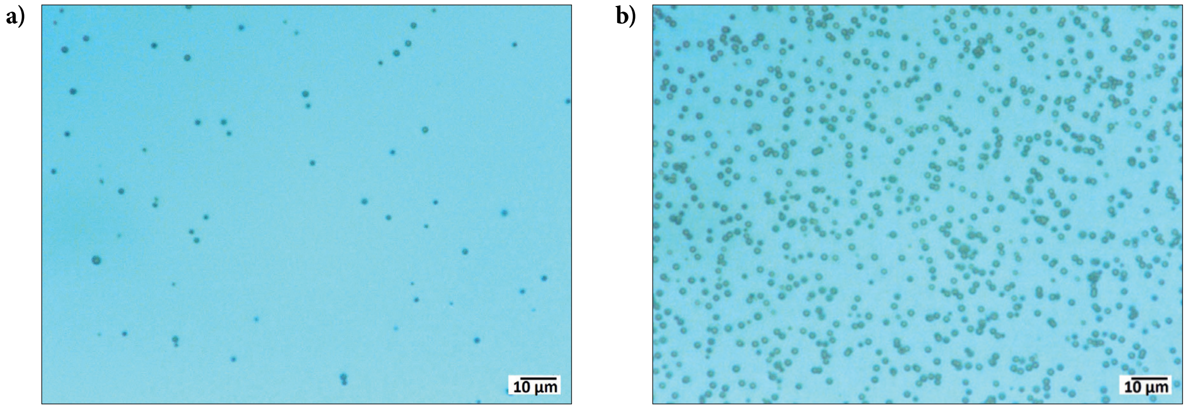

Figure 2 Digital microscopy images of hydrochar prepared from 0.5 M sucrose and 1 wt.-% CMC (180 °C, 2h) dispersed in de-ionized water with concentrations of a) 1 g L^{-1} and b) 10 g L^{-1}

of the frequency of particle collisions and the probability of attachment in the collision events [56]. As close approach and collisions of the particles cannot be prevented in highly concentrated suspensions, attachment probability needs to be reduced in order to obtain stable suspensions. The synthesized CS_1% particles exhibit a strongly negative zeta potential of -43.5 mV at pH 6 which can be transcribed to a high density of negative surface charges, due to abundant oxygen-containing functional groups [57]. The latter were confirmed by TPD analyses, which resulted in a total of 12.3 wt.-% of thermally labile oxygen (data not shown). The determined zeta potential value is higher than the empirical value of $\geq |\pm 30\ \text{mV}|$, which was found as a prerequisite for suspension stability for many types of colloids [58]. In such cases, electrostatic repulsion leads to an energy barrier which has to be overcome for agglomeration. Thus, agglomeration phenomena are highly dependent on the ionic strength of the suspension, the ion valence of electrolytes present and the pH of the suspension [56].

The suspension stability of the samples produced under various HTC conditions was characterized comparatively by determining the total organic carbon (TOC) content of the resting samples at 0 h (immediately after agitation) and after 18 h at a depth of 2 cm below the suspension surface. This criterion was chosen based on Stokes' law (eq. (1)), which describes the correlation of particle diameters with sedimentation velocities of spherical particles in suspensions.

$$\frac{d_{\text{Stokes}}}{2} = r = \sqrt{\frac{v_{\text{sedimentation}} \bullet 9\eta}{2(\rho_{\text{particle}} - \rho_{\text{medium}}) \bullet g}} \tag{1}$$

In eq. (1), d_{Stokes} is the Stokes diameter of particles (m), $v_{\text{sedimentation}}$ the sedimentation velocity (m s^{-1}), η is the shear viscosity of the medium (kg m^{-1} s^{-1}), ρ is the density of the particles or the medium respectively (kg m^{-3}), and g is the apparent gravity (= 9.81 m s^{-2}). The particle density was determined *via* mixing dichloromethane and chloroform in various ratios and observing at which medium density the particles floated in a stable manner for > 60 h. With this method, a mass density of about (1.45 ± 0.03) g cm^{-3} was identified for two representative CS samples synthesized at two different hydrothermal carbonization temperatures: 180 °C and 200 °C. This density was assumed for all synthesized CS samples as the method is not able to determine the suspected minor differences with higher resolution. In the literature, a comparable mass density of 1.445 g cm^{-3} is given for hydrochar pellets prepared from food waste (220 °C, 1 h) [59].

According to Stokes' equation (1), particles which pass 2 cm within 18 h are ≥ 1.1 µm in diameter. Figure 3 shows that for the CS which were synthesized in the presence of 1 wt.-% CMC, a particle mass fraction of 50–60 % did not pass the 2 cm limit, *i.e.* has a diameter < 1.1 µm. This is in good accordance with the d_{50} value of 1.2 µm determined by microscopy (*cf.* Table 1). In contrast, merely ≤ 10 % of the CS samples synthesized in the presence of lower or higher CMC concentrations are still in suspension after 18 h (*cf.* Fig 3). This can again readily be explained when referring to Table 1, as only 10 % of the particles of these samples have diameters below 1.1 µm.

When comparing the suspension stabilities of all synthesized samples, equivalent trends are visible within the various test series (*cf.* Figure S1): the stability of aqueous suspensions

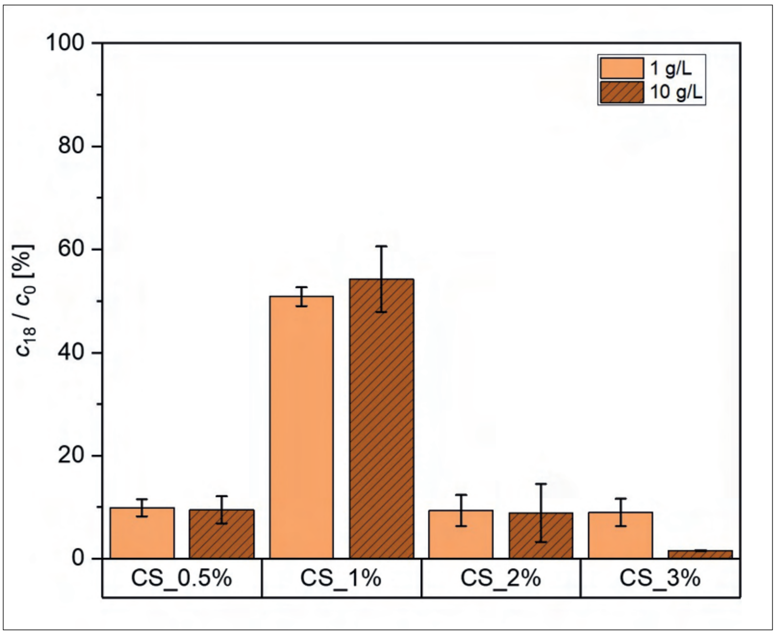

Figure 3 Suspension stability of various CS samples in de-ionized water (suspended particle fraction after 18 h); the native pH value of the samples was between 3.5 and 4.5; CS were synthesized from 0.5 M sucrose in the presence of various weight percentages of CMC at 180 °C for 2 h as detailed in Table 1.

decreases with increasing particle diameter. The latter results from a higher initial sucrose concentration, reaction time and/or reaction temperature applied in the HTC process (*cf.* Figure 3). Furthermore, the experimental observations of the sedimentation behavior are in good relation with Stokes' law (eq. (1)). For example, the samples CS_0.25M and CS_170C are the most stable ones where 80–90 % of particles were found in suspension at the 2-cm-sampling point after 18 h. Accordingly, the d_{90} value of these samples can be assumed to be below 1.1 µm, as confirmed by microscopy of the dry particles (Table 1). These findings indicate that the sedimentation of particles proceeds practically unhindered and without agglomeration processes. Furthermore, in all cases, higher particle concentrations (causing more frequent collisions) did not lead to faster sedimentation, which in turn speaks against significant agglomeration or, more precisely, for a low probability of attachment in collisions.

In order to investigate how tolerant the suspended CS are to higher ionic strengths, analogous experiments were conducted where 1 g L^{-1} CS_1% were dispersed in two different electrolyte solutions and again allowed to sediment for 18 h. Various concentrations of KNO_3 and $CaCl_2$ were applied. It was found that the suspensions "collapsed" at a certain ionic strength, meaning that the particles agglomerated increasingly and completely sedimented within a few hours. As expected, the tolerated salt concentrations depend strongly on the ion valence as well as on the pH of the suspension. At a pH of 4, the particles in suspension of 1 g L^{-1} CS_1% were present in an agglomerated state at 90 mM KNO_3 (pH 3.8) and 7 mM $CaCl_2$ (pH 4.1), whereas an analogous suspension tolerated up to 168 mM KNO_3 at pH 6.0 and 12 mM $CaCl_2$ at pH 6.6 until particles agglomerated (*cf.* Figures S8, S9). As a higher ionic strength in the solution leads to the compression of the electric double layer, the particles can approach each other more closely, so that van-der-Waals interactions predominate and agglomeration occurs [56] (Figures S8, S9). The amount of surface charge, and consequently the thickness of the electric double layer, varies at different pH values. Therefore, the salt concentration which leads to a sufficient compression of the double layer is pH-dependent [56], as was also observed within this study.

The tolerated concentration of K^+ was around 13-fold higher (pH 4) and 14-fold higher (pH 6) than that of Ca^{2+}. These results are in accordance with previous findings regarding colloidal particle suspensions. Sun *et al.* (2020) found that colloidal kaolinite suspensions tolerated a 14-fold higher concentration of Na^+ than of Mg^{2+} before the particles agglomerated [56]. As the ionic strength of a $CaCl_2$ solution is only threefold as high as that of a KNO_3 solution at equal molar concentrations, it can be deduced that specific effects of the bivalent Ca^{2+} lead to a greater destabilization than that due to the effect of monovalent ions. This is also known as the Schulze-Hardy rule. Bivalent ions are, for example, able to form a single ion-layer between two particles and consequently interlink the particles [60].

3.3 Sorption of various hydrophobic compounds on the hydrothermally synthesized carbonaceous microspheres

The sorption characteristics of the synthesized CS were tested on the basis of the sample CS_1% (0.5 M suc, 1 wt.-% CMC, 180 °C, 2 h) which was chosen due to its desirable colloidal properties in combination with a sufficient mass yield. The sorption of PHE was investigated regarding the time frame for approaching an equilibrium state (Figure S13) and the thermodynamic characteristics (Figure 4). The sorption isotherm was fitted according to the Freundlich model (eq. 2), where q (mg kg^{-1}) refers to the mass loading, c_e (mg L^{-1}) is the equilibrium concentration of the sorbate in the aqueous phase, K_F is the Freundlich coefficient and n the Freundlich exponent.

$$q = K_F \cdot c_e^{1/n} \tag{2}$$

Fitting the isotherm in Figure 4 according to eq. 2 leads to K_F = 17 500 (mg kg^{-1}) (mg L^{-1})$^{-1/n}$ and $1/n$ of 0.70. As the CS are largely non-porous with a specific surface area < 5 m^2 g^{-1}, the high sorption affinity up to $K_{D,CS} = q/c_e = 10^{5.1}$ L kg^{-1} at c_e = 1.5 µg L^{-1} and the PHE loading up to 1.3 wt.-% at c_e = 0.7 mg L^{-1} lead us to the presumption that an *ab*sorption process into the carbonaceous bulk material takes place in addition to the sole *ad*sorption onto the particle surface. This was further elucidated by estimating the theoretical maximum loading of the outer particle surface. Based on a calculated smooth geometrical particle surface area of 3.6 m^2 g^{-1} and the approximate monolayer capacity of $1.7 \cdot 10^{-6}$ mol m^{-2} PHE [61], the maximum monolayer loading at the outer particle surface would amount to merely 0.1 wt.-%. As the experimentally

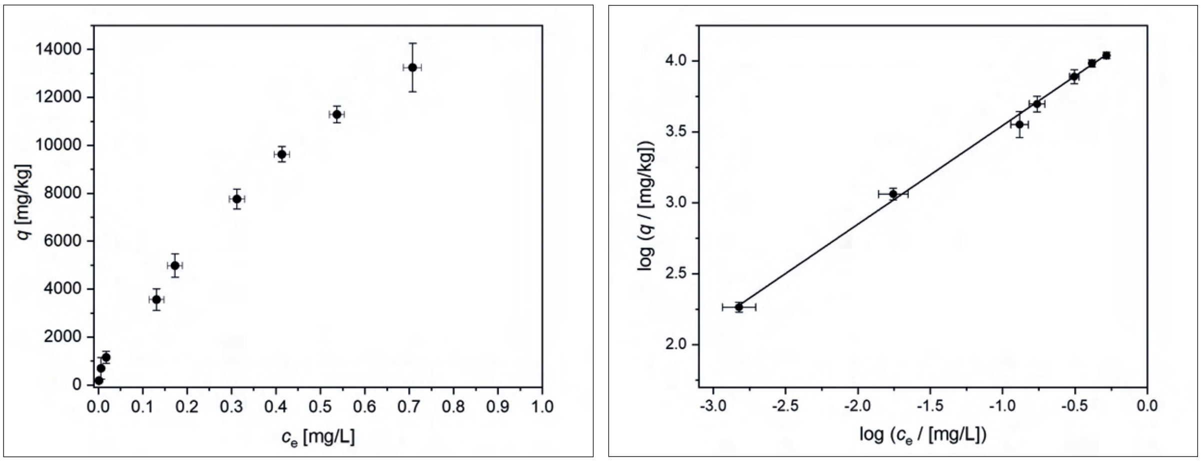

Figure 4 Sorption of phenanthrene onto hydrothermally synthesized CS (0.5 M suc, 1 wt.-% CMC, 180 °C, 2 h); the last data point of the sorption isotherm showed a relatively high uncertainty (left) and was omitted when fitting according to the linearized Freundlich model (right); error bars were calculated *via* error propagation from the measurement uncertainty regarding the aqueous PHE concentration; $c_{\mathrm{CS}} = 50$ mg L^{-1}, $c_{0,\mathrm{PHE}} = 0.01–1.4$ mg L^{-1}, $c_{\mathrm{KNO_3}} = 1$ g L^{-1}, pH = 4.8.

determined loadings are much higher, it can indeed be assumed that the sorption process of PHE onto the hydrothermally synthesized CS is dominated by absorption into the char. The latter could happen through intercalation of the polyaromatic ring system into the polymer-like carbonaceous material. This so-called partitioning has also been observed for carbonaceous materials such as peat and lignite [62]. The determined value of the Freundlich exponent $n = 1/0.70 = 1.43$ indicates a heterogeneous composition of the carbonaceous bulk material with more and less sorption affine regions. Similar sorption isotherms have been observed regarding the sorption of polycyclic aromatic hydrocarbons (PAHs) onto organic fractions in soil and sediment [63]. In additional sorption experiments, we compared the sorption behavior of the CS towards further organic pollutants with different hydrophobicities and with or without presence of aromatic rings and chlorine substituents. In order to eliminate possible competition effects between the different sorbates, the experiments were designed to keep the overall loading below 500 mg kg^{-1} which is only 3 % of the estimated maximum loading of the CS (*cf.* Figure 4). Figure 5 shows a plot of the experimentally determined sorption coefficients ($K_{\mathrm{D,CS}}$) of the investigated substances *vs.* their octanol-water partitioning coefficients (K_{OW}) [1]. For comparison, we also calculated sorption coefficients to soil organic matter ($K_{\mathrm{D,SOM}}$) for the various compounds using the freely accessible UFZ-LSER (linear solvation energy relationship) database [2] which is based on polyparameter linear free energy relationships (LFER) as common concept for predicting partitioning sorption processes. $K_{\mathrm{D,SOM}}$ was calculated by multiplying the distribution coefficient between water and

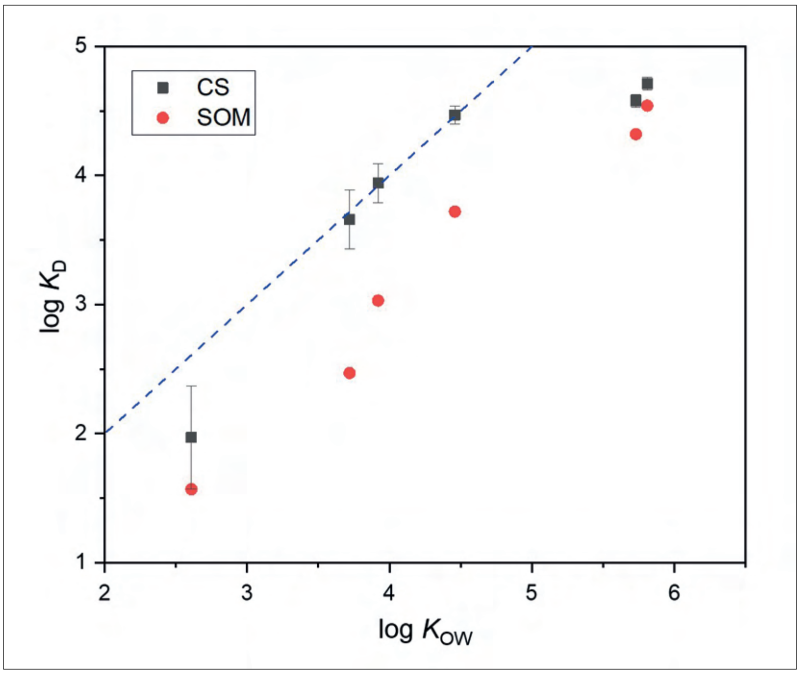

Figure 5 Experimentally determined sorption coefficient of phenanthrene on CS log $K_{\mathrm{D,CS}}$ ($c_{\mathrm{CS}} = 50$ mg L^{-1}, $c_{0,\mathrm{pollutant}} = 10$ µg L^{-1}, $c_{\mathrm{KNO_3}} = 1$ g L^{-1}, pH = 7.2) in comparison with log K_{OW} [1] and the sorption coefficient on soil organic matter log $K_{\mathrm{D,SOM}}$ based on [2]; the dotted line represents log K_{OW} = log K_{D}.

soil organic carbon as obtained from the LSER database (K_{OC} [2]) with the mass fraction of organic carbon in peat as model for soil organic matter (f_{OC} = 0.47 g C/g peat [64]). In Figure 5, it can be seen that the sorption affinities of the investigated substances generally increase with increasing K_{OW} as a measure of their hydrophobicity. This is of course expected as substances with higher hydrophobicities tend to leave the water phase and sorb to carbon-rich surroundings. For LIN, ACE and PHE, $K_{D,CS}$ values mirror the K_{OW} values, meaning that the affinities of these substances for octanol and CS are equal. The affinity of the sorbent phase depends on the ability of sorbate and sorbent to take part in various intermolecular interactions. LFER models thus include several parameters such as polarizability and H-bond basicity/acidity of the sorbate and corresponding parameters for the sorbent phase. It is obvious from the differences in $K_{D,CS}$ and $K_{D,SOM}$ that the sorbent properties of both types of carbonaceous materials are not identical and that hydrochar materials such as the studied CS require the development of an individual LSER parameter set for the prediction of sorption coefficients. This clearly needs to be based on a large set of experimental sorption data which is a task for future research.

When comparing the $K_{D,CS}$ values for the CS with $K_{D,SOM}$ values, it can be seen that the CS provide higher sorption affinities than peat soil for all probed molecules which is most significant for the compounds with moderate hydrophobicity with factors of 15 (LIN) over 8 (ACE) to 5 (PHE) in $K_{D,CS}$ *vs.* $K_{D,SOM}$. This means that the synthesized CS could be used at contaminated sites with soils and sediments having low organic matter fractions (such as sandy aquifers) in order to increase the retention capacity and thus prevent the spreading of hydrophobic pollutants with the groundwater flow.

3.4 Estimation of the retardation factor for phenanthrene as well as the effective lifetime of a hypothetical *in-situ* sorption barrier

The effective lifetime of such an *in-situ* sorption barrier was estimated with a model described by Georgi *et al.* (2015). The retardation factor R_{PHE} was calculated with eq. 3 [6] from the experimentally determined single-point sorption coefficient at pH = 7 $K_{D,PHE,CS}$ = 30 000 L kg^{-1} at $c_{e,PHE}$ = 5 µg L^{-1} as the assumed PHE concentration in the contaminated groundwater influent.

$$R_{PHE} = 1 + \frac{\rho}{\varepsilon} f_{CS} K_{D,PHE,CS} \tag{3}$$

ρ (kg L^{-1}) and ε (unitless) are the bulk density and the porosity of the sediment for which typical values of 1.75 kg L^{-1} and 0.3 were supposed [65]. Assuming a fraction f_{CS} = 0.002 (= 0.2 wt.-%) of CS immobilized on the sediment, an R_{PHE} of 345 was calculated. When the latter is put into relation with the average linear velocity of the groundwater u (m d^{-1}) and a length of the sorption barrier l (m) in the direction of the groundwater flow, the useable lifetime t (d) of the sorption barrier can be calculated according to eq. 4 [6]:

$$t = \frac{l}{u} \cdot R_{PHE} \tag{4}$$

This is a simplified approach which assumes a step-function breakthrough curve, *i.e.* approaching sorption equilibria during the slow passage of groundwater through the sorption barrier, and neglecting dispersion effects. Nevertheless, it provides a first estimate on expected useable operation times of *in-situ* sorption barriers. With an assumed groundwater velocity of 0.5 m d^{-1} and a barrier length of 10 m [6], the estimated lifetime of the *in-situ* sorption barrier with the herein synthesized CS would be 19 years regarding the retention of PHE as a typical 3-ring PAH representative of oil-derived hydrophobic pollutants detected in groundwater. More hydrophobic compounds such as PAHs with 4 and more rings or the tested HCB and TCB can be reasonably predicted to have even longer breakthrough times (see SI, Table S2). For LIN and ACE (log K_{OW} > 3), the predicted retention times in the order of 3–6 years are still noteworthy while the remediation approach is not suitable for less hydrophobic contaminants such as TCE (log K_{OW} < 3).

The measured sorption kinetics (see SI, Figure S13) yields a half-life of about 15 h for approaching sorption equilibrium with PHE under batch conditions in a shaken suspension. This indicates a relatively slow sorption process compared to activated carbon particles of comparable size [66]. The finding is in conformity with the dominating sorption mechanism and the assumed rate-controlling process: bulk phase diffusion in a highly viscous polymer-like phase of the CS particles, in contrast to activated carbon particles where the film or pore diffusion in an aqueous medium are the slowest steps of the adsorption process. Nevertheless, the sorption process is still sufficiently fast to approach sorption equilibria under *in-situ* conditions, taking into account the long residence times (τ = barrier length / groundwater velocity) of groundwater in a permeable sorption barrier. An assumed groundwater velocity of 0.5 m d^{-1} and a barrier length of 10 m [6] lead to a residence time of 20 d, which would be completely sufficient to approach sorption equilibrium (*cf.* Figure S13).

4 Conclusion

Uniform and dispersible CS with tunable mean particle diameters from 1–1.5 µm were synthesized within a single step *via* HTC of sucrose in the presence of CMC as a cheap, non-toxic and environmentally friendly polyelectrolyte stabilizer. The synthesized uniform CS samples were dispersible into single spheres in water, and suspensions remained stable over several hours. Due to these excellent colloidal properties, CS are suitable for *in-situ* application in aquifers using simple infiltration processes. High sorption coefficients of up to $K_{D,CS} = 10^5$ L kg^{-1} were found for phenanthrene (at low concentrations of about 10 µg L^{-1}) combined with high sorption capacities of CS, > 1 wt.-%. This indicates absorption as the dominating sorption mechanism for hydrophobic pollutants. The obtained results are promising for the potential application of the hydrothermally synthesized CS in *in-situ* sorption barriers providing an alternative to finely-ground activated carbon colloids at least for hydrophobic pollutants such as PAHs, with predicted operating lifetimes in the range of several decades. Benefits of the proposed synthesis method are the renewable carbon source, the bottom-up generation of highly uniform microparticles in the desired size range and the anticipated smaller "carbon footprint" due to the absence of a high-temperature ($T \geq 600$ °C) activation/pyrolysis procedure such as typically applied in activated carbon production. This encourages further studies in terms of up-scaling of the process, also including the search for suitable waste carbon sources, *e.g.* from food-grade sugar production. Preliminary experiments suggest that – due to the CMC as stabilizing agent – the herein described process is also applicable to more complex feedstocks with a greater amount of impurities like sugar beet syrup. Further studies should also involve experiments on the mobility of the synthesized CS particles in real aquifer matrices which is an essential requirement for installing *in-situ* sorption barriers. The highly uniform spherical shape and size around 1 µm in combination with the strongly negative zeta potential (-43.5 mV at pH = 6) of the particles provide excellent conditions for high subsurface mobility with low tendency of blocking the passages.

Acknowledgement: The authors acknowledge the financial support from "Deutsche Forschungsgemeinschaft" (DFG), project number 392011053. They also thank Dr. Matthias Schmidt for the SEM analysis which was done at ProVIS – Centre for Chemical Microscopy at the UFZ, Leipzig, which is supported by European Regional Development Funds (EFRE-Europe funds Saxony) and the Helmholtz Association. Furthermore, the authors sincerely thank Birgit Würz for kindly assisting with the zeta potential measurement which was performed at the Department of Environmental Microbiology of the UFZ, Leipzig. Last but not least, he authors are much obliged to Birgit Forkert, Kerstin Lehmann, Dr. Robert Köhler and Silke Woszidlo from the Department of Environmental Engineering (UFZ, Leipzig) for their support by conducting the BET analysis, the elemental analysis of the synthesized particles and additional sorption experiments.

References

[1] S. Kim, J. Chen, T. Cheng, A. Gindulyte, J. He, S. He, Q. Li, B.A. Shoemaker, P.A. Thiessen, B. Yu, L. Zaslavsky, J. Zhang, E.E. Bolton, *PubChem in 2021: new data content and improved web interfaces*, Nucleic Acids Res. 49 (2019) D1388–D1395.

[2] N. Ulrich, S. Endo, T.N. Brown, N. Watanabe, G. Bronner, M.H. Abraham, K.-U. Goss, *UFZ-LSER database v 3.2.1*, Leipzig, Germany, Helmholtz-Centre for Environmental Research-UFZ, 2017. (Accessed 09.05.2022 2022).

[3] T. Zhang, G.V. Lowry, N.L. Capiro, J. Chen, W. Chen, Y. Chen, D.D. Dionysiou, D.W. Elliott, S. Ghoshal, T. Hofmann, H. Hsu-Kim, S. Liu, J. Ma, B. Pan, T. Phenrat, X. Qu, X. Quan, V. Saleh, P.J. Vikesland, Q. Wang, P. Westerhoff, M.S. Wong, T. Xia, B. Xing, B. Yan, L. Zhang, D. Zhou, P.J.J. Alvarez, In situ *remediation of subsurface contamination: opportunities and challenges for nanotechnology and advanced materials*, Environ. Sci.: Nano 6 (2019) 1283–1302.

[4] P. Bardos, C. Merly, P. Kvapil, H.-P. Koschitzky, *Status of nanoremediation and its potential for future deployment: risk-benefit and benchmarking appraisals*, Remediation Journal 28 (2018) 43–56.

[5] K. Mackenzie, A. Georgi, *NZVI synthesis and characterization*, in: T. Phenrat, G.V. Lowry (Eds.), *Nanoscale zerovalent iron particles for environmental restoration*, Springer International Publishing AG, Basel, 2019, pp. 45–95.

[6] A. Georgi, A. Schierz, K. Mackenzie, F.-D. Kopinke, *Colloidal activated carbon for* in-situ *groundwater remediation – Transport characteristics and adsorption of organic compounds in water-saturated sediment columns*, Journal of Contaminant Hydrology 179 (2015) 76–88.

[7] M. Sørengard, B.K. D., L. Ahrens, *Stabilization of per- and polyfluoroalkyl substances (PFASs) with colloidal activated carbon (PlumeStop®) as a function of soil clay and organic matter content*, J. Environ. Manage. 249 (2019).

[8] G.R. Carey, R. McGregor, A.L. Pham, B. Sleep, S. Hakimabadi, *Evaluating the longevity of a PFAS* in situ *colloidal activated carbon remedy*, Remediation J. (29) (2019) 17–31.

[9] Intrapore, *Particle-based ground-water remediation*. https://intrapore.com/en/, accessed on 21.05.2022, 2022. https://intrapore.com/en/.

[10] K. Mackenzie, A. Schierz, A. Georgi, F.-D. Kopinke, *Colloidal activated carbon and CARBO-IRON – Novel materials for in-situ groundwater treatment*, Glob. NEST J. 10 (2008) 54–61.

[11] Regenesis, *PlumeStop® Liquid Activated CarbonTM*. https://regenesis.com/en/remediation-products/plumestop-liquid-activated-carbon/, accessed on 21.05.2022, (2022).

[12] M.M. Titirici, M. Antonietti, *Chemistry and materials options of sustainable carbon materials made by hydrothermal carbonization*, Chemical Society Reviews 39 (2010) 103–116.

[13] A. Jain, R. Balasubramanian, M.P. Srinivasan, *Hydrothermal conversion of biomass waste to activated carbon with high porosity: a review*, Chem. Eng. J. 283 (2016) 789–805.

[14] S. Nizamuddin, H.A. Baloch, G.J. Griffin, N.M. Mubarak, A.W. Bhutto, R. Abro, S.A. Mazari, B.S. Ali, *An overview of effect of process parameters on hydrothermal carbonization of biomass*, Renew. Sust. Energ. Rev. 73 (2017) 1289–1299.

[15] J.R. White, K. Tauer, M. Antonietti, M.M. Titirici, *Functional hollow carbon nanospheres by latex templating*, JACS Communications 132 (2010) 17360–17363.

[16] Z.-C. Yang, Y. Zhang, J.-H. Kong, S.-Y. Wong, X. Li, J. Wang, *Hollow carbon nanoparticles of tunable size and wall thickness by hydrothermal treatment of α-Cyclodextrin templated by F127 block copolymers*, Chemistry of Materials 25 (2013) 704–710.

[17] M.-M. Titirici, A. Thomas, M. Antonietti, *Replication and coating of silica templates by hydrothermal carbonization*, Adv. Funct. Mater. 17 (2007) 1010–1018.

[18] S. Kubo, J.R. White, K. Tauer, M.M. Titirici, *Flexible coral-like carbon nanoarchitectures* via *a dual block copolymer-latex templating approach*, Chemistry of Materials 25 (2013) 4781–4790.

[19] J. Su, C. Fang, M. Yang, Y. Cheng, Z. Wang, Z. Huang, C. You, *A controllable soft-templating approach to synthesize mesoporous carbon microspheres derived from D-xylose* via *hydrothermal method*, Journals of Materials Science & Technology 38 (2020) 183–188.

[20] X. Sun, Y. Li, *Colloidal carbon spheres and their core/shell structures with noble-metal nanoparticles*, Angew. Chem. 116 (2004) 607–611.

[21] C. Liu, Y. He, L. Wei, Y. Zhang, Y. Zhao, J. Hong, S. Chen, L. Wang, J. Li, *Hydrothermal carbon-coated TiO_2 as support for co-based catalyst in Fischer-Tropsch synthesis*, ACS Catalysis 8 (2018) 1591–1600.

[22] J. Yang, J.-Y. Li, J.-Q. Qian, H.-Z. Lian, H.-Y. Chen, *Solid phase extraction of magnetic carbon doped Fe_3O_4 nanoparticles*, Journal of Chromatography A 1325 (2014) 8–15.

[23] M. Sevilla, A.B. Fuertes, *Chemical and structural properties of carbonaceous products obtained by hydrothermal carbonization of saccharides*, Chem. Eur. J. 15(16) (2009) 4195–4203.

[24] Y. Gong, L. Xie, H. Li, Y. Wang, *Sustainable and scalable production of monodisperse and highly uniform colloidal carbonaceous spheres using sodium polyacrylate as the dispersant*, Chemical Communications 50 (2014) 12633–12636.

[25] B. Hu, K. Wang, L. Wu, S.-H. Yu, M. Antonietti, M.-M. Titirici, *Engineering carbon materials from the hyrothermal carbonization process of biomass*, Adv. Mater. 22 (2010) 813–828.

[26] R. Li, A. Shahbazi, *A review of hydrothermal carbonization of carbohydrates for carbon spheres preparation*, Trends in Renewable Energy 1 (2015) 43–56.

[27] V.K. LaMer, *Nucleation in phase transitions*, Ind. Eng. Chem. 44 (1952) 1270–1277.

[28] D. Jung, M. Zimmermann, A. Kruse, *Hydrothermal carbonization of fructose: growth mechanism and kinetic model*, ACS Sustainable Chemistry & Engineering 6 (2018) 13877–13887.

[29] E. Dinjus, A. Kruse, N. Tröger, *Hydrothermale Karbonisierung: 1. Einfluss des Lignins in Lignocellulosen*, CIT 83 (2011) 1734.

[30] M. Zheng, Y. Liu, Y. Xiao, Y. Zhu, Q. Guan, D. Yuan, J. Zhang, *An easy catalyst-free hydrothermal method to prepare monodisperse carbon microspheres on a large scale*, J. Phys. Chem. C 113 (2009) 8455–8459.

[31] H. Yang, G. Wang, N. Ding, C. Yin, Y. Chen, *Size-controllable synthesis of carbon spheres with assistance of metal ions*, Synthetic Metals 214 (2016) 1–4.

[32] M. Liang, J. Wang, M. Zhao, J. Cai, M. Zhang, N. Deng, B. Wang, B. Li, K. Zhang, *Borax-assisted hydrothermal carbonization to fabricate monodisperse carbon spheres with high thermostability*, Materials Research Express 6 (2019).

[33] P. Liu, W. Cai, J. Wei, Z. Cai, M. Zhu, B. Han, Z. Yang, J. Chen, M. Jaroniec, *Ultrafast preparation of saccharide-derived carbon microspheres with excellent dispersibility* via *ammonium persulfate-assisted hydrothermal carbonization*, J. Mater. Chem. A 7 (2019) 18840–18845.

[34] A. Philippe, G.E. Schaumann, *Interactions of dissolved organic matter with natural and engineered inorganic colloids – a review*, Environ. Sci. Technol. 48 (2014) 8946–8962.

[35] C. Falco, N. Baccile, M.M. Titirici, *Morphological and structural differences between glucose, cellulose and lignocellulosic biomass derived hydrothermal carbons*, Green Chemistry 13 (2011) 3273–3281.

[36] H. Cai, X. Lin, L. Tian, X. Luo, *One-step hydrothermal synthesis of carbonaceous spheres from glucose with an aluminum chloride catalyst and its adsorption characteristic for uranium (VI)*, Industrial & Engineering Chemistry Research 55 (2016) 9648–9656.

[37] Z.Z. Chowdhury, B. Krishnan, S. Sagadevan, R.F. Rafique, N.A.B. Hamizi, Y.A. Wahab, A.A. Khan, R.B. Johan, Y. Al-douri, S.N. Kazi, S.T. Shah, *Effect of temperature on the physical, electro-chemical and adsorption properties of carbon micro-spheres using hydrothermal carbonization process*, Nanomaterials 8 (2018) 597–616.

[38] Y. Liu, S. Ma, J. Chen, *A novel pyro-hydrochar via sequential carbonization of biomass waste: preparation, characterization and adsorption capacity*, Journal of Cleaner Production 176 (2018) 187–195.

[39] X. Zhao, W. Li, S.-X. Liu, *Coupled soft-template/hydrothermal process synthesis of mesoporous carbon spheres from liquefied larch sawdust*, Materials Letters 107 (2013) 5–8.

[40] S. Li, F. Liang, J. Wang, H. Zhang, S. Zhang, *Preparation of mono-dispersed carbonaceous spheres via a hydrothermal process*, Advanced Powder Technology 28 (2017) 2648–2657.

[41] L. Macron, J. Oliveras, V.F. Puntes, In situ *nanoremediation of soils and groundwaters from the nanoparticle's standpoint: A review*, Sci. Total Environm. 791 (2021) 148324.

[42] C. Bianco, J.E.P. Higuita, T. Tosco, A. Tiraferri, R. Sethi, *Controlled deposition of particles in porous media for effective aquifer nanoremediation*, Sci. Rep. 7 (2017) 12992.

[43] N. Tufenkji, M. Elimelech, *Correlation equation for predicting single-collector efficiency in physicochemical filtration in saturated porous media*, Environ. Sci. Technol. 38 (2004) 529–536.

[44] S. Comba, J. Braun, *A new physical model based on cascading column experiments to reproduce the radial flow and transport of micro-iron particles*, Journal of Contaminant Hydrology 140-141 (2012) 1–11.

[45] I. Corsi, M. Winther-Nielsen, R. Sethi, R. Punta, D.C. Torre, G. Libralato, G. Lofrano, L. Sabatini, M. Aiello, L. Fiordi, F. Cinuzzi, A. Caneschi, D. Pellegrini, I. Buttino, *Ecofriendly nanotechnologies and nanomaterials for environmental applications: Key issue and consensus recommendations for sustainable and ecosafe nanoremediation*, Ecotoxicol. Environ. Saf. 154 (2018) 237–244.

[46] C. Tang, Z. Pingping, Y. Sun, L. Bai, *Size-tunable synthesis of mono-disperse wastewater-derived carbon spheres with polyacrylamide as a directing agent*, Micro Nano Lett. 10 (2015) 603–606.

[47] M. Sevilla, A.B. Fuertes, *The production of carbon materials by hydrothermal carbonization of cellulose*, Carbon 47 (2009) 2281–2289.

[48] S. Kang, X. Li, J. Fan, J. Chang, *Characterization of hydrochars produced by hydrothermal carbonization of lignin, cellulose, D-xylose, and wood meal*, Industrial & Engineering Chemistry Research 51 (2012) 9023–9031.

[49] Q. Wu, W. Li, S. Liu, C. Jin, *Hydrothermal synthesis of N-doped spherical carbon from carboxymethylcellulose for* CO_2 *capture*, Applied Surface Science 369 (2016) 101–107.

[50] K. Mackenzie, S. Bleyl, F.-D. Kopinke, H. Doose, J. Bruns, *Carbo-Iron as improvement of the nanoiron technology: from laboratory design to the field test*, Sci. Total Environm. 563–564 (2016) 641–648.

[51] L. Bai, B. Mei, Q.-Z. Guo, Z.-G. Shi, Y.-Q. Feng, *Magnetic solid-phase extraction of hydrophobic analytes in environmental samples by a surface hydrophilic carbon-ferromagnetic nanocomposite*, Journal of Chromatography A 1217 (2010) 7331–7336.

[52] Z. Wang, H. Guo, Y. Yu, N. He, *Synthesis and characterization of a novel magnetic carrier with its composition of* Fe_3O_4*/carbon using hydrothermal reaction*, Journal of Magnetism and Magnetic Materials 302 (2006) 397–404.

[53] X.-W. Wei, G.-X. Zhu, C.-J. Xia, Y. Ye, *A solution phase fabrication of magnetic nanoparticles encapsulated in carbon*, Nanotechnology 17 (2006) 4307–4311.

[54] S. Zhang, H. Niu, Z. Hu, Y. Cai, Y. Shi, *Preparation of carbon coated* Fe_3O_4 *nanoparticles and their application for solid-phase extraction of polycyclic aromatic hydrocarbons from environmental water samples*, Journal of Chromatography A 1217 (2010) 4757–4764.

[55] Q. Zhao, S. Wu, P. Zhang, Y. Zhu, *Green polyelectrolyte-functionalization of carbonaceous nanospheres and its application in ion chromatography*, ACS Sustainable Chemistry & Engineering 5 (2017) 112–118.

[56] Y. Sun, D. Pan, X. Wei, D. Xian, P. Wang, J. Hou, Z. Xu, C. Liu, W. Wu, *Insight into the stability and correlated transport of kaolinite colloid: Effect of pH, electrolytes and humic substances*, Environ. Pollut. 266 (2020) Article 115189.

[57] L.J.R. Higgins, A.P. Brown, J.P. Harrington, A.B. Ross, B. Kaulich, B. Mishra, *Evidence for a core-shell structure of hydrothermal carbon*, Carbon 161 (2020) 423–431.

[58] R. Xu, *Particle characterization: light scattering methods*, Springer, Netherlands, 2000.

[59] H.B. Sharma, B.K. Dubey, *Co-hydrothermal carbonization of food waste with yard waste for solid biofuel production: Hydrochar characterization and its pelletization*, Waste Management 118 (2020) 521–533.

[60] G. Trefalt, I. Szilágyi, M. Borkovec, *Schulze-Hardy rule revisited*, Colloid Polym. Sci. 298 (2020) 961–967.

[61] D. Werner, *Comment on "Modelling maximum adsorption capacities of soot and soot-like materials for PAHs and PCBs"*, Environ. Sci. Technol. 39 (2005) 381–382.

[62] S. Kleineidam, C. Schüth, P. Grathwohl, *Solubility-normalized combined adsorption-partitioning sorption isotherms for organic pollutants*, Environ. Sci. Technol. 36 (2002) 4680–4697.

[63] K. Sun, B. Gao, Z. Zhang, G. Zhang, Y. Zhao, B. Xing, *Sorption of atrazine and phenanthrene by organic matter fractions in soil and sediment*, Environ. Pollut. 158 (2010) 3520–3526.

[64] H.C. Tülp, K. Fenner, R.P. Schwarzenbach, K.-U. Goss, *pH-Dependent Sorption of Acidic Organic Chemicals to Soil Organic Matter*, Environ. Sci. Technol. 43 (2009) 9189–9195.

[65] R.P. Schwarzenbach, P.M. Gschwend, D.M. Imboden, *Environmental Organic Chemistry*, John Wiley and Sons Inc., New York, 1993.

[66] P. Grathwohl, *Diffusion in natural porous media: Contaminant transport, sorption/desorption and dissolution kinetics*, Springer, Berlin, 1998.

Supporting Information

Experimental setup for investigating the suspension stability of CS

CS suspensions were generated in de-ionized water or solutions with defined amounts of KNO_3 and $CaCl_2$, respectively *via* ultrasonic treatment for 10 min (for specifications please see section 2.3). 30 mL of the suspensions were left resting for 18 h. Samples were taken by syringe from 2 cm below the water surface at 0 h and at 18 h. The sampling volume amounted to 0.1 mL in order not to affect the height level of the suspension. The samples were diluted for analysis of the total organic carbon (TOC) content.

Total organic carbon (TOC) analysis

The diluted aqueous samples were injected *via* syringe into a two-zone combustion unit consisting of a combustion zone (780 °C) and a catalytic post-oxidation zone containing a Pt/Al_2O_3-catalyst (700 °C). The samples were fully oxidized and the resulting gas stream was dried with a membrane dryer. CO_2 was detected with a nondispersive infrared detector. Potassium hydrogen phthalate was used as calibration standard.

Suspension stabilities of differently synthesized CS

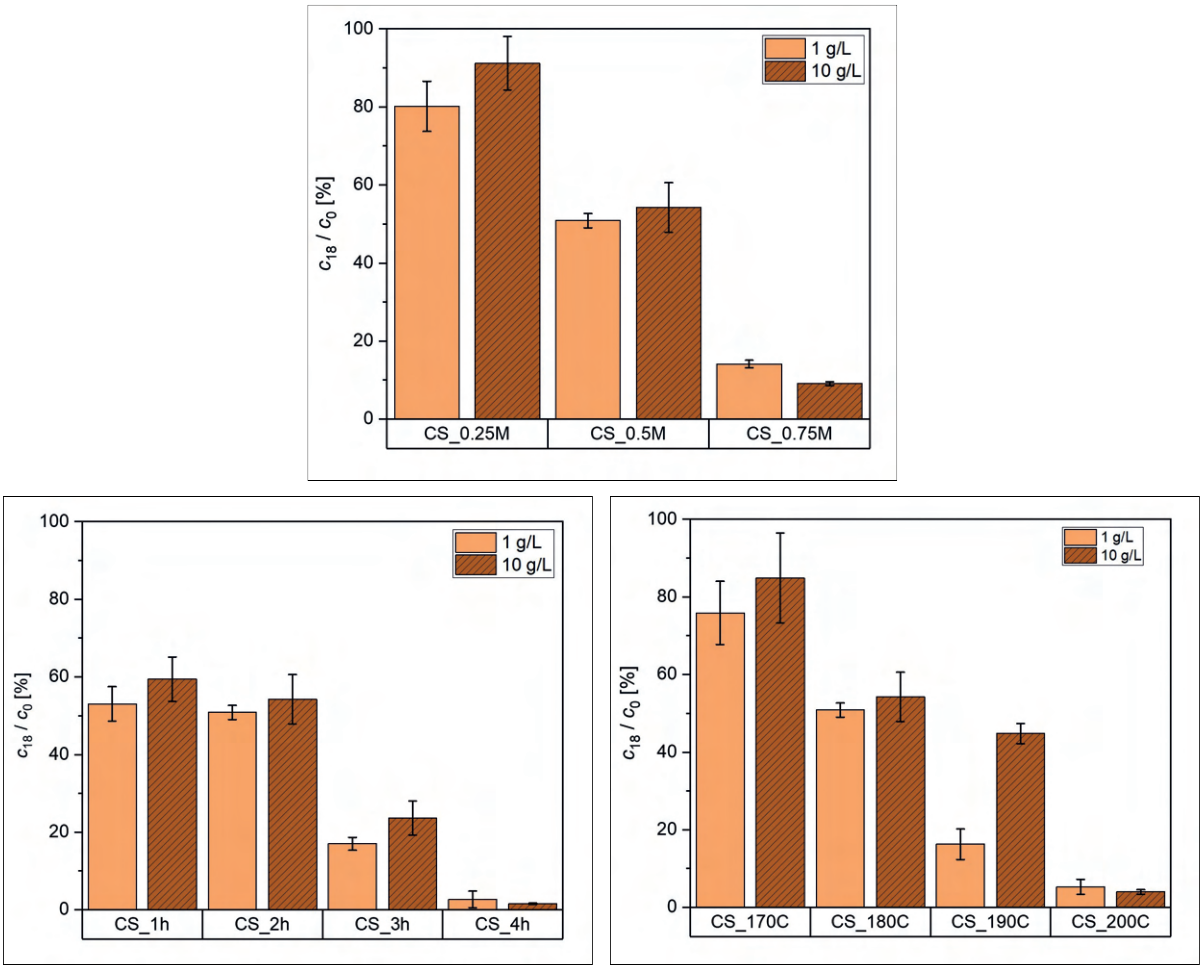

Figure S1 Suspension stability of the various CS suspensions in de-ionized water (determined by measuring the carbon concentration in 2 cm depth below the water surface at 0 and 18 h); The native pH value of the samples was between 3.5 and 4.5; CS were synthesized from 0.25–0.75 M sucrose and 1 wt.-% CMC at 170–200 °C for 1–4 h

Variation of the CMC concentration

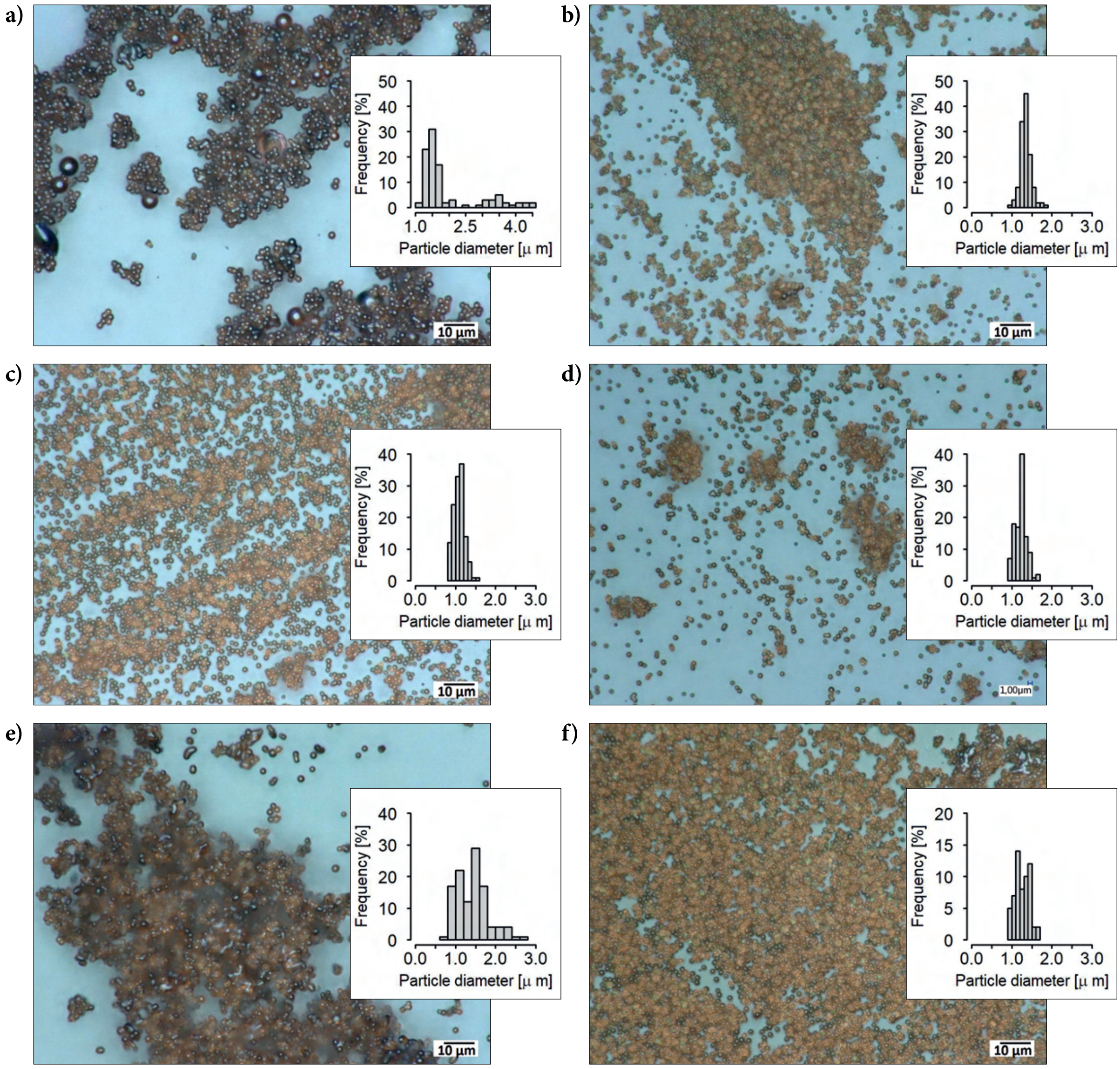

Figure S2 CS prepared from 0.5 M sucrose at 180 °C for 2 h with (a) 0.3 wt.-% CMC (b) 0.5 wt.-% CMC (c) 1 wt.-% CMC (d) 2 wt.-% CMC (e) 3 wt.-% CMC and (f) CS prepared from 0.5 M sucrose at 180 °C for 1 h without CMC.

Variation of the sucrose concentration

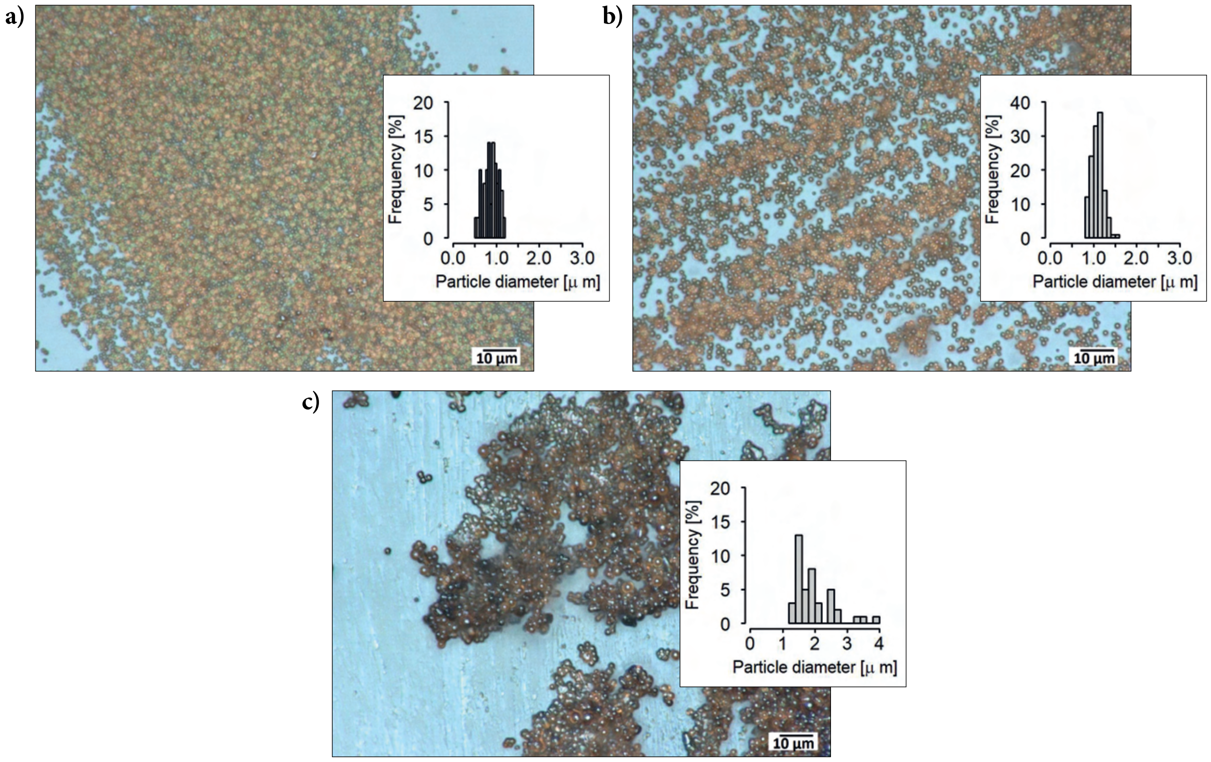

Figure S3 CS prepared from sucrose with 1 wt.-% CMC at 180 °C for 2 h with concentrations of (a) 0.25 M (b) 0.5 M (c) 0.75 M sucrose.

Variation of the reaction time

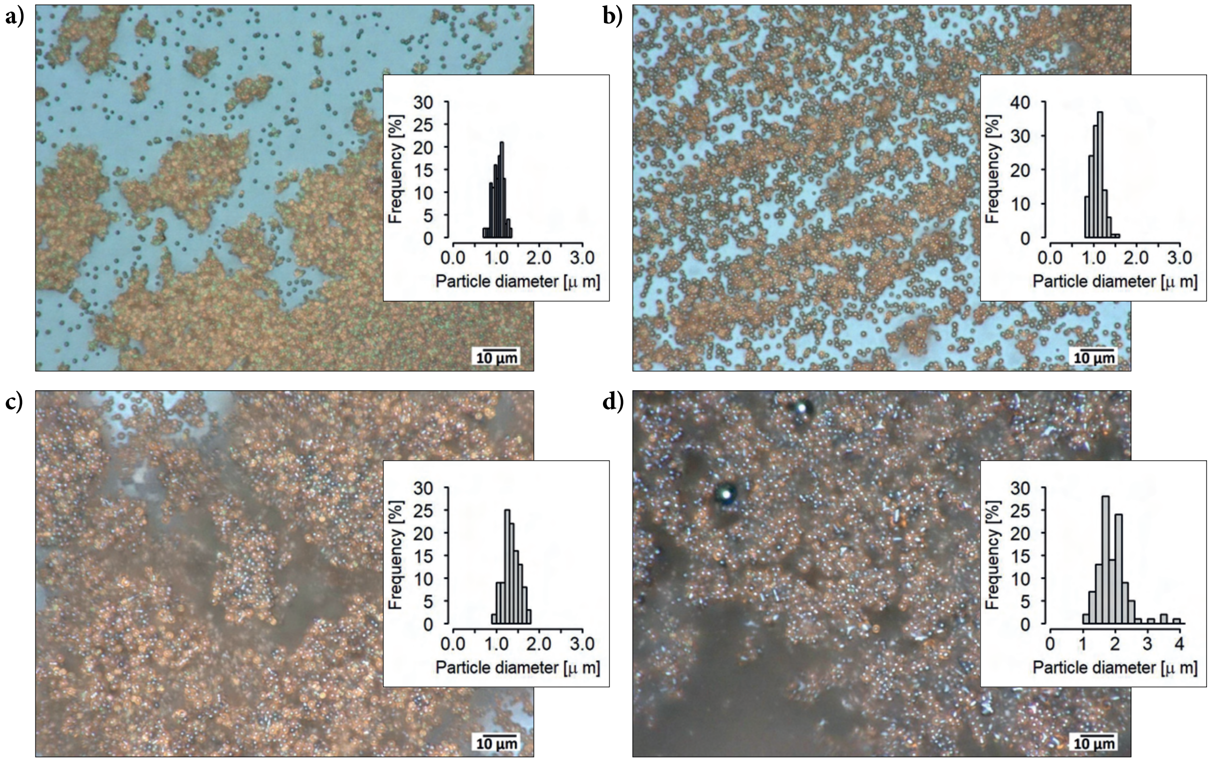

Figure S4 CS prepared from 0.5 M sucrose with 1 wt.-% CMC at 180 °C for (a) 1 (b) 2 h (c) 3 h (d) 4 h.

Variation of the reaction temperature

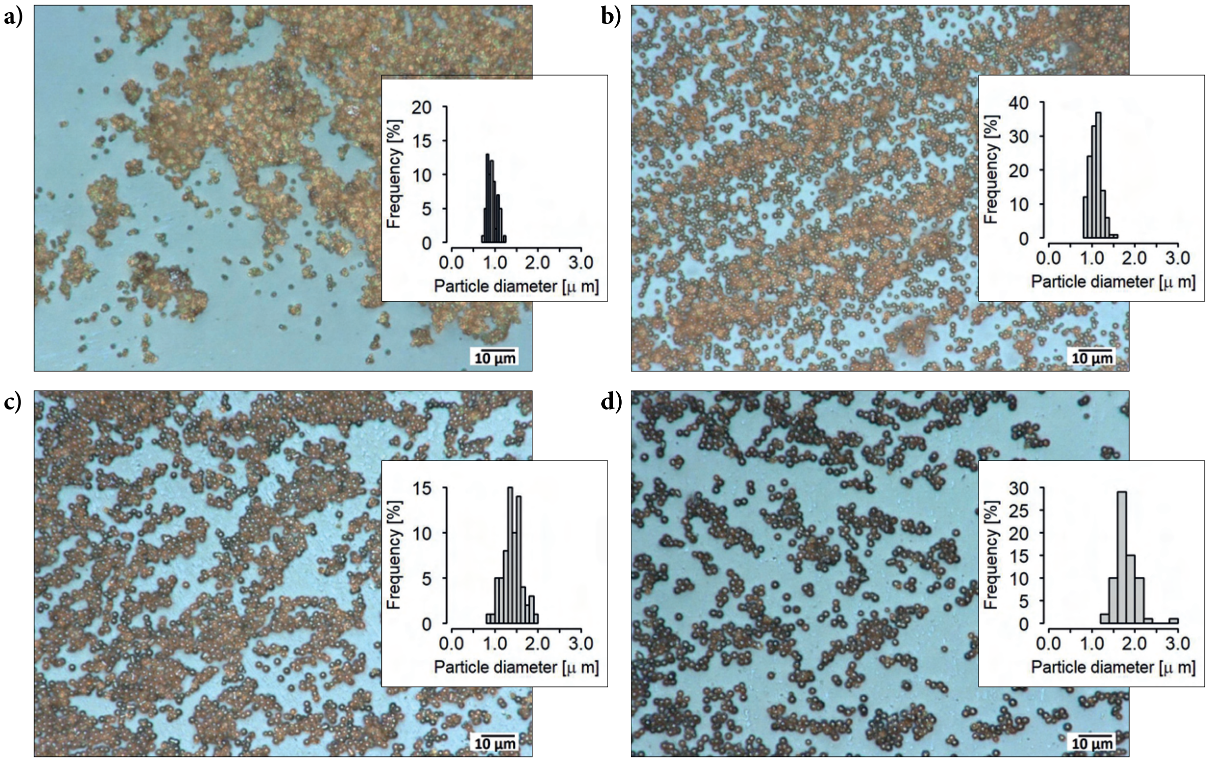

Figure S5 CS prepared from 0.5 M sucrose with 1 wt.-% CMC for 2 h at (a) 170 °C (b) 180 °C (c) 190 °C (d) 200 °C.

Table S1 Content of C, H and O of the CS generated *via* HTC of sucrose under variation of process parameters.

Fixed parameters	Varied Parameter	Sample name	C	H	O
			[wt.-%]		
0.5 M sucrose, 180 °C	1 h	CS_0%1h	62.9	5.1	32.0
	2 h	CS_0%	63.6±0.1	4.8±0.1	31.6
0.5 M sucrose, 180 °C, 2 h	0.3 % CMC	CS_0.3%	65.0±0.1	4.5±0.1	30.5±0.2
	0.5 % CMC	CS_0.5%	62.6±1.2	4.3±0.1	33.1±1.3
	1 % CMC	CS_1%	65.0±0.6	4.3±0.2	30.7±0.8
	2 % CMC	CS_2%	63.3±1.6	4.7±0.1	32.0±1.7
	3 % CMC	CS_3%	64.1±0.1	4.6±0.1	31.3±0.2
1 % CMC, 180 °C, 2 h	0.25 M sucrose	CS_0.25M	62.8±3.2	3.9±0.6	33.3 ±3.8
	0.5 M sucrose	CS_0.5M	65.0±0.6	4.3±0.2	30.7±0.8
	0.75 M sucrose	CS_0.75M	63.7±1.0	4.7±0.1	31.6±1.1
0.5 M sucrose, 1 % CMC, 180 °C	1 h	CS_1h	62.5±1.0	4.8±0.1	32.7±1.1
	2 h	CS_2h	65.0±0.6	4.3±0.2	30.7±0.8
	3 h	CS_3h	62.8±2.4	4.6±0.1	32.6±2.5
	4 h	CS_4h	65.8±0.2	4.3±0.1	29.9±0.3
0.5 M sucrose, 1 % CMC, 2 h	170 °C	CS_170C	62.2±2.9	4.3±0.3	33.5±3.2
	180 °C	CS_180C	65.0±0.6	4.3±0.2	30.7±0.8
	190 °C	CS_190C	63.9±1.8	4.5±0.1	31.6±1.9
	200 °C	CS_200C	65.6±2.0	4.4±0.1	30.0±2.1

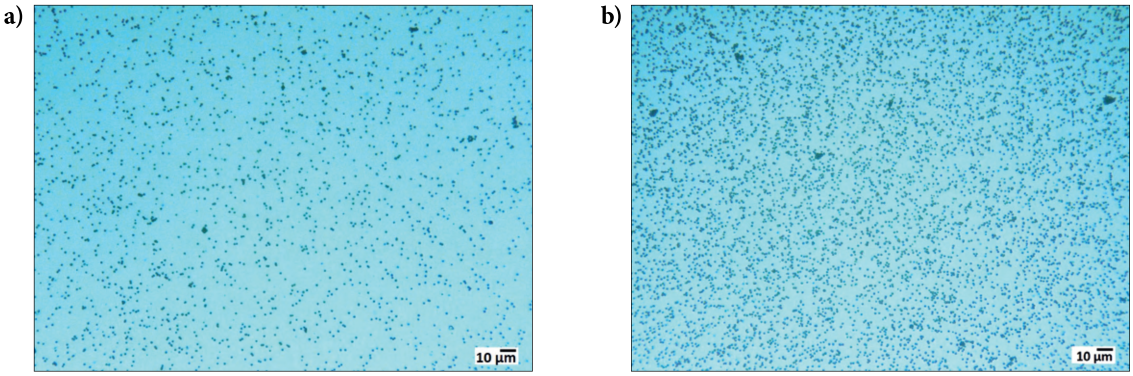

Figure S6 Digital microscopy of CS prepared from 0.5 M sucrose and 1 wt.-% CMC (180 °C, 2 h) and dispersed in de-ionized water in the concentrations of a) 1 g L^{-1} and b) 10 g L^{-1} after 1 month of ageing.

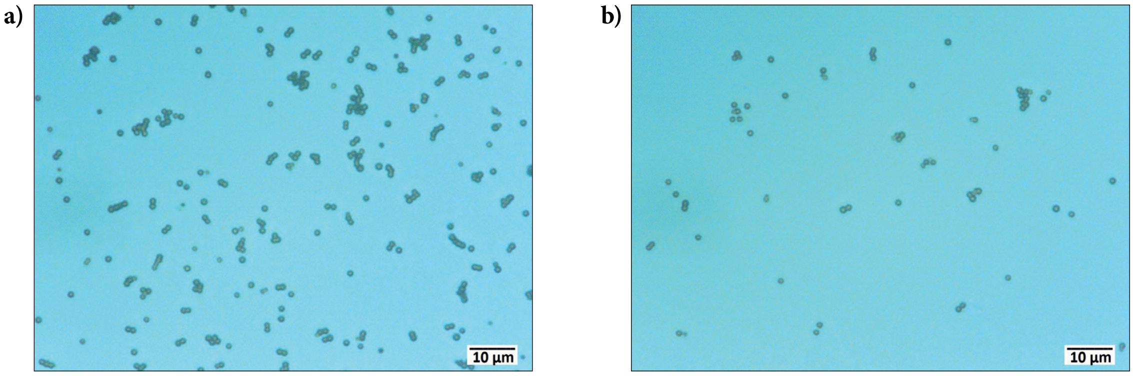

Figure S7 Digital microscopy of 1 g L^{-1} CS prepared from 0.5 M sucrose and 1 wt.-% CMC (180 °C, 2 h) dispersed in a) 89 mM KNO_3 (pH = 3.8) and b) 168 mM KNO_3 (pH = 6.0).

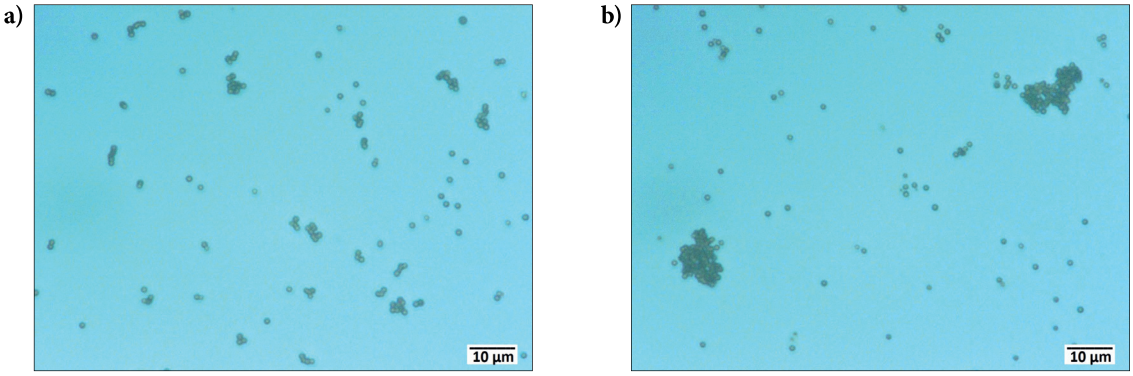

Figure S8 Digital microscopy of CS prepared from 0.5 M sucrose and 1 wt.-% CMC (180 °C, 2 h) dispersed in a) 7 mM $CaCl_2$ (pH = 4.1) and b) 12 mM $CaCl_2$ (pH = 6.6).

Aqueous suspensions of CS synthesized in the presence of various CMC concentrations

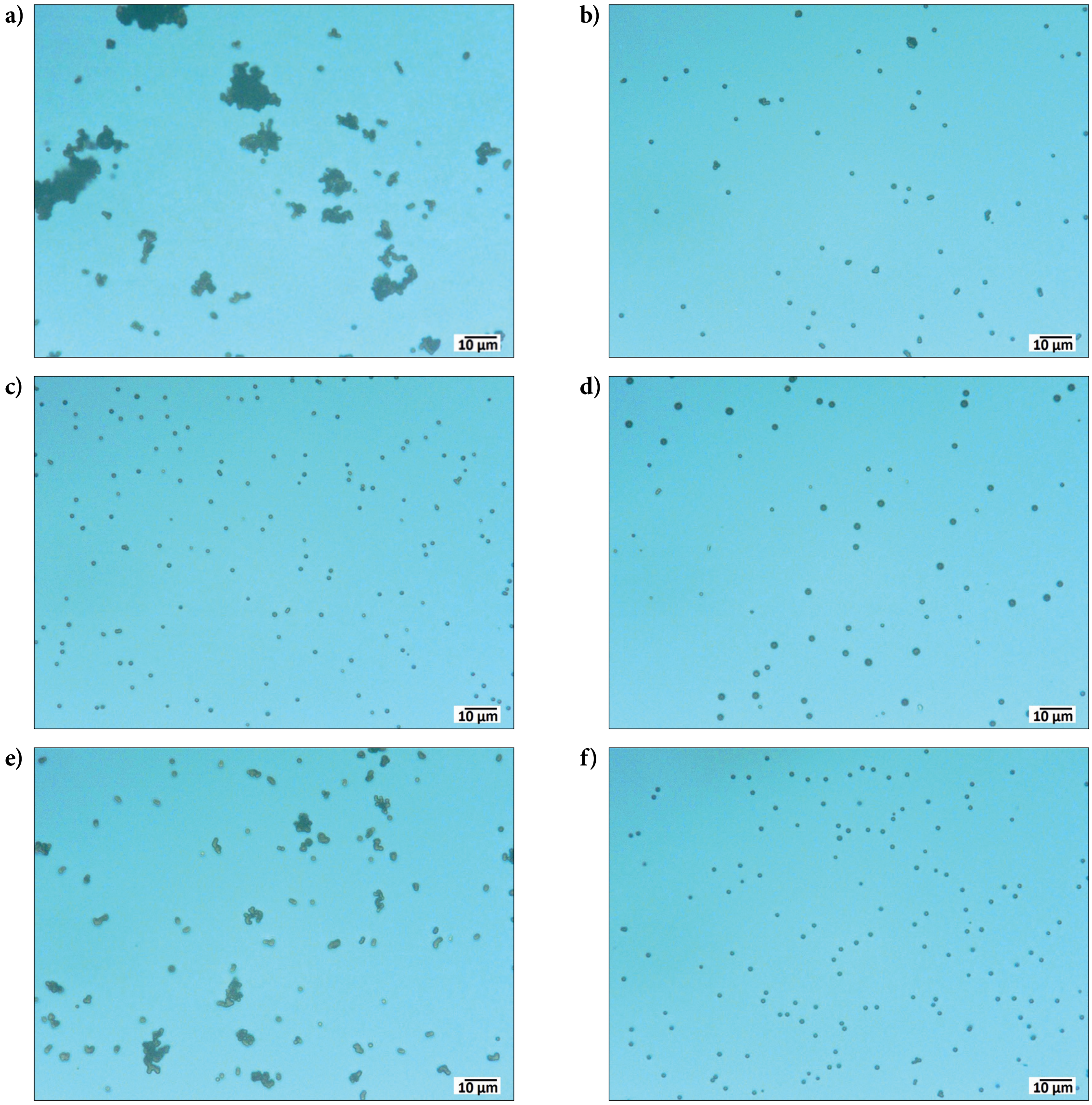

Figure S9 CS prepared from 0.5 M sucrose at 180 °C for 2 h with (a) 0.3 wt.-% CMC (b) 0.5 wt.-% CMC (c) 1 wt.-% CMC (d) 2 wt.-% CMC (e) 3 wt.-% CMC and (f) CS prepared from 0.5 M sucrose at 180 °C for 1 h without CMC; dispersed in de-ionized water at a particle concentration of 1 g L^{-1} *via* 10 min of ultrasonic treatment.

Aqueous suspensions of CS synthesized from various concentrations of sucrose

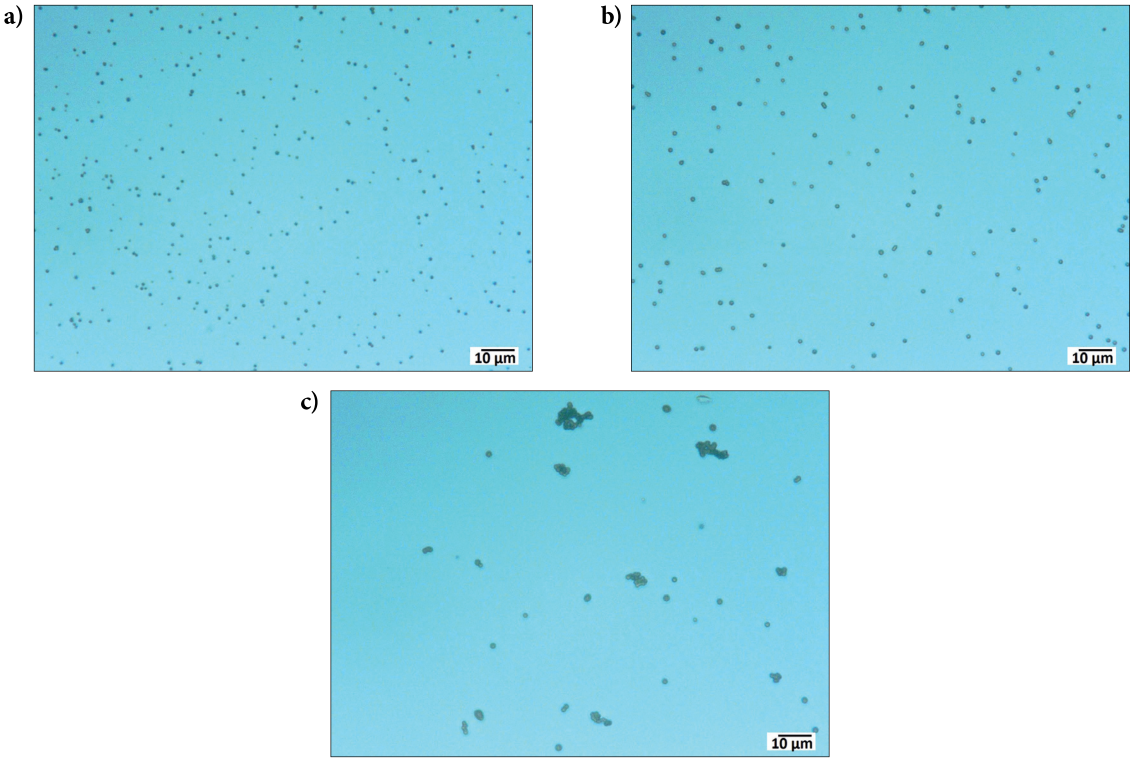

Figure S10 CS prepared from sucrose with 1 wt.-% CMC at 180 °C for 2 h with concentrations of (a) 0.25 M (b) 0.5 M (c) 0.75 M sucrose; dispersed in de-ionized water at a particle concentration of 1 g L^{-1} *via* 10 min of ultrasonic

Aqueous suspensions of CS synthesized at various reaction times

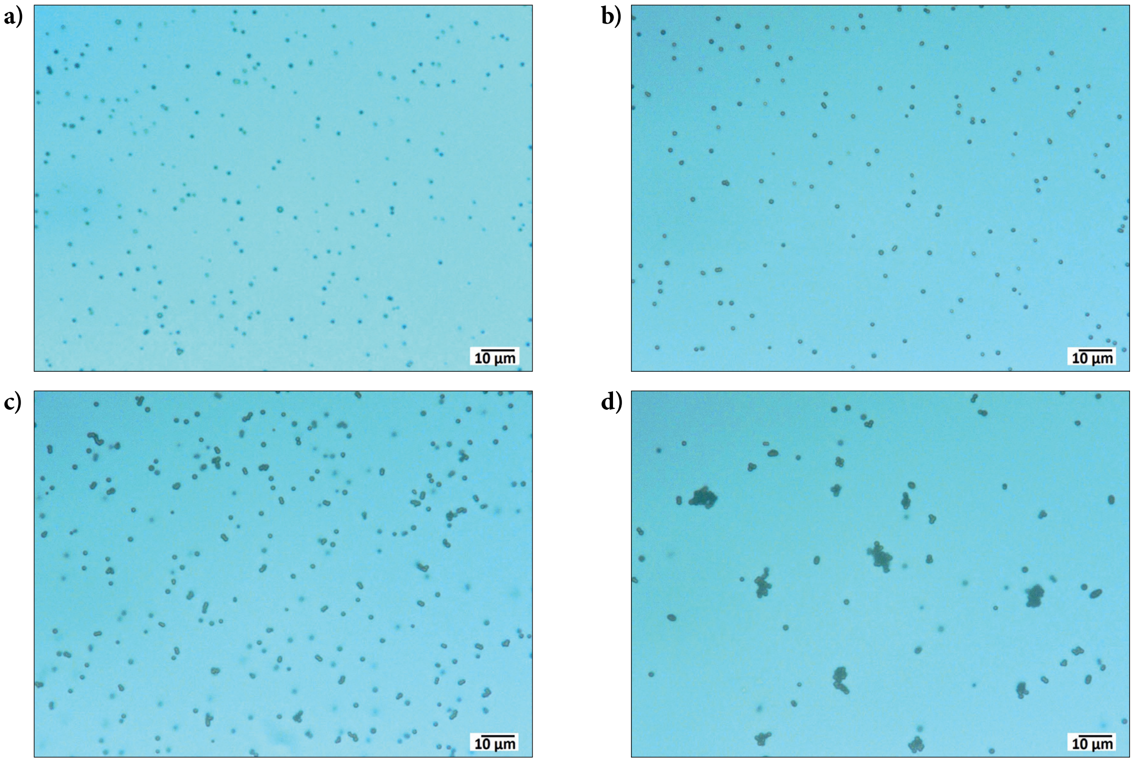

Figure S11 CS prepared from 0.5 M sucrose with 1 wt.-% CMC at 180 °C for (a) 1 (b) 2 h (c) 3 h (d) 4 h; dispersed in de-ionized water at a particle concentration of 1 g L^{-1} *via* 10 min of ultrasonic treatment.

Aqueous suspensions of CS synthesized at various temperatures

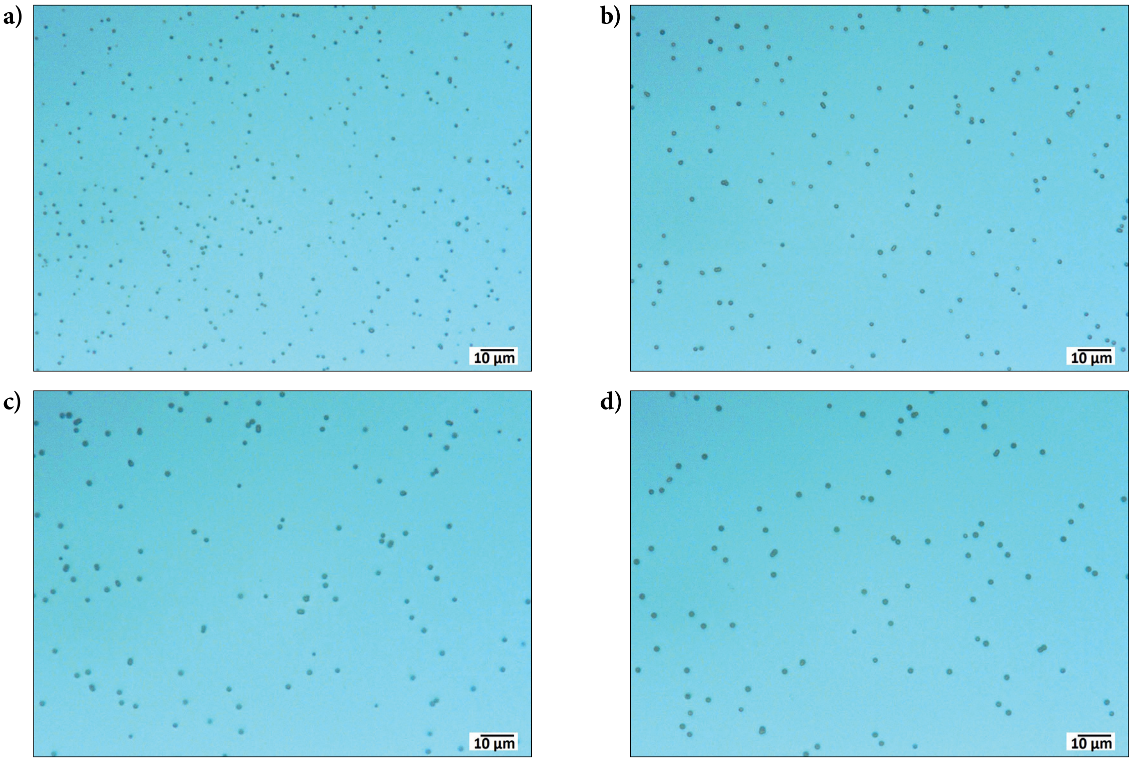

Figure S12 CS prepared from 0.5 M sucrose with 1 wt.-% CMC for 2 h at (a) 170 °C (b) 180 °C (c) 190 °C (d) 200 °C; dispersed in de-ionized water at a particle concentration of 1 g L^{-1} *via* 10 min of ultrasonic treatment.

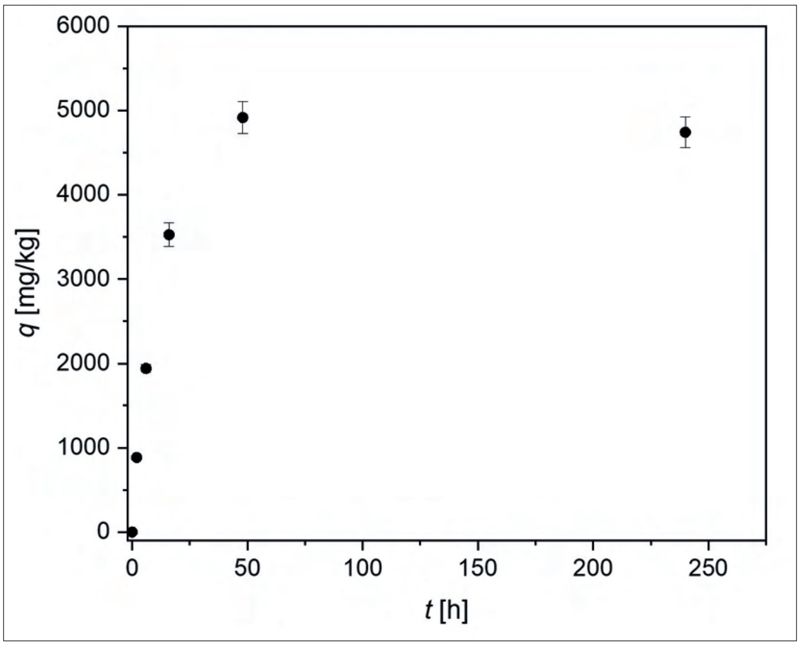

Figure S13 Sorption of PHE onto hydrothermally synthesized CS (0.5 M suc, 1 wt.-% CMC, 180 °C, 2 h) monitored over time in order to determine the time to approach sorption equilibrium; error bars were calculated *via* error propagation from the measurement uncertainty with respect to the aqueous PHE concentration; c_{CS} = 50 mg L^{-1}, $c_{0,PHE}$ = 0.5 mg L^{-1}, c_{KNO_3} = 1 g L^{-1}, pH = 4.8.

Alternative methods for CS dispersion

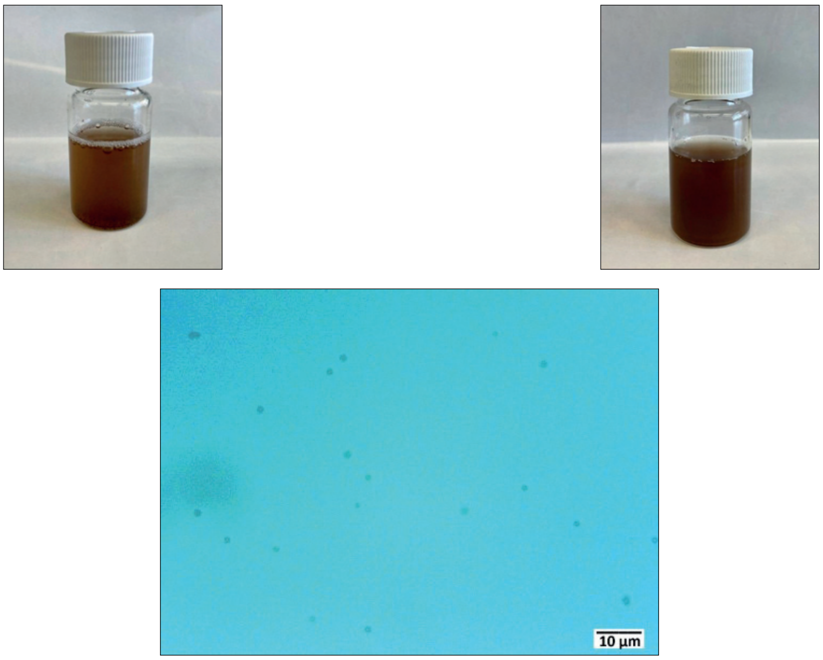

after 2 h shaking at 200 rpm

after 1 min UltraTurrax® at 5000 rpm

Figure S14 CS dispersed in water *via* shaking for several hours at 200 rpm or treatment with UltraTurrax® for 1 min at 5000 rpm and confirmation of single suspended particles *via* digital microscopy.

Table S2 Estimated lifetimes of *in-situ* sorption barriers with the herein synthesized CS regarding different organic pollutants.

Compound	log K_{OW}	$K_{D,CS}$ [L kg^{-1}]	Retardation factor	Time until breakthrough [a]
TCE	2.6	90	2	0.1
LIN	3.7	4600	54	3
ACE	3.9	8700	103	6
PHE	4.5	30 000	345	19
HCB	5.7	38 000	445	24
TCB	5.8	51 000	599	33

4.2 Bottom-up synthesis of de-functionalized and dispersible carbon spheres as colloidal adsorbent

Maria Balda[1], Katrin Mackenzie[1], Silke Woszidlo[1], Hans Uhlig[2], Jens Möllmer[2], Frank-Dieter Kopinke[1], Gerrit Schüürmann[3,4], Anett Georgi[1]

[1] Department of Environmental Engineering, Helmholtz Centre for Environmental Research – UFZ,
04318 Leipzig, Germany
[2] Institut für Nichtklassische Chemie e.V. – INC,
04318 Leipzig, Germany
[3] Institute of Organic Chemistry, Technical University Bergakademie Freiberg,
09599 Freiberg, Germany
[4] Department of Ecological Chemistry, Helmholtz Centre for Environmental Research – UFZ,
04318 Leipzig, Germany

Abstract: Recent innovative adsorption technologies for water purification rely on micrometer-sized particles as so-called super-fine powdered activated carbon (AC) for ultrafast adsorption or colloidal AC for *in-situ* remediation by infiltration of adsorbent suspensions into the subsurface. In this study, the bottom-up synthesis of tailored activated carbon spheres (aCS) from sucrose as renewable feedstock is demonstrated. The synthesis is based on a hydrothermal carbonization (HTC) step followed by a targeted thermal activation of the raw material. This preserves its excellent colloid properties, *i.e.* narrow particle size distribution around 1 µm, ideal spherical shape and excellent aqueous dispersibility. We investigated the ageing of the freshly synthesized, highly de-functionalized AC surface in air and different aqueous media under conditions relevant to practice. The stability of oxygen-poor AC products against re-oxidation is crucial for material optimization. A slow but significant ageing due to hydrolysis and oxidation reactions was observed for all carbon samples, leading to an increase of the oxygen contents with storage time. In this study, a tailored aCS product was generated within a single pyrolysis step with 3 vol.-% H_2O in N_2 in order to obtain the desired pore diameters and surface properties. Adsorption characteristics including sorption isotherms and kinetics were investigated with monochlorobenzene and perfluorooctanoic acid as adsorbates.

Keywords: activated carbon spheres; dispersibility; hydrothermal carbonization; adsorption; groundwater remediation

1 Introduction

Activated carbon (AC) in the particle size of about 1 µm has recently gained increasing attention as so-called super-fine powdered activated carbon (SPAC) or colloidal AC. Compared to conventional powdered activated carbon (PAC) in the size range of 10-100 µm, SPAC typically provides very fast adsorption kinetics which is a necessary adsorbent property for efficient wastewater treatment [1, 2]. Furthermore, colloidal activated carbon is already applied at large scale in the field of *in-situ* groundwater remediation [3–5]. In this case, the suspended particles are injected directly into the contaminated aquifer. There, they are deposited on the aquifer sediment and form a permeable sorption barrier in order to retain pollutants and prevent them from further spreading with the groundwater flow. *In-situ* groundwater remediation is often the only way to provide damage control at polluted sites which are difficult to access or where the remediation *via* pump-and-treat of polluted water would be too expensive and time-consuming. One of the major environmental problems we are currently facing are poly- and perfluorinated aliphatic substances (PFAS). Various PFAS congeners are known to have adverse-health effects such as endocrine disruption [6, 7]. Due to their high mobility and simultaneous persistency, these so-called “forever-chemicals” are a serious environmental issue [8]. Regarding PFAS, the remediation with well-adapted colloidal AC is currently the only *in-situ* treatment option applied at technical scale for an efficient damage mitigation [9, 10].

For production of SPAC, commercially available PAC is crushed to a mean particle size close to 1 µm in a wet-milling process with a duration of several hours [2, 11]. In this work, an alternative synthesis strategy for an SPAC-like product was developed and denominated activated carbon spheres (aCS). aCS particles in the desired size-range were generated bottom-up *via* the hydrothermal carbonization (HTC) of sucrose with subsequent activation under pyrolysis conditions.

To obtain the desired product, we had to solve the following research questions:

1. How can the dispersibility of the individual particles be maintained during pyrolysis?
2. How can the pore size distribution and surface chemistry of the aCS be tuned during the pyrolysis step?
3. How does the surface of the synthesized aCS change over time and how can it be stabilized?

As mentioned in a former publication [12], the dispersibility of HTC-generated carbonaceous spheres (CS), especially after pyrolysis, has not yet been closely investigated but was merely mentioned in passing [13, 14]. However, for designing the desired product, its dispersibility is a crucial property and can too easily be erased by choosing unfavorable pyrolysis conditions. Therefore, the impact of the pyrolysis process on the product quality was intensively investigated within this work. A low heating rate was identified as the deciding parameter for maintaining the particle dispersibility. To our knowledge, this has not been described in literature before. Furthermore, for the *in-situ* application, the behavior of the aCS in aqueous suspensions over time is important. The sedimentation and/or agglomeration was monitored in aqueous suspension for the synthesized aCS in comparison with a finely-ground commercial AC sample.

Due to the presence of water and the high energy input during the milling process, the surface of the AC particles is prone to be oxidized. It was found that this decreases the adsorption capacities for non-ionic organic compounds [15]. This is thought to have an even greater impact on more challenging substances such as perfluorooctanoic acid (PFOA) which has a highly hydrophobic chain and an anionic head-group. It was recently shown that also a slight oxidation of the AC surface could have a negative influence on the sorption performance [16]. With the herein developed bottom-up synthesis, aCS properties, *e.g.* pore size distribution and surface functional groups can be tuned by choosing suitable parameters during the pyrolysis/activation step.

Monitoring the aCS in aqueous suspensions eventually led us to our last research questions: (i) how fast does the particle surface age under relevant conditions regarding storage and application, and (ii) what are possible underlying mechanisms? Some mechanisms have been studied regarding AC surfaces, *e.g.* for the role of water vapor in activated carbon ageing at 150 °C [17]. However, to the best of our knowledge, there are no literature studies which investigate the surface oxidation of (pyro-)hydrochar under ambient conditions in water or air. Furthermore, for de-functionalized AC surfaces, additional treatment with hydrogen gas might be necessary in order to maintain very low oxygen contents of the surface [18]. As an additional high-temperature treatment with hydrogen is energy-consuming and safety-relevant, we developed a pyrolysis procedure where the desired porosity as well as de-functionalization and stabilization of the surface were achieved directly within one pyrolysis step. For potential applications in wastewater treatment and *in-situ* aquifer remediation, changes of the adsorbent surface upon storage/application in water are crucial. This applies especially when it comes to more demanding pollutants like PFOA that favors a very hydrophobic carbon sorbent surface. Therefore, we further investigated the ageing of our synthesized aCS in oxygen-containing water and air of different humidity over 30 days. In order to characterize their performance as colloidal adsorbent, the sorption of monochlorobenzene (MCB) as well as PFOA was studied in more detail.

2 Materials and Methods

2.1 Chemicals

Commercially available sugar was used as starting material for the HTC synthesis. PFOA (96 %) and carboxymethyl cellulose (CMC) sodium salt with a molecular weight of 90 kDa, a polymerization degree of 400, a substitution degree of 0.65–0.90 with a sodium content of approximately 8 wt.-% and a purity of 99.5 % was purchased from Sigma-Aldrich. MCB (≥ 99 %), sodium chloride, sodium sulfate, sodium borohydride, sodium hydroxide, hydrochloric acid (37 %) potassium hydroxide and potassium nitrate were all analytical grade and purchased from Merck. Potassium hydrogen phthalate (p.a.) was purchased from Riedel-de Haën.

2.2 Preparation of activated carbon spheres

Activated carbon spheres were prepared from hydrothermal carbonaceous spheres (CS). The synthesis was described in our previous work [12]. In brief, 0.5 M sucrose (171.2 g L^{-1}) dissolved in de-ionized water with 1 wt.-% of CMC (in relation to the initial amount of sucrose) was placed in a stainless steel autoclave with a glass insert and heated in an oven for 2 h at 180 °C. The formed precipitate was separated from the liquid phase through centrifugation, washed once with de-ionized water and then air-dried. CS were pyrolyzed in a horizontal quartz reactor tube with a continuous N_2 gas flow of 200 mL min^{-1} under various conditions. Initially, the heating rate was varied between 100, 10 and 1 K min^{-1}. If not stated otherwise, the latter was used for all pyrolysis experiments in order to ensure an optimal dispersibility of the product. CS pyrolyzed (pCS) under N_2 at 400, 600 and 800 °C for 1 h were named pCS400, pCS600 and pCS800, respectively. The addition of "-H_2O" after the temperature indicates pyrolysis in a 3 vol.-% H_2O/N_2 mixture. For this, the dry nitrogen flow passed a water reservoir in order to allow water uptake into the gas flow at room temperature (23 ± 2) °C before it entered the pyrolysis reactor. If the pyrolysis time deviated from 1 h, this was indicated at the end of the respective sample names ("pCS800-H_2O-2h" and "pCS800-H_2O-4h"). CS treated under H_2O/N_2 at 800 °C for 4 h were called aCS.

2.3 Ageing of activated carbon spheres

The ageing of aCS was conducted under various conditions: in laboratory air atmosphere, in a desiccator with silica gel as drying agent and suspended in different aqueous media (de-ionized water and salt solutions containing 10 mM KNO_3, NaCl, Na_2SO_4 or $NaBH_4$, respectively). The surface oxygen content of the aCS was analyzed *via* TPD directly after the preparation and after storage for various time periods. The ageing in air/water of aCS was compared with two differently prepared samples: pCS800 (pyrolyzed at 800 °C in N_2) and aCS-H_2 for which aCS were post-treated at 900 °C in 10 vol.-% H_2/N_2.

For the ageing in air, 50 mg of the samples were stored in open beakers under laboratory atmosphere or in the desiccator (not evacuated), respectively. The ageing in water was conducted with sample amounts of 15 mg in closed vials with 25 mL oxygen-containing de-ionized water and 5 mL air in the headspace. They were continuously shaken on a horizontal shaker with 180 rpm during the defined ageing time. For experiments in oxygen-free water, the water-containing vials were flushed with N_2 for 20 min prior to the addition of aCS and 10 min afterwards, before closing the vials airtight and shaking them likewise. After defined periods of ageing time, the aCS samples were transferred to a tubular furnace and dried at 100 °C in an N_2-flow.

2.4 Adsorption experiments

The synthesized aCS were prepared for sorption experiments by shaking 100–200 mg L^{-1} of aCS in a salt solution (10 mM KNO_3 or 10 mM NaCl) at (23 ± 2) °C for at least 24 h at 180 rpm. After that, the pH of the mixture was checked and, if necessary, adjusted to 6.5 with 0.1 M NaOH or HCl. aCS were then fully dispersed by ultrasonication for 10 min and spiked with the according amount of stock solutions of the pollutants (MCB in acetone, PFOA in 10 mM aqueous NaCl). After 1 min of vigorous shaking by hand, the spiked suspensions were continuously shaken on a horizontal shaker with 180 rpm. MCB was monitored using gas chromatography coupled with mass spectrometry (GC-MS) through manual sampling of the batch headspace with a gas-tight syringe. For PFOA analysis, aliquots of the aqueous suspensions were taken, filtered through 0.45 µm cellulose acetate filters and afterwards diluted with methanol and subsequently analyzed *via* liquid chromatography coupled with mass spectrometry (LC-MS, see below). For kinetic experiments, headspace or aqueous samples were taken after defined periods of time and analyzed accordingly.

The thermodynamic data of MCB adsorption were evaluated according to the Langmuir model with the software OriginPro 2018G (© 1991–2017 OriginLab Corporation). For fitting the MCB adsorption on the different pCS samples, a linearized form of the Langmuir eq. (1) was used.

$$q_e = q_m - \left[\frac{1}{K_L}\right]\frac{q_e}{c_e} \tag{1}$$

q_m [mg g^{-1}] is the maximum monolayer loading of MCB on the adsorbent, c_e [mg L^{-1}] and q_e [mg g^{-1}] are the equilibrium sorbate concentration and loading, respectively. K_L [L mg^{-1}] is the Langmuir constant which is a measure of the affinity between adsorbent and adsorbate.

For evaluation of the PFOA adsorption, the linearized form of the Freundlich model (eq. (2)) was used.

$$\log q_e = n^{-1} \cdot \log c_e + \log K_F \tag{2}$$

q_e [mg kg^{-1}] and c_e [mg L^{-1}] are the equilibrium loading and dissolved concentration of PFOA. The Freundlich constant K_F [(mg kg^{-1})/(mg L^{-1})$^{1/n}$] is a measure of the adsorption affinity and n^{-1} is the Freundlich exponent which expresses the deviation of the isotherm from a linear correlation.

Single point adsorption coefficients K_D [L kg^{-1}] were determined as ratios q_e/c_e.

The kinetic evaluation of time-resolved adsorption data was performed according to the method described by Yao *et al.* [19].

The film mass transfer coefficient k_f [m s^{-1}] was estimated based on the adsorbent radius R [m], the adsorbent particle density of the air-filled particles ρ_p [g L^{-1}], the initial adsorbate concentration c_0 [mg L^{-1}] and the initial adsorption rate $r_0 = dq_t/dt$ [mg g^{-1} s^{-1}] (eq. (3)). In the present work, the latter was defined as the initial change in the loading q between $t = 0$ and 0.5 min.

$$k_f = \frac{R\rho_p r_0}{3c_0} \tag{3}$$

The surface diffusion coefficient D_s [m^2 s^{-1}] can be obtained *via* eq. (4)

$$D_s = \frac{R/\pi^2}{\frac{1}{k_e}\left[1+\frac{m}{V}\left(\frac{dq}{dc}\right)_e\right] - \frac{R\rho_p}{3k_f}\left(\frac{dq}{dc}\right)_e} \tag{4}$$

where m/V is the dosage of adsorbent [g L^{-1}], $(dq/dc)_e$ [L g^{-1}] is the slope of the adsorption isotherm at the respective equilibrium loading and k_e [s^{-1}] is the late stage first-order adsorption rate coefficient. The estimation of k_e was carried out through the following method:

$$-\ln\left(1-\frac{q_t}{q_e}\right) = b + k_e t \tag{5}$$

After plotting $-\ln(1-q_t/q_e)$ versus t, k_e can be obtained from the slope of the linear regression line. b represents an integration constant. Eq. (5) is only used in the late adsorption stage close to the equilibrium state [19].

2.5 Analytical methods

Optical microscopic images of particles and suspensions were recorded with a VHX digital microscope (Keyence). Random samples of 100-150 particles were measured with the open-source software ImageJ 1.52a in order to determine the particle diameters for the dry CS samples. The measured values were processed with RStudio 1.4 (© 2009–2021 RStudio, PBC) in order to obtain the frequency distribution of particle size.

The scanning electron microscopy (SEM) analyses were conducted with a Zeiss Merlin VP compact microscope. The beam current was 250 pA and the electron landing energy added up to 10 kV.

The C-contents of the dry CS samples were determined either with a TruSpec® CHN macro-analyzer (LECO) or with a C-Mat 5500 (Ströhlein Instruments).

For analysis of the total organic carbon (TOC) concentration in particle suspensions, the diluted aqueous samples were injected *via* syringe into a two-zone combustion unit consisting of a thermal combustion zone (780 °C) and a catalytic post-oxidation zone containing a Pt/Al_2O_3 catalyst (700 °C). The samples were fully oxidized and the resulting gas stream was dried with a membrane dryer. CO_2 was detected with a nondispersive infrared detector. Potassium hydrogen phthalate was used as calibration standard.

The zeta potential as well as the particle size distribution of the samples in aqueous suspension were characterized with a Zetasizer Ultra (Malvern Panalytical). Samples were prepared by dispersing the aCS in 10 mM KNO_3 at a concentration of 5 mg L^{-1} and the pH was adjusted to 6 with 1 M KOH.

TPD was performed under Ar (50 mL min^{-1}) with a BELCAT-B chemisorption analyzer (BEL). The samples were pretreated at 50 °C for 30 min, then heated to 1100 °C with 10 K min^{-1} and held for 30 min. Evolving CO and CO_2 were detected with an Infralyt detector (SAXON Junkalor).

The specific surface area as well as the pore-size distribution were determined from CO_2 ad and desorption isotherms measured at 273 K by using the Software ASiQwin (Version 5.0) and included density functional theory (DFT) model (non-local DFT for CO_2 sorption at 273 K in carbon slit pore, equilibrium model). Prior to the data evaluation, the CO_2 ad- and desorption isotherms at 273 K were measured with the manometric sorption analyzer AUTOSORB-iQ (Quantachrome Instruments, US). For temperature control a cryoTune (3P Instruments GmbH & Co. KG, Germany) was used. Before starting the measurement, about 50–100 mg of the carbon material was transferred to the measuring cell and then pre-treated for 10 h at 423 K and a final vacuum of $< 10^{-2}$ Pa. Subsequently, the sample was weighed again, the activated sample amount was determined and the measurement started. The measurement began with the determination of the void volume with He (Air Products, Purity 5.2; 99.9992 %) at ambient temperature (298 K). After that, vacuum was applied again for approx. 30 min, the temperature was lowered to 273 K and the actual measurement with CO_2 (Air Products, purity 4.5; 99.995 %) was started. The equilibration times were set to at least 8 min per step. The generated measurement data were automatically converted to a volume-based loading of carbon dioxide per gram of carbon material as a function of the detected absolute pressure at the constant temperature of 273 K. The mean pore diameter represents the pore width at one half of the total pore volume.

Headspace GC-MS samples were injected into a GCMS-QP2010 (Shimadzu) at 180 °C with a column temperature of 140 °C and a He flow of 1 mL min^{-1}. A DB-5ms column (Agilent, 30 m × 0.25 mm × 0.25 μm) was used.

LC-MS measurements were carried out with a LCMS-2020 (Shimadzu) equipped with a Gemini C6-Phenyl column (100 mm × 2 mm, Phenomenex, with a particle size of 3 μm and pore size of 110 Å) at a column temperature of 40 °C. The mobile phase consisted of a mixture of 35 vol.-% solvent A (20 mM ammonium acetate in a 9:1 mixture of de-ionized water and methanol and 65 vol.-% solvent B (20 mM ammonium acetate in a 9:1 mixture of methanol and de-ionized water) and was delivered at a flow rate of 0.25 mL min^{-1}.

3 Results and Discussion

3.1 Maintaining the excellent dispersibility of carbon spheres after the pyrolysis step

When the CS generated *via* HTC were pyrolyzed under nitrogen atmosphere, they were further carbonized and developed a microporous structure (*cf.* Table 1). Upon carbonization, the CS changed their color from brown to black (Figure 1, (**a**) and (**b**)) and appeared to be hardened (Figure 1, bottom). The particles' mean diameters did not change significantly. In order to find the optimal heating scheme to maintain the dispersibility in water of the HTC-derived CS, three different heating rates – 100 K min^{-1}, 10 K min^{-1} and 1 K min^{-1} – were investigated. After the pyrolysis at 600 °C for 1 h under N_2 the different samples were added into water, shaken for at least 24 h and then treated with sonication for 10 min.

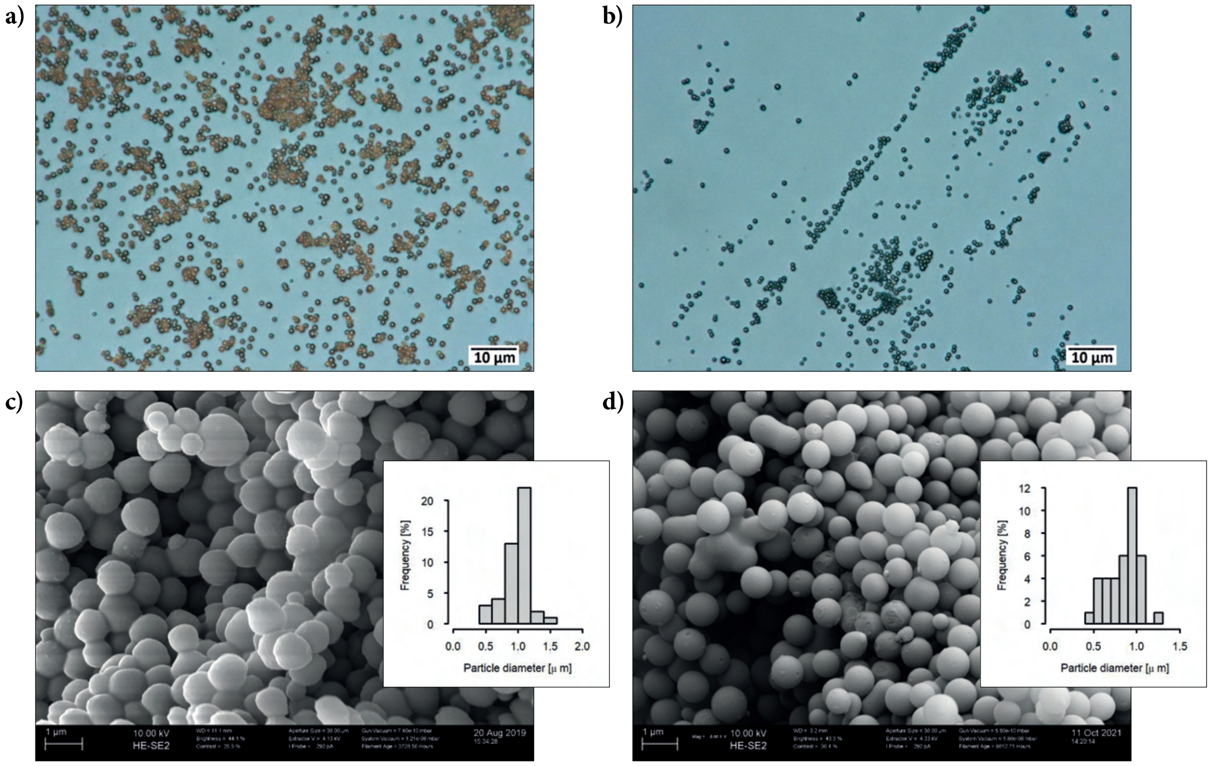

Figure 1 a) Digital microscopy of carbon spheres (CS) and b) activated CS (aCS); c) SEM of CS and d) CS pyrolyzed at 600 °C (N_2) for 1 h; histograms of the particle distribution were obtained through measurement of 100–150 particles (ImageJ) and data evaluation (RStudio).

In Figure 2 a, the drastic differences between the three differently heated samples are shown. The CS samples which were heated with 100 or 10 K min^{-1}, could not be dispersed into individual particles. Instead, the particles remain predominantly as large aggregates on the bottom of the flask (Figure 2 a, vials 1 and 2). In contrast, the sample which was obtained with very slow heating (1 K min^{-1}) was well dispersible, forming a homogeneous and stable black dispersion. That the primary particle size of the CS was preserved in the latter sample was confirmed through microscopic analysis, shown in Figure 2 b. The particle size distribution in aqueous suspension remained monomodal. It was measured by dynamic light scattering (Figure S3) and exhibited a Gaussian distribution with a mean value of (1.02 ± 0.03) µm which is consistent with the d_{90} of 1.04 µm obtained from particle characterization in the dry state.

For understanding the effect of the heating rate on the dispersibility of the CS, the mechanisms behind pyrolysis processes have to be considered. At low temperatures (< 260 °C), mainly dehydration reactions occur which can proceed either in an intra-particulate or inter-particulate way. At higher temperatures (> 400 °C) condensation and aromatization processes are favoured which can lead to further crosslinking [20]. Intra-particulate condensation and aromatization lead to the solidification of the individual lignite-like hydrochar particles whereas the respective inter-particulate reactions may result in aggregation of

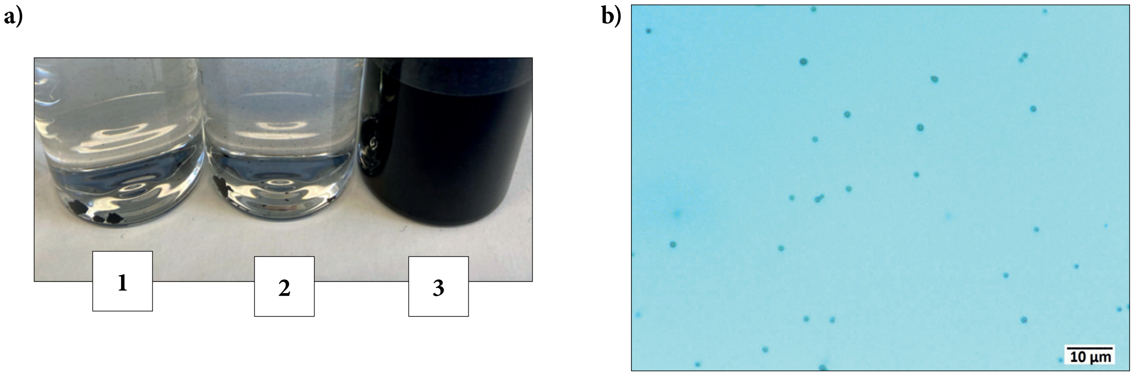

Figure 2 a) CS pyrolyzed at 600 °C for 1 h under N_2 with heating rates of (1) 100, (2) 10 and (3) 1 K min^{-1} respectively (with (1) and (2) showing large non-dispersible aggregates at the bottom); b) digital microscopy of sample (3).

particles. As a result, lower heating rates favour higher degrees of solidification of 'visco-plastic' particles prior to cross-linking reactions between particles at higher temperatures. Solid particles may have less contact areas compared to visco-plastic particles.

3.2 Tuning of surface properties and mean pore diameters during the pyrolysis step

In order to understand the influence of the pyrolysis parameters on the pore structure as well as the surface of the synthesized CS, an extensive set of experiments was performed, where pyrolysis temperature, gas atmosphere and holding time were varied. The resulting CS samples were characterized by temperature-programmed decomposition (TPD) as well as CO_2 ad-/desorption measurements. The samples pyrolyzed under N_2 showed a decrease in oxygen content with increasing pyrolysis temperature from 8.8 wt.-% oxygen (pCS400) over 2.3 wt.-% O (pCS600) to 1.3 wt.-% O (pCS800). This effect is generally known in literature and was recently shown for the pyrolysis of hydrochars derived from cellulose and woody biomass [21]. For these types of hydrochars, the oxygen contents typically decreased from 25–30 wt.-% to 14 wt.-% at pyrolysis temperatures of 400 and 600 °C, respectively.

In order to investigate the type of functional groups more closely, the temperature-resolved TPD profiles are shown in Figure 3. The total content of oxygen functional groups was decreased as thermally labile groups were detached during the pyrolysis at higher temperatures, leaving behind solely the functional groups with higher thermal stabilities. Therefore, the major CO peak shifted to higher temperatures for materials which were pyrolyzed at higher temperatures under N_2 (Figure 3, top left). According to the assignment of T-dependent CO release from O-groups on carbon surfaces presented by Figueiredo *et al.* [22], this means that the major amount of CO-releasing functional groups was shifted from α-substituted carbonyls/aldehydes to aromatic carbonyls/quinones and/or phenols. The major peak in the CO_2 thermogram of pCS400 could be assigned to anhydride groups. It can be observed that after the pyrolysis at temperatures > 600 °C anhydride groups are almost completely annihilated and a small amount of free carboxylic groups remains as the only CO_2-releasing functional groups on the pCS surface, probably due to re-oxidation after pyrolysis.

The de-functionalization effect of the conducted pyrolysis was significantly enhanced when 3 vol.-% H_2O were added to the inert pyrolysis atmosphere. The overall TPD-derived oxygen contents decreased from (2.6 ± 0.2) wt.-% for pCS800 to as low as (0.5 ± 0.2) wt.-% for pCS800-H_2O.

Furthermore, Figure 3 shows that the de-functionalization of the carbon surface was more pronounced at higher temperatures. The CO and CO_2 release decreased from pCS800-H_2O over pCS840-H_2O to pCS880-H_2O. Longer reaction times further reduced the CO_2 release but also led to a slight increase in CO release again, resulting in slightly higher TPD-derived O-contents of (0.9 ± 0.2) wt.-% for pCS800-H_2O-2h and (1.2 ± 0.2) wt.-% for pCS800-H_2O-4h.

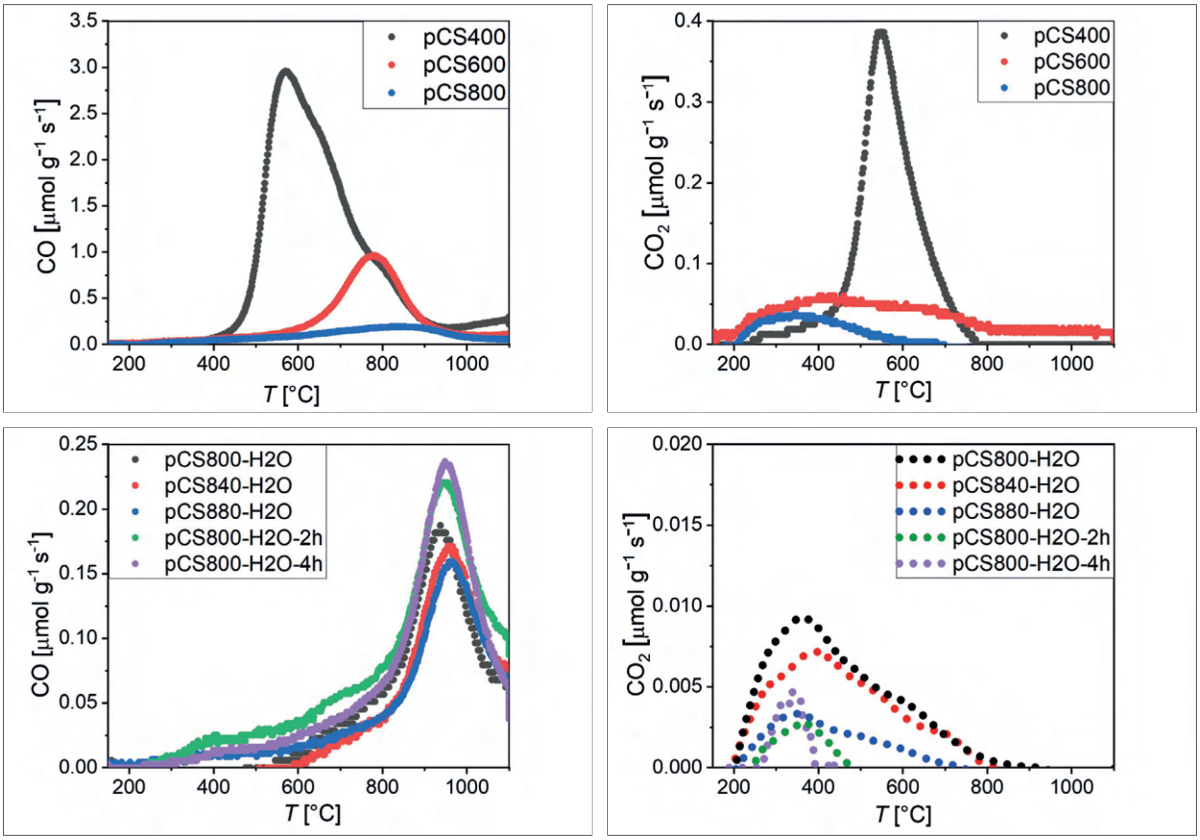

Figure 3 CO and CO_2 release from temperature-programmed decomposition (TPD) up to 1100 °C (10 K min^{-1}) of all pyrolyzed CS samples; CO_2 thermograms of the steam activated samples (bottom right) were smoothed *via* locally weighted scatterplot smoothing (LOWESS) with a smoothing parameter of 0.1.

Table 1 Summary of CS samples pyrolyzed under different conditions along with their specific surface areas derived from CO_2 ad-/desorption (density functional theory (DFT) method) and their C-contents determined by combustion. The error ranges were derived from the relative mean deviation of single values from the mean value of at least two independent experiments.

Treatment conditions (gas atmosphere, final temperature, heating rate and holding time)					
Fixed parameters	**Varied parameter**	**Sample name**	**Surface area by applying DFT method [m² g⁻¹]**	**Mean pore diameter [nm]**	**Carbon content [wt.-%]**
1 K min^{-1}, N_2, 1h	400 °C	pCS400	386 ± 5	0.60 ± 0.01	78 ± 1
	600 °C	pCS600	653 ± 8	0.58 ± 0.01	88 ± 1
	800 °C	pCS800	877 ± 10	0.56 ± 0.01	92 ± 2
1 K min^{-1}, H_2O/ N_2, 1h	800 °C	pCS800-H_2O	954 ± 11	0.58 ± 0.01	96 ± 2
	840 °C	pCS840-H_2O	1178 ± 14	0.63 ± 0.01	98 ± 2
	880 °C	pCS880-H_2O	1386 ± 17	0.68 ± 0.01	96 ± 2
1 K min^{-1}, H_2O/N_2, 800 °C	2 h	pCS800-H_2O-2h	1031 ± 12	0.60 ± 0.01	87 ± 2
	4 h	pCS800-H_2O-4h = aCS	1015 ± 12	0.60 ± 0.01	91 ± 2
1 K min^{-1}, H_2O/N_2, 800 °C, 4h	post-treatment at 900 °C, 2 h, 10 vol.-% H_2/N_2	aCS-H_2	1030 ± 12	0.61 ± 0.01	92 ± 2

The CS pyrolyzed under different conditions all provide a strictly microporous system with pore sizes < 1 nm (see Figure S2). The distinct main pore fraction of all samples exhibits diameters of around 0.5–0.7 nm. Only small differences between all CS samples could be monitored regarding the mean pore diameter. CS pyrolyzed under pure N_2 showed an increase of the C content as well as of the CO_2-sorption-derived surface area with increasing pyrolysis temperature. Overall, the pore volume in the size range of 0.5 to 0.7 nm increased with increasing pyrolysis temperature and in addition a larger contribution of even smaller pores appeared (Figure S2). In contrast, pyrolysis under 3 vol.-% H_2O/N_2 at three different temperatures (800, 840 and 880 °C) led to a significant widening of the mean pore diameter from 0.58 nm over 0.63 nm to 0.68 nm, respectively. It is known from literature that steam can widen the microporosity of carbonaceous materials, as was shown for the activation of carbonized olive stones [23, 24].

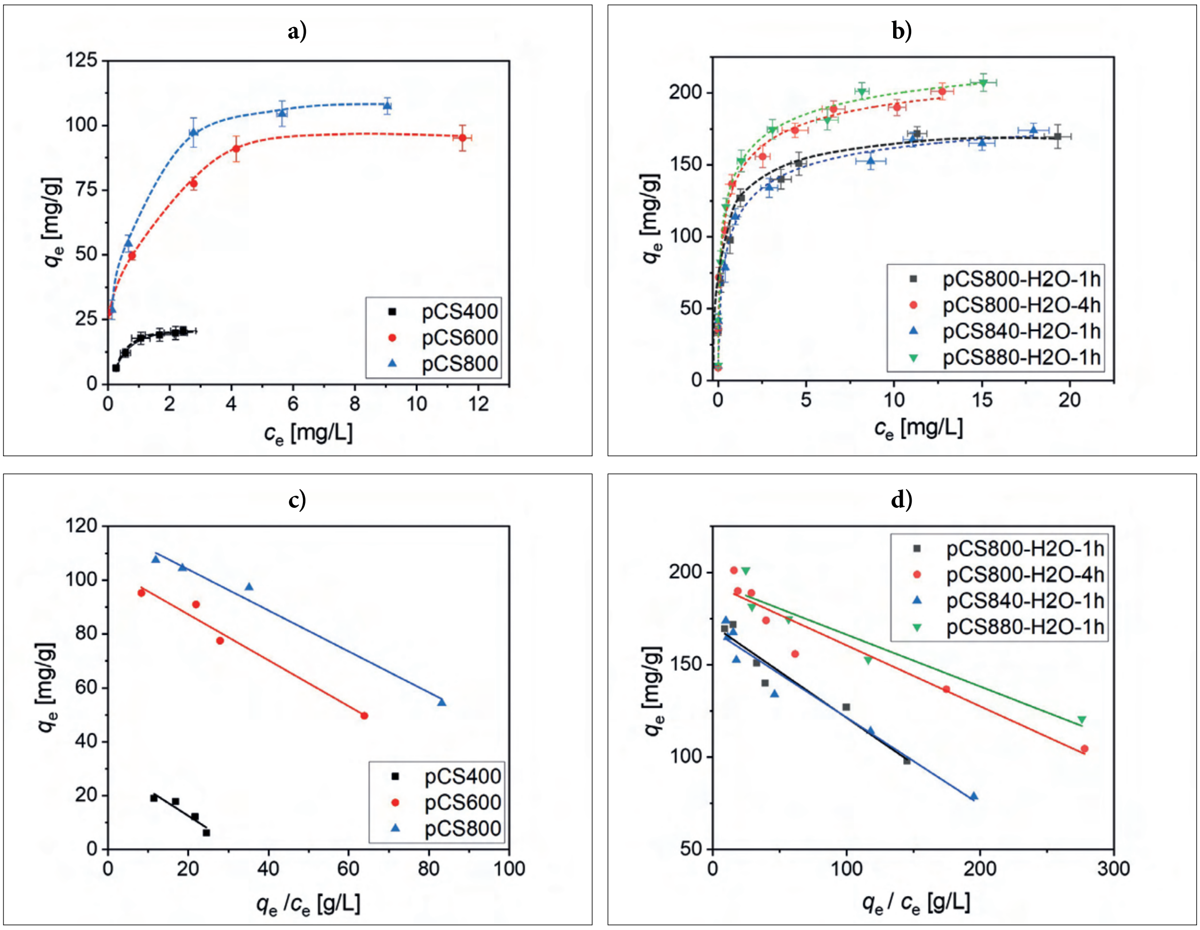

Figure 4 Isotherms of monochlorobenzene (MCB) sorption on hydrochar samples pyrolyzed under N_2 (a, c) or under H_2O/N_2 (b, d). Error bars represent the mean deviation of single values from the mean value based on the experimental and analytical duplicates (*i.e.* n = 4). The dotted lines are a guide for the eye and the solid lines are fitted according the linearized Langmuir model. The results are summarized in Table 2. c_{MCB} = 2.5–30 mg L^{-1}, c_{pCS} = 100 mg L^{-1}, 10 mM KNO_3, pH = 6.5.

It is noteworthy that the steam concentration of 3 vol.-% which was applied in this work is low compared to typical dosages of 70 vol.-% used in literature studies [25]. Nevertheless, it had a significant effect on the resulting carbonaceous material regarding the additionally generated porosity and the widening of pores as well as on the surface de-functionalization as discussed above. A similar effect was found by Mestre *et al.* who generated activated carbon with basic properties from the activation of sucrose-derived hydrochar with 40 vol.-% steam [26]. In contrast to the pyrolysis temperature, the holding time up to 4 h at 800 °C had a less significant impact on the mean pore size.

In the first step, the sorption performance of the differently pyrolyzed samples was characterized by determining the adsorption of MCB as a non-ionic compound and frequently occurring groundwater contaminant (Figure 4). The experimentally obtained adsorption isotherms were evaluated and fitted according to the Langmuir model (eq. (1), Figure 4 bottom). The results are shown in Table 2. The steam-activated samples showed the highest sorption affinities (indicated by the highest K_L values). It is noteworthy that the sample obtained at a moderate pyrolysis temperature of 600 °C (pCS600) exhibits already rather good adsorption properties for MCB which are not improved by further increasing the pyrolysis temperature under N_2 atmosphere. In contrast, activation with steam with 1 h holding time at 800 °C (pCS800-H_2O) significantly improved the adsorption compared to sample pCS800.

Table 2 Fitting parameters for the evaluation of the experimentally obtained sorption isotherms for monochlorobenzene (MCB) according to the linearized Langmuir eq. (1) and compared with the experimentally obtained maximum loading (q_{max} (exp) derived from at least two replicate experimental data points). The error ranges of the experimental values represent the mean deviation of single values from the mean value of at least two independent experiments. The error ranges of the fitted parameters were derived from the standard error of regression *via* propagation of uncertainty.

Sample name	**q_{max} (exp)** **[mg g^{-1}]**	**q_{max} (fit)** **[mg g^{-1}]**	**K_L** **[L mg^{-1}]**	**R_2**
pCS400	20 ± 1	32 ± 5	1.0 ± 0.3	0.81
pCS600	104 ± 3	104 ± 4	1.2 ± 0.2	0.95
pCS800	106 ± 2	119 ± 3	1.3 ± 0.1	0.97
pCS800-H_2O	171 ± 1	171 ± 5	2.0 ± 0.3	0.94
pCS840-H_2O	169 ± 4	168 ± 4	2.1 ± 0.2	0.95
pCS880-H_2O	204 ± 3	194 ± 7	3.6 ± 0.6	0.89
aCS	196 ± 6	193 ± 5	3.0 ± 0.4	0.92

The maximum loading as well as K_L of the synthesized adsorbents could be gradually increased either with activation at higher temperature or prolonging of the holding time. The sample pCS800-H_2O-4h, called “activated carbon spheres” = aCS, was selected for further thorough characterization.

When shifting from the small target molecule MCB to PFOA, the impact of the activation step on the accessibility of the CS pores for adsorption became more obvious. For chain-like molecules like PFOA, the effective cross-sectional molecular diameter at maximum elongation is relevant to evaluate its fit into the CS pores. By means of the calculation tool CROSS[2] [27], a diameter of 0.6 nm was determined for PFOA. This is in good agreement with literature findings [28] and fits well to the experimentally determined mean pore diameter of aCS of 0.6 nm (*cf.* Table 1). Even though there was nearly no change in the pore size distribution apparent between the two particle types activated with 1 and 4 h holding time, *i.e.* pCS800-H_2O and aCS (Figure S2), and although a slight tendency towards a larger mean pore diameter was observed, the longer activation time for aCS drastically improved PFOA adsorption as shown in Figure 5. The single-point adsorption coefficient was increased by four orders of magnitude from log ($K_{D,PFOA}$/(L kg^{-1})) = 2.6 to 6.6.

Therefore, it is assumed that on pCS800-H_2O, PFOA can merely adsorb at the outer surface of the spherical particles while on aCS, PFOA molecules are able to enter the microporous system. This assumption was supported by calculating the theoretically possible surface coverage of the particulate adsorbents with PFOA molecules (see SI). In order to elucidate the strong effect of the close tailoring of the pore diameter on the adsorption of a target compound, the adsorption of PFOA was investigated in more detail regarding kinetics as well as thermodynamics (Figure 6). Most of the PFOA is adsorbed within a few hours. This can be expected for porous adsorbents in the microscale. Regarding the *in-situ* application of aCS particles as

---

[2] G. Schüürmann. 1988. Program for the approximate calculation of the effective largest, effective second largest (= effective) and effective smallest diameters of three-dimensional Cartesian coordinate representations of molecules. The effective largest diameter D_{max} is defined such that the respective perpendicular diameter is minimal, the latter being the effective second largest or simply effective diameter D_{eff}; the effective third largest diameter D_{min}, is the diameter perpendicular to both D_{max} and D_{eff}.

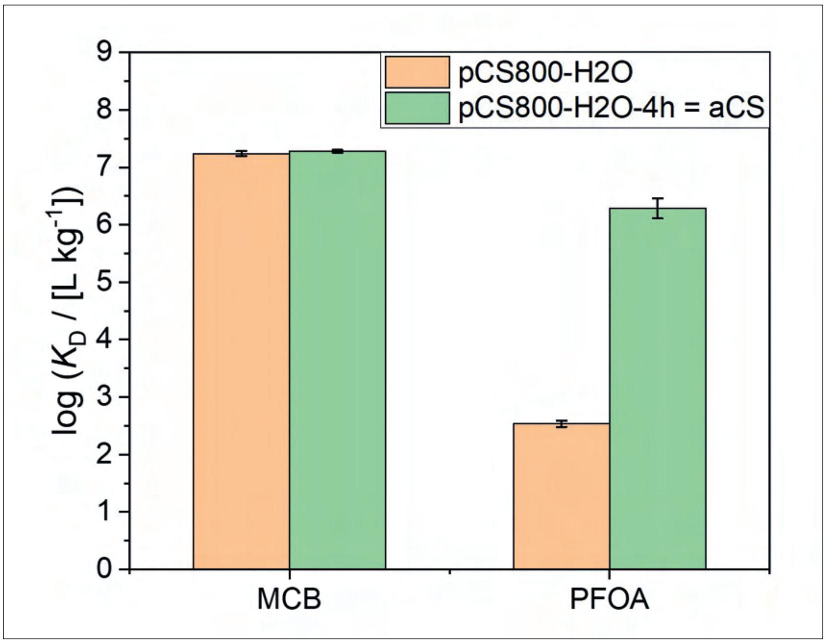

Figure 5 Single point adsorption coefficients log K_D on pCS800-H_2O *vs.* aCS for MCB ($c_{0,\mathrm{MCB}}$ = 2.5 mg L^{-1}; $c_{e,\mathrm{MCB}}$ = 2 µg L^{-1}; c_{aCS} = 70 mg L^{-1}; 10 mM KNO_3; 6 < pH < 7) and PFOA ($c_{0,\mathrm{PFOA}}$ = 0.5 mg L^{-1}; $c_{e,\mathrm{PFOA}}$ = 2 µg L^{-1}; c_{aCS} = 200 mg L^{-1}; 10 mM NaCl; pH = 6.5). Error bars represent the mean deviation of single values from the mean value of at least two independent experiments.

adsorbents in groundwater, the PFOA adsorption kinetics can be considered sufficiently fast due to typically low groundwater velocities of below 1 m d^{-1} [11]. The adsorption isotherm of PFOA on the microporous aCS was fitted according to the linearized Freundlich model (eq. (2)) with $R^2 = 0.995$. The obtained adsorption parameters log (K_F/[(mg kg^{-1})/(mg L^{-1})$^{1/n}$]) = 4.43 and $n^{-1} = 0.46$ are comparable with literature data for PFOA adsorption on AC. For example, Wang *et al.* (2015) determined log K_F = 4.48 and $n^{-1} = 0.43$ for the PFOA adsorption on microporous AC fibers with a mean pore diameter of 0.56 nm and a BET surface area of 1226 m^2 g^{-1}. The obtained low n^{-1} values reflect strongly non-linear sorption isotherms, *i.e.* a spectrum of high-affinity sorption sites. The maximum adsorption capacity of aCS was not yet reached at an equilibrium PFOA concentration of $c_{e,\mathrm{PFOA}}$ = 7.1 mg L^{-1} and loading of $q_{e,\mathrm{PFOA}}$ = 66,000 mg kg^{-1}.

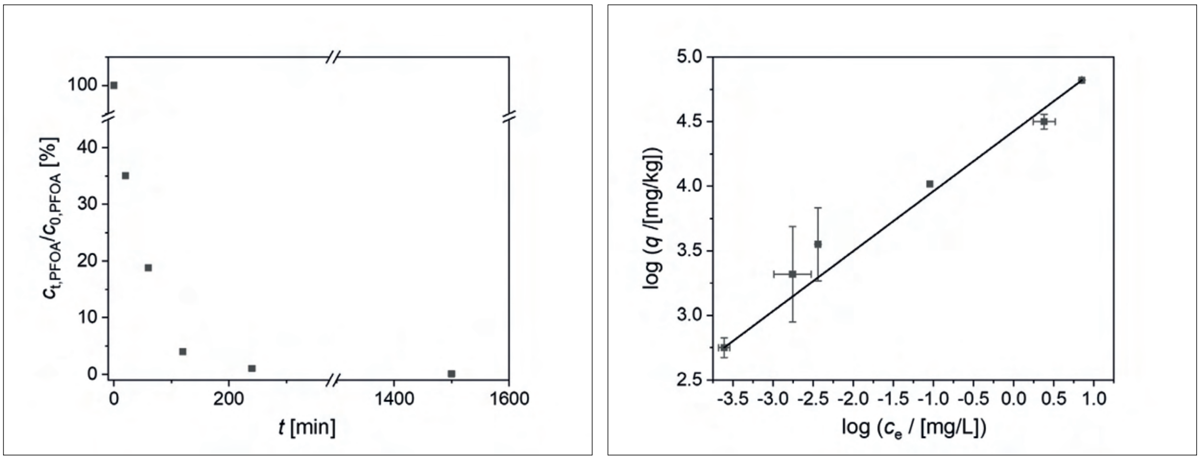

Figure 6 Time-resolved perfluorooctanoic acid (PFOA) adsorption (left) as well as the linearized adsorption isotherm (right) according to the Freundlich model (eq. (2)) on aCS. Error bars represent the minimum and maximum deviation from the mean value based on the experimental and analytical duplicates (*i.e.* n = 4); $c_{0,\mathrm{PFOA,kinetics}}$ = 0.2 mg L^{-1}; $c_{0,\mathrm{PFOA,isotherm}}$ = 0.2–20 mg L^{-1}, c_{aCS} = 200 mg L^{-1}, 10 mM NaCl, pH = 6.5.

3.3 Suspension stability of the activated carbon spheres

Considering a possible future *in-situ* application for the synthesized aCS, the aqueous suspension properties of the particles are crucial and therefore were carefully investigated. The sedimentation of the particles in an aqueous suspension was monitored over 18 h in comparison with a commercial colloidal activated carbon (Intraplex®). When the aCS as well as Intraplex® particles were not stabilized with CMC they showed agglomeration and relatively fast sedimentation of the formed agglomerates. However, due to their perfectly spherical shape, the aCS particles were less prone to agglomeration compared to the commercial sample (Intraplex®) as shown in Figure 7. When stabilized with CMC, both herein synthesized and commercial particles sedimented slowly as mostly individual particles and stayed in suspension much longer than without CMC. The effect can be attributed to an introduction of surface charge by CMC sorption onto the external particle surface and the resulting electro-sterical stabilization effect [29].

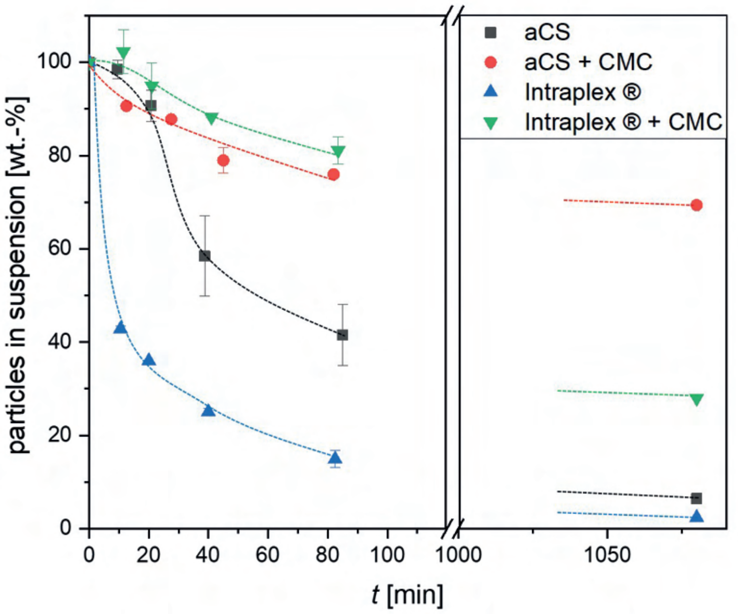

Figure 7 Sedimentation of the synthesized aCS in aqueous suspension in the absence and in the presence of CMC in comparison with a commercial finely-powdered activated carbon (AC, Intraplex®). Dotted lines are a guide for the eye. Error bars represent the mean deviation of single values from the mean value of at least two independent experiments.

This was confirmed by zeta potential measurements which showed decreases from (-31.7 ± 3.6) mV for aCS to (-45.5 ± 1.0) mV for aCS + CMC and from (-35.1 ± 0.8) mV for Intraplex® to (-40.0 ± 2.5) mV for Intraplex® + CMC. Here as well, the aCS were stable for a longer time. After storage for 18 h in a non-agitated state, 70 wt.-% of aCS + CMC remained in suspension while only 28 wt.-% of Intraplex® + CMC were still suspended. On the one hand, this can be explained by the lower zeta potential of aCS + CMC compared to the commercial sample stabilized with CMC. On the other hand, the commercial finely-ground particles are not spherical and thus provide a greater external surface for adhesive forces when particles get in contact. Furthermore, the rougher surface of the ground particles counteracts the shearing forces induced by Brownian motion of the particles and consequently hinders their separation. This enhanced agglomeration of the commercial AC sample (in the absence of stabilizing CMC) can be impressively viewed under the microscope (Figure 8, sample "Intraplex®").

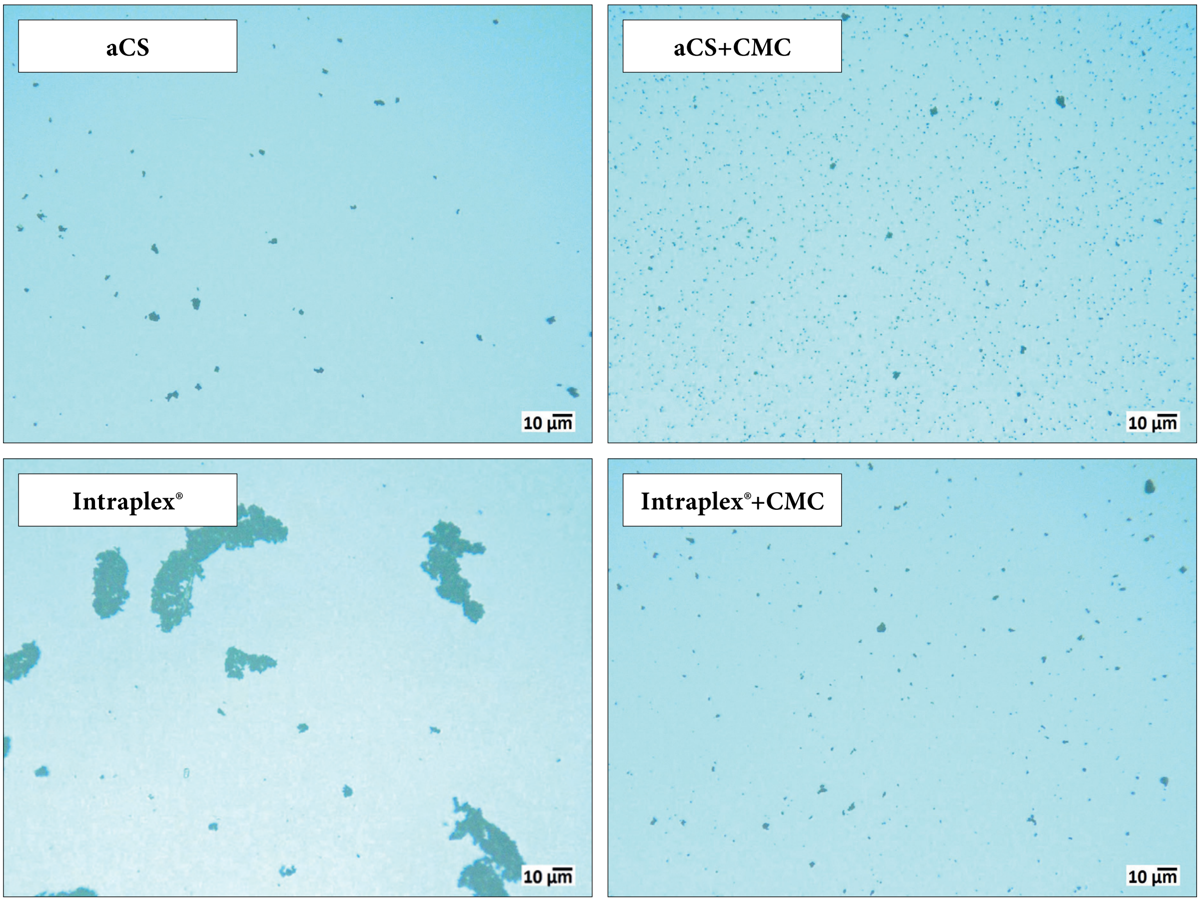

Figure 8 1 g L^{-1} AC particles in 10 mM KNO_3 after > 18 h in non-agitated suspensions in the presence and in the absence of 10 wt.-% carboxymethyl cellulose (CMC) (relating to the AC particles).

3.4 Ageing of the activated carbon spheres

The oxygen content of the carbon surface is important for surface hydrophobicity and charge and is thus a crucial factor for adsorption performance especially towards ionic organic compounds [16, 30]. The surface ageing of aCS (pyrolyzed in 3 vol.-% H_2O/N_2) over time was monitored in comparison with the ageing processes of pCS800 (pyrolyzed in dry N_2) and aCS-H_2 (aCS treated with 10 vol.-% H_2/N_2 at 900 °C). From Figure 9 it becomes evident that all samples age fastest upon storage in open beakers under laboratory atmosphere and slowest in the desiccator. Sample pCS800 which was pyrolyzed under only N_2 aged to the highest extent which could not be prevented even by storage under reduced humidity in the desiccator. Furthermore, the high deviations of replicate experiments indicate that the ageing of pCS800 is least predictable. The de-functionalization of the carbon surface during the high-temperature treatment in N_2 creates reactive centers which are not saturated by N_2 [31]. High-temperature treatment with H_2 on the contrary not only de-functionalizes the carbon surface but also saturates the resulting reactive carbon atoms and un-saturated aliphatic structures [18]. This procedure was recently applied in order to obtain AC felts with very low O-content and positive surface charge and proved to be suitable to generate excellent adsorbents for PFAS anions and other anionic persistent and mobile organic compounds (PMOCs) [32]. Most interestingly, the effect of high-temperature treatment in 3 vol.-% H_2O/N_2 applied in this study was comparable to the treatment with H_2. On the one hand, both treatment conditions, H_2O/N_2 as well as H_2/N_2 atmosphere, de-functionalized the surface more than the high-temperature treatment in pure N_2. On the other hand, they both stabilized the surface afterwards which resulted in a suppressed and thus slower and overall less ageing of the aCS surface. However, it is worth mentioning that the very low oxygen content of the samples treated in H_2O/N_2 as well as H_2/N_2 could not be completely maintained. Even upon storage in a desiccator, functional groups releasing CO_2 during TPD got introduced presumably due to the chemisorption of O_2. Nevertheless, the re-oxidation of the surface only occurred to a certain degree and could be kept at a relatively low amount of surface oxygen.

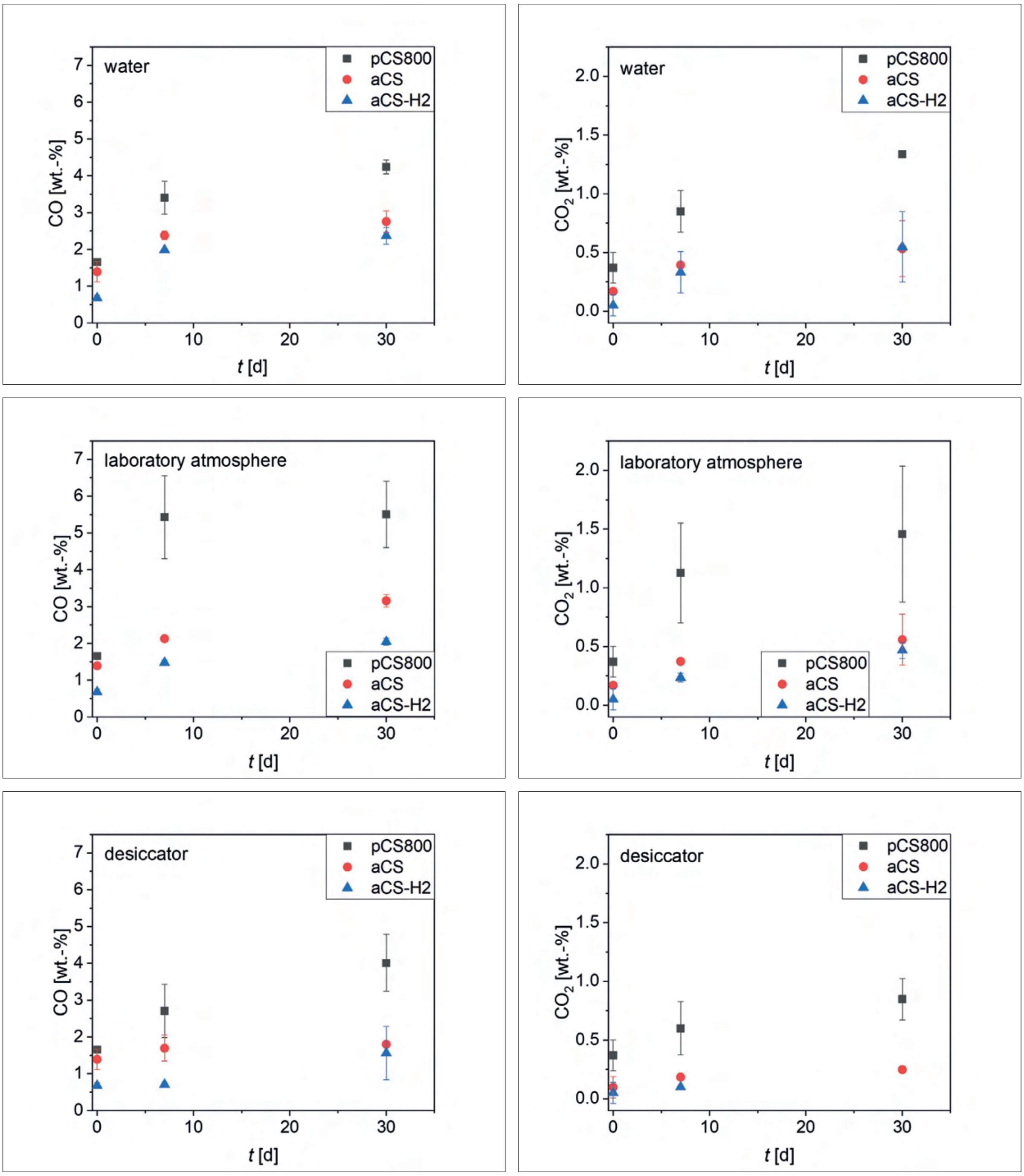

Figure 9 CO and CO_2 released during TPD up to 1100 °C of the samples after various storage times *t* as indicator of the amount of functional groups on the carbon surface. Error bars represent the mean deviation of single values from the mean value of at least two independent experiments. The titles of the diagrams represent the ageing conditions of the freshly synthesized aCS samples.

Due to the planned application of the aCS in water, the according ageing mechanism was further investigated. In addition to the experiments in water shown in Figure 9 that were conducted in the presence of a limited amount of oxygen and for at least 7 d, experiments in oxygen-free water with exposure in shorter time-frames were performed. In Figure 10 (left), it is shown that the surface ageing monitored through the introduction of oxygen occurred also at very short ageing times of 1 h and even in oxygen-free water. Hence, it can be deduced that the major part of the observed ageing occurs upon the first contact with water due to the rapid saturation of reactive surface centers [31]. Specifically, half of the increase in surface oxygen content of the sample that was aged for 7 d in water was already introduced after 1 h in water. The ageing in water was slightly enhanced or suppressed when different inorganic salts were added. KNO_3

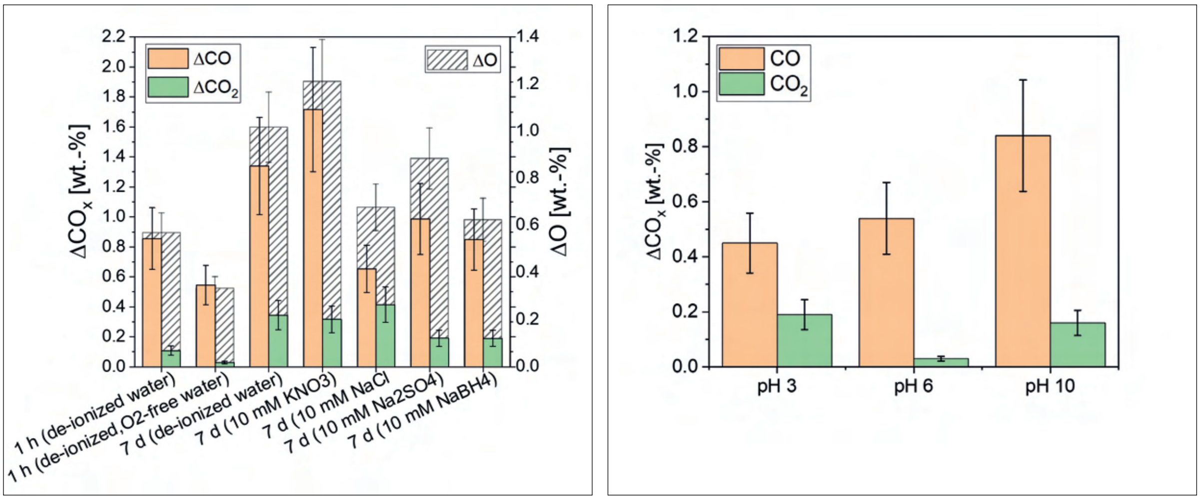

Figure 10 Increase of the CO- and CO_2-releasing groups analyzed *via* TPD up to 1100 °C after ageing of aCS in different aqueous media (left) and in oxygen-free water for 1 h at three different pH values adjusted with HCl or NaOH (right). The given ΔCO_x values are differences between fresh and aged samples. Error bars represent the mean deviation of single values from the mean value of at least two independent experiments.

moderately enhanced surface ageing, possibly due to a slight oxidizing effect of nitrate and/or inducing a small change of pH. Sodium borohydride, in contrast, suppressed the oxygen-introduction due to the reducing effect of borohydride. Also sodium chloride and sodium sulfate showed a slightly suppressing effect on the introduction of oxygen on the aCS surface but had the opposite effect regarding the introduction of carboxylic and quinone/phenol groups. The ageing *via* introduction of oxygen-containing groups could not be prevented in aqueous media as it was also observed in oxygen-free water. This means that there is a significant contribution of hydrolysis to the ageing process. In order to investigate the effect of hydrolysis on the aCS surface ageing, further experiments in O_2-free water at different pH values were conducted. From Figure 10 (right), it can be seen that the introduction of CO_2-releasing functionalities such as carboxylic groups is augmented at pH 3 as well as at pH 10. Therefore, it is assumed that these functionalities are introduced upon hydrolysis of surface sites that is facilitated in acidic and alkaline media. Furthermore, it is noteworthy that the amount of CO-releasing groups is significantly enhanced only at pH 10. This could mean that, *e.g.* phenolic groups can be introduced by the reaction of hydroxide with reactive moieties on the aCS surface, presumably by a nucleophilic addition-like mechanism.

The influence of the observed activated carbon ageing on the sorption behavior was characterized by monitoring the MCB sorption kinetics of freshly prepared aCS with an aged aCS sample in comparison with the commercial finely-ground AC sample (Intraplex®) (Figure 11). The aged aCS sample was prepared by suspending the aCS sample in water and keeping it for 45 d in an abundant oxygen atmosphere. After this, “aCS aged” exhibited 4.6 wt.-% ‘TPD-oxygen’, meaning oxygen which is released as CO and CO_2 upon heating up to 1100 °C. Note that this oxygen content is significantly higher than that of the above-shown aged samples (Figure 9).

In Figure 11, it can be seen that the three finely-powdered AC samples show very fast adsorption kinetics as they all provide mean particle diameters of about 1 µm. The herein freshly prepared aCS adsorb the MCB almost completely within the first minute. After the very fast initial adsorption, both aCS samples exhibit a slow pore diffusion due to the narrow microporous system. The equilibrium state is approached within 48 h. The equilibrium sorption distribution coefficients log (K_D/(L kg^{-1})) for MCB significantly decrease from aCS (7.2 ± 0.1) > aCS aged (6.6 ± 0.1) > Intraplex® (5.9 ± 0.2). This correlates with the increase in oxygen content of the samples from aCS (1.6 wt.-% O) < aCS aged (4.6 wt.-% O) < Intraplex® (6.5 wt.-% O). The detailed TPD profiles can be viewed in the SI (Figure S1). The results of the kinetic evaluation according to eqs. 3 and 4 are displayed in Table 3. The initial adsorption rate r_0 was roughly estimated through the increase of the loading at the first sampling point of 30 s. However, due to the extremely fast initial adsorption this parameter may be afflicted with a high error as the actual duration of the fast initial adsorption is unknown. The linear fitting for the estimation of the late-stage adsorption rate coefficient k_e (eq. (5)) is shown in Figure S4.

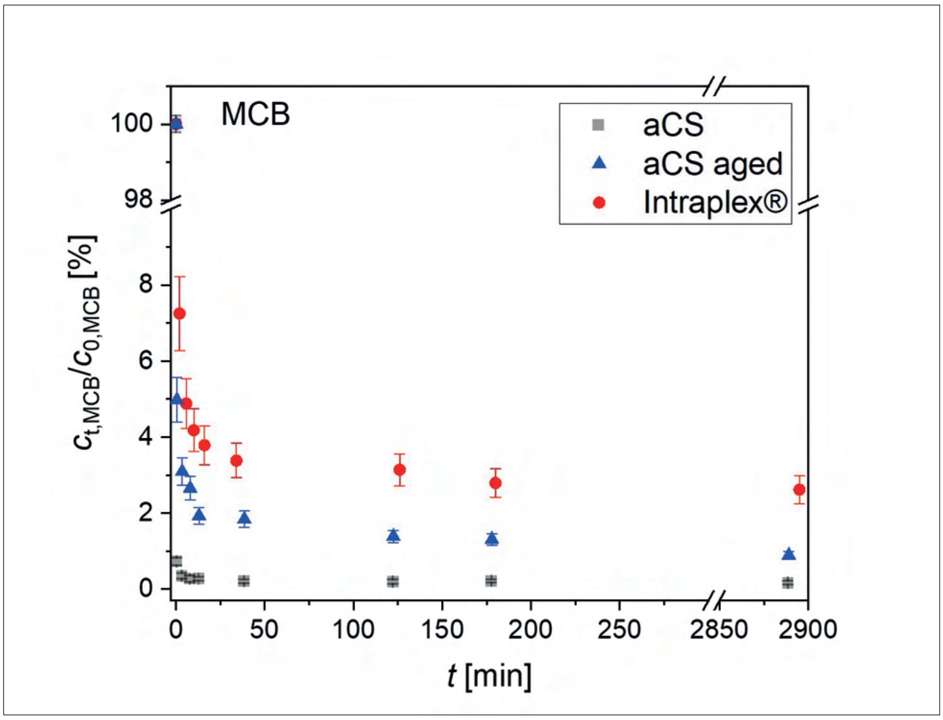

Figure 11 Time-resolved adsorption of MCB on aCS *vs.* aCS aged for MCB in comparison with the commercial finely ground AC sample Intraplex®. Error bars represent the minimum and maximum deviation from the mean value based on the experimental and analytical duplicates (*i.e.* n = 4); $c_{0,\mathrm{MCB}}$ = 2.5 mg L^{-1}; c_{aCS} = 70 mg L^{-1}; 10 mM KNO_3; pH = 6.5.

Table 3 Derived parameters r_0 and k_e for the estimation of the film mass transfer (k_f) and surface diffusion (D_s) coefficients of the MCB adsorption on the different activated carbon samples according to the method proposed in [19].

AC sample	r_0 [mg g^{-1} s^{-1}]	$k_e \cdot 10^4$ [s^{-1}]	$k_f \cdot 10^4$ [m s^{-1}]	$D_s \cdot 10^{20}$ [m^2 s^{-1}]
aCS	1.2	7.9	1.3	2.3
aCS aged	1.3	5.4	1.4	1.0
Intraplex®	1.2	1.1	1.3	25.7

The film-mass-transfer coefficients k_f for the MCB adsorption on the three AC samples are essentially the same due to their comparable particle size. They are in the same order of magnitude as literature results for the adsorption of toluene and phenol on adsorbent particles with radii of around 500 and 200 µm, respectively [19]. However, the k_f values in Table 3 seem to overestimate the thickness of the stagnant boundary layer around the small AC particles ($d_{\mathrm{film}} = D_{\mathrm{MCB,water}} / k_f = 10^{-9}$ m^2 s^{-1} / ($1.3 \cdot 10^{-4}$ m s^{-1}) ≈ 10 µm). This may be due to the very short contact time of about 30 s which does not ensure an instantaneous ideal mixing of the added MCB into the AC suspension. The surface diffusion coefficients D_s decrease from Intraplex® > aCS > aCS aged and are several orders of magnitude smaller compared to literature data [19, 33]. This might be attributed to the predominant microporosity of the herein investigated adsorbents which can impede fast surface diffusion processes [33]. This could also explain why the experimentally obtained D_s for Intraplex® is an order of magnitude higher than that for the aCS samples. Intraplex® provides larger micropores between 1 and 1.5 nm which could facilitate intra-particle substance transport (*cf.* Figures S2 and S5).

It was assumed that the ageing of aCS surface might have an even greater effect on the adsorption of PFOA than on the adsorption of MCB. Therefore, the adsorption affinity of freshly prepared aCS (1.6 wt.-% O) in comparison with aCS aged (4.6 wt.-% O) towards PFOA was monitored by means of single point adsorption coefficients K_D. In order to follow the observed trend, additionally the adsorption on a highly aged sample (9.2 wt.-% O) was investigated. The latter represents ageing in abundant

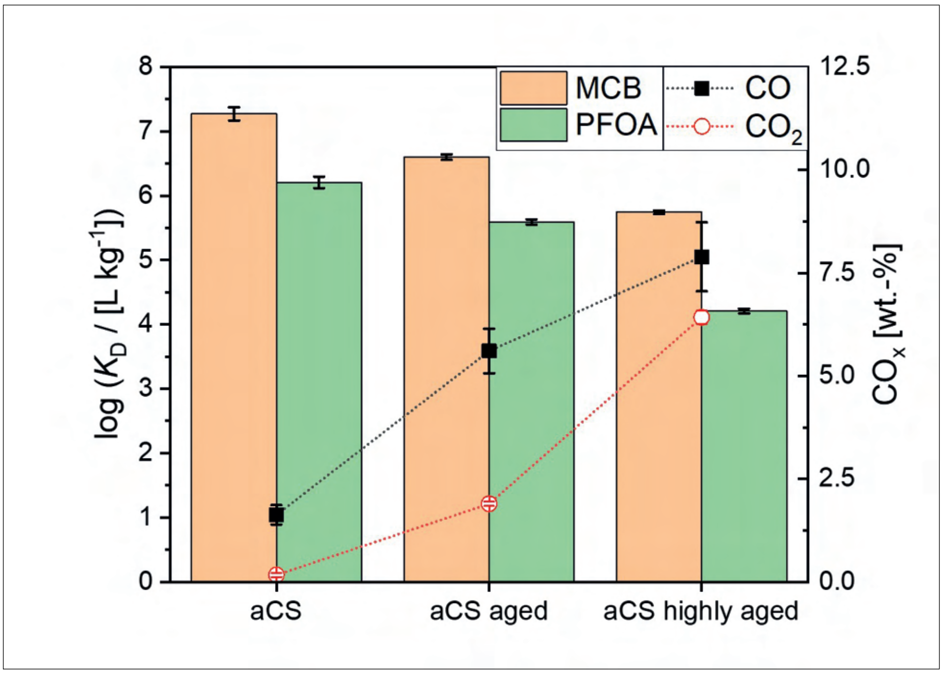

Figure 12 Adsorption coefficients log K_D on aCS *vs.* aCS aged for MCB ($c_{0,MCB}$ = 2.5 mg L^{-1}; c_{aCS} = 70 mg L^{-1}; 10 mM KNO_3; pH = 6.5) and PFOA ($c_{0,PFOA}$ = 0.2 mg L^{-1}; c_{aCS} = 200 mg L^{-1}; 10 mM NaCl; pH = 6.5). Error bars represent the mean deviation of single values from the mean value of at least two independent experiments.

oxygen for more than 8 months. The resulting log K_D values for the PFOA adsorption are displayed in Figure 12 in comparison with those for the MCB adsorption. As discussed above, the log $K_{D,MCB}$ is significantly decreased for aCS aged compared to aCS. Regarding the adsorption of PFOA on 'aCS aged', the adsorption is decreased as well, however not more than for the neutral MCB molecule. For the highly aged sample the decrease of log K_D becomes slightly more pronounced for PFOA compared to MCB. At the experimental pH of 6.5, the aged adsorbents exhibit a negative net charge on the surface as the point of zero net charge (PZNC) decreases from pH = 7.0 ± 0.2 for aCS to pH ≤ 6.3 for the aged aCS samples. Accordingly, the decrease of adsorbent affinity towards PFOA with decreasing PZNC due to electrostatic repulsion of the oxidized surface and the anionic PFOA molecule is in conformity with observed trends in literature [34]. The adsorption affinity of an adsorbent towards PFOA is a complex interplay of the adsorbent characteristics such as charge, ion exchange capacities and various functional groups but also a matter of pore size [16, 28, 35]. Nevertheless, the decrease in the adsorption affinity of the aged adsorbents towards MCB is also significant. These results highlight the need for monitoring adsorbent ageing and the investigation of the influence on the adsorption of different pollutant classes. Furthermore, it is necessary to avoid preventable oxidation during and directly after synthesis of freshly de-functionalized surfaces. The herein proposed synthesis of aCS may be an alternative for either wet-grinding of AC or pyrolysis of hydrochar particles under N_2 as both procedures can lead to enhanced surface oxidation.

4 Conclusion

Uniform and dispersible aCS were synthesized bottom-up *via* hydrothermal carbonization of sucrose with subsequent pyrolysis. The dosage of 3 vol.-% H_2O in N_2 flow led to high specific surface areas up to 1400 $m^2\ g^{-1}$ with a well-pronounced microporosity and a highly de-functionalized surface which was moderately stable against hydrolysis and oxidation at ambient conditions. Pyrolysis with 3 vol.-% H_2O/N_2 could replace 10 vol.-% H_2/N_2 for the generation of sufficiently stable, hydrophobic carbonaceous adsorbent surfaces. However, a certain degree of re-oxidation could not be prevented for all investigated samples, even the ones where the surface was saturated with H_2 after de-functionalization. This has to be kept in mind, especially when adsorbents are characterized in the dry state and then applied in water. A comparative experiment where the enhanced surface ageing of the adsorbent was induced in water with abundant oxygen showed that the aCS suffered a significant loss regarding their sorption affinity, even when it comes to the neutral MCB molecule. This negative effect becomes even stronger for negatively charged adsorbates like PFOA. Therefore, it was attempted to even out decreases regarding the sorption performance upon inevitable surface ageing in water by adjusting the pore system of the synthesized aCS. The very narrow and strictly microporous system performed well regarding the PFOA adsorption with adsorption coefficients up to $10^{6.5}$ L kg^{-1}.

Funding: This research was funded by "Deutsche Forschungsgemeinschaft" (DFG), project number 392011053.

Acknowledgments: The authors thank Dr. Matthias Schmidt for the SEM analysis which was done at ProVIS – Centre for Chemical Microscopy at the UFZ, Leipzig, which is supported by European Regional Development Funds (EFRE-Europe funds Saxony) and the Helmholtz Association.

Furthermore, the authors sincerely thank Birgit Würz for kindly assisting with the zeta potential measurement which was performed at the Department of Environmental Microbiology of the UFZ, Leipzig. The authors are obliged to Kerstin Lehmann and Dr. Robert Köhler from the Department of Environmental Engineering (UFZ, Leipzig) for conducting the elemental analysis of the synthesized particles.

References

[1] L. Decrey, F. Bonvin, C. Bonvin, E. Bonvin, T. Kohn, *Removal of trace organic contaminants from wastewater by superfine powdered activated carbon (SPAC) is neither affected by SPAC dispersal nor coagulation*, Water Res. 185 (2020) 116302.

[2] F. Bonvin, L. Jost, L. Randin, E. Bonvin, T. Kohn, *Super-fine powdered activated carbon (SPAC) for efficient removal of micropollutants from wastewater treatment plant effluent*, Water Res. 90 (2016) 90–99.

[3] Regenesis, *PlumeStop® Liquid Activated Carbon^{TM}*. https://regenesis.com/en/remediation-products/plumestop-liquid-activated-carbon/, accessed on 21.05.2022, (2022).

[4] P. Bardos, C. Merly, P. Kvapil, H.-P. Koschitzky, *Status of nanoremediation and its potential for future deployment: risk-benefit and benchmarking appraisals*, Remediation Journal 28 (2018) 43–56.

[5] Intrapore, *Particle-based ground-water remediation*. https://intrapore.com/en/, accessed on 21.05.2022, 2022. https://intrapore.com/en/.

[6] F. Coperchini, O. Awwad, M. Rotondi, F. Santini, M. Imbriani, L. Chiovato, *Thyroid disruption by perfluorooctane sulfonate (PFOS) and perfluorooctanoate (PFOA)*, J. Endocrinol. Invest. 40 (2017) 105–121.

[7] H. Holbech, P. Matthiessen, M. Hansen, G. Schüürmann, D. Knapen, M. Reuver, F. Flamant, L. Sachs, W. Kloas, K. Hilscherova, M. Leonard, J. Arning, V. Strauss, T. Iguchi, L. Baumann, *ERGO: Breaking down the wall between human health and environmental testing of endocrine disrupters*, Int. J. Mol. Sci. 21 (2020) 2954–2972.

[8] A. Cordner, G. Goldenman, L. Birnbaum, M. Brown, M.F. Miller, R. Mueller, S. Patton, D.H. Salvatore, L. Trasande, *The true cost of PFAS and the benefits of acting now*, Environ. Sci. Technol. 55 (2021) 9630–9633.

[9] R. McGregor, *In situ treatment of PFAS-impacted groundwater using colloidal activated carbon*, Remediation Journal 28 (2018) 33–41.

[10] G.R. Carey, R. McGregor, A.L. Pham, B. Sleep, S. Hakimabadi, *Evaluating the logevity of a PFAS* in situ *colloidal activated carbon remedy*, Remediation 29 (2019) 17–31.

[11] A. Georgi, A. Schierz, K. Mackenzie, F.-D. Kopinke, *Colloidal activated carbon for in-situ groundwater remediation – Transport characteristics and adsorption of organic compounds in water-saturated sediment columns*, Journal of Contaminant Hydrology 179 (2015) 76–88.

[12] M. Balda, K. Mackenzie, F.-D. Kopinke, A. Georgi, *Uniform and dispersible carbonaceous microspheres as quasi-liquid sorbent*, Chemosphere (2022) 136079.

[13] X. Sun, Y. Li, *Colloidal carbon spheres and their core/shell structures with noble-metal nanoparticles*, Angew. Chem. 116 (2004) 607–611.

[14] J. Yang, J.-Y. Li, J.-Q. Qian, H.-Z. Lian, H.-Y. Chen, *Solid phase extraction of magnetic carbon doped Fe_3O_4 nanoparticles*, Journal of Chromatography A 1325 (2014) 8–15.

[15] H. Takaesu, H. Matsui, Y. Nishimura, T. Matsushita, N. Shirasaki, *Micro-milling super-fine powdered activated carbon decreases adsorption capacity by introducing oxygen/hydrogen-containing functional groups on carbon surface from water*, Water Res. 155 (2019) 66–75.

[16] N. Saeidi, F.-D. Kopinke, A. Georgi, *What is specific in adsorption of perfluoroalkyl acids on carbon materials?*, Chemosphere 273 (2021) 128520.

[17] J.C. Petit, Y. Bahaddi, *New insight on the chemical role of water vapour in the ageing of activated carbon*, Carbon 31 (1993) 821–825.

[18] J.A. Menéndez, J. Philips, B. Xia, L.R. Radovic, *On the modification and characterization of chemical surface properties of activated carbon: in the search of carbons with stable basic properties*, Langmuir 12 (1996) 4404–4410.

[19] C. Yao, T. Chen, *A new simplified method for estimating film mass transfer and surface diffusion coefficients from batch adsorption kinetic data*, Chem. Eng. J. 265 (2015) 93–99.

[20] N.M. Osmond, *Activated carbon fibre adsorbent materials*, Adsorp. Sci. Technol. 18 (2000) 529–539.

[21] N. Saha, D. Xin, P.C. Chiu, M. Toufiq Reza, *Effect of pyrolysis temperature on acidic oxygen-containing functional groups and electron storage capacities of pyrolyzed hydrochars*, ACS Sustainable Chemistry & Engineering 7 (2019) 8387–8396.

[22] J.L. Figueiredo, M.F.R. Pereira, M.M.A. Freitas, J.J.M. Órfao, *Characterization of active sites on carbon catalysts*, Industrial & Engineering Chemistry Research 46 (2007) 4110–4115.

[23] A.A. Azzaz, B. Khiari, S. Jellali, C.M. Ghimbeu, M. Jeguirim, *Hydrochars production, characterization and application for wastewater treatment: A review*, Renew. Sust. Energ. Rev. 127 (2020) 109882.

[24] S. Román, J.M. Nabais Valente, B. Ledesma, M.T. González, C. Laginhas, M.M. Titirici, *Production of low-cost adsorbents with tunable surface chemistry by conjunction of hydrothermal carbonization and activation processes*, Microporous Mesoporous Mater. 165 (2013) 127–133.

[25] G. Chegini, C. Briens, D. Pjontek, *Production and characterization of adsorbents from a hydrothermal char by pyrolysis, carbon dioxide and steam activation*, Biomass Conv. Bioref. (2022).

[26] A.S. Mestre, E. Tyszko, A. Andrade, M. Galhetas, F. C., A.P. Carvalho, *Sustainable activated carbons prepared from a sucrose-derived hydrochar: remarkable adsorbents for pharmaceutical compounds*, RSC Advances 5 (2015) 19696–19707.

[27] G. Schüürmann, *QSAR analysis of the acute fish toxicity of organic phosphorothionates using theoretically derived molecular descriptors*, Environ. Toxicol. Chem. 9 (1990) 417–428.

[28] K.M. Krahn, G. Cornelissen, G. Castro, H.P.H. Arp, A.G. Asimakopoulos, R. Wolf, R. Holmstad, A.R. Zimmemann, E. Sørmo, *Sewage sludge biochars as effective PFAS-sorbents*, J. Hazard. Mater. 445 (2023) 130449.

[29] K. Mackenzie, A. Georgi, *NZVI synthesis and characterization*, in: T. Phenrat, G.V. Lowry (Eds.), *Nanoscale zerovalent iron particles for environmental restoration*, Springer International Publishing AG, Basel, 2019, pp. 45–95.

[30] J. Zhou, N. Saeidi, L.Y. Wick, Y. Xie, F.-D. Kopinke, A. Georgi, *Efficient removal of trifluoroacetic acid from water using surface-modified activated carbon and electro-assisted desorption*, J. Hazard. Mater. 436 (2022) 129051.

[31] J.J. Pignatello, W.A. Mitch, W. Xu, *Activity and reactivity of pyrogenic carbonaceous matter toward organic compounds*, Environ. Sci. Technol. 51 (2017) 8893–8908.

[32] J. Zhou, Y. Zhang, M. Balda, V. Presser, F.-D. Kopinke, A. Georgi, *Electro-assisted removal of polar and ionic organic compounds from water using activated carbon felts*, Chem. Eng. J. 433 (2022) 133544.

[33] R. Ocampo-Pérez, R. Leyva-Ramos, M. Sanchez-Polo, J. Utrilla-Rivera, *Role of pore volume and surface diffusion in the adsorption of aromatic compounds on activated carbon*, Adsorption 19 (2013) 945–957.

[34] Z. Du, S. Deng, Y. Bei, Q. Huang, B. Wang, J. Huang, G. Yu, *Adsorption behavior and mechanism of perfluorinated compounds on various adsorbents – a review*, J. Hazard. Mater. 274 (2014) 443–454.

[35] J. Fabregat-Palau, M. Vidal, A. Rigol, *Examining sorption of perfluoroalkyl substances (PFAS) in biochars and other carbon-rich materials*, Chemosphere 302 (2022) 134733.

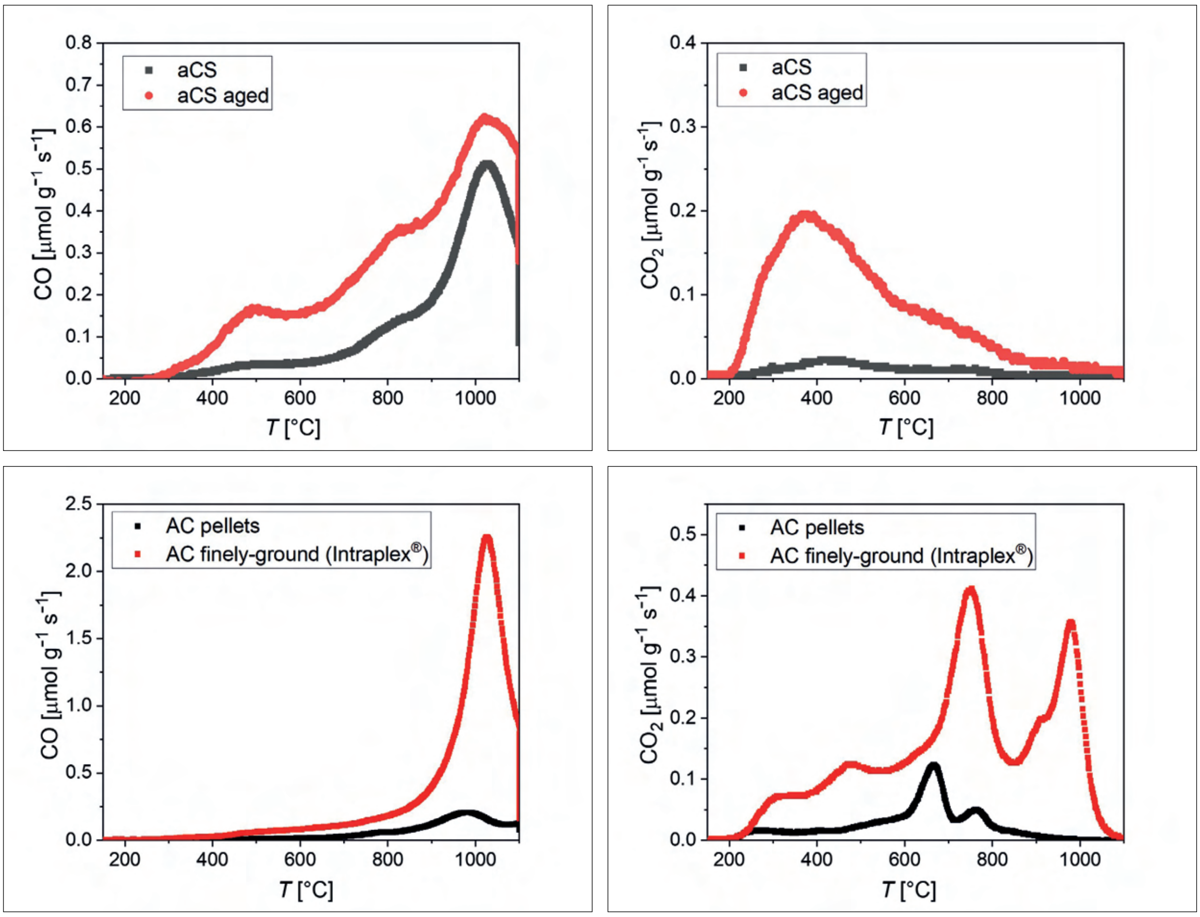

Figure S1 Temperature-programmed decomposition (TPD) up to 1100 °C (10 K min^{-1}) of activated carbon spheres (aCS) compared with aCS aged (top) and a commercial activated carbon (AC) sample Intraplex® obtained by a wet-milling process (“AC finely-ground”) compared with the respective precursor material in pellet-form (“AC pellets”)

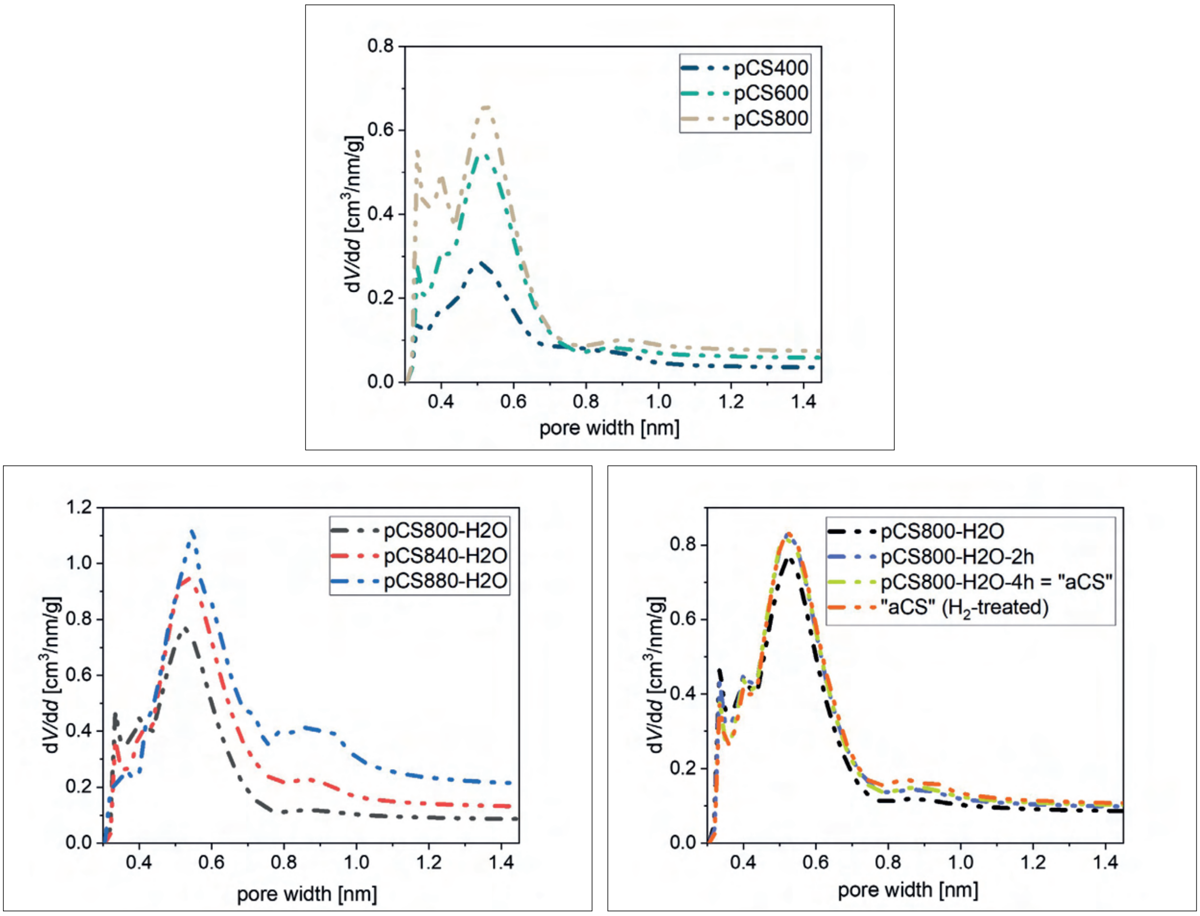

Figure S2 Pore size distributions for all pyrolyzed and activated CS samples determined with NLDFT based on CO_2 ad- and desorption (isotherms measured up to $p/p_0 = 0.0287$ equals to $p = 0.1$ MPa).

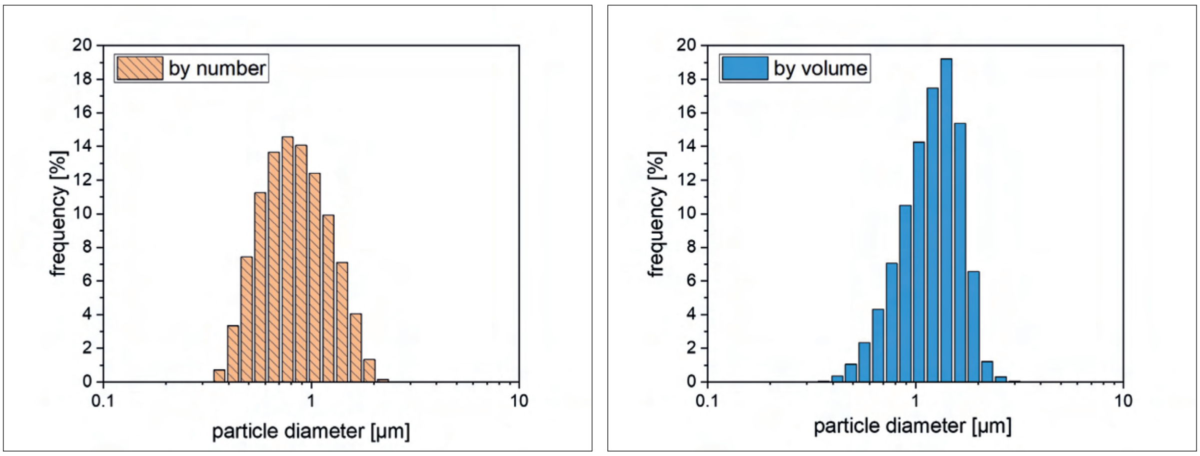

Figure S3 Differential particle size distribution by number and by volume determined via dynamic light scattering (DLS) analysis of 5 mg L^{-1} aCS particles dispersed in 10 mM KNO_3 solution at pH = 6.

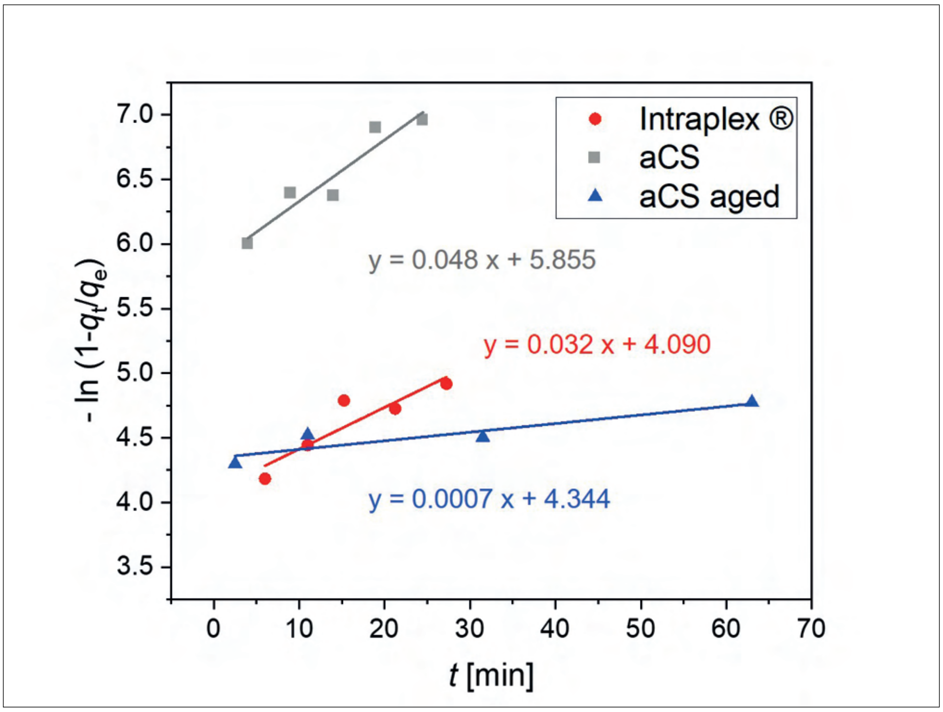

Figure S4 Linear fitting of the kinetic data of the monochlorobenzene (MCB) adsorption according to eq. (5) for estimation of the late stage adsorption rates of MCB on the different activated carbon samples.

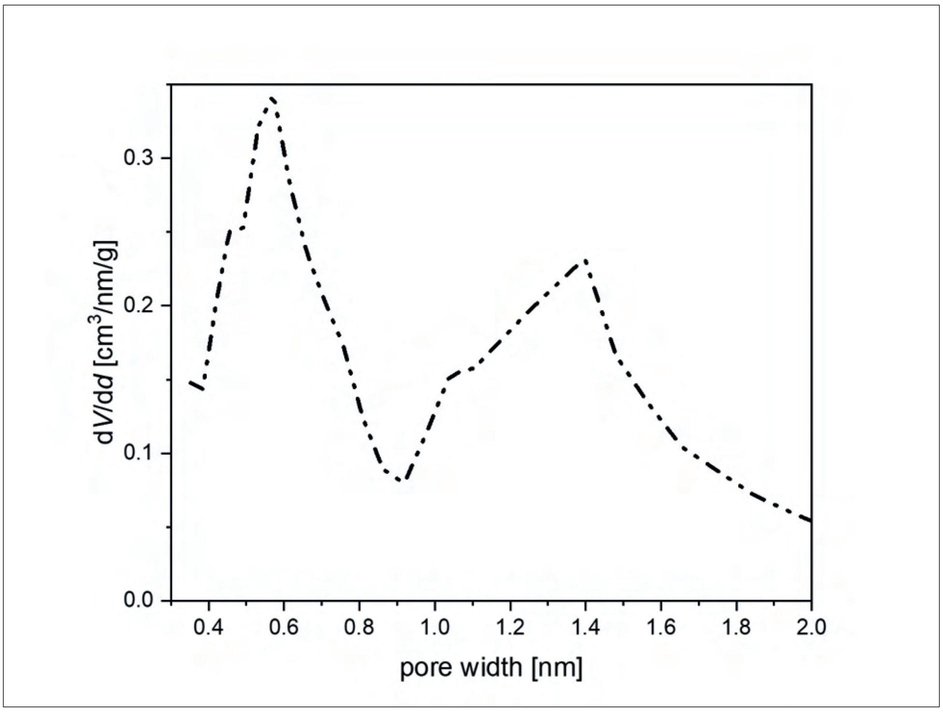

Figure S5 Pore size distribution of the AC Intraplex® determined with NLDFT based on CO_2 adsorption (up to $p/p_0 = 1$, with $p_0 = 3.4851$ MPa).

4.3 Generating colloidal Fe/C composites *via* hydrothermal carbonization – a critical study[3]

Maria Balda, Anett Georgi, Frank-Dieter Kopinke, Katrin Mackenzie

Department of Environmental Engineering, Helmholtz Centre for Environmental Research – UFZ, D-04318 Leipzig, Germany

Abstract: The aim of this work was to develop an approach for the bottom-up synthesis of colloidal Fe/C composites. It was tested whether the composites meet the main criteria for use as injectable adsorbents and reducing agents for the removal of chlorinated pollutants in *in-situ* groundwater remediation. After the screening of different Fe and C precursors, the bottom-up synthesis of a particulate and reactive Fe/C composite was developed *via* one-pot hydrothermal carbonization (HTC) of mixtures of ferrous and sodium gluconate and subsequent carbothermal reduction at 800 °C. The generated particles exhibit a good dispersibility with particle diameters in the range of $d_{10} \geq 2$ µm, $d_{50} \approx 11$ µm and $d_{90} \leq 40$ µm in aqueous suspensions. By varying the molar ratio of Fe to gluconate in the HTC process, the final content of zero-valent iron equivalents (ZVI) in the composite was adjusted between (24 ± 12) and (49 ± 15) wt.-%. The chemical reactivity of the composite was tested using reductive dechlorination of chloroform (CF). Characterization of the composites before and after reductive dechlorination with XRD indicates that not only pristine Fe^0 but also Fe_3C is active in the reductive dechlorination reaction. Palladization of the composite material shifts the product selectivity from dichloromethane as the main product to the non-chlorinated products methane (up to 77 mol-%) and ethane (up to 9 mol-%) without any external H_2 feed. The dispersiblity and intrinsic reactivity of the synthesized composites is favorable for the application in water remediation where contaminants need to be retained and degraded, *e.g.* for groundwater remediation or protection by the *in-situ* generation of permeable barriers using modern injection technologies.

Keywords: Fe/C composites; hydrothermal carbonization; dispersible; reductive dechlorination; chloroform; water remediation

---

[3] This article was published in Separation and Purification Technology, Vol. 335, MARIA BALDA, ANETT GEORGI, FRANK-DIETER KOPINKE, KATRIN MACKENZIE, *Generating colloidal Fe/C composites via hydrothermal carbonization – A critical study*, 126082, © Elsevier (2024).

1 Introduction

Water scarcity is a global problem, so it is important to safeguard the water quality of groundwater bodies in order to ensure high quality standards for drinking water. For this purpose, it is not only necessary to provide the required amount of water, *e.g.* by artificial groundwater recharge systems, but also to maintain and restore the desired water quality. However, the typically low concentrations of contaminants at polluted groundwater sites make effective remediation measures difficult. Therefore, innovative technologies combine adsorptive and reactive techniques to enrich the pollutants in the adsorbent phase and degrade them with an added reactant [2, 3]. The adsorbents and reactants used for remediation should be effective and cost-efficient while posing no additional threats to the treated water bodies. For this purpose, iron and carbon have proven to be suitable components due to their natural abundance, low price and non-toxic nature [4, 5]. Ideally, the degradation of the pollutant leads to the regeneration of the adsorptive function of the material. This combinatory approach has been established on the remediation market for *in-situ* groundwater remediation, *e.g.* Carbo-Iron® [6] or BOS 100® [7].

For the construction of permeable reactive zones by low-pressure injections into the aquifer, the adsorptive reagents should be quasi-dissolved and form sufficiently stable suspensions [8]. Particles with densities of about 1.1–2.6 g cm^{-3} ideally have diameters of about 1–2 µm in order to reach larger transport ranges [9, 10]. Nonetheless, it is also possible to inject larger particles, *e.g.* by stabilizing the suspensions in the form of biopolymer gels and applying higher injection pressures [11]. Beyond *in-situ* remediation, alike reactive adsorbents could also be useful in treating other water bodies where retention and degradation of pollutants are critical such as stormwater. For stormwater retention in urban areas for the local reuse and groundwater recharge such 'enrich & treat' options can help to prevent pollutants from reaching groundwater bodies *via* infiltration. Thus, there is a need to develop new materials or more sustainable synthesis ways for these kinds of remediation tasks.

The beneficial interaction of adsorptive and reactive material components of colloidal particles have been investigated with respect to environmental remediation, where highly selective and stable materials are required and contaminant concentrations are low, *e.g.* in groundwater remediation [12, 13]. The transfer of 'chemical reactivity' from ZVI to carbon was also demonstrated when both particles were in the suspended state, even in the micro rather than the nano scale [14–17]. The corresponding transfer process of electrons or hydrogen species (H^*) is referred to as spill-over.

In order to combine iron and carbon (Fe/C) in well-dispersible composite materials, usually multi-step synthesis approaches are used. The carbon material is pre-synthesized and then provided with the reactive component. In the case of iron, this is realized by wet impregnation of the carbon's pore system with iron salts and subsequent reduction [18]. In some cases, the reduction of oxidic iron on AC can be achieved with $NaBH_4$ [19]. Similar wet impregnation processes have also been reported for the preparation of Fe-containing composites using hydrochar instead of AC, where the (pre-pyrolyzed) hydrochar was soaked in a suspension containing iron salts and then thermally activated to produce porosity and form Fe particles [20, 21]. More recently, other processes have been investigated in which solid feedstocks were impregnated prior to hydrothermal treatment [22] or where the Fe was introduced into the hydrochar in particulate form, *e.g.* as magnetite *via* the co-precipitation method with $FeCl_2$ and $FeCl_3$ [23]. It should be noted, however, that when solid biomass or pre-synthesized (activated) carbons are used, the dispersibility and suitable particle sizes for low-pressure injections cannot be adjusted in a single synthesis step, but must be achieved either by separate synthesis of the carbonaceous precursor in the desired particle sizes [21] or through milling of either the precursor or the final composite [22–24].

An alternative to these multi-step syntheses described above is the one-pot synthesis of Fe/C composites, starting from dissolved precursors, preferably from renewable resources. There are already several studies dealing with the combination of iron and carbon within one step using hydrothermal carbonization (HTC). However, it has been shown that effectively combining iron and carbon in this manner is not trivial, as the iron precursors are typically hydrophilic and the carbonaceous phase formed is comparatively hydrophobic. In order to gain more insight into the possibilities and limitations of HTC-based bottom-up syntheses, particularly of colloidal Fe/C composites for *in-situ* application, the existing literature studies were comprehensively reviewed and evaluated.

1.1 State of knowledge on the bottom-up synthesis of colloidal Fe/C composites *via* HTC

In order to fabricate functional Fe/C composites as colloidal particles during HTC, in principal two different approaches are followed in literature: (I) HTC of freshly synthesized Fe-containing NPs combined with sugar solutions (Table 1) and (II) HTC of fully dissolved Fe and C precursors (Table 2). Based on the objective of the present work, we focused on two criteria for our review, namely if the dispersibility of the composites was explicitly investigated and if the composites were tested regarding reductive dechlorination reactions.

Approach (I) typically led to Fe/C composites with particle diameters of 35–200 nm (*cf.* Table 1). This is due to the coating of the original particles and their aggregates with thin carbon shells of about 5–40 nm [25–27]. It seems that with this approach, Fe dominates the composite and the compatability with carbon is limited. For the planned *in-situ* application, the final ratio of Fe/C is crucial and should preferentially be adjusted between 10–30 wt.-% Fe. A sufficient proportion of C is needed to shield the magnetic attraction of ZVI, otherwise leading to excessive agglomeration of the particle during injection known from pure ZVI. For nZVI this has been identified as major limitation for the *in-situ* application [12, 28, 29]. Furthermore, approach (I) has the drawback that the Fe-containing NPs have to be synthesized individually, resulting in an additional step prior to HTC.

Table 1 Literature studies on the synthesis of colloidal Fe/C composites *via* HTC of solid Fe precursors and dissolved C precursors.

Ref.	Experimental	Result/Comments	Suggested Application(s)
Wang *et al.* [26]	• Oleic acid stabilized magnetite NPs (2.5 g L^{-1}) + glucose (0.6 M) in Teflon-sealed autoclave • HTC at 170 °C for 3 h	• Nanocomposites in the size range 100–200 nm • Fe_3O_4-NPs homogeneously distributed in the center of the carbon spheres (10 nm carbon shell) • Dispersible nanocomposites (Fe_3O_4/C) • No stability tests	Magnetic carrier (not tested)
Wei *et al.* [25]	• Freshly synthesized FeNi-NPs (0.5 g L^{-1}) + glucose (0.4 M) in Teflon®-sealed autoclave • HTC at 160 °C for 3.5 h/2.5 h	• Core-shell structured particles with 35 nm FeNi-core and 5–12 nm carbon shell • Composites dispersible in H_2O, EtOH and MeOH *via* ultrasonication • No stability tests	Magnetic carrier (not tested)
Bai *et al.* [30]	• Freshly synthesized Fe_3O_4-NPs (10 g L^{-1}) + glucose (0.5 M) mixed for 30 min and put in an autoclave • HTC at 160 °C for 8 h	• Core-shell particles of about 70 nm • Easily dispersible Fe_3O_4/C composites due to the hydrophilic C surface • No stability tests	Solid-phase extractant (tested for PAHs)
Zhang *et al.* [31]	• Freshly synthesized Fe_3O_4-NPs (5 g L^{-1}) + glucose (0.5 M) ultrasonicated for 20 min and put in a Teflon®-lined autoclave • HTC at 180 °C for 4 h	• Agglomerates of Fe_3O_4-NPs (primary particle size 10 nm) are coated with carbon • Hydrophilic C shell of Fe_3O_4 ameliorates dispersibility in H_2O • No stability tests	Solid-phase extractant (tested for PAHs)
Yang *et al.* [27]	• Freshly synthesized Fe_3O_4-NPs (6.7 g L^{-1}) + glucose (0.5 M) • HTC at 180 °C for 4 h	• Core-shell particles with an Fe_3O_4 core (70–80 nm) and a carbon shell (30–40 nm) • Overall diameter 100–120 nm Fe_3O_4/C dispersible via ultrasonication • No tests of suspension stability	Solid-phase extractant (tested for PAHs)

The literature studies that investigated approach (II) can be divided into two categories with respect to their results: the composite particles had diameters of either a few micrometers or below 100 nm, depending on the ratio of Fe to C precursor and additives (*cf.* Table 2). When moderate concentrations of glucose (about 0.5 M) were mixed with 0.05–0.15 M Fe salts, the excess of C precursor together with the catalyzing effect of Fe during the HTC process generated particle sizes of the carbonaceous phase of 5–8 µm separately from Fe-NPs [32–34]. In contrast, when the glucose concentrations were decreased to 0.17–0.25 M and combined with 0.06–0.2 M of Fe precursor, true composites were formed which exclusively consisted of Fe-NPs coated with thin carbon shells. Presumably, the deficit of C precursor led to an increased Fe content of the resulting composites which thus feature the typical behavior of nano-sized Fe-containing particles [35, 36]. Similarly sized composites were generated *via* HTC of more complex sugar-containing solutions such as olive mill wastewater [37, 38] and hydrolysates derived from pinewood chips [39]. These substrates contain phenols which can act as chelating agents for Fe. Correcher *et al.* studied the influence of gallic acid as a model chelating agent on the HTC of glucose and $Fe(NO_3)_3$ solutions [35]. Their results suggest that the addition of chelating agents that do not carbonize themselves leads to a smaller particle size, higher Fe content and Fe-NP-like properties. For our planned application, we are aiming for composites with higher C contents in order to receive the favorable properties of a porous C phase with regard to local enrichment of pollutants and enhanced reactivity of the Fe phase [17, 40]. Gluconate, as used by *Luo et al.*, could be a compromise between a complexing agent and a C precursor that is able to carbonize in the presence of Fe [1]. An advantage might be that the Fe content of the resulting product can be adjusted more freely compared to the other synthesis methods. It is worth noting that approach (II) with dissolved iron salts gives rise to iron oxide particles rather than ZVI because HTC conditions are not strongly reducing. Reactivity for reduction processes (*e.g.* dechlorination) has to be implemented in a subsequent treatment step such as pyrolysis (carbothermal reduction: $FeO_x + C \rightarrow Fe^0 + CO_x$).

1.2 Derived approach for the experimental study presented here

The goal of this work was to find a bottom-up synthesis of an Fe/C composite, *i.e.* starting from dissolved Fe and C precursors and combining them within one step. The composite material should be mechanically stable, have a small particle size (in the lower µm range) and colloidal properties, and provide reactivity for reductive dechlorination reactions. Starting from dissolved iron/carbon precursors, different one-pot processes were investigated and the resulting product morphologies were evaluated.

Carbothermal reduction/activation of the HTC-generated Fe/C composite was used to further process the most promising material obtained from HTC of iron and sodium gluconate for application. To date, there are no studies in the literature investigating colloidal Fe/C composites from one-pot HTC synthesis and carbothermal reduction for dechlorination reactions. Therefore, we characterized for the first time the colloidal properties of the HTC-derived Fe/C composites in aqueous suspensions and the reactivity of the synthesized composite with respect to reductive dechlorination, including XRD and XPS analyses of the fresh *vs.* spent composites. In addition, the Fe/C composites were palladized and the product selectivity regarding the chloroform (CF) degradation was monitored. The known change in the reaction mechanism of palladized ZVI-based materials from electron-driven reductive dechlorination (Fe/C) to hydrodechlorination (Pd/Fe/C) [41] led to a significant enhancement of the selectivity towards fully dechlorinated and hydrogenated products. The selectivity of Pd/Fe/C was compared with Pd/Carbo-Iron® and other typical Pd-containing catalyst materials (Pd/AC, Pd/ZVI, Pd/magnetite, Pd/Al_2O_3 and Pd-NPs). The effects of palladization were tested because Pd not only increases the reaction rate but also broadens the spectrum of degradable compounds. For example, ZVI alone is not capable of attacking chlorinated aromatics, but Pd/ZVI is [42]. We are aware that Pd can have some adverse health effects when exposure to dissolved Pd^{2+} occurs [43]. However, Pd on ZVI is usually very stable and does not tend to dissolve, as Pd is more noble than ZVI [44]. The use of Pd-containing materials has been demonstrated regarding *in-situ* purification of groundwater [45] and it might remain necessary to use them in the future at contaminated sites with challenging pollutants – always subject to country-specific regulations. The herein synthesized composites could potentially be applied for *in-situ* contaminant retention and degradation, *e.g.* in percolation systems or aquifers.

Table 2 Literature studies on the synthesis of colloidal Fe/C composites *via* HTC with dissolved Fe and C precursors.

Ref.	Experimental	Result/Comments	Planned Application(s)
Xuan *et al.* [36]	• Glucose (0.25 M), $FeCl_3$ (0.15 M) + urea (2.5 M) in water • HTC at 180 °C for 14 h	• Well-dispersed particles (100–200 nm diameter) • Carbon shell and single crystalline Fe_3O_4 core	Magnetic carrier (not tested)
Luo *et al.* [1]	• $FeCl_3$ (0.05 M) + sodium gluconate (0.15 M) in water • HTC at 180 °C for 48 h	• Dispersible and spherical Fe/C composites with multiple Fe_3O_4 cores, coated with a carbonaceous phase	Reagent for photo-Fenton reaction (tested for the oxidation of methylene blue)
Sun *et al.* [33]	• Glucose (0.5 M), $Fe(NO_3)_3$ (0.1 M) • HTC at 180 °C for 18 h • Thermal treatment at 350, 550 or 750 °C for 2 h	• Carbonaceous spheres of about 6–8 µm decorated with Fe-NPs	Catalyst for the activation of peroxymono-sulfate (tested for the oxidation of phenol with sulfate radicals)
Yan *et al.* [39]	• $FeCl_2$ (0.2 M) dissolved in a sugar solution derived from the acid hydrolysis of pine wood chips • HTC at 160–180 °C for 8 h • Thermal treatment at 700 °C for 1 h	• Aggregates with diameters of a few microns consisting of spherical Fe-NPs coated with a thin carbon shell	Catalyst for Fischer-Tropsch synthesis (tested with biomass derived syngas)
Liang *et al.* [34]	• $Fe(NO_3)_3$ and glucose in a 1:6 molar ratio • pH adjusted to 2, 4, 6 or 8 • HTC at 180 °C for 12 h	• Depending on pH during HTC microspheres from approx. 2–10 µm decorated with dispersed or large aggregates of NPs	Reagent for photo-Fenton reaction (tested for the oxidation of Orange II)
Calderon *et al.* [38]	• $Fe(NO_3)_3$ (0.2 M) dissolved in olive mill wastewater • HTC at 180–275 °C for 0.5–18 h	• Aggregates with diameters of (130 ± 50) nm consisting of Fe-NPs with 4 nm diameter coated with 1 nm carbon shell	Adsorbent/Reagent for removal of heavy metals (tested for Cu, Zn, Cr, Ni, Cd)
Correcher *et al.* [35]	• Glucose (0.17 M), gallic acid (0.02–0.06 M) $Fe(NO_3)_3$ (0.06–0.09 M), pH adjustment to various starting pHs between 1 and 12 • HTC at 180 °C for 5 h	• Aggregates consisting of Fe-NPs with thin carbon shells	Catalyst for Fischer-Tropsch-synthesis
Munoz *et al.* [37]	• $Fe(NO_3)_3$ (0.2 M) dissolved in olive mill wastewater • HTC at 225 °C for 3 h • Thermal treatment at 800 °C for 3 h	• Aggregates with diameters of a few microns consisting of Fe-NPs with a carbon shell (30–50 nm composite diameters)	Adsorbent (tested for diclofenac, sulfamethoxazole, metronidazole)
Jiang *et al.* [32]	• Glucose (0.6 M), $FeCl_2$ (0.05 M), $FeCl_3$ (0.07 M) + Urea (0.8 M) in water • HTC at 200 °C for 10 h • Functionalization with sulfonic acid groups	• Carbonaceous spheres of about 5 µm with partially attached ‘clouds’ of Fe_3O_4-NPs in between the spheres	Adsorbent (tested for methylene blue)

2 Materials and Methods

2.1 Chemicals

All chemicals were purchased in analytical grade or higher. The detailed information about chemicals used in the experiments and materials used as catalyst support can be found in the supporting information (SI) in Text S1.

2.2 Bottom-up synthesis of Fe/C

After the screening of different Fe and C precursors (*cf.* SI Text S2 and Figure S1), colloidal Fe/C composites were synthesized *via* HTC of ferrous gluconate dihydrate (30–60 g L^{-1}) at 180 °C for 24 h in the absence and in the presence of CMC (0.6–1.5 g L^{-1}, resulting in 1 wt.-% related to the combined weight of ferrous and sodium gluconate). In order to adjust the Fe/C ratio, different concentrations of sodium gluconate (0–120 g L^{-1}) were added to the reaction mixture. The native pH_0 values prior to HTC were 4.6 ± 0.1 for mixtures with molar ratios of $n_{Fe}/n_{gluconate}$ = 1/2 and 5.3 ± 0.1 for $n_{Fe}/n_{gluconate}$ = 1/10, respectively. In some cases, the pH_0 was adjusted with 1 M HCl or 1 M NaOH above or below the native values. The dark brown/ black precipitates obtained after HTC were washed with de-ionized water, dried and pyrolyzed at 800 °C for 2 h under N_2 with a heating rate of 1 K min^{-1}, in order to (partially) reduce the iron oxide species in the composite to ZVI. The resulting Fe/C composites were characterized for their material properties as well as their reactivity in the dechlorination of chloroform (CF). In order to ameliorate the selectivity of the CF degradation to fully dechlorinated products, the composites were palladized and their dechlorination performance was compared with that of various other palladized catalysts.

2.3 Preparation of palladized catalyst materials

2.3.1 Pd/Fe/C

For palladization of the Fe/C as well as Carbo-Iron® colloids, the particles were dispersed in de-oxygenated and de-ionized water *via* 10 min of ultrasonic treatment after shaking for approximately 24 h. Afterwards, the appropriate amount of a stock solution of Pd(II) acetate ($Pd(CH_3COO)_2$) was added to achieve Pd contents of 1–4 wt.-%, the mixture was vigorously shaken by hand for 30 s and then placed onto a horizontal shaker for 30 min until the aqueous phase was completely colorless. The palladization took place *via* the redox reaction according to eq. (1):

$$Fe + Pd^{2+} \rightarrow Fe^{2+} + Pd \qquad (1)$$

Afterwards, the composite was washed with de-oxygenated methanol and dried under N_2 atmosphere.

2.3.2 Pd/AC

A slightly modified method as previously reported by [46] was used to prepare Pd/AC. Pd ions were reduced with H_2. 10 g of AC ($d \approx 1$ µm) were suspended in 1 L deionized water, dispersed for 30 min in an ultrasonic bath and spiked with the calculated amount of $Pd(ac)_2$ stock solution resulting in a Pd content of 1 wt.-%. The mixture was vigorously shaken for 1 h and centrifuged to separate liquid and solids. The separated solids were suspended in 1 L de-ionized water and purged with H_2 (100 mL min^{-1}) for 1 h to ensure the complete reduction to Pd^0. The resulting catalyst was washed with de-ionized water and ethanol and then dried in an oven at 100 °C under N_2 overnight.

2.3.3 Pd/ZVI

For Pd/ZVI synthesis, Nanofer Star iron was used as the carrier material. 3 g of the commercial nZVI was suspended in de-ionized and de-oxygenated water, dispersed for 15 min in an ultrasonic bath and then spiked with the calculated amount of $Pd(ac)_2$ stock solution resulting in a Pd content of 1 wt.-%. The mixture was vigorously shaken for about 3 h to ensure the complete reduction of Pd^{2+} (de-colorization of the solution). The solid was washed with de-ionized water and ethanol and then dried under N_2 atmosphere. To exclude possibly formed free Pd-NPs, a magnet was used to exclusively separate Pd/ZVI from the mixture.

2.4 Dechlorination reactions

Dechlorination tests of CF were performed with all synthesized materials in 10 mM $NaHCO_3$ solution (pH = 8.5). For this, 25 mL solution was filled in a 55 mL vial and purged with N_2 for 20 min. 15–25 mg of composite material was added and the suspension including headspace was purged for another 10 min. The reaction system was pre-conditioned by shaking the mixture overnight. Afterwards, it was placed in an ultrasonic bath for 10 min, in order to ensure the dispersion of the particulate composite. The batches were then spiked with the according amount of acetonic stock solution of CF resulting in $c_{0,CF} = 10$ mg L^{-1} in the aqueous reaction mixture. The progression of the reaction was checked by analyzing the educts and products *via* headspace sampling and gas chromatography coupled with mass spectrometry (GC/MS) or with a flame-ionization detector (FID, for light hydrocarbons).

For the comparison of various palladized materials, external H_2 supply was ensured by purging the reaction batches additionally with H_2 for 15 min before sealing them in an airtight way and starting the reaction by adding CF.

In order to compare the performance of the synthesized composites, product selectivities (*S*) towards fully dechlorinated products were determined, using eq. (2) where $Y_{C1,C2}$ is the amount of carbon in the respective products (CH_4, C_2H_4, C_2H_6) and X_{CHCl_3} the amount of converted CF carbon. The extent of CF conversion was ≥ 90 mol-% for all monitored reactions.

$$S = \frac{Y_{C1,C2}}{X_{CHCl_3}} \tag{2}$$

The kinetics of the CF degradation was evaluated according to a first-order model. This description is rather simplified as the reaction system is complex regarding three fractions of CF in equilibrium – adsorbed on the solid composite, dissolved in the aqueous phase and gasous in the batch headspace. Less than 20 % of the CF present in the reaction batches was adsorbed on the composite materials under the applied conditions. Due to the overlying processes of adsorption and reductive dechlorination of the CF with the Fe/C composites, the reaction kinetics was investigated based on product formation as the main products are not significantly adsorbed. Specifically, the total CF concentration at a certain reaction time c_t was estimated based on the molar concentrations of the volatile main products DCM, ethane and methane formed at that time *t*. Despite the complex reaction system, the linearized graphs were well fitted with eq. (3) (*cf.* Figure S3) and an observed rate constant k_{obs} was determined in order to describe the reaction rates of the monitored CF degradation.

$$\ln (c_{0,CF} - \Sigma\, c_{products,i} \cdot n_{carbon,i}) = -k_{obs} \cdot t + \ln (c_{0,CF}) \tag{3}$$

$c_{0,CF}$ is the initial molar concentration of CF and $c_{0,CF} - \Sigma\, c_{products,i} \cdot n_{carbon,i}$ is the estimated CF concentration after certain reaction times. The number of carbon atoms $n_{carbon,i}$ in the products *i* takes into account the reaction stoichiometry.

For the comparison of ZVI reactivities, the observed rate constants were normalized to the mass concentrations of ZVI in suspension (c_{ZVI} [g L^{-1}], eq. (4)).

$$k_{\text{norm}} = \frac{k_{\text{obs}}}{c_{\text{ZVI}}} \tag{4}$$

For the comparison of the various palladized composite materials, a second-order rate constant expression was used: the specific catalytic activity A_{Pd} [L g^{-1} min^{-1}] according to eq. (5).

$$A_{\text{Pd}} = \frac{1}{c_{\text{Pd}} \cdot \tau_{1/2}} = \frac{k_{\text{obs}}}{c_{\text{Pd}} \cdot \ln(2)} \tag{5}$$

A_{Pd} is based on the applied concentration of palladium c_{Pd} [g L^{-1}] and the substrate half-life $\tau_{1/2}$ [min].

For the characterization of selected materials *via* XPS and XRD after palladization and after the reductive dechlorination of CF, the composites were washed with de-oxygenated water and methanol several times and dried at 80 °C under N_2. This approach was used to get an impression of the change of material components. We are aware that the state of the material during the reaction in aqueous media cannot be depicted by these analysis techniques.

2.5 Analysis methods

Microscopic images were recorded with a VHX digital microscope (Keyence).

The scanning electron microscopy (SEM) analyses were conducted with a Zeiss Merlin VP compact with a beam current of 250 pA and electron landing energy of 10 kV.

The particle diameters in aqueous suspension were analyzed with a Mastersizer 3000 (Malvern Panalytical). Samples were prepared by dispersing the Fe/C composites in 10 mM $NaHCO_3$ solution in the presence of CMC as stabilizing agent. The native pH (8.5 ± 0.3) of the suspensions was recorded with a pH meter (MP225, Mettler Toledo) equipped with a glass electrode (InLab® Micro, Mettler Toledo).

The specific surface area (*SSA*) was determined with a Belsorp MINI (BEL Japan). Adsorption/desorption of N_2 was performed at -196 °C after pretreatment of the samples under vacuum at 100 °C overnight. The obtained data were evaluated according to the BET theory.

In order to determine the reactive ZVI equivalents in the synthesized Fe/C composites (simplistically called 'ZVI' in the following text), 1 mL of half-concentrated HCl was added to 10 mg of the dry composites under inert atmosphere (V = 250 mL) and measuring the evolved H_2 with a GC-6850 (Agilent) coupled with a thermal conductivity detector (TCD) and a HP plot column.

The solid sample composition was explored by X-ray photoelectron spectroscopy (XPS, Kratos Ultra DLD) and X-ray diffraction (XRD, ULTIMA IV, Rigaku). The analyses parameters are described in detail in the SI (Text S5).

For the determination of dissolved chloride, aqueous samples were filtered by cellulose acetate filters (Ø 0.45 µm) and were analysed by ion chromatography (Dionex Integrion HPIC, Thermo Scientific).

GC/MS analyses were performed with a GCMS-QP2010 (Shimadzu) equipped with a DB-5ms column (Agilent) (30 m × 0.25 mm × 0.25 µm). Headspace samples (CF, DCM, monochloromethane) were injected at 200 °C with a column temperature of 60 °C and a He flow of 1 mL min^{-1}. The MS detector conditions were as follows: ion source at 250 °C, 70 eV, detection in the single-ion monitoring (SIM) mode.

Methane, ethane and ethene were measured with a GC-2010 plus (Shimadzu, GS-Q Plot column (Agilent)) coupled with an FID at an injection temperature of 200 °C and a column temperature of 60 °C. The quantification of the GC/MS and GC/FID analyses was based on external calibration with vials containing defined concentrations of CF/DCM and methane/ethane/ethene, respectively.

3 Results and Discussion

3.1 HTC of ferrous and sodium gluconate for generating colloidal Fe/C composites

After the screening of various Fe and C precursors (*cf.* SI, Text S2. And Figure S1), ferrous gluconate was chosen as precursor in order to benefit from the complexation of the Fe ions by gluconate during the early particle formation process under HTC conditions (*cf.* Figure 2). The final ZVI content of the composite was modified by the addition of sodium gluconate resulting in different molar ratios of Fe/gluconate ranging from 1/2 to 1/10. The HTC was performed in the presence and in the absence of CMC in order to investigate a possible influence of the stabilizing agent on the particle morphology [47]. The SEM images of the prepared samples are displayed in Figure S2. In principle, no significant differences between the samples were observed with digital microscopy. The SEM analysis (Figure 1) of the Fe/C composite shows rather small and spherical primary particles. However, the effective particle size observed in aqueous suspensions was much larger (*cf.* Table 3), suggesting that the primary particles become agglomerated during the hydrothermal synthesis and form aggregates of a few microns.

Fe/gluc 1/2

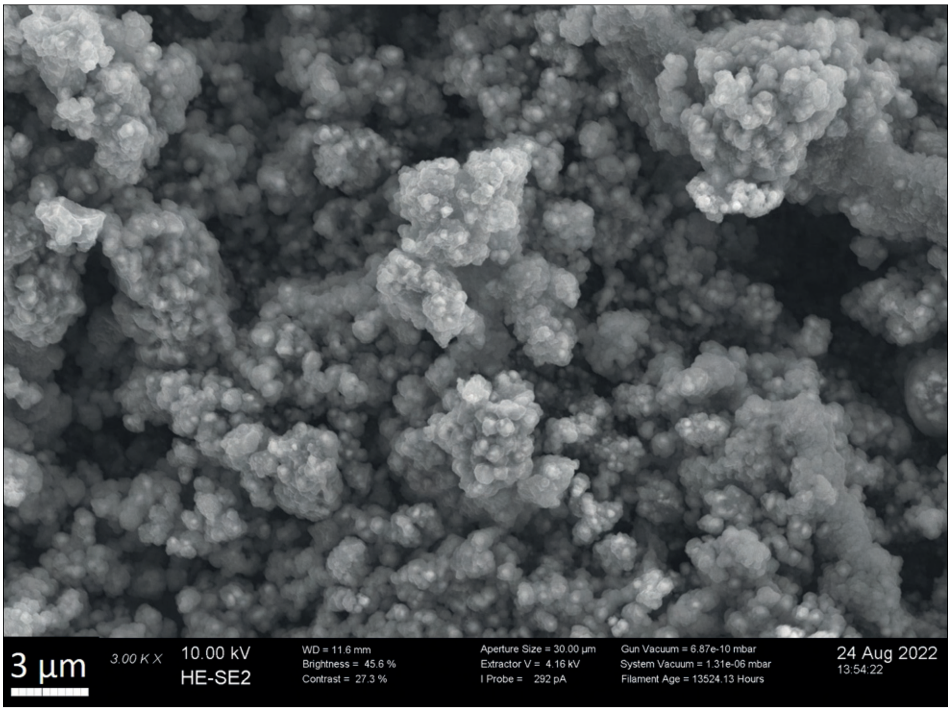

Figure 1 SEM image of the Fe/C composite synthesized *via* HTC of 120 g L^{-1} Na gluconate + 30 g L^{-1} Fe gluconate dihydate with subsequent carbothermal reduction at 800 °C under N_2.

We assume that due to the formation of the $Fe^{2+/3+}$ gluconate complexes during synthesis the reaction system provides an inherent stability avoiding the disintegration of the two elements. However, a too low Fe concentration would lead to an insufficient carbonization of the C precursor, as gluconate alone does not carbonize into particles under the applied HTC conditions ($pH_{0,adjusted}$ = 5.3, 180 °C, 24 h). Due to its properties regarding the HTC process [48], the addition of Fe enables the carbonization of gluconate in our system. Typically, it is proposed that the promoting effect of iron acts mainly in the form of acidification and complexation with the organic matter formed [48]. Considering the growth mechanism proposed by Jung *et al.*, the agglomeration of the initially formed nuclei is indeed a crucial step during the HTC process of soluble carbohydrates to enable particle growth [49]. However, in our case, we could rule out the sole pH effect because, as mentioned above, we did not observe any particle formation after the HTC of a sodium-gluconate solution that had been adjusted to the native pH of the ferrous gluconate solutions ($pH_0 \leq 5.3$). Therefore, we assume that the complexation of gluconate with ferrous/ferric ions might ensure local carbohydrate concentrations which are sufficiently high for enabling the intermolecular dehydration and polymerization reactions that lead to nucleation of the carbonaceous phase. Furthermore, it is assumed that the Fe ions not only ensure the complexation but might also participate in redox reactions [48, 50] that enable decarboxylation and dehydration reactions which are the initial steps during HTC processes. That is why we propose that a more homogeneous distribution of the Fe throughout the reaction mixture ensures a controlled carbonization process.

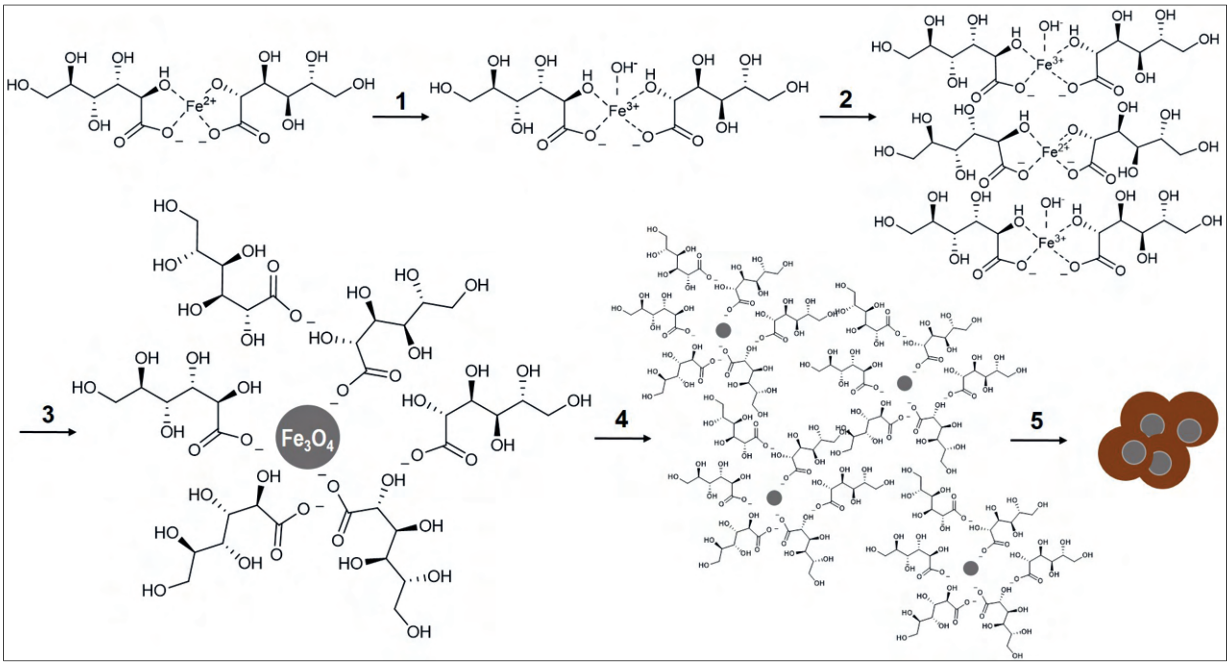

Figure 2 Proposed formation mechanism of Fe/C composites during the HTC of ferrous and sodium gluconate (scheme developed based on the proposed mechanism of [1]). The arrows represent simplified synthesis steps during the HTC process of ferrous gluconate: **1)** partial oxidation of Fe^{2+} to Fe^{3+}, **2)** assembly, **3)** formation of magnetite, **4)** coordination/agglomeration, **5)** formation of carbonaceous particles through dehydration, condensation, polymerization and aromatization reactions

This effect might be most distinct when the Fe/gluconate molar ratio is 1/2 in order to ensure a complete complex formation throughout the reaction mixture. In Table 3 the resulting ZVI contents of the samples with different molar Fe/gluconate ratios are displayed and ranged from (24 ± 12) to (49 ± 15) wt.-% after carbothermal reduction at 800 °C. Due to the necessity of Fe species for carbonization of the gluconate, it is anticipated that the ZVI contents of the resulting composites cannot be adjusted fully independently. Furthermore, the high variability of the lowest synthesized ZVI content of (24 ± 12) wt.-% in three replicate samples suggests a poorly controlled carbonization process presumably resulting in a more heterogeneous composite. Additionally, when the molar ratio of Fe/gluconate was decreased to 1/10, a decrease in the overall mass yield of composite particles down to (4 ± 1) wt.-% (related to the total mass of the introduced precursors Fe and gluconate) indicates in turn an incomplete carbonization of the sodium gluconate due to an iron deficiency. The mass yield was slightly increased and the deviation between replicates was decreased when 1 wt.-% CMC was added during the HTC compared to the synthesis in the absence of CMC. This could be due to the known stabilization effect of CMC which might reinforce a homogeneous distribution of the Fe throughout the reaction mixture and thus slightly enhancing the carbonization of gluconate. This assumption was tested with the HTC of $n_{\mathrm{Fe}}/n_{\mathrm{gluconate}} = 1/2$ in the presence of 2 wt.-% CMC (related to the combined weight of ferrous and sodium gluconate) where the char yield increased from 20 to 24 wt.-% after HTC (data not shown). However, the higher mass yield was accompanied by a loss of product homogeneity, confirming previous findings that small particle sizes and mass yields are a natural trade-off in HTC processes [47, 51].

From Table 3 it can be seen that all synthesized composites provide broad particle size distributions from $d_{10} \geq 2$ to $d_{90} \leq 40$ µm in suspension. It is assumed that this is mostly due to agglomeration of the primary particles as a result of their ferromagnetic properties. The optimization of the resulting particle diameters towards a narrow size distribution in the range of a few µm was aspired but not achieved neither

Table 3 Characterization of Fe/C composites synthesized *via* HTC of ferrous and sodium gluconate and subsequent carbothermal reduction. Listing of ZVI contents (after carbothermal reduction), particle diameters in aqueous suspension (determined with dynamic light scattering), specific surface areas (SSA_{BET}) and mean pore diameters (d_{pore}) (both determined *via* N_2 ad/desorption) and their overall mass yields after carbothermal reduction. Note that the error ranges of the ZVI-contents, SSA_{BET}, d_{pore} and yield represent the mean deviation of single values from the mean value of at least two replicate synthesis experiments; the error ranges of the particle diameters represent the mean deviation of single values from the mean value of two measurements of the same sample.

n_{Fe} / $n_{gluconate}$	ZVI content [wt.-%]	Particle diameters [µm]			SSA_{BET} [m^2 g^{-1}]	d_{pore} [nm]	Yield [wt.-%]
		d_{10}	d_{50}	d_{90}			
1/10 + CMC	24 ± 12	2.2 ± 0.1	7.5 ± 0.3	31 ± 2	220 ± 50	6 ± 1	5 ± 1
1/5 + CMC	37 ± 5	n/d	n/d	n/d	150 ± 30	7 ± 1	9 ± 1
1/2 + CMC	42 ± 6	3.5 ± 0.1	12.6 ± 0.1	34.6 ± 0.4	140 ± 30	7 ± 1	11 ± 1
1/10	31 ± 4	3.4 ± 0.1	14.0 ± 0.1	36.2 ± 0.2	280 ± 60	4 ± 1	4 ± 1
1/5	34 ± 13	n/d	n/d	n/d	160 ± 40	7 ± 1	8 ± 2
1/2	49 ± 15	2.6 ± 0.1	9.2 ± 0.1	31.1 ± 0.1	160 ± 40	7 ± 1	10 ± 5

through the addition of CMC during the HTC process nor through the adjustment of initial pH values (*cf.* Figure S3 and Text S4). Nevertheless, the suspension stability of the herein synthesized composites was effectively enhanced compared to nZVI particles (*cf.* Figure S10). Although the particle diameters of the composite material might be too large for low-pressure injections into aquifers or soils [52], injection techniques for micro-sized ZVI could be used in order to apply the material *in situ* [11].

In order to generate the desired reactivity for *in-situ* remediation, carbothermal reduction of the composites was necessary. During this pyrolysis process, the composites encountered a mass loss (46 ± 2) wt.-% enabling the formation of a porous structure. This resulted in overall mass yields of ≤ 10 wt.-% (related to the Fe and gluconate input) of the herein applied synthesis process. The influence of the pyrolysis step on the particle diameters in aqueous suspension was investigated regarding the composite synthesized at n_{Fe}/$n_{gluconate}$ = 1/10. After the HTC synthesis and prior to pyrolysis, the composite featured particle diameters ranging from $d_{10} \geq 4$ to $d_{90} \leq 80$ µm. Those were significantly reduced during the carbothermal reduction to $d_{10} \geq 3$ and $d_{90} \leq 35$ µm (*cf.* Table 3). This effect might on the one hand be rooted in the partial volatilization of the carbonaceous phase (decrease of oxygen content) due to pyrolysis and porosity generation. On the other hand, the Fe phase in the composite after HTC consists mainly of magnetite while, after carbothermal reduction, ZVI and Fe_3C are present (*cf.* Figure S6-S7). The latter exhibit different magnetic properties which may lead to less pronounced agglomeration effects.

The *SSA* of the composites were in the range of 140–280 m^2 g^{-1} with an increasing trend when the ZVI content was decreased. The resulting carbonaceous phase provided mean pore diameters in the mesopore range of about 4–7 nm. Regarding this, the samples differ from hydrochar which is pyrolyzed in the absence of iron where a strictly microporous system is developed [53, 54]. The increase in pore diameters results from the catalytic effect of iron oxides on the pyrolysis of carbon materials [55].

3.2 Reductive dechlorination of CF with the synthesized Fe/C composites

In order to test the accessibility and activity of the reactive iron in the composite for reductive dechlorination, CF was chosen as substrate. CF is a challenging target compound as its dechlorination proceeds *via* transfer of electrons or atomic hydrogen to DCM and methane as the two main products. Therefore, it not only allows to measure reaction kinetics of the reductive dechlorination but also the selectivities towards chlorinated and non-chlorinated products. The kinetic evaluation throughout this work was performed according to the first-order model as shown for exemplary samples in Figure S4.

Table 4 Normalized rate constants k_{norm} of CF degradation (*cf.* eq. 4) and distribution of the main products methane and DCM at 90 % CF conversion in relation to $c_{0,CF}$ with various Fe/C composites synthesized by HTC and carbothermal reduction ($c_{0,CF}$ = 10 mg L^{-1}, $c_{Fe/C}$ = 400–1200 mg L^{-1}, 10 mM $NaHCO_3$, pH_0 = 8.5. The error ranges represent the mean deviation of single values from the mean value of two replicate experiments

n_{Fe} / $n_{gluconate}$	ZVI-content [wt.-%]	k_{norm} [L g^{-1} h^{-1}]	Methane [mol-%]	DCM [mol-%]
1/10 + CMC	21 ± 1	0.04 ± 0.02	9 ± 2	72 ± 1
1/5 + CMC	39 ± 1	0.03 ± 0.01	10 ± 1	71 ± 1
1/2 + CMC	44 ± 6	0.017 ± 0.001	21 ± 3	48 ± 1
1/10	25 ± 2	0.023 ± 0.009	6 ± 1	60 ± 10
1/5	32 ± 1	0.020 ± 0.005	12 ± 2	62 ± 2
1/2	48 ± 2	0.023 ± 0.004	13 ± 1	73 ± 3

Table 4 shows that all Fe/C samples provide mass-normalized rate coefficients of (3 ± 1) · 10^{-2} L g^{-1} h^{-1} which is one order of magnitude higher than the rate coefficients recently reported in [56]. DCM is the dominant reaction product. Only traces of monochloromethane (MCM), ethene and ethane were found in all monitored reactions.

The formation of DCM is unfavorable with respect to remediation goals. DCM is hardly reactive towards further dechlorination with ZVI as reductant. Similar DCM yields were also observed for nZVI [41]. Thus, the Fe/C composites prepared in a one-pot HTC synthesis followed by carbothermal reduction

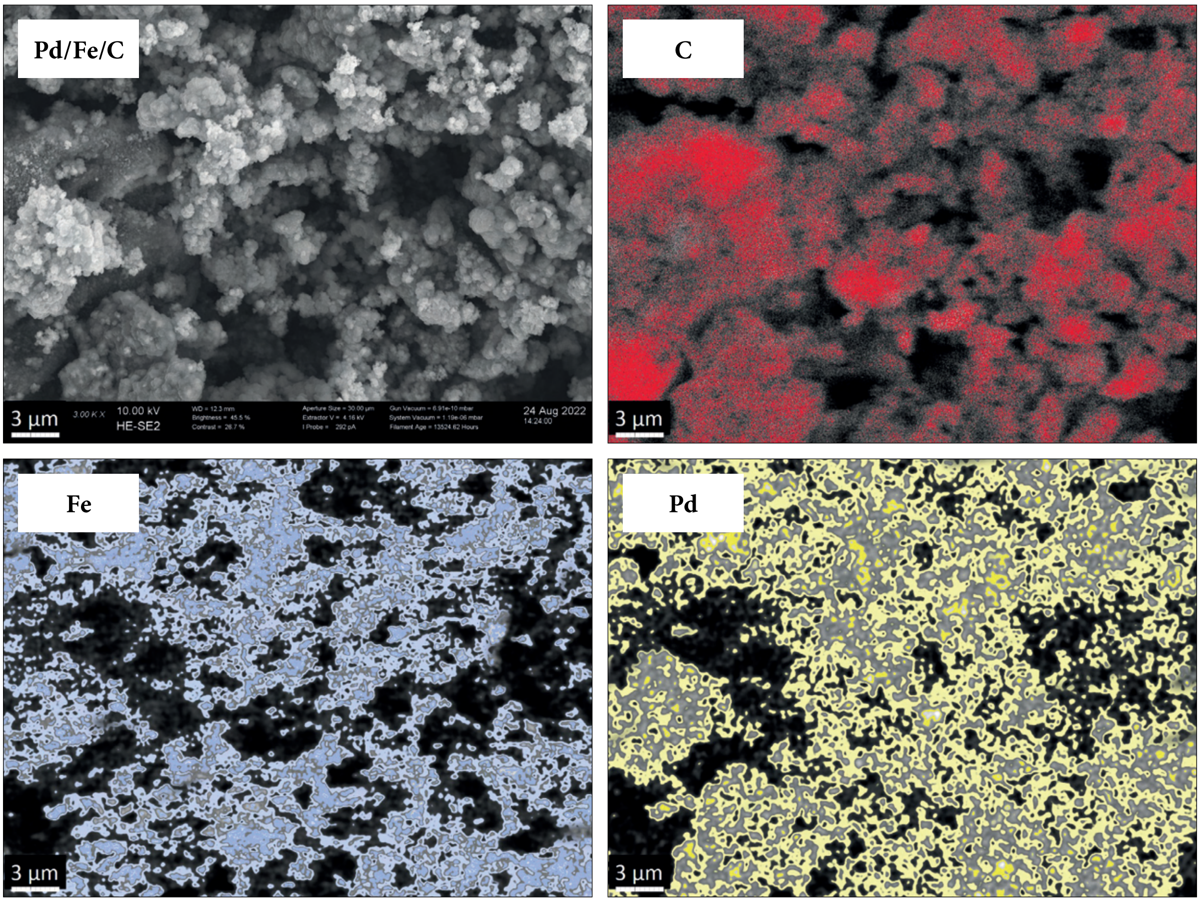

Figure 3 Elemental mapping with SEM/EDX analysis of a Pd/Fe/C composite containing ca. 30 wt.-% ZVI and 1 wt.-% Pd; C: red, Fe: blue, Pd: yellow.

are active in reductive dechlorination but show the same shortcomings for the dechlorination of chloromethanes as nZVI. In contrast, reactions involving Cu or noble metal catalysts and H_2 or borohydride as reductants show higher selectivities towards non-chlorinated products [41].

Accordingly, in order to improve the product selectivities of the Fe/C materials, their palladization with (1.2 ± 0.5) or (3.6 ± 0.5) wt.-% Pd was carried out resulting in Pd/Fe/C composites which were characterized with SEM-EDX. The elemental mapping shown in Figure 3 reveals that Pd is deposited predominantly as distinct clusters on the Fe-rich sites, as expected.

After palladization, CF dechlorination activities were greatly enhanced. Furthermore, ethane was observed as additional product in significant amounts. When the samples were palladized with (1.2 ± 0.5) wt.-% Pd, significant gaps in carbon mass balances were observed which ranged from 20–40 mol-% (*cf.* Figure S5 and Tab. S2).

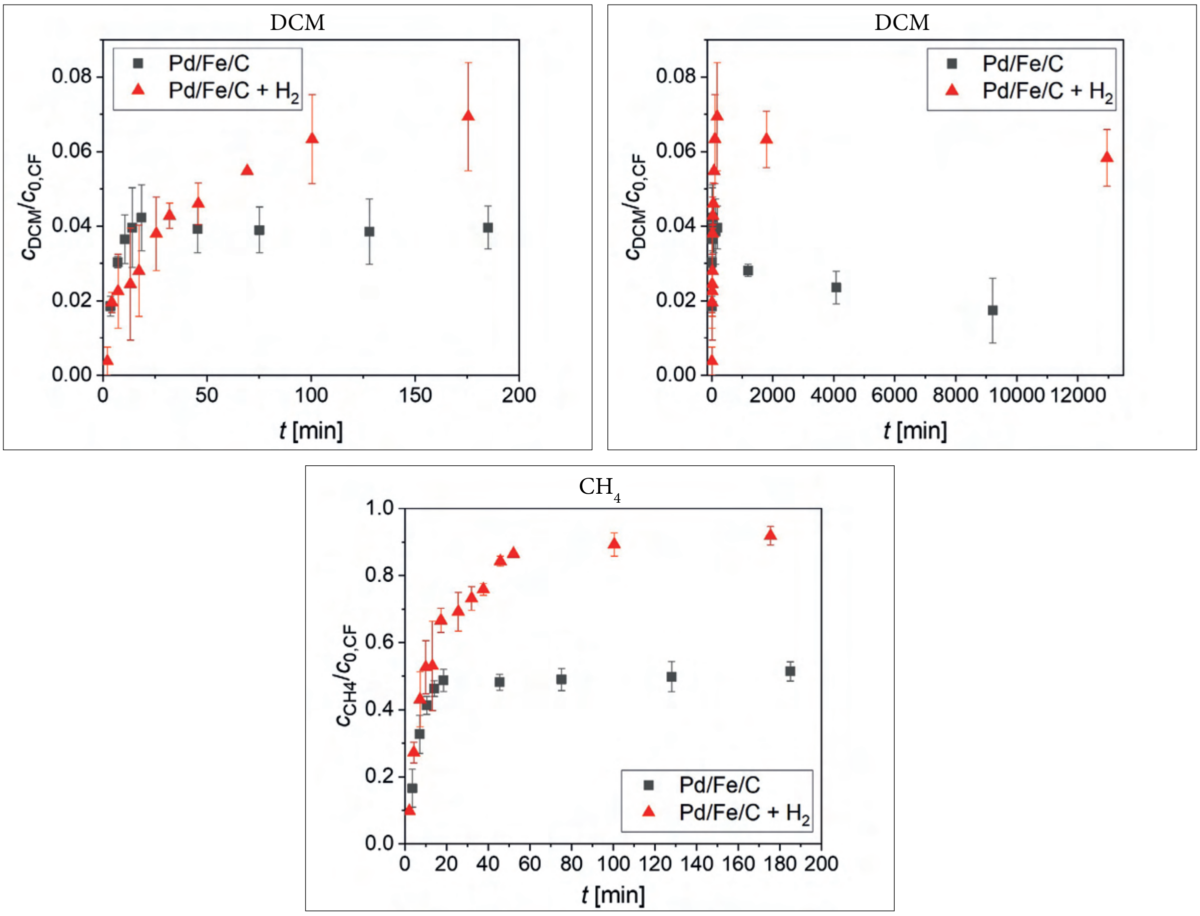

Figure 4 Formation of dichloromethane (DCM) and methane during reductive degradation of chloroform with Pd/Fe/C composites with 1.8 wt.-% Pd and 26 wt.-% ZVI under inert conditions and in H_2 atmosphere; note the different time scales in the two upper diagrams; the error bars represent the mean deviation of single values from the mean value of two replicate experiments.
$c_{0,CF}$= 7 mg L^{-1}, $c_{Pd/Fe/C}$ = 740 mg L^{-1}, c_{NaHCO_3} = 10 mM, pH_0 = 8.5.

In order to investigate the reason behind these gaps, the CF degradation was performed with Pd/Fe/C (35 wt.-% ZVI and 1.5 wt.-% Pd) in a pure H_2 atmosphere (*cf.* Figure 4). The resulting rate constants and catalytic activities for the CF degradation with Pd/Fe/C were essentially the same in the absence and in the presence of abundant H_2 (k_{norm} = (32 ± 7) L g^{-1} h^{-1} *vs.* (28 ± 4) L g^{-1} h^{-1} and A_{Pd} = (13 ± 3) L g^{-1} min^{-1} *vs.* A_{Pd} = (12 ± 2) L g^{-1} min^{-1}, respectively). This indicates that the availability of hydrogen is not rate limiting for the CF conversion, even with an initially inert gas atmosphere (N_2). This may be due to the fact that Pd is able to 'store' active hydrogen from the corrosion period prior to the reaction by chemisorption and make it available for CF degradation in the early reaction phase. However, with external H_2 supply, the selectivity towards methane at > 99 % CF conversion was drastically enhanced from (51 ± 1) to

(92 ± 1) mol-%. As the chloride yield with Pd/Fe/C ((87 ± 2) mol-%) was comparably high as the one with Pd/Fe/C + H_2 ((98 ± 5) mol-%), it is assumed that in both cases no excess amount of non-detected chlorinated byproducts besides DCM was formed. Instead, the observed propane formation led us to the assumption that radical-induced oligomerization processes take place [57, 58] which are obviously suppressed in the presence of abundant H_2 in the system. This assumption was strengthened by increasing the Pd content on the Pd/Fe/C samples to (3.6 ± 0.5) wt.-% Pd. At higher Pd contents and without external H_2 feed, the selectivities towards methane were increased up to 77 mol-% while the selectivities towards DCM were decreased to values as low as 2 mol-% at > 95 % CF conversion (*cf.* Figure S5 and Text S4). This was attributed to an increase in anaerobic ZVI corrosion when more Pd was present due to the formation of local galvanic couples on the composite surfaces [59, 60]. Figure 4 reveals a slow but significant conversion of DCM with Pd/Fe/C in the absence and in the presence of external H_2. The comparison of k_{norm} of DCM and CF of around 0.02 L g^{-1} h^{-1} *vs.* around 30 L g^{-1} h^{-1} shows that DCM is significantly less reactive than CF. This is in line with relative reactivities of halogenated compounds in hydrodehalogenation reactions on Pd/Al_2O_3 as catalyst in aqueous media [61].

In order to gain more insight into the material composition, the samples Fe/C (1/10, 35 wt.-% ZVI) and Pd/Fe/C (1/10, 35 wt.-% ZVI and 1.1 wt.-% Pd) were characterized by XRD and XPS before and after the degradation of CF. The XRD spectra are displayed in the SI part (Figs. S6–S7). The crystalline structures of the Fe/C sample "1/10" consist mainly of Fe_3C (23 wt.-%), Fe^0 (15 wt.-%) and graphite (62 wt.-%) before the reaction. It should be noted that it was not analyzed to what extent the composite material is crystalline or amorphous. The formation of crystalline phases like iron carbide and graphite during the one-pot synthesis of Fe/C materials have been reported earlier for the HTC starting from the lignocellulosic matrix pinewood and iron(III) nitrate with subsequent calcination [62]. Gai *et al.* stated that the formation of iron carbide phases contributes to the mechanical stability of the composite material. Fe_3C as well as Fe^0 seem to be consumed during the CF degradation and the crystalline phases of the resulting composite consisted of magnetite (15 wt.-%) and graphite (85 wt.-%), suggesting that the Fe_3C phase might play a role in the reductive dechlorination of CF. This phenomenon was recently investigated by Meng *et al.* who identified the potential of iron carbides to act as donor for electrons as well as atomic hydrogen (H^*) in the reductive dechlorination of trichloroethene [63].

The crystalline phases of the synthesized Pd/Fe/C composite consisted of Fe_3C (18 wt.-%), Fe^0 (3 wt.-%), magnetite (21 wt.-%), graphite (46 wt.-%) and Pd (0.3 wt.-%) previous to the reaction. After the reaction, Fe^0 was absent and an increase in magnetite was observed (29 wt.-%). Graphite was depleted to 30 wt.-%. This might be due to conversion into amorphous carbonaceous species resulting in an overall decrease of the crystalline phase of the composite during the contact with water. This could explain why the Fe_3C content formally increased (36 wt.-%) in the crystalline phase of the composite. The Pd content stayed essentially the same (0.8 wt.-%), indicating the prevention of Pd leaching when in contact with Fe [44]. It is assumed that due to the preparation method of wet impregnation with Pd, Fe^0 was used up to some extent prior to the dechlorination and converted into magnetite. However, most of the Fe_3C remained and might enable the efficient hydrodechlorination in the presence of Pd resulting in a very active composite despite the low Fe^0 content. The significant decrease of the XRD signal intensities for both Fe/C and Pd/Fe/C after the reaction indicated that the crystalline phases were partially converted to more amorphous structures. The surface of the composite materials before and after reaction was characterized with XPS (*cf.* Figs. S8–S9). For Fe/C, the same trends as in the XRD analyses could be followed, namely an increase in surface oxygen content due to the consumption of Fe^0 and Fe_3C during the anaerobic corrosion in the aqueous phase. The binding energy of the most pronounced peak (C1s) at 284.5 eV indicated a state of mostly C=C double bonds which is in agreement with the graphite content verified by XRD. In the palladized samples, about 0.5 at.-% Pd were found on the surface.

The performance of Pd/Fe/C regarding the product selectivities (eq. (2)) and specific catalytic activities (eq. (6)) were compared with Pd/Carbo-Iron® as well as Pd/AC, Pd/ZVI, Pd/magnetite Pd/Al_2O_3 and Pd nanoparticles (*cf.* Table 5). It should be noted that in order to compare all catalyst materials without possible rate limiting H_2-formation steps, external H_2 was supplied (p_{H_2} = 100 kPa). Under these conditions, methane was the main product with selectivities ≥ 85 mol-% for all investigated Pd-containing materials. Except of Pd/magnetite (with 1.5 mol-%), all investigated catalysts exhibited selectivities towards DCM of ≥ 5 mol-% increasing from Pd/Al_2O_3 (5.5 mol-%) < Pd/ZVI (5.8 mol-%) < Pd/Fe/C (6 mol-%) < Pd/Carbo-Iron® (7.4 mol-%) < Pd-NP (9.3 mol-%) and Pd/AC (10 mol-%). As the tested catalyst materials provided

Table 5 Specific catalytic activities A_{Pd} and product selectivities S of the CF dechlorination at 95 % conversion for various palladized materials; $c_{0,CF}$ = 10 mg L^{-1}, $c_{Pd/Fe/C,1/10}$ = 500 mg L^{-1}, $c_{Pd/Carbo\text{-}Iron}$ = 26 mg L^{-1}, $c_{Pd/AC}$ = 63 mg L^{-1}, $c_{Pd/magnetite}$ = 241 mg L^{-1}, c_{Pd/Al_2O_3} = 766 mg L^{-1}, c_{NaHCO_3} = 100 mM, pH$_0$ = 8.0–8.5, p_{H_2} = 100 kPa. The error ranges represent the mean deviation of single values from the mean value of two replicate experiments.

Pd-catalysts	**Pd-content**	**A_{Pd}**	***S* [mol-%]**			
	[wt.-%]	**[L g^{-1} min^{-1}]**	**methane**	**ethane**	**DCM**	**MCM**
Pd/Fe/C (w/o H_2)	4.0	9 ± 1	71	9.0	3.2	0.3
Pd/Fe/C	1.8	13 ± 1	85	3	6	0.6
Pd/Carbo-Iron®	1.1	190 ± 20	91.3	0.8	7.4	0.5
Pd/AC	0.8	40 ± 6	86	2.6	10	1.4
Pd-NP	100	20 ± 4	90.2	0.4	9.3	0.1
Pd/ZVI	0.8	1.4 ± 0.5	93.5	0.5	5.8	0.2
Pd/magnetite	0.2	10 ± 1	97.6	0.4	1.5	0.5
Pd/Al_2O_3	0.5	9 ± 1	94.4	0.3	5.5	< LOQ

various particle sizes ranging from Pd-NPs (< 100 nm) to Pd/Al_2O_3 (25–63 µm), it has to be noted that the estimated catalytic activities can only be compared to some extent. The specific catalytic activity of Pd/Fe/C with external H_2 supply was in the same range as Pd/magnetite and Pd/Al_2O_3. In contrast, Pd/Carbo-Iron® featured the highest specific catalytic activity of (190 ± 20) L g^{-1} min^{-1} even though not having the lowest particle size and thus indicating the presence of most favorable Pd species. Presumably, the higher SSA_{BET} of 720 m^2 g^{-1} and the well-dispersed ZVI-NPs on the surface may also lead to a more favorable Pd dispersion.

In this work, it was shown that the synthesized Pd/Fe/C composites degraded CF with a high chloride and low DCM yield even without external supply of H_2 but solely by intrinsic H_2 or H^* from the anaerobic ZVI corrosion as required for *in-situ* remediation materials (*cf.* Figure S5). It is noteworthy, that for the reactions in the absence of external H_2, equally high selectivities towards non-chlorinated products and even a decrease of the selectivities towards the chlorinated by-products DCM and MCM could be achieved. However, this favorable effect was only observed at high Pd contents of up to 4 wt.-% (*cf.* Table 5 and S2) which was necessary to ensure a sufficient internal H_2 supply from enhanced ZVI corrosion. This would be certainly a matter of cost for individual applications. Furthermore, the increase in ZVI corrosion naturally leads to a faster ZVI depletion in the composite and thus limits the time of the availability of H_2 which is not favorable for *in-situ* applications where long-term activities of the applied reagents are desired [64]. Therefore, the palladized materials might only be suitable for urgent remediation measures over a short time-frame. Regarding the Fe/C material, longer life times are expected comparable to similar *in-situ* reagents which can even be extended by sulfidation of the material [65].

4 Conclusion

Bottom-up synthesis of a colloidal and reactive Fe/C composite was demonstrated based on the HTC of ferrous and sodium gluconate and a subsequent carbothermal reduction step with mass yields of ≤ 11 wt.-%, depending on the molar ratio of Fe/gluconate. The resulting Fe/C composites provide specific surface areas of 140–280 $m^2 g^{-1}$ and a particle size distribution characterized by $d_{10} \geq 2$ µm, $d_{50} \approx 11$ µm and $d_{90} \leq 40$ µm. Thus, it can be concluded that the formation of dispersible Fe/C composites with uniform composition by a one-pot HTC process and subsequent carbothermal reduction is possible, but at the expense of a low mass yield and rather wide particle size distribution. The ZVI contents of the mechanically stable composites were adjusted from (24 ± 12) to (49 ± 15) wt.-%. The composite material was proven to provide reductive dechlorination activity as demonstrated for CF. However, the degradation reaction produced DCM as main product, showing as unfavorable selectivities as common ZVI-based reagents. The composite components of the synthesized Fe/C were characterized by XPS and XRD before and after the reaction, suggesting that Fe_3C could be an additional active Fe species besides pristine Fe^0. Palladization of the composites resulted in faster CF degradation and a shift in selectivity towards fully dechlorinated reaction products without external H_2 feed. Compared to other typical catalyst supports, selectivities of Pd/Fe/C were favorable as the selectivities were higher towards ethane and lower towards DCM. In the presence of external H_2, the palladized Fe/C composites behaved similarly to Pd/AC in terms of selectivities and to Pd/magnetite and Pd/Al_2O_3 in terms of specific catalyst activities. The dispersibility with particle diameters below 50 µm, and mechanical stability of the synthesized composites could be advantageous for water treatment applications. However, despite considerable efforts, perfectly uniform composite particles in the size range suitable for low-pressure injection, *i.e.*, about 1 µm, could not be achieved. Nevertheless, the synthesized composites could be used *in-situ* with technologies that are already used for the application of µZVI or in percolation systems where adsorbents/reagents need to be added to retain and degrade contaminants. Future studies should therefore include additional reactivity testing in environmental media and long-term activity.

Acknowledgement: This study was funded by “Deutsche Forschungsgemeinschaft” (DFG), project number 392011053.

The authors thank Dr. Robert Köhler and Dr. Matthias Schmidt for the SEM analysis which was done at ProVIS – Centre for Chemical Microscopy at the UFZ, Leipzig, supported by European Regional Development Funds (EFRE-Europe funds Saxony) and the Helmholtz Association.

The authors are much obliged to Birgit Forkert and Wenbi Guan from the Department of Environmental Engineering (UFZ, Leipzig) for their experimental support by conducting the ion chromatography and BET analyses and performing additional dechlorination experiments. The authors acknowledge the laser diffraction analytics performed by ZetA Partikelanalytik GmbH, Mainz, under the direction of Dr. Andreas Hahn, and the XRD as well as the XPS measurements performed under the direction of Dr. Jan Griebel at the Institute of Surface Engineering (IOM), Leipzig.

References

[1] Z. Luo, H. Tang, L. Qu, T. Han, X. Wu, *A visible-light-driven solid state photo-Fenton reagent basedon magnetite/carboxylate-rich carbon spheres*, CrystEngComm 14 (2012) 5710–5713.

[2] H. Tang, D.Q. Zhu, T.L. Li, H.N. Kong, W. Chen, *Reductive dechlorination of activated carbon-adsorbed trichloroethylene by zero-valent iron: carbon as electron shuttle*, Journal of Environmental Quality 40(6) (2011) 1878–1885.

[3] K. Mackenzie, S. Bleyl, F.-D. Kopinke, H. Doose, J. Bruns, *Carbo-Iron as improvement of the nanoiron technology: from laboratory design to the field test*, Sci. Total Environm. 563–564 (2016) 641–648.

[4] S. Bleyl, F.-D. Kopinke, K. Mackenzie, *Carbo-Iron® – synthesis and stabilization of Fe^0-doped colloidal activated carbon for in situ groundwater treatment*, Chem. Eng. J. 191 (2012) 588–595.

[5] H. Choi, S. Agarwal, S.R. Al-Abed, *Adsorption and simultaneous dechlorination of PCBs on GAC/Fe/Pd: mechanistic aspects and reactive capping barrier concept*, Environ. Sci. Technol. 43(2) (2009) 488–493.

[6] Intrapore, *CarboIron® – For the degradation of halogenated pollutants*, 2023. (Accessed 20.08.2023 2023).

[7] RPI®, *Safe & effective solutions: BOS 100*, 2023. https://www.trapandtreat.com/products/. (Accessed 19.09.2023).

[8] T. Tosco, M.P. Papini, C.C. Viggi, R. Sethi, *Nanoscale zerovalent iron particles for groundwater remediation: A review*, Journal of Cleaner Production 15 (2014) 10–21.

[9] N. Tufenkji, M. Elimelech, *Correlation equation for predicting single-collector efficiency in physicochemical filtration in saturated porous media*, Environ. Sci. Technol. 38 (2004) 529–536.

[10] A. Georgi, J. Bosch, J. Bruns, K. Mackenzie, N. Saeidi, F.-D. Kopinke, *Kolloidale Aktivkohle für die In-situ-Sanierung von PFAS-kontaminierten Grundwasserleitern*, altlasten spektrum 6 (2020) 221–264.

[11] F. Mondino, A. Piscitello, C. Bianco, A. Gallo, A. Folly D'Auris, T. Tosco, M. Tagliabue, R. Sethi, *Injection of Zerovalent Iron Gels for Aquifer Nanoremediation: Lab experiments and modeling*, Water 12 (2020) 826–841.

[12] K. Pandey, S. Sharma, S. Saha, *Advances in design and synthesis of stabilized zero-valent iron nanoparticles for groundwater remediation*, J. Environ. Chem. Eng. 10 (2022) 107993.

[13] D. Fan, D.M. O'Carroll, D.W. Elliott, Z. Xiong, P.G. Tratnyek, R.L. Johnson, A.N. Garcia, *Selectivity of nano zerovalent iron in* in situ *chemical reduction: challenges and improvements*, Remediation 26 (2016) 27–40.

[14] F.-D. Kopinke, G. Speichert, K. Mackenzie, E. Hey-Hawkins, *Reductive dechlorination in water: interplay of sorption and reactivity*, Appl. Catal. B 181 (2016) 747–753.

[15] B.H. Tan, K.C. Tam, Y.C. Lam, C.B. Tan, *Osmotic compressibility of soft colloidal systems*, Langmuir 21 (2005) 4283–4290.

[16] F.-D. Kopinke, S. Suehnholz, A. Georgi, K. Mackenzie, *Interaction of zero-valent iron and carbonaceous materials for reduction of DDT*, Chemosphere 253 (2020) 126712.

[17] M. Vogel, F.-D. Kopinke, K. Mackenzie, *Acceleration of microiron-based dechlorination in water by contact with fibrous activated carbon*, Sci. Total Environm. 660 (2019) 1274–1282.

[18] K. Mackenzie, A. Schierz, A. Georgi, F.-D. Kopinke, *Colloidal activated carbon and CARBO-IRON – Novel materials for in-situ groundwater treatment*, Glob. NEST J. 10 (2008) 54–61.

[19] J. Zhan, I. Kolesnichenko, B. Sunkara, J. He, G.L. McPherson, G. Piringer, V.T. John, *Multifunctional iron-carbon nanocomposites through an aerosol-based process for the* in situ *remediation of chlorinated hydrocarbons*, Environ. Sci. Technol. 45 (2011) 1949–1954.

[20] Q. Ning, Y. Liu, S. Liu, L. Jaing, G. Zeng, Z. Zeng, X. Wang, J. Li, Z. Kare, *Fabrication of hydrochar functionalized Fe-Mn binary oxide nanocomposites: characterization and 17β-estradiol removal*, RSC Advances 7 (2017) 37122–37129.

[21] J. Zhan, B. Sunkara, L. Le, V.T. John, J. He, G.L. McPherson, G. Piringer, Y. Lu, *Multifunctional colloidal particles for* in situ *remediation of chlorinated hydrocarbons*, Environ. Sci. Technol. 43 (2009) 8616–8621.

[22] G. Davies, J. McGregor, *Hydrothermal synthesis of biomass-derived magnetic carbon composites for adsorption and catalysis*, ACS Omega 6 (2021) 33000–33009.

[23] F. Di Caprio, A. Pellini, R. Zanoni, M.L. Astolfi, P. Altimari, F. Pagnanelli, *Two-phase synthesis of Fe-loaded hydrochar for As removal: The distinct effects of pH, reaction time and Fe/hydrochar ratio*, J. Environ. Manage. 302 (2022) 114058.

[24] H. Takaesu, H. Matsui, Y. Nishimura, T. Matsushita, N. Shirasaki, *Micro-milling super-fine powdered activated carbon decreases adsorption capacity by introducing oxygen/hydrogen-containing functional groups on carbon surface from water*, Water Res. 155 (2019) 66–75.

[25] X.-W. Wei, G.-X. Zhu, C.-J. Xia, Y. Ye, *A solution phase fabrication of magnetic nanoparticles encapsulated in carbon*, Nanotechnology 17 (2006) 4307–4311.

[26] Z. Wang, H. Guo, Y. Yu, N. He, *Synthesis and characterization of a novel magnetic carrier with its composition of Fe_3O_4/carbon using hydrothermal reaction*, Journal of Magnetism and Magnetic Materials 302 (2006) 397–404.

[27] J. Yang, J.-Y. Li, J.-Q. Qian, H.-Z. Lian, H.-Y. Chen, *Solid phase extraction of magnetic carbon doped Fe_3O_4 nanoparticles*, Journal of Chromatography A 1325 (2014) 8–15.

[28] N. Saleh, H.J. Kim, T. Phenrat, K. Matyjaszewski, R.D. Tilton, G.V. Lowry, *Ionic strength and composition affect the mobility of surface-modified Fe^0 nanoparticles in water-saturated sand columns*, Environ. Sci. Technol. 42 (2008) 3349–3355.

[29] K. Mackenzie, A. Georgi, *NZVI synthesis and characterization*, in: T. Phenrat, G.V. Lowry (Eds.), *Nanoscale zerovalent iron particles for environmental restoration*, Springer International Publishing AG, Basel, 2019, pp. 45–95.

[30] L. Bai, B. Mei, Q.-Z. Guo, Z.-G. Shi, Y.-Q. Feng, *Magnetic solid-phase extraction of hydrophobic analytes in environmental samples by a surface hydrophilic carbon-ferromagnetic nanocomposite*, Journal of Chromatography A 1217 (2010) 7331–7336.

[31] S. Zhang, H. Niu, Z. Hu, Y. Cai, Y. Shi, *Preparation of carbon coated Fe_3O_4 nanoparticles and their application for solid-phase extraction of polycyclic aromatic hydrocarbons from environmental water samples*, Journal of Chromatography A 1217 (2010) 4757–4764.

[32] X. Jiang, Y. Jia, D. Ren, N. Zhang, T. Peng, Z. Huo, *Magnetic seeds promoted high-density sulfonic acid-based hydrochar derived from sugar-rich wastewater for removal of methylene blue*, Environ. Sci. Pollut. 30 (2022) 36872–36882.

[33] H. Sun, G. Zhou, S. Liu, H.M. Ang, M. O Tadé, S. Wang, *Nano-Fe^0 encapsulated in microcarbon spheres: Synthesis, characterization and environmental applications*, ACS Appl. Mater. Interfaces 4 (2012) 6235–6241.

[34] C. Liang, W. Zhao, Z. Song, S. Xing, *Influence of precursor pH on the structure and photo-Fenton performance of Fe/hydrochar*, RSC Advances 7 (2017) 35257–35264.

[35] R. Correcher, Y. Budyk, A. Fullana, *Role of gallic acid in the synthesis of carbon-encapsulated iron nanoparticles by hydrothermal carbonization: Selecting iron oxide composition*, ACS Omega 6 (2021) 29547–29554.

[36] S. Xuan, L. Hao, W. Jiang, X. Gong, Y. Hu, Z. Chen, *A facile method to fabricate carbon-encapsulated Fe_3O_4 core/shell composites*, Nanotechnology 18 (2007).

[37] M. Munoz, J. Nieto-Sandoval, S. Torrellas-Álvarez, E. Sanz-Santos, B. Calderón, Z.M. de Pedro, M. Larriba, A. Fullana, J. García, J.A. Casas, *Carbon-encapsulated iron nanoparticles as reusable adsorbents for micropollutants removal from water*, Sep. Purif. Technol. 257 (2021) 117974.

[38] B. Calderon, F. Smith, I. Aracil, A. Fullana, *Green synthesis of thin shell carbon-encapsulated iron nanoparticles via hydrothermal carbonization*, ACS Sustainable Chemistry & Engineering 6 (2018) 7995–8002.

[39] Q. Yan, J. Street, F. Yu, *Synthesis of carbon-encapsulated iron nanoparticles from wood derived sugars by hydrothermal carbonization (HTC) and their application to convert bio-syngas into liquid hydrocarbons*, Biomass Bioenerg. 83 (2015) 85–95.

[40] Z.G. Liu, F. Zhang, S.K. Hoekman, T.T. Liu, C. Gai, N.N. Peng, *Homogeneously dispersed zerovalent iron nanoparticles supported on hydrochar-derived porous carbon: simple,* in situ *synthesis and use for dechlorination of PCBs*, ACS Sustainable Chemistry & Engineering 4(6) (2016) 3261–3267.

[41] A. Shee, F.-D. Kopinke, K. Mackenzie, *Borohydride and metallic copper as a robust dehalogenation system: Selectivity assessment and system optimization*, Sci. Total Environm. 810 (2022) 152065.

[42] H. Hildebrand, K. Mackenzie, F.-D. Kopinke, *Pd/Fe_2O_3 nano-catalysts for selective dehalogenation in wastewater treatment processes: Influence of water constituents*, Appl. Catal. B 91 (2009) 389–396.

[43] J. KIELHORN, C. MELBER, D. KELLER, I. MANGELSDORF, *Palladium - A review of exposure and effects to human health*, Int. J. Hyg. Environ. Health 205 (2002) 417–432.

[44] D.W. ELLIOTT, W.-X. ZHANG, *Field assessment of nanoscale bimetallic particles for groundwater treatment*, Environ. Sci. Technol. 35 (2001) 4922–4926.

[45] F. HE, D. ZHAO, C. PAUL, *Field assessment of carboxymethyl cellulose stabilized iron for in situ destruction of chlorinated solvents*, Water Res. 44 (2010) 2360–2370.

[46] H. HILDEBRAND, K. MACKENZIE, F.-D. KOPINKE, *Highly active Pd-on-magnetite nanocatalysts for aqueous phase hydrodechlorination reactions*, Environ. Sci. Technol. 43 (2009) 3254–3259.

[47] M. BALDA, K. MACKENZIE, F.-D. KOPINKE, A. GEORGI, *Uniform and dispersible carbonaceous microspheres as quasi-liquid sorbent*, Chemosphere (2022) 136079.

[48] V. SAADATTALAB, X. WANG, A.E. SZEGO, N. HEDIN, *Effects of metal ions, metal and metal oxide particles on the synthesis of hydrochars*, ACS Omega 5 (2020) 5601–5607.

[49] D. JUNG, M. ZIMMERMANN, A. KRUSE, *Hydrothermal carbonization of fructose: growth mechanism and kinetic model*, ACS Sustainable Chemistry & Engineering 6 (2018) 13877–13887.

[50] A.M. VINDEDAHL, J.H. STREHLAU, W.A. ARNOLD, R.L. PENN, *Organic matter and iron oxide nanoparticles: aggregation, interactions and reactivity*, Environmental Science: Nano 3 (2016) 494–505.

[51] M. SEVILLA, A.B. FUERTES, *Chemical and structural properties of carbonaceous products obtained by hydrothermal carbonization of saccharides*, Chem. Eur. J. 15(16) (2009) 4195–4203.

[52] A. GEORGI, A. SCHIERZ, K. MACKENZIE, F.-D. KOPINKE, *Colloidal activated carbon for* in-situ *groundwater remediation – Transport characteristics and adsorption of organic compounds in water-saturated sediment columns*, Journal of Contaminant Hydrology 179 (2015) 76–88.

[53] L. MAO, Y. ZHANG, Y. HU, K.H. HO, Q. KE, H. LIU, Z. HU, D. ZHAO, J. WANG, *Activation of sucrose-derived carbon spheres for high performance supercapacitor electrodes*, RSC Advances 5 (2015) 9307–9313.

[54] M. BALDA, K. MACKENZIE, S. WOSZIDLO, H. UHLIG, J. MÖLLMER, F.-D. KOPINKE, G. SCHÜÜRMANN, A. GEORGI, *Bottom-up synthesis of de-functionalized and dispersible carbon spheres as colloidal adsorbent*, Int. J. Mol. Sci. 24 (2023) 3831.

[55] M.B. AHMED, J.L. ZHOU, H.H. NGO, W. GUO, M. CHEN, *Progress in the preparation and application of modified biochar for improved contaminant removal from water and wastewater*, Bioresource Technology 214 (2016) 836–851.

[56] L. GONG, J. CHEN, Y. HU, K. HE, E.J. BYLASKA, P.G. TRATNYEK, F. HE, *Degradation of chloroform by zerovalent iron: effect of mechanochemical sulfidation and nitridation on the kinetics and mechanism*, Environ. Sci. Technol. 57 (2023) 9811–9821.

[57] J. FENG, T.T. LIM, *Pathways and kinetics of carbon tetrachloride and chloroform reductions by nanoscale Fe and Fe/Ni particles: comparison with commercial micro-scale Fe and Zn*, Chemosphere 59(9) (2005) 1267–1277.

[58] H.-L. LIEN, S. YUAN-PANG, W.-X. ZHANG, *Nanoscale Bimetallic Pd/Fe particles for remediation of halogenated methanes*, in: I.M.C. LO, R.Y. SURAMPALLI, K.C.K. LAI (EDS.), *Zero-valent iron reactive materials for hazardous waste and inorganics removal2006.*

[59] Y. XU, W.-X. ZHANG, *Subcolloidal Fe/Ag particles for reductive dehalogenation of chlorinated benzenes*, Ind. Eng. Chem. Res. 39 (2000) 2238–2244.

[60] K. MONDAL, G. JEGADEESAN, S.B. LALVANI, *Removal of selenate by Fe an NiFe nanosized particles*, Ind. Eng. Chem. Res. 43 (2004) 4922–4934.

[61] K. MACKENZIE, H. FRENZEL, F.-D. KOPINKE, *Hydrodehalogenation of halogenated hydrocarbons in water with Pd catalysts: Reaction rates and surface competition*, Appl. Catal. B 63 (2006) 161–167.

[62] C. GAI, F. ZHANG, Q. LANG, T. LIU, N. PENG, Z. LIU, *Facile one-pot synthesis of iron nanoparticles immobilized into the porous hydrochar for catalytic decomposition of phenol*, Appl. Catal. B 204 (2017) 566–576.

[63] F. MENG, Z. LI, C. LEI, K. YANG, D. LIN, *Removal of trichloroethene by iron-based biochar from anaerobic water: key roles of Fe/C ratio and iron carbides*, Chem. Eng. J. 413 (2021) 127391.

[64] A. PAVELKOVÁ, V. STEJSKAL, O. VOLOŠČUKOVÁ, J. NOSEK, *Cost-effective remediation using microscale ZVI: comparison of commercially available products*, Ecol. Chem. Eng. S. 27 (2020) 211–224.

[65] M. VOGEL, A. GEORGI, F.-D. KOPINKE, K. MACKENZIE, *Sulfidation of ZVI/AC composite leads to highly corrosion-resistant nanoremediation particles with extended life-time*, Sci. Total Environm. 665 (2019) 235–245.

Text S1. As carbon precursors, sodium gluconate (Kraft) or commercially available sucrose were used. The tested iron precursors were ferrous gluconate dihydrate (Thermo Scientific), iron(II) sulfate heptahydrate (Roth), iron(III) nitrate (Alfa-Aesar), iron(II) chloride tetrahydrate (Kraft) and iron(III) chloride hexahydrate (Riedel-de-Haen). Carboxymethyl cellulose (CMC) sodium salt was purchased from Sigma-Aldrich. The CMC had a molecular weight of 90 kDa, a polymerization degree of 400 and a substitution degree of 0.65–0.90 with a sodium content of approximately 8 wt.-%. The viscosity in a 4 wt.-% aqueous solution is 85 cPs at 25 °C. The (hydroxypropyl)methyl cellulose (HPMC) had a molecular weight of 26 kDa and substitution degrees of 0.19–0.24 (methoxyl) and 0.07–0.12 (hydroxypropoxyl). The viscosity in a 2 wt.-% aqueous solution is 112 cPs at 20 °C. Chloroform (CF) and dichloromethane (DCM) were purchased from Sigma-Aldrich. Palladium(II) acetate was obtained from Chempur. Methanol, ethanol, acetone, toluene, hydrochloric acid, potassium nitrate and sodium bicarbonate were purchased from Merck. Gaseous methane, ethane and ethene were provided by SIAD and Linde.

The activated carbon SA Super was purchased from Norit® and ground to a mean particle diameter of about 1 µm. Carbo-Iron® colloids ($d_{\mathrm{particle}} \approx 1$ µm) with 25 wt.-% zero-valent iron (ZVI) were palladized and used for comparison experiments. They were characterized with Brunauer-Emmet-Teller (BET) specific surface area (SSA_{BET} = 720 m^2 g^{-1}), pore volume (4.0 cm^3 g^{-1}) and iron cluster size ($d_{\mathrm{Fe\text{-}crystallite}}$ = 47 nm, by XRD). Details about the synthesis and characterization of CIC are provided in [1]. Nanofer Star iron, provided by NANO IRON s.r.o., is an air-stable commercially available nanocale ZVI (nZVI). The average particle size of the nZVI is 50 nm and its SSA_{BET} is about 25 m^2 g^{-1}. Pd/magnetite NPs were prepared on the basis of commercially available magnetite NPs (Chempur); the synthesis methods are shown in [2]. The eggshell catalyst G-133D with 0.5 wt.-% Pd on γ-Al_2O_3 was purchased from Commercia, Germany, crushed and sieved. The size fraction of 25–63 µm was used for the dechlorination experiments.

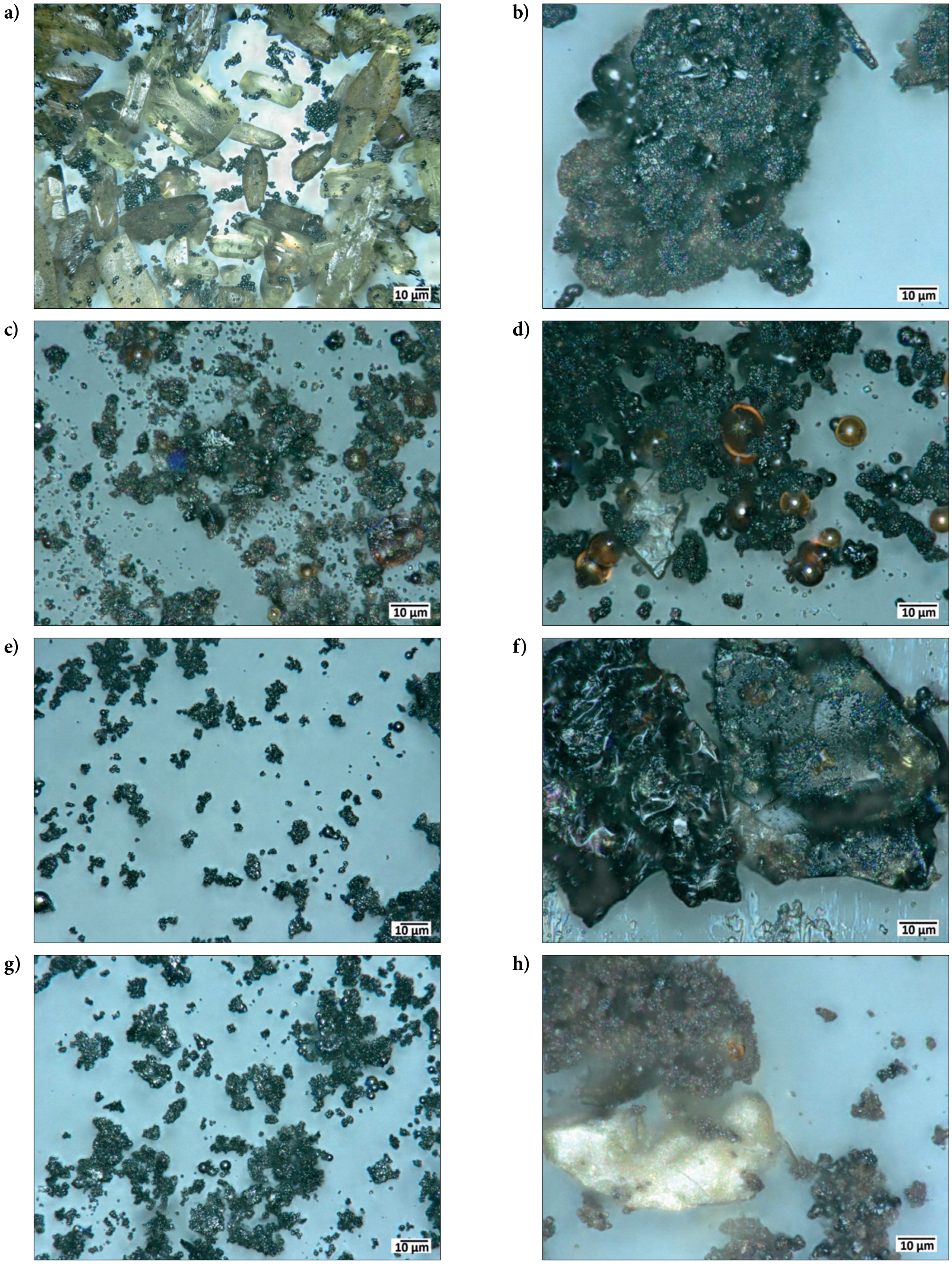

Figure S1 HTC of different Fe and C precursors;

a) 180 g L^{-1} sucrose + 1.5 g L^{-1} CMC + 130 g L^{-1} $Fe(NO_3)_3 \cdot 9\ H_2O$, $pH_0 = 1.0$, 140 °C, 2h
b) 170 g L^{-1} sucrose + 1.8 g L^{-1} CMC + 60 g L^{-1} $Fe(OH)_2$, $pH_0 = 6.8$, 160 °C, 2 h
c) 30 g L^{-1} Na gluconate + 10 g L^{-1} $FeCl_2 \cdot 4\ H_2O$, $pH_0 = 4.7$, 180 °C, 24 h
d) 30 g L^{-1} Na gluconate + 15 g L^{-1} $FeCl_3 \cdot 6\ H_2O$, $pH_0 = 3.5$, 180 °C, 48 h
e) 120 g L^{-1} Na gluconate + 30 g L^{-1} Fe gluconate $\cdot\ 2\ H_2O$, $pH_0 = 5.3$, 180 °C, 24 h
f) 60 g L^{-1} sucrose + 60 g L^{-1} Fe gluconate $\cdot\ 2\ H_2O$ + 1.5 g L^{-1} CMC, $pH_0 = 4.5$, 180 °C, 24 h
g) 120 g L^{-1} Na gluconate + 30 g L^{-1} Fe gluconate $\cdot\ 2\ H_2O$ + 1.5 g L^{-1} CMC, $pH_0 = 5.3$, 180 °C, 24 h
h) 40 g L^{-1} Na gluconate + 60 g L^{-1} Fe gluconate $\cdot\ 2\ H_2O$ + 1.4 g L^{-1} HPMC, $pH_0 = 5.3$, 180 °C, 24 h

Text S2. Initially, a screening of potential Fe and C precursors was performed. As Fe precursors, $Fe(NO_3)_3 \cdot 9\ H_2O$ (130–200 g L^{-1}), $FeSO_4 \cdot 7\ H_2O$ (20–190 g L^{-1}), $FeCl_2 \cdot 4\ H_2O$ (10 g L^{-1}), $FeCl_3 \cdot 6\ H_2O$ (7–30 g L^{-1}) were tested and as C precursors commercial sucrose (60–200 g L^{-1}) and sodium gluconate (30–100 g L^{-1}) were used. All precursors were mixed in solutions with various ratios and the native pH_0 values prior to HTC were recorded with a pH meter. In the case of $FeSO_4 \cdot 7\ H_2O$, the pH was adjusted to ca. 7 in order to form dark blue precipitates of $Fe(OH)_2$. This was the only approach tested with particulate Fe, as some positive effects of freshly precipitated $Fe(OH)_2$ had initially been observed. The resulting mixtures were subject to HTC at 140–180 °C for 2–24 h. During this screening process, the morphologies of the obtained particles were characterized with the digital microscope (*cf.* Figure S1).

Without any additives, the generation of stable composite materials was not achieved when using commercial sucrose as the C precursor together with any tested iron salt as the Fe precursor. Only those experiments starting from ferrous gluconate were successful in generating a comparably homogeneous distribution regarding particle sizes and the combination of Fe and C. We attribute this finding to the complex formation between ferrous/ferric ions and gluconate as shown in Figure 2 of the manuscript. In contrast to our previous results regarding the HTC of sucrose [3], the addition of CMC during the HTC of ferrous gluconate did not have a distinct favorable effect on the particle morphology. However, as it did not act as detrimental as other stabilizers (*e.g.* HPMC), the potential influence of CMC on the particle sizes, morphologies and reactivities of the composites was investigated more closely.

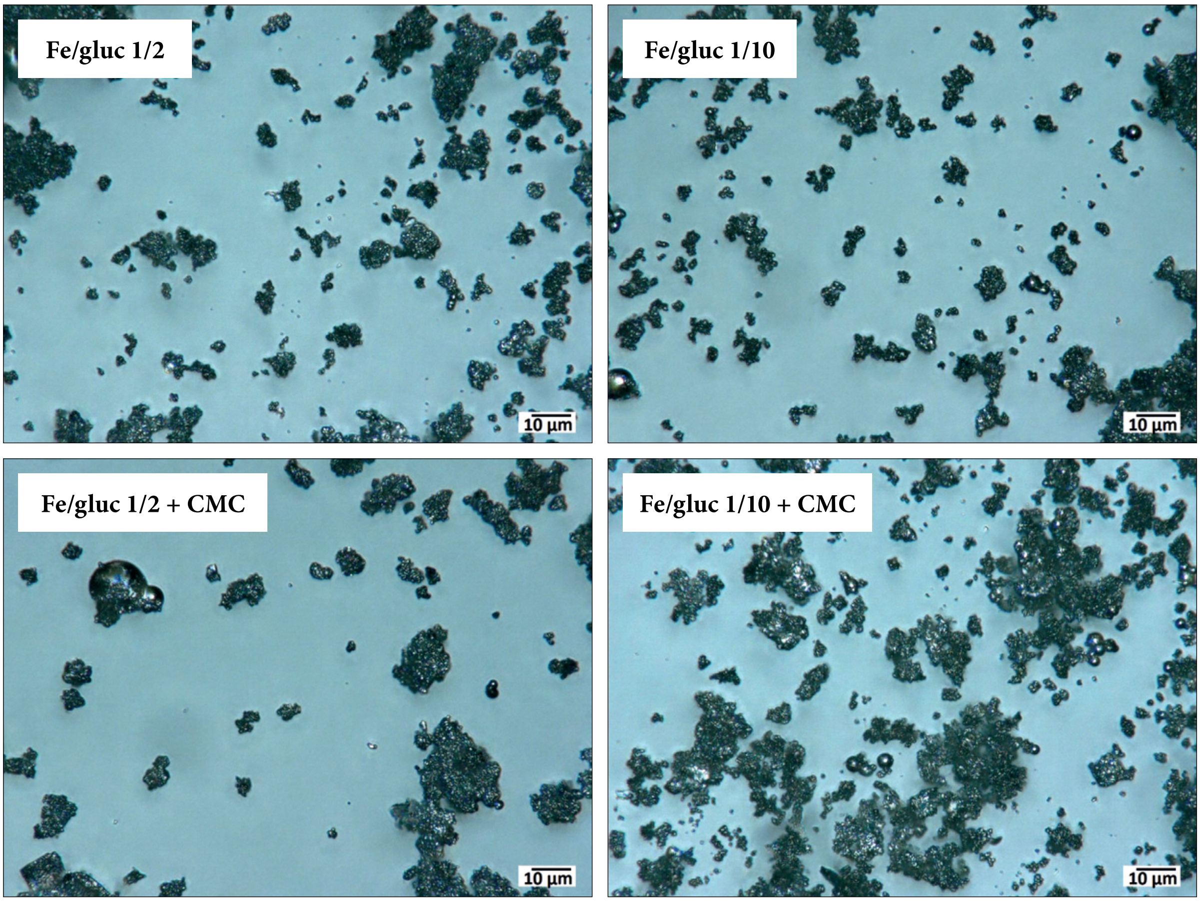

Figure S2 Digital microscopy of the dry Fe/C composites synthesized *via* HTC of ferrous gluconate and sodium gluconate at different molar ratios of $n_{Fe}/n_{gluconate}$ = 1/2 or 1/10 (60 g L^{-1} Fe gluconate dihydrate or 120 g L^{-1} Na gluconate + 30 g L^{-1} Fe gluconate dihydrate, respectively) in the absence and presence of 0.6 and 1.5 g L^{-1} CMC (1 wt.-% related to the combined weight of Fe + C precursors); HTC at 180 °C for 24 h at pH_0 = 4.6 ($n_{Fe}/n_{gluconate}$ = 1/2) or 5.3 ($n_{Fe}/n_{gluconate}$ = 1/10); subsequent carbothermal reduction at 800 °C for 2 h under N_2.

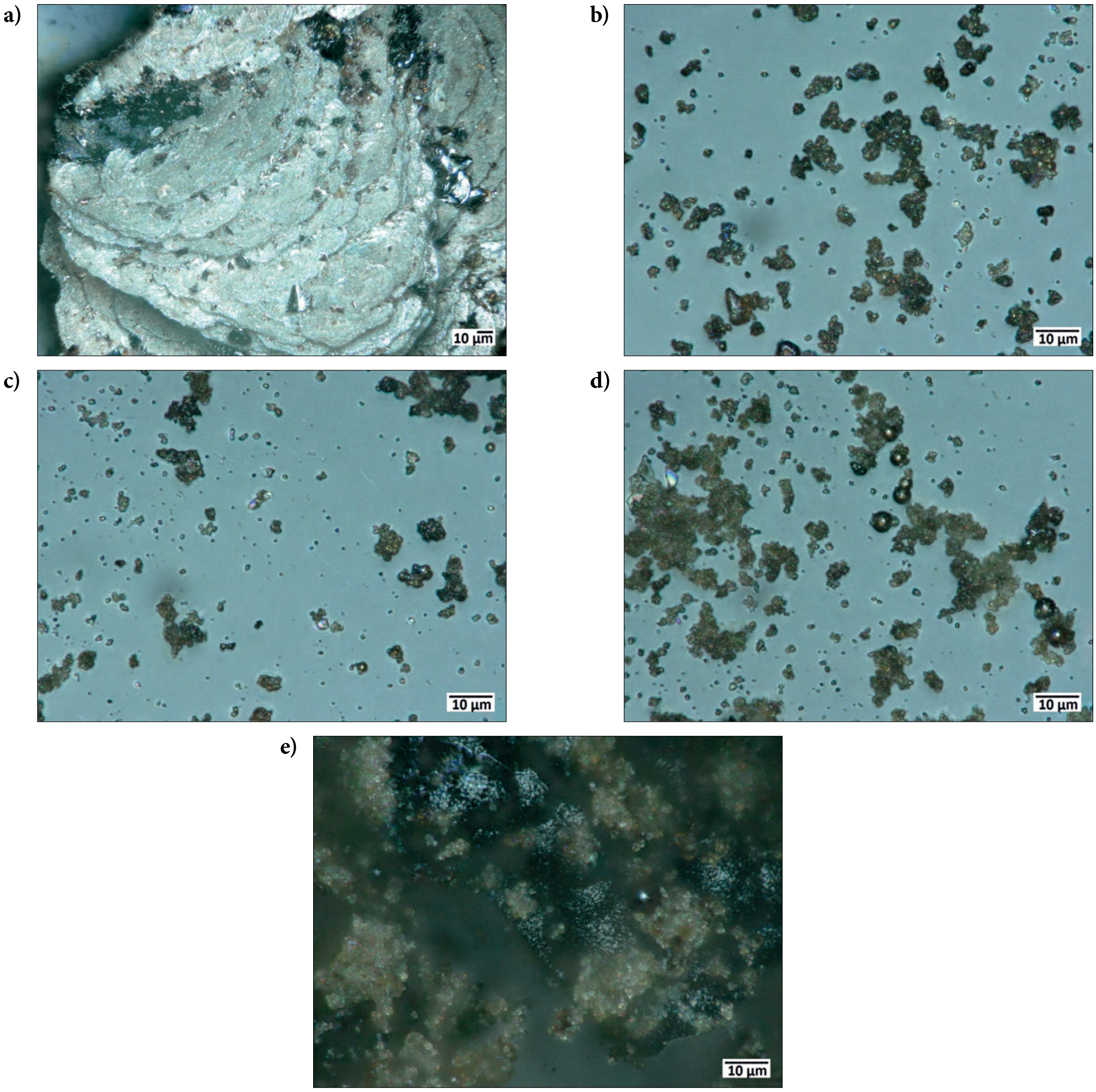

Figure S3 HTC of 120 g L^{-1} Na gluconate + 30 g L^{-1} Fe gluconate dihydrate (molar ratio 1/10) at 180 °C for 24 h with various adjusted pH_0 values;

a) $pH_0 = 2.6$
b) $pH_0 = 4.3$
c) $pH_0 = 5.3$ (native)
d) $pH_0 = 6.3$
e) $pH_0 = 8.0$

Text S3. The influence of pH_0 prior to HTC on the resulting particle size distributions was investigated. At initial pH values of 2.6 and 8.0 large aggregates were formed (*cf.* Figure S2 a) and e)). In contrast, the moderate adjustments to 4.3 or 6.3 had no significant effects on the particle morphologies compared to the native pH_0 (5.3) (*cf.* Figure S2 b), c) and d) and Table S1). However, an increase in mass yields after HTC at pH_0 = 4.3 to 11 wt.-% could be denoted whereas the yield decreased to 6 wt.-% at pH_0 = 6.3.

Table S1 Particle diameters in aqueous suspension (determined with dynamic light scattering; values are intensity-weighted diameters) and the mass yield after HTC of Fe/C composites synthesized *via* HTC of ferrous and sodium gluconate at different initial pH values (pH_0) with a molar ratios of $n_{Fe}/n_{gluconate}$ = 1/10. The error ranges of the particle diameters represent the mean deviation of single values from two measurements of the same sample.

pH_0	Particle diameters [µm]			Yields [wt.-%]
	d_{10}	d_{50}	d_{90}	
2.6	n/d	n/d	n/d	25
4.3	4.8 ± 0.1	27.1 ± 0.1	72 ± 2	11
5.3	4.4 ± 0.1	34.7 ± 0.3	80.7 ± 0.4	8 ± 1
6.3	4.3 ± 0.1	24.8 ± 0.2	68.0 ± 0.2	6
8.0	n/d	n/d	n/d	10

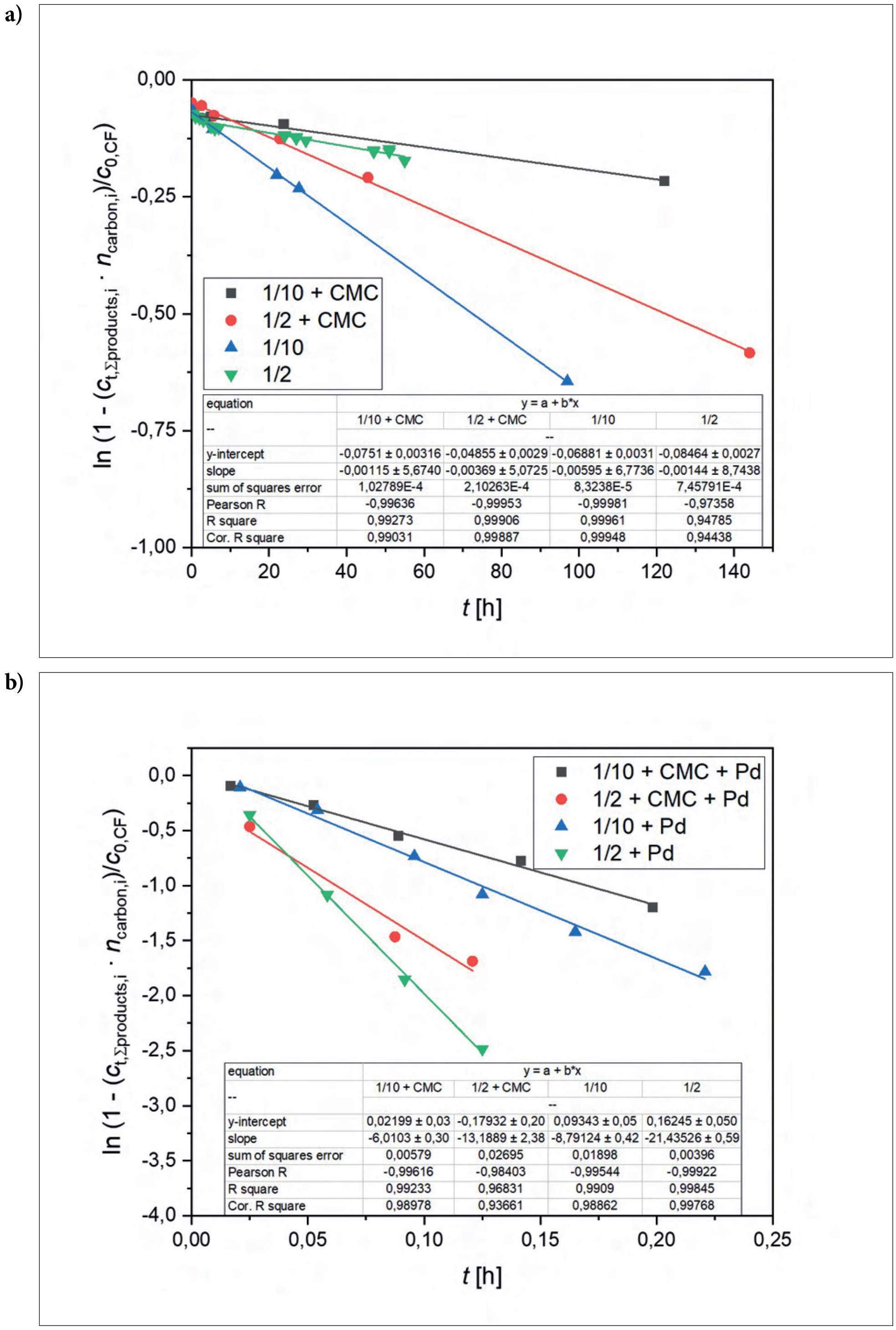

equation	y = a + b*x			
--	1/10 + CMC	1/2 + CMC	1/10	1/2
	--			
y-intercept	-0,0751 ± 0,00316	-0,04855 ± 0,0029	-0,06881 ± 0,0031	-0,08464 ± 0,0027
slope	-0,00115 ± 5,6740	-0,00369 ± 5,0725	-0,00595 ± 6,7736	-0,00144 ± 8,7438
sum of squares error	1,02789E-4	2,10263E-4	8,3238E-5	7,45791E-4
Pearson R	-0,99636	-0,99953	-0,99981	-0,97358
R square	0,99273	0,99906	0,99961	0,94785
Cor. R square	0,99031	0,99887	0,99948	0,94438

equation	y = a + b*x			
--	1/10 + CMC	1/2 + CMC	1/10	1/2
	--			
y-intercept	0,02199 ± 0,03	-0,17932 ± 0,20	0,09343 ± 0,05	0,16245 ± 0,050
slope	-6,0103 ± 0,30	-13,1889 ± 2,38	-8,79124 ± 0,42	-21,43526 ± 0,59
sum of squares error	0,00579	0,02695	0,01898	0,00396
Pearson R	-0,99616	-0,98403	-0,99544	-0,99922
R square	0,99233	0,96831	0,9909	0,99845
Cor. R square	0,98978	0,93661	0,98862	0,99768

Figure S4 First-order kinetic evaluation of the CF degradation shown exemplarily for a) Fe/C and b) Pd/Fe/C with different precursor Fe/gluconate molar ratios of 1/2 or 1/10; $c_{0,CF}$ = 10 mg L^{-1}, $c_{Fe/C}$ = 400–1000 mg L^{-1}, 3.6 wt.-% Pd, 10 mM $NaHCO_3$, pH_0 = 8.5.

Table S2 Normalized rate constants k_{norm} of the CF degradation with Pd/Fe/C samples derived from Fe/C composites *via* HTC with different molar Fe/gluconate ratios synthesized in presence or absence of CMC displayed together with the specific catalyst acitivites A as well as the selectivities S towards the main products methane, ethane and DCM at 95 % CF conversion; $c_{0,CF} = 10$ mg L^{-1}, $c_{Pd/Fe/C} = 400–1000$ mg L^{-1}, (1.2 ± 0.5) or (3.6 ± 0.5) wt.-% Pd, 10 mM $NaHCO_3$, $pH_0 = 8.5$; the error ranges of the particle diameters represent the mean deviation of single values from the mean value of two measurements of the same sample.

n_{Fe} / $n_{gluconate}$	**Pd-content [wt.-%]**	**ZVI-content [wt.-%]**	**k_{norm} [L (g h)$^{-1}$]**	**A [L g^{-1} min^{-1}]**	**S [mol-%]**		
					methane	**ethane**	**DCM**
1/10 + CMC	1.0 ± 0.2	20 ± 2	18 ± 2	8 ± 1	49 ± 1	7 ± 1	5.0 ± 0.5
1/2 + CMC	1.0 ± 0.1	47 ± 2	14 ± 1	9 ± 1	63 ± 1	6 ± 1	4.0 ± 0.5
1/10	1.5 ± 0.3	25 ± 2	12 ± 1	9 ± 1	48 ± 1	6 ± 1	4 ± 1
1/2	1.4 ± 0.5	48 ± 2	11 ± 2	11 ± 1	69 ± 1	7 ± 1	7 ± 1
1/10 + CMC	3.7 ± 0.5	20 ± 2	65 ± 8	7 ± 1	71 ± 3	7.9 ± 0.5	2.4 ± 0.5
1/2 + CMC	3.0 ± 0.4	47 ± 2	29 ± 3	14 ± 1	68 ± 1	7 ± 1	2 ± 1
1/10	4.0 ± 0.5	25 ± 2	80 ± 10	10 ± 1	71 ± 3	9.0 ± 0.5	3.2 ± 0.5
1/2	3.7 ± 0.5	48 ± 2	80 ± 5	24 ± 1	77 ± 3	7 ± 1	5.0 ± 0.5

Text S4. When the Pd-content for Pd/Fe/C samples was increased to (3.6 ± 0.5) wt.-% Pd, the selectivities towards methane as well as k_{norm} and the resulting activities increased by trend, while the selectivities towards DCM decreased. This suggests that also with a high content of (3.6 ± 0.5) wt.-% Pd, the deposited Pd has an approximately equal specific activity. Similar trends were observed for the hydrodechlorination of chlorinated benzenes with Ag/Fe bimetallic particles [4] as well as for the reduction of selenite with Ni/Fe as long as a sufficiently high ZVI content continuously ensured the supply with H_2 [5]. In contrast, Wang *et al.* observed an increase only up to low Pd loadings of 0.2 wt.-% and a subsequent decrease in specific catalytic activity with increasing Pd loading for the hydrodechlorination of CF with Pd/ZVI bimetallic particles [6]. This could be an effect of full surface coverage with Pd of the non-porous metal support and thus hindering the production of reactive species from the ZVI. In the present work the Fe/C supports provide higher specific surface areas of 140–280 m^2 g^{-1} (*cf.* Table 3) compared to nZVI (about 30 m^2 g^{-1} [6]). Although, it is likely that the composite surface does not only provide Fe species, it could explain that even high Pd contents up to 4 wt.-% can be deposited in a catalytically active form without eliminating the reactivity of ZVI. As displayed in Figure S4, S_{CH_4} was especially low for Fe/C composites synthesized at molar ratios of $n_{Fe}/n_{gluconate} = 1/10$ and palladized with (1.2 ± 0.5) wt.-% Pd. This might be due to the lower ZVI contents of 20–25 wt.-% compared to the samples synthesized at $n_{Fe}/n_{gluconate} = 1/2$ with ZVI-contents of 47–48 wt.-% (*cf.* Table S2). These might result in lower rate constants for H_2 formation indicating in turn the increased formation of longer-chain byproducts instead of methane when a H_2 shortage was present during the reactions. In contrast, when the Fe/C samples were palladized with higher Pd contents of (3.6 ± 0.5) wt.-% Pd, S_{CH_4} was significantly increased for all samples and the increase was most pronounced for samples which featured a low S_{CH_4} before. This indicated an increase in anaerobic ZVI corrosion when more Pd was present due to the formation of local galvanic couples on the composite surfaces [4, 5].

In comparison with the non-palladized Fe/C composites (*cf.* Table 4), Table S2 shows that the palladization of Fe/C drastically increased the rate constant up to $k_{norm,Pd/Fe/C} = (70 \pm 10)$ L g^{-1} h^{-1} as well as shifted the selectivity towards fully dechlorinated products for all investigated samples. The CF degradation on the Pd/Fe/C samples with (3.6 ± 0.5) wt.-% Pd featured selectivities of 68–77 mol-% methane and 2–5 mol-% DCM after > 95 % CF conversion.

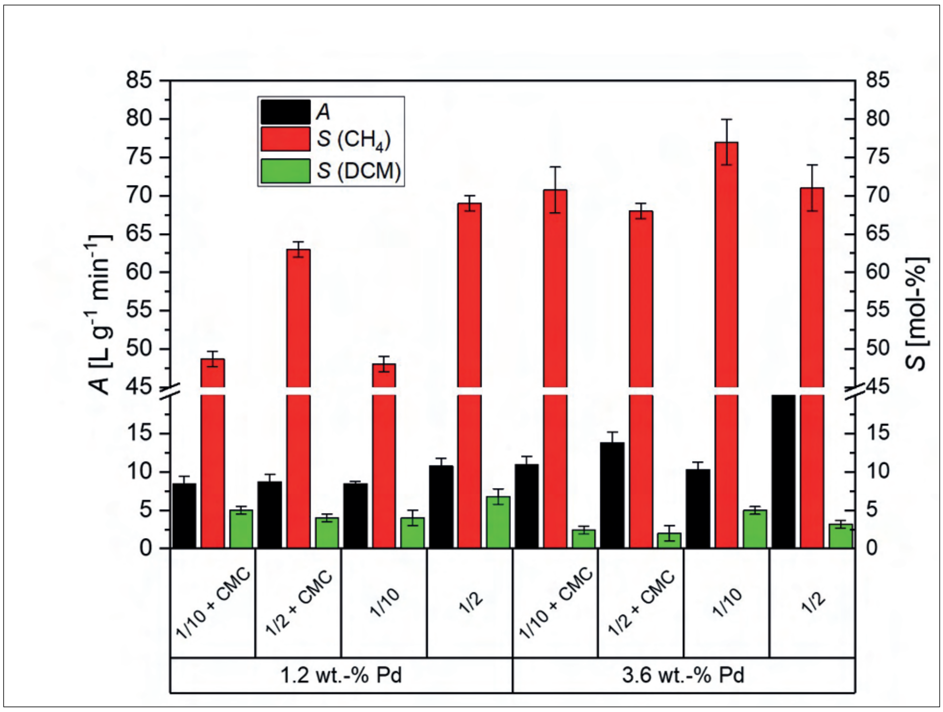

Figure S5 Catalytic activities A_{Pd} and selectivities S towards methane and DCM determined from the reductive dechlorination of CF with Pd/Fe/C composites palladized with either (1.2 ± 0.5) or (3.6 ± 0.5) wt.-% Pd; $c_{0,CF}$ = 10 mg L^{-1}, $c_{Pd/Fe/C}$ = 400–1000 mg L^{-1}, c_{NaHCO_3} = 10 mM, pH_0 = 8.5. Error bars represent the mean deviation of single values from the mean value of two replicate experiments.

Text S5. The solid sample composition was explored by X-ray photoelectron spectroscopy (XPS, Kratos Ultra DLD). The measurements were performed at room temperature with a background pressure of 10^{-7} Pa. For excitation, monochromic Al K_α radiation at 1486.6 eV was used while the X-ray source was operated at 150 W. Photoelectrons were released from the 300 µm · 700 µm analysis area and analyzed under normal incidence configuration. In order to enhance the photoelectron yield, a magnetic immersion lens was applied. Thermal electrons were supplied to the analysis area by a neutralizer in order to avoid sample charging. For energy separation, a retarding lens system coupled by a hemispherical analyser with 40 eV pass energy was used. The energy-filtered photoelectrons were amplified passing a microchannel plate and recorded by a delay line detector. The UNIFIT 2023 software was used for spectra analysis and composition calculation considering the specific transmission correction of the XPS machine. For curve fitting convolved Gaussian-Lorentzian peak profiles were simultaneously optimized with a Shirley background profile. The spectral calibration was performed by the adventitious carbon peak in the C-1s core-level spectrum at 284.4 eV.

For the X-ray diffraction (XRD) analyses, the $2\theta/\omega$ scans were measured with a diffractometer (ULTIMA IV, Rigaku) in out-of-plane geometry with parallel beam optics. A copper anode (K_α, $\lambda = 0.15406$ nm) was used as X-ray source. The diffractometer was equipped with a scintillation detector. The diffractograms were analysed using the software package PDXL (Rigaku).

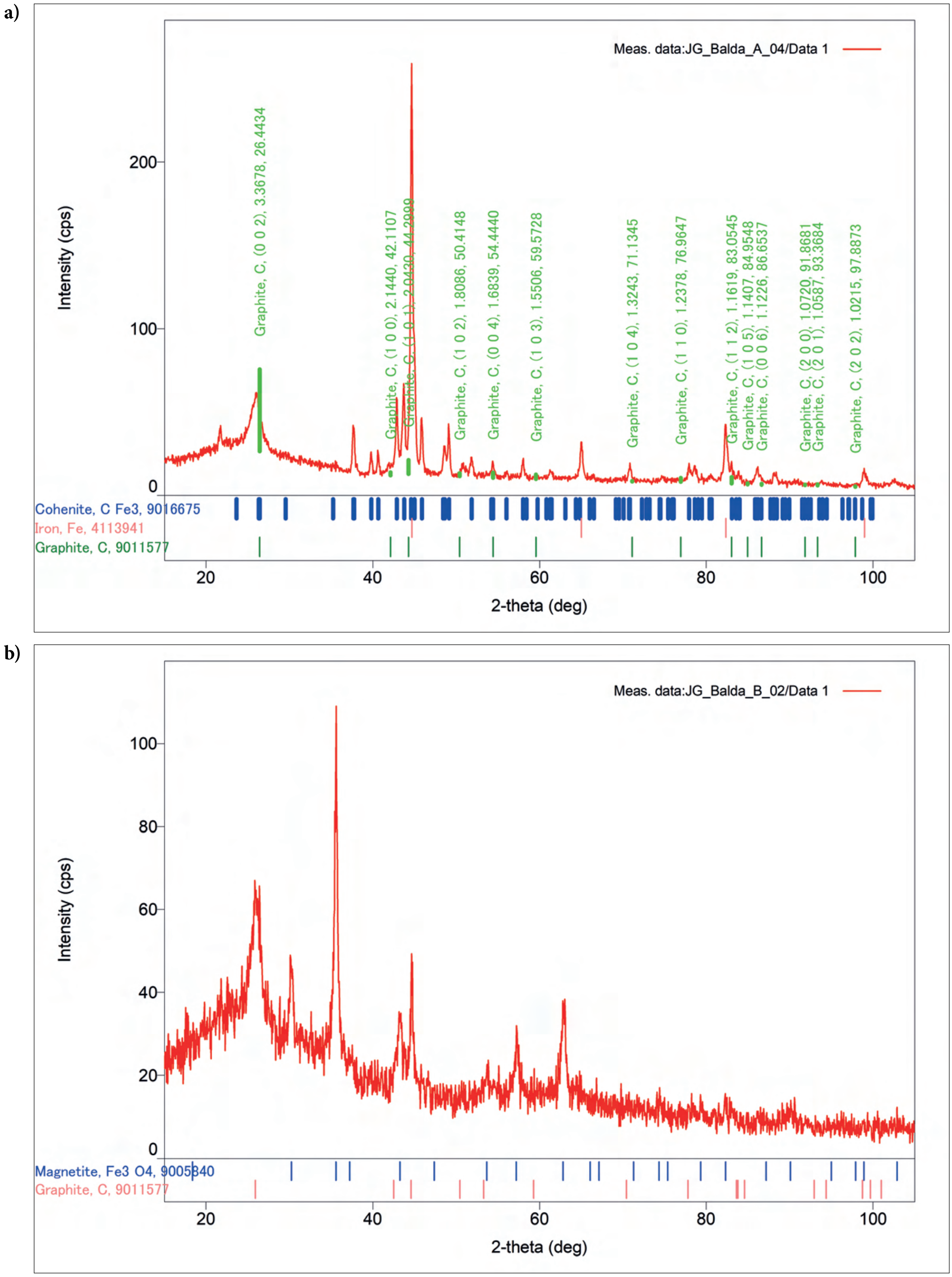

Figure S6 XRD spectra of Fe/C “1/10” containing 35 wt.-% ZVI a) before and b) after CF degradation.

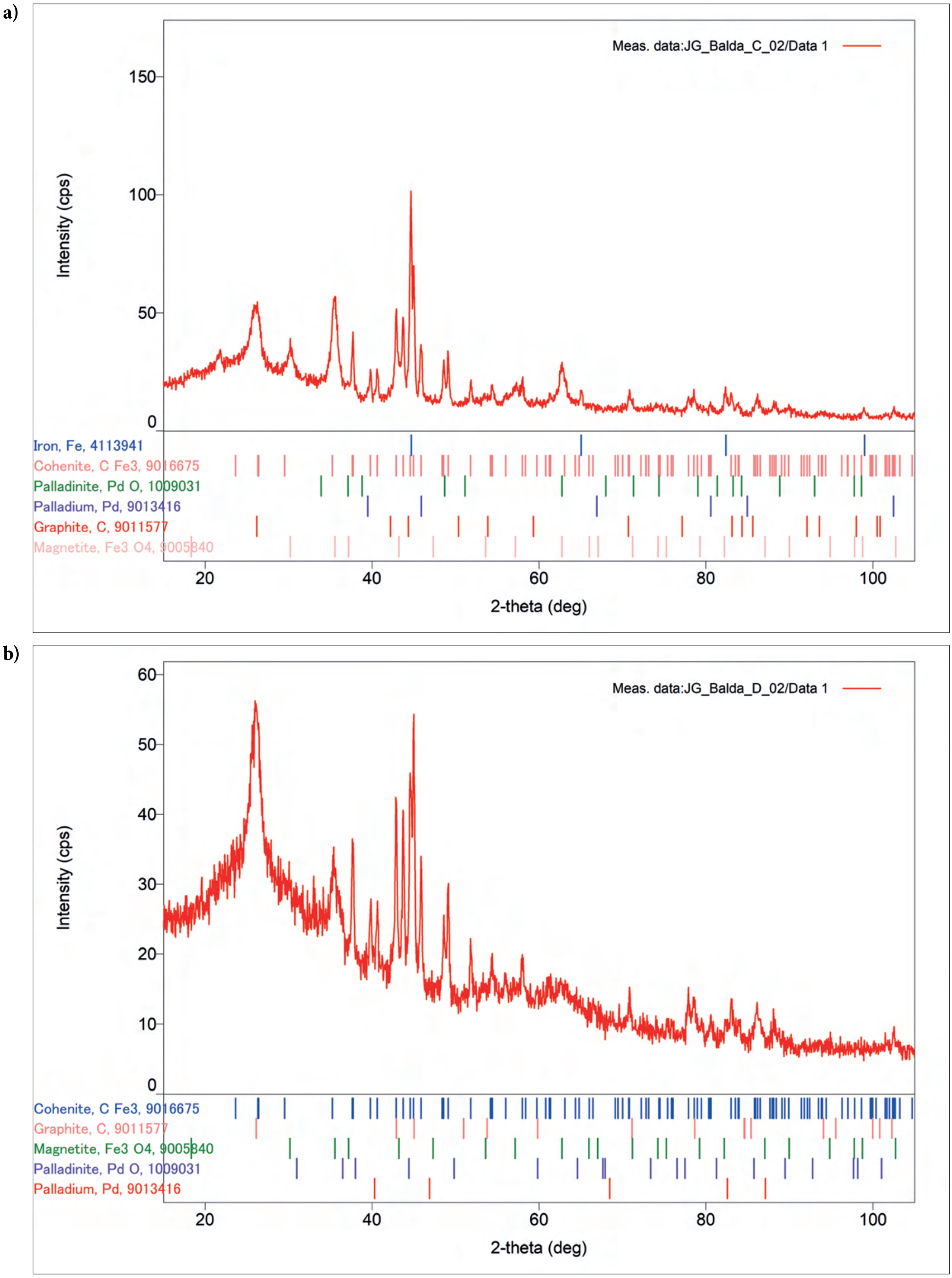

Figure S7 XRD spectra of Pd/Fe/C “1/10” containing 35 wt.-% ZVI and 1.1 wt.-% Pd a) before and b) after CF degradation.

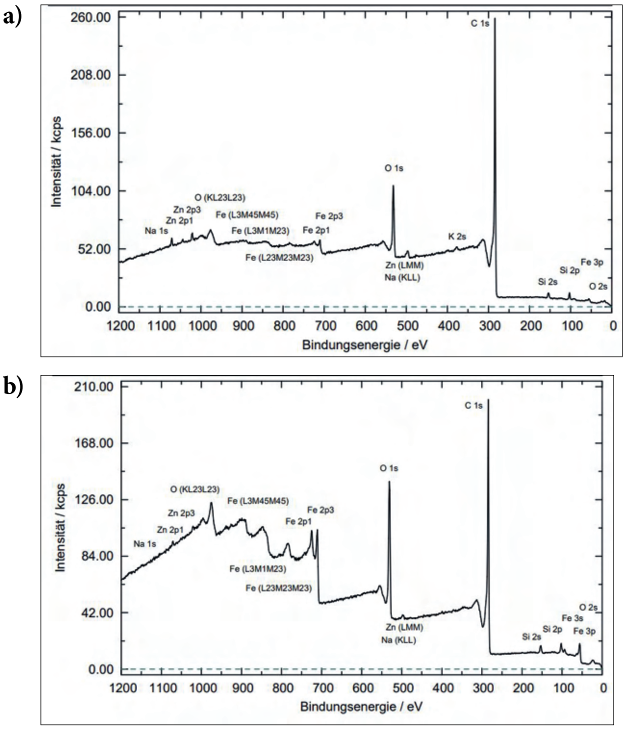

Figure S8 XPS spectra of Fe/C "1/10" containing 35 wt.-% ZVI a) before and b) after CF degradation.

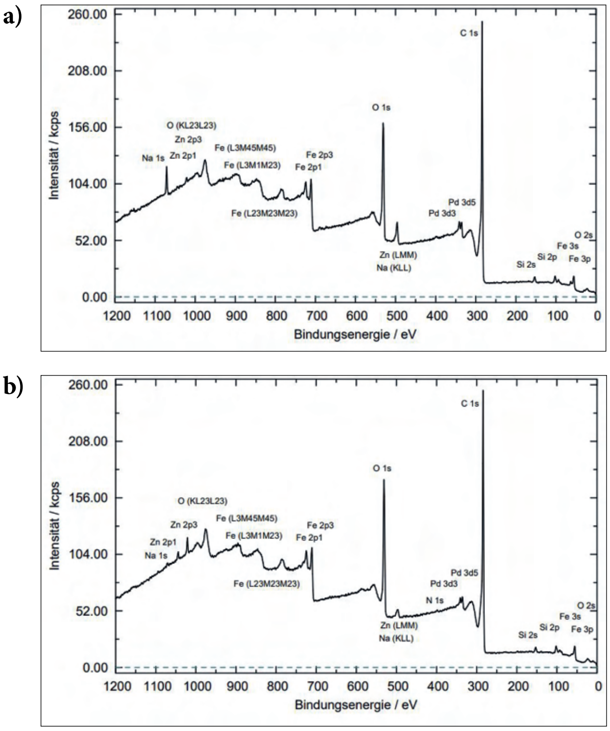

Figure S9 XPS spectra of Pd/Fe/C "1/10" containing 35 wt.-% ZVI and 1.1 wt.-% Pd a) before and b) after CF degradation.

Figure S10 Aqueous suspensions (from left to right) of activated carbon spheres (aCS, [7], Fe/C 1/10, Fe/C 1/2 and freshly synthesized nZVI as described in [8] after 30 min of sedimentation; c_{NaHCO_3} = 10 mM, $c_{particles}$ = 1 g L^{-1}, c_{CMC} = 10 mg L^{-1}.

References

[1] K. Mackenzie, S. Bleyl, A. Georgi, F.-D. Kopinke, *Carbo-Iron – an Fe/AC composite – as alternative to nano-iron for groundwater treatment*, Water Res. 46(12) (2012) 3817–3826.

[2] H. Hildebrand, K. Mackenzie, F.-D. Kopinke, *Highly active Pd-on-magnetite nanocatalysts for aqueous phase hydrodechlorination reactions*, Environ. Sci. Technol. 43 (2009) 3254–3259.

[3] M. Balda, K. Mackenzie, F.-D. Kopinke, A. Georgi, *Uniform and dispersible carbonaceous microspheres as quasi-liquid sorbent*, Chemosphere (2022) 136079.

[4] Y. Xu, W.-X. Zhang, *Subcolloidal Fe/Ag particles for reductive dehalogenation of chlorinated benzenes*, Ind. Eng. Chem. Res. 39 (2000) 2238–2244.

[5] K. Mondal, G. Jegadeesan, S.B. Lalvani, *Removal of selenate by Fe an NiFe nanosized particles*, Ind. Eng. Chem. Res. 43 (2004) 4922–4934.

[6] X. Wang, C. Chen, Y. Chang, H. Liu, *Dechlorination of chlorinated methanes by Pd/Fe bimetallic nanoparticles*, J. Hazard. Mater. 161 (2009) 815–823.

[7] M. Balda, K. Mackenzie, S. Woszidlo, H. Uhlig, J. Möllmer, F.-D. Kopinke, G. Schüürmann, A. Georgi, *Bottom-up synthesis of de-functionalized and dispersible carbon spheres as colloidal adsorbent*, Int. J. Mol. Sci. 24 (2023) 3831.

[8] M. Balda, F.-D. Kopinke, *The role of nickel traces in fine chemicals for hydrodechlorination reactions with zero-valent iron*, Chem. Eng. J. 388 (2020) 124185.

5 Conclusion

In this work, the research questions posed in section 3. were answered consecutively. Research question (I) was complemented with research question (I).i (see below) and answered within the first manuscript "Uniform and dispersible carbonaceous microspheres as quasi-liquid sorbent" which was published in *Chemosphere* in 2022. Research questions (II) and (III) (extended to (III).i, see below) were answered in the second manuscript "Bottom-up synthesis of de-functionalized and dispersible activated carbon spheres as colloidal adsorbent" (published in the *International Journal of Molecular Sciences* in 2023). The last three research questions (IV, V and VI) were processed in the third manuscript "Generating colloidal Fe/C composites *via* hydrothermal carbonization – a critical study" was published in *Separation and Purification Technology* in 2024. The deduced and summarized answers are given in the following.

(I) How can the yield of microparticles in the desired size range be optimized without potentially hazardous additives during the HTC process?

i. Do the synthesized microparticles exhibit the capability for sorption of organic groundwater pollutants?

The addition of CMC during the HTC of sucrose at 180 h for 2 h optimized the mass yield of spherical CS with a narrow size distribution around 1 µm. These 'raw' CS exhibited an extraordinary suspension stability due to their hydrophilic surface and negative surface charges characterized by a zeta potential of -43.5 mV at pH 6 which makes them suitable for *in-situ* injection into aquifers. That is why their capability for the sorption of various groundwater pollutants with different hydrophobicities was investigated. The highest sorption coefficients of up to $K_D = 10^5$ L kg^{-1} were found for hydrophobic substances such as phenanthrene. The proposed sorption mechanism is the diffusion of hydrophobic molecules, especially polyaromatic systems, into the lignite-like matrix of the CS. This interaction may be classified as absorption. One has to take into account, however, that the absorption coefficients with CS are lower than the adsorption coefficients achievable with AC. That is why, for the cost-efficient remediation, CS would have to be cheaper than AC which might be achieved by using alternative (waste) substrates in the HTC process.

(II) How can the high aqueous dispersibility of the microparticles be kept after pyrolysis?

The parameters for pyrolysis of the CS were investigated closely and suitable conditions were found in order to maintain the aqueous dispersiblity of the aCS also after the pyrolysis step. Under all applied pyrolysis conditions, a low heating rate of about 1 K min^{-1} was crucial in order to minimize inter-particulate polymerization processes and to ensure sufficient dispersibility of the aCS in water. However, in order to prevent increased agglomeration of the particles, CMC had to be added as stabilizer in aqueous suspensions.

(III) How can the porosity and surface characteristics of the AC be tailored according to specific classes of pollutants?

i. How (fast) does the surface of the de-functionalized aCS age under ambient conditions?

It was demonstrated that the microporous system of the resulting aCS could be finely tuned with mean pore diameters ranging from 0.5 to 0.7 nm depending on the pyrolysis atmosphere, treatment time and temperature. The addition of 3 vol.-% steam to the N_2-atmosphere during pyrolysis not only led to a slight increase in mean pore diameter but also to a further de-functionalized surface of the aCS. Due to the de-functionalization in combination with tuning the mean pore diameter according to the molecular diameter of PFOA, the synthesized aCS exhibited high adsorption coefficients up to $K_{D,PFOA} = 10^{6.5}$ L kg^{-1}. It is concluded that the developed synthesis parameters can be adjusted further depending on specific pollutants' needs. However, the ageing of the de-functionalized surface could not be prevented even in dry air under ambient conditions. The spontaneous ageing of the aCS surface in water with abundant oxygen resulted in a significant negative effect on the adsorption of PFOA. Nevertheless, the aCS synthesized under 3 vol.-%

H_2O/N_2 at 800 °C exhibited equally stable surface properties as aCS treated in 10 vol.-% H_2/N_2 at 900 °C. It was concluded that the applied steam activation process stabilized the de-functionalized aCS surface comparable to hydrogen treatment as opposed to sole high-temperature treatment in pure N_2 which left a rather reactive surface prone to ageing. Therefore, it can be concluded that both molecular hydrogen and water are appropriate reagents to saturate/deactivate most of the reactive surface sites.

(IV) Is it possible to generate a functional iron-carbon composite with the desired morphology within a one-pot synthesis based on HTC?

The extensive screening of possible Fe and C precursors for HTC led to the conclusion that specific interactions between carbon precursors and metal ions are needed in order to generate mechanically stable Fe/C composite materials with the desired colloidal properties. Finally, ferrous gluconate proved as most promising precursor due to the complexation of $Fe^{2+/3+}$ by gluconate. The morphologies of the primary particles in the Fe/C composites were characterized *via* SEM. In future studies, the investigation of the particle morphologies with transmission electron microscopy can give more information about the possible core-shell structure of the composite material.

(V) Do the morphology and speciation of the composite after carbothermal reduction allow the reductive dechlorination of chlorinated hydrocarbons in water?

It was shown that the morphology of the synthesized Fe/C composite enables reductive dechlorination with specific activities comparable to nZVI. Specific surface areas of the composites of 140–280 $m^2\ g^{-1}$ and their mesoporous character suggest a carbonaceous phase with a well-pronounced porosity, ensuring the accessibility of the reactive ZVI surface. XRD and XPS analyses revealed that, besides pristine Fe^0, also Fe_3C was present in the material which was suspected to additionally generate reactive species (e^- and H^*) needed for the reductive dechlorination (*cf.* section 4.3) Furthermore, graphitic structures were observed that might facilitate the transfer of reactive species, likely electrons. Further investigations should also take into account the functional groups on the carbonaceous surface which can mediate redox processes. They may act as shuttle for reactive species [102, 103].

(VI) What is the gain in selectivity towards fully dechlorinated products achievable by palladization of the composite?

As the reactive ZVI equivalents within the composites were accessible (as demonstrated by relatively fast reductive dechlorination) also the facile palladization of the composite by impregnation with Pd^{2+} and reduction to Pd on the ZVI surface under ambient conditions was effective (*cf.* section 4.3, Figure 3). The resulting Pd/Fe/C composites exhibit drastically higher reaction velocities and greater selectivities towards fully dechlorinated products such as methane. The comparison with various other palladized materials showed lower selectivities of Pd/Fe/C to dichloromethane (DCM) and higher selectivities to ethane, even without external feed of H_2. A gap in mass balance was observed after summarizing the volatile products methane, ethane, DCM and monochloromethane. High extents of dechlorination of CF were verified by chloride analysis after the complete CF conversion.

The reactivity of the synthesized Fe/C in reductive dechlorination processes was demonstrated. However, there are many pollutants which cannot be degraded with ZVI, *e.g.* PFOA and DCM. In future studies, it could be explored if the synthesized material is also active as catalyst/reagent in oxidation processes typical for ISCO. However, as carbonaceous materials are also prone to oxidation they can be destroyed in the process and act as scavengers for oxidizing species.

In conclusion, it was shown that the bottom-up synthesis of finely powdered AC with particle sizes of about 1 µm as well as a colloidal Fe/C composite in the size range below 50 µm is possible *via* HTC and subsequent pyrolysis. The hydrothermally generated particles were optimized regarding their application by adjusting various process parameters. However, the hydrothermal synthesis of micrometer-sized particles with controllable diameters comes with the inevitable tradeoff of small mass yields. This diminishes the overall sustainable, facile and resource-efficient character of HTC processes. Nevertheless, it is shown within this work that mass yields can be optimized within certain boundaries. Consequently, the process parameters derived here can be seen as a basis for future studies in which the mass yield or material properties can be further optimized with regard to various applications. Moreover, alternative substrates, *e.g.* derived from regional waste sources, can be explored within the developed scopes in order to improve the sustainability of the synthesis.

Author Contribution Statement

Section 4.1 "Uniform and dispersible carbonaceous microspheres as quasi-liquid sorbent" (2022):

Unless acknowledged otherwise, Maria Balda (MB) performed the investigative experiments, specifically the development of the HTC synthesis process, material characterization as well as the sedimentation and sorption studies. MB performed the formal data analysis, curation and validation. MB visualized the results with exception of the graphical abstract that was visualized by Katrin Mackenzie (KM). MB wrote the original draft and Anett Georgi (AG) helped with the original draft, specifically on pp. 22, 30 and 32 of the manuscript. AG and KM acquired the funding and administrated the project. Frank-Dieter Kopinke (FDK) and KM provided the infrastructural resources for experimentation. AG, KM and FDK supervised the project. All authors were involved in developing methodologies, the conceptualization and reviewing and editing of the manuscript.

Section 4.2 "Bottom-up synthesis of de-functionalized and dispersible carbon spheres as colloidal adsorbent" (2023):

MB performed the investigative experiments, specifically the pyrolysis of CS, characterization of the materials *via* TPD, dispersibility, ageing and sedimentation tests as well as the adsorption studies with MCB. Silke Woszidlo (SW) performed the adsorption studies with PFOA. Hans Uhlig (HU) and Jens Möllmer (JM) conducted the CO_2 ad-/desorption measurements. MB, SW, HU and JM formally analyzed, curated and validated the data. MB visualized the results. Gerrit Schüürmann (GS), MB, KM, FDK and AG developed methodologies. MB wrote the original draft. AG helped on pp. 50 and 58 of the manuscript. AG and KM acquired the funding and administrated the project. KM provided the infrastructural resources for experimentation. AG, KM and FDK supervised the project. MB, AG, KM and FDK conceptualized the work. All authors were involved in reviewing and editing of the manuscript.

Section 4.3 "Generating colloidal Fe/C composites via HTC – a critical study" (2024):

Unless acknowledged otherwise, MB performed the investigative experiments, *i.e.* the precursor screening and material synthesis *via* HTC and pyrolysis, material characterization and testing of the dispersibility, sedimentation and reductive dechlorination. MB did the formal data analysis, curation, validation and visualization. AG and KM acquired the funding and administrated the project. KM provided the infrastructural resources for experimentation. AG, KM and FDK supervised the project. All authors were involved in conceptualization, developing methodologies as well as reviewing and editing of the manuscript.

The project that led to the three manuscripts was funded by "Deutsche Forschungsgemeinschaft" (DFG) under project number 392011053.

Acknowledgement

First and foremost, I would like to thank Prof. Dr. Frank-Dieter Kopinke for giving me this research opportunity, for sharing his expertise and providing me with valuable guidance throughout the whole project. My equally heartfelt thanks goes to Dr. Anett Georgi and Dr. Katrin Mackenzie for their relentless support and supervision.

I express my gratitude towards Lisa Frenzel, Silke Woszidlo, Dr. Robert Köhler, Birgit Forkert, Kerstin Lehmann, Dr. Sarah Sühnholz, Dr. Maria Vogel, Dr. Ulf Trommler, Dr. Ulf Roland and all current and former colleagues of the Department of Environmental Engineering at the UFZ for their untiring help during scientific, technical and emotional trials.

I thank my whole family, especially my parents and my brothers for mentally and financially preparing me for my studies. I also thank my friends for always being by my side and being patient.

Last but not least, I thank my life partner for being a constant source of inspiration and strength during the most intensive working phase of my life so far.

Curriculum vitae

Personal Data

Name	Maria Balda
Date of birth	30.01.1994
place of birth	Freyung (Germany)

Education

Time frame	**Degree**
Oct 2018 – Apr 2024	***Doctor rerum naturalium* in Chemistry** • Faculty of Chemistry and Mineralogy, Leipzig University • Thesis conducted at the Helmholtz Centre for Environmental Research – UFZ, Leipzig (Department of Environmental Engineering)
Oct 2018 – Dec 2021	**Graduate Training** • Helmholtz Interdisciplinary Graduate School for Environmental Research (HIGRADE), UFZ Leipzig
Oct 2016 – Sep 2018	**Master of Science in Chemistry** • Faculty of Chemistry and Mineralogy, Leipzig University • Thesis conducted at the Helmholtz Centre for Environmental Research – UFZ, Leipzig (Department of Environmental Engineering)
Oct 2012 – Oct 2016	**Bachelor of Science in Chemistry** • Faculty of Chemistry and Mineralogy, Leipzig University • Thesis conducted at the Faculty of Chemistry and Mineralogy, University of Leipzig (Institute of Chemical Technology)

Scientific experience

Time frame	Occupation
Mar 2024 – Sep 2024	Research associate at UFZ, Leipzig (Department of Environmental Engineering) Topic: *Activation/modification of hydrochar and its performance as adsorbent*
Aug 2023 – Dez 2023	Research associate at UFZ, Leipzig (Department of Environmental Engineering) Topic: *Adsorption of pollutants emerging from street-runoff and modification of adsorbents*
Feb 2023 – Apr 2023	Research associate at UFZ, Leipzig (Department of Environmental Engineering) Topic: *Tailor-made finely-powdered activated carbon from renewable sources for* in-situ *groundwater remediation of PFAS*
Jan 2023 – Dez 2024	Research associate in the junior research group „GreenInnoSax“ at the University of Applied Sciences (Hochschule für Technik, Wirtschaft und Kultur (HTWK)), Leipzig Topic: *Development of innovative remediation strategies for biocides leached from paint and render*
Jun 2022 – Dez 2022	Research associate in the junior research group „GreenHydroSax“ at the University of Applied Sciences (HTWK), Leipzig Topic: *Development of analytics for biocides leached from paint and render*
Oct 2018 – Sep 2022	PhD position at UFZ, Leipzig (Department of Environmental Engineering) Topic: *Colloidal activated carbon and Fe/C composites by hydrothermal carbonization and subsequent pyrolysis: mechanisms of formation, pollutant adsorption and reductive dechlorination*

Conference contributions

Conference contributions / science communication relating to the PhD topic

Oral presentation at the Forum for Hydrothermal Processes, Deutsches Biomasseforschungszentrum GmbH, Leipzig, **2020**

Poster presentation at the Summer School of the European Federation of Catalysis Societies, online, **2020**

First Prize in the competition *Three Minute Thesis* held by JCF local committee, Faculty of Chemistry and Mineralogy, University of Leipzig, **2019**

Other conference contributions

Oral presentation at the International Conference on Chemistry and the Environment (ICCE), Venice, **2023**

Publications

Publications relating to the PhD topic

M. Balda, A. Georgi, F.-D. Kopinke, K. Mackenzie, *Generating colloidal Fe/C composites* via *HTC – a critical study*, Sep. Purif. Technol., 335, 2024, 126082.

M. Balda, K. Mackenzie, S. Woszidlo, H. Uhlig, J. Möllmer, F.-D. Kopinke, G. Schüürmann, A. Georgi, *Bottom-up synthesis of de-functionalized and dispersible carbon spheres as colloidal adsorbent*, Int. J. Mol. Sci., 24, 2023, 3831.

M. Balda, K. Mackenzie, F.-D. Kopinke, A. Georgi, *Uniform and dispersible carbonaceous microspheres as quasi-liquid sorbent*, Chemosphere, 307, 2022, 136079.

Other publications

J. Zhou, Y. Zhang, **M. Balda**, V. Presser, F.-D. Kopinke, A. Georgi, *Electro-assisted removal of polar and ionic organic compounds from water using activated carbon felts*, Chem. Eng. J., 433, 2022, 133544.

M. Balda, F.-D. Kopinke, *The role of nickel traces in fine chemicals for hydrodechlorination reactions with zero-valent iron*, Chem. Eng. J., 388, 2020, 124185.

Kurzfassung der wissenschaftlichen Ergebnisse der Dissertation

---

Colloidal activated carbon and Fe/C composites by hydrothermal carbonization and subsequent pyrolysis: mechanisms of formation, pollutant adsorption and reductive dechlorination

---

Der Fakultät für Chemie und Mineralogie der Universität Leipzig
vorgelegt von

M. Sc. Maria Balda

im November 2023

Angefertigt am Helmholtz-Zentrum für Umweltforschung GmbH – UFZ

1 Motivation and research questions

Due to the increasing water shortage, it is important to remediate contaminated water resources. Care should be taken to ensure that sustainable principles are applied both in the remediation process and in the production of the materials required for this purpose. The *in-situ* remediation of contaminated groundwater using finely powdered activated carbon (AC) or iron-carbon (Fe/C) composites represents an innovative and low-impact remediation method without any excavation or lifting of contaminated soil and water. The particles are injected into the subsoil in the form of aqueous suspensions and, once deposited on the aquifer sediment, form an adsorptive and/or reactive zone that effectively stops the further spreading of the pollutants with the flow of groundwater [1]. The fine-grained AC used in this established process is obtained by grinding commercial AC, which is often imported or produced from fossil materials in Germany (*e.g.* hard coal). During the grinding process, the particle morphology and the surface properties can hardly be controlled. For the synthesis of iron-carbon composites, the finely powdered AC is typically impregnated with iron salts and subject to a carbothermal reduction at high temperatures in order to reduce oxidic Fe species to the reductant zero-valent iron (ZVI) [2].

In this work, alternative synthesis routes for fine-grained AC as well as iron-carbon composites should be developed based on hydrothermal carbonization (HTC). The HTC process has the advantage that colloidal particles can be produced from locally available, renewable raw materials and the morphology of the particles can be controlled by adjusting the process parameters. In a subsequent pyrolysis step, the pore system and surface properties of the AC can be finely tuned towards persistent pollutants.

A bottom-up HTC process was chosen to synthesize colloidal carbonaceous particles, as soluble carbohydrates naturally form lignite-like spherical microparticles under HTC conditions. In order to generate these in the desired size range and simultaneously increase the mass yield, typical stabilizing agents like hazardous and/or expensive polyelectrolytes or high salt concentrations were added to the HTC in previous studies. These additives might compromise or even annihilate the sustainable character of the process. Consequently, alternative additives were sought which are not hazardous but functional as well as cheap. The second crucial aspect of the bottom-up synthesis is the preservation of the dispersibility of the formed individual particles. For the generation of porous carbon particles a pyrolysis or activation step is needed during which the dispersibility can easily be eradicated. Therefore, the pyrolysis conditions were investigated closely in order to find suitable parameters for maintaining the dispersibility of the product. In addition, the porous system and surface properties of the adsorbent should be tailored during the pyrolysis. The surface should preferentially be de-functionalized which has proven to be beneficial for the adsorption of challenging organic pollutants such as the anionic perfluorooctanoic acid (PFOA) [3]. Unfortunately, especially de-functionalized surfaces are prone to 'ageing' due to oxidation processes in (humid) air and water under ambient conditions. To tackle these issues, the following three research questions were important for the bottom-up preparation of very fine (activated) carbon particles:

(I) How can the yield of microparticles in the desired size range be optimized without potentially hazardous additives during the HTC process?
(II) How can the high aqueous dispersibility of the microparticles be kept after pyrolysis?
(III) How can the porosity and surface characteristics of the AC be tailored to benefit the adsorption of certain pollutant classes?

When iron is added in the synthesis process, further aspects have to be considered for the generation of a reactive composite material. As iron salts promote the HTC, the process parameters must be adjusted accordingly in order to achieve a similar particle size compared to the process without Fe. Furthermore, the (composite) particles provide different morphologies depending on the initially used iron source. It was tested if the resulting composite morphologies enable the generation of reactive species, *e.g.* electrons from ZVI that are needed for reductive dechlorination reactions. Although not all classes of pollutants can be degraded with ZVI, we focused on the capability as reductant of the synthesized Fe/C composites within this work. The mechanisms of reductive dechlorination are well understood, however, the reactivity of colloidal composites synthesized by an initial bottom-up HTC process and subsequent carbothermal reduction has not yet been investigated. Herein, the reactivity of the composite materials was tested by using chloroform (CF) as a model compound as it not only allows to measure reaction kinetics but also selectivities to chlorinated and non-chlorinated products. While ZVI and ZVI/C systems are able to dechlorinate aliphatic (and highly chlorinated aromatic) compounds, the selectivities might be poor and desirable products may not be formed within desired time frames, *i.e.* the lifetime of ZVI in water. Therefore, a palladization of the Fe/C composite was conducted in order to broaden the spectrum of degradable pollutants while shifting the selectivity towards products with lower chlorination and higher hydrogenation degrees. The specific catalyst activities were compared to those of other typical Pd-containing catalysts. Consequently, the following research questions were posed:

(IV) Is it possible to generate a functional iron-carbon composite with the desired morphology within a one-pot synthesis based on HTC?

(V) Do the morphology and speciation of the composite after carbothermal reduction allow the reductive dechlorination of chlorinated hydrocarbons in water?

(VI) What is the gain in selectivity towards fully dechlorinated products achievable by palladization of the composite?

2 Materials and Methods

2.1 Experimental procedures

2.1.1 Synthesis via HTC and pyrolysis

In order to generate uniform carbonaceous spheres (CS), HTC of 0.5 M sucrose was performed for 1–4 h at 170–200 °C together with 0–3 wt.-% carboxymethyl cellulose (CMC). CS synthesized from 0.5 M sucrose with 1 wt.-% CMC at 180 °C for 2 h were heated in N_2 or 3 vol.-% H_2O/N_2 gas flow. Heating rates of 1–100 K min^{-1}, final temperatures of 400–880 °C and holding times of 1–4 h were applied. Colloidal Fe/C composites were synthesized *via* HTC of ferrous gluconate dihydrate (30–60 g L^{-1}) at 180 °C for 24 h together with CMC (0.6–1.5 g L^{-1}) and sodium gluconate (0–120 g L^{-1}). The Fe_xO_y/C composites obtained after HTC were heated with 1 K min^{-1} to 800 °C for 2 h under N_2 in order to (partially) reduce the iron oxide species in the composite to ZVI or equivalents. The latter were determined by acid digestion with HCl and measurement of the evolved H_2 with a GC-6850 (Agilent, HP plot column) coupled with a thermal conductivity detector. All samples were characterized with a VHX digital microscope (Keyence) and with a Zeiss Merlin VP compact scanning electron microscope (SEM). The specific surface area (*SSA*) of CS, activated CS (aCS, pyrolyzed at 800 °C (1 K min^{-1}) in 3 vol.-% H_2O/N_2) and Fe/C was determined with a Belsorp MINI (BEL Japan). The pore-size distribution of aCS in the small micropore range below 1 nm was determined from CO_2 ad and desorption at 0 °C with the manometric sorption analyzer AUTOSORB-iQ (Quantachrome Instruments, US).

For palladization, the particles were dispersed in de-oxygenated and de-ionized water *via* 10 min of US after shaking for 24 h. Afterwards, the appropriate amount of a stock solution of Pd(II) acetate was added to achieve Pd contents of 1–4 wt.-% (related to solid mass) and the mixture was shaken vigorously. For particles or composites containing reactive ZVI (Fe/C, ZVI/AC and Carbo-Iron®) the reduction of Pd^{2+} to Pd occurred spontaneously through oxidation of Fe^0 to Fe^{2+}. For the palladization of AC, H_2 was used as a reducing agent. For the CF degradation with palladized materials, external H_2 supply was ensured and specific catalyst activities for Pd were determined. The solid sample composition was explored by X-ray photoelectron spectroscopy (XPS, Kratos Ultra DLD) and X-ray diffraction (XRD, ULTIMA IV, Rigaku).

2.1.2 Dispersibility, sedimentation and ageing

The dried CS, aCS or Fe/C were dispersed in aqueous media by treatment with an ultrasonic bath (US) RK 100 SH Sonorex (Bandelin Electronic, P = 160 W and f = 35 kHz). For sedimentation studies, non-agitated suspensions were probed from a defined height below the surface and analyzed for their total organic carbon content. The zeta potentials and particle size distributions of (a)CS and Fe/C in aqueous suspensions were characterized with a Zetasizer Ultra or a Mastersizer 3000 (both from Malvern Panalytical), respectively. For aCS, the ageing in laboratory air atmosphere, in a desiccator (SiO_2 as drying agent) and in aqueous media was monitored under ambient conditions. The content of thermally labile oxygen of the aCS, largely corresponding to the oxygen-containing functional groups on the aCS surface, was analyzed *via* temperature-programmed decomposition (TPD, up to 1100 °C in Ar) directly after the preparation and after storage under different conditions.

2.1.3 Sorption experiments

0.05–0.2 g L^{-1} CS/aCS were agitated in salt solutions (10 mM KNO_3 or 10 mM NaCl) at (23 ± 2) °C for at least 24 h at 180 rpm. CS/aCS were then fully dispersed by US for 10 min and spiked with the according amount of stock solutions of the various pollutants and placed on a horizontal shaker at 180 rpm. For CS, single-point sorption coefficients of trichloroethylene (TCE), lindane (LIN), acenaphthene (ACE), hexachlorobenzene (HCB) and 2,3,4-trichlorobiphenyl (TCB) were determined in a combined batch with initial concentrations of 10 µg L^{-1} for each analyte. For the sorption of phenanthrene (PHE), a sorption isotherm was determined. For aCS, adsorption isotherms of MCB and PFOA were investigated. LIN, ACE, HCB, TCB and PHE were extracted and analyzed by means of gas chromatography with coupled mass-spectrometry (GC-MS) using a GCMS-QP2010 (Shimadzu) with liquid injection and a column temperature gradient. TCE and MCB were analyzed *via* headspace sampling and isothermal GC methods. PFOA was analyzed *via* liquid chromatography coupled with MS (LC-MS-2020, Shimadzu).

2.1.4 Degradation experiments

Dechlorination tests of CF were performed under N_2 with all synthesized Fe/C composites in 10 mM $NaHCO_3$ solution (pH = 8.5) after pre-conditioning by shaking overnight and dispersion *via* US. CF and products were analyzed *via* headspace sampling and GC-MS or, for light hydrocarbons, GC coupled with a flame-ionization detector for methane/ethene/ethane and quantified with external calibration. In order to compare the performance of the synthesized composites, product selectivities (S_i) towards fully dechlorinated products and kinetics in relation to ZVI concentrations were evaluated.

3 Results and Discussion

In this work, the research questions posed in section 1 were answered consecutively. Research question (I) was complemented with research question (I).i and question (III) was extended to (III).i (see below).

(I) How can the yield of microparticles in the desired size range be optimized without potentially hazardous additives during the HTC process?

i. Do the synthesized microparticles exhibit the capability for sorption of organic groundwater pollutants?

The addition of CMC as environmentally friendly and cheap stabilizing agent during the HTC of sucrose at 180 h for 2 h optimized the mass yield of spherical CS with a narrow size distribution around 1 µm. These 'raw' CS exhibit an extraordinary suspension stability which was investigated in detail for the first time. Due to their hydrophilic surface and negative surface charge characterized by a zeta potential of –43.5 mV at pH 6, the CS form stable suspensions even in the presence of relatively high salt concentrations of up to 168 mM KNO_3 (pH 6.0) and 12 mM $CaCl_2$ (pH 6.6). This makes them suitable for *in-situ* injection into aquifers. The highest sorption coefficients of up to $K_D = 10^5$ L kg^{-1} were found for hydrophobic substances such as PHE in environmental concentrations. Therefore, hydrothermally synthesized CS might be a more sustainable alternative to colloidal AC for the formation of *in-situ* sorption barriers at contaminated sites where hydrophobic pollutants are dominating (s. Figure 1). One has to take into account, however, that the sorption coefficients with CS are generally lower than those achievable with AC. For the cost-efficient remediation, CS would have to be cheaper than AC which might be achieved by using alternative (waste) substrates in the HTC process.

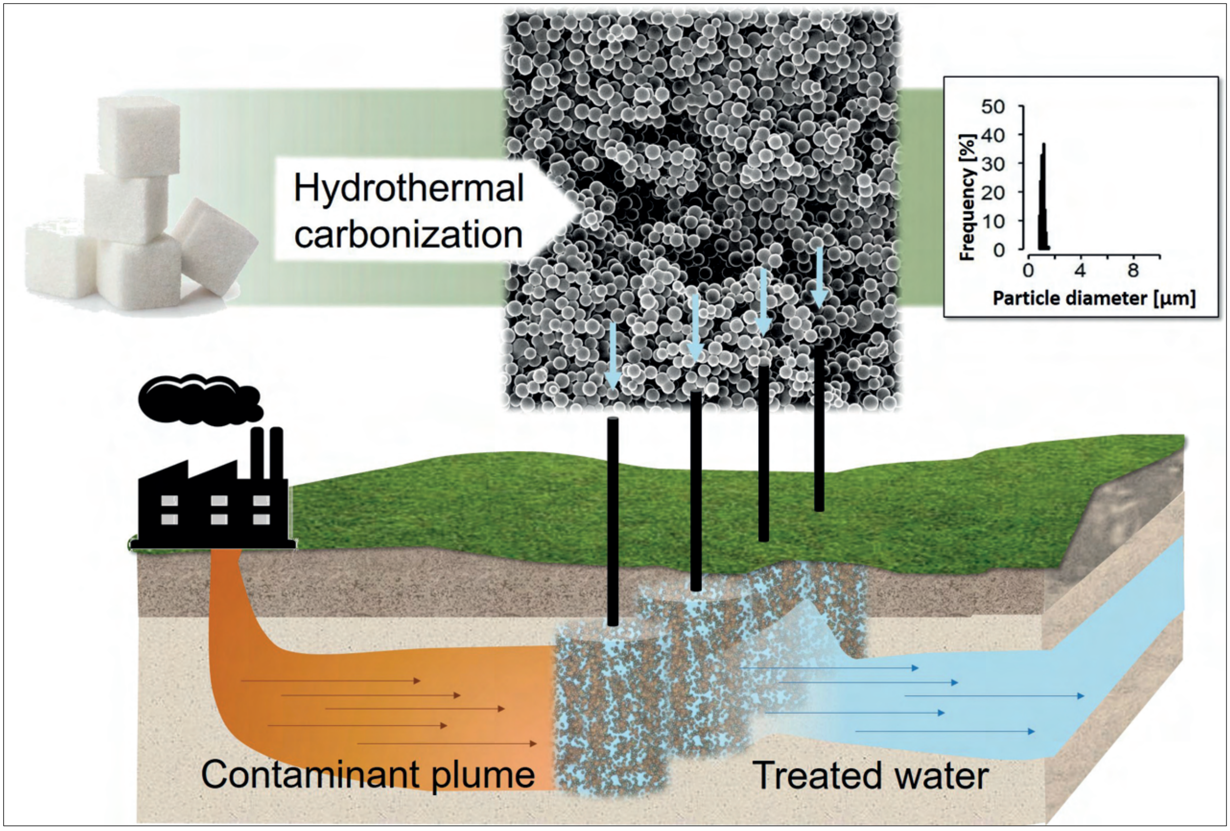

Figure 1 Synthesis and possible application of carbonaceous spheres as sorbent for *in-situ* groundwater remediation.

(II) How can the high aqueous dispersibility of the microparticles be kept after pyrolysis?

The influence of the parameters for pyrolysis on the aqueous dispersibility of the CS were investigated in detail for the first time and suitable conditions were found to maintain the aqueous dispersiblity of the aCS even after the pyrolysis step. Under all applied pyrolysis conditions, a low heating rate of about 1 K min^{-1} was crucial in order to minimize inter-particle polymerization processes and to ensure sufficient dispersibility of the resulting aCS in water. In order to prevent increased agglomeration of the hydrophobic particles after dispersion, CMC had to be added as stabilizer in aqueous suspensions.

(III) How can the porosity and surface characteristics of the AC be tailored according to specific classes of pollutants?

i. How (fast) does the surface of the de-functionalized aCS age under ambient conditions?

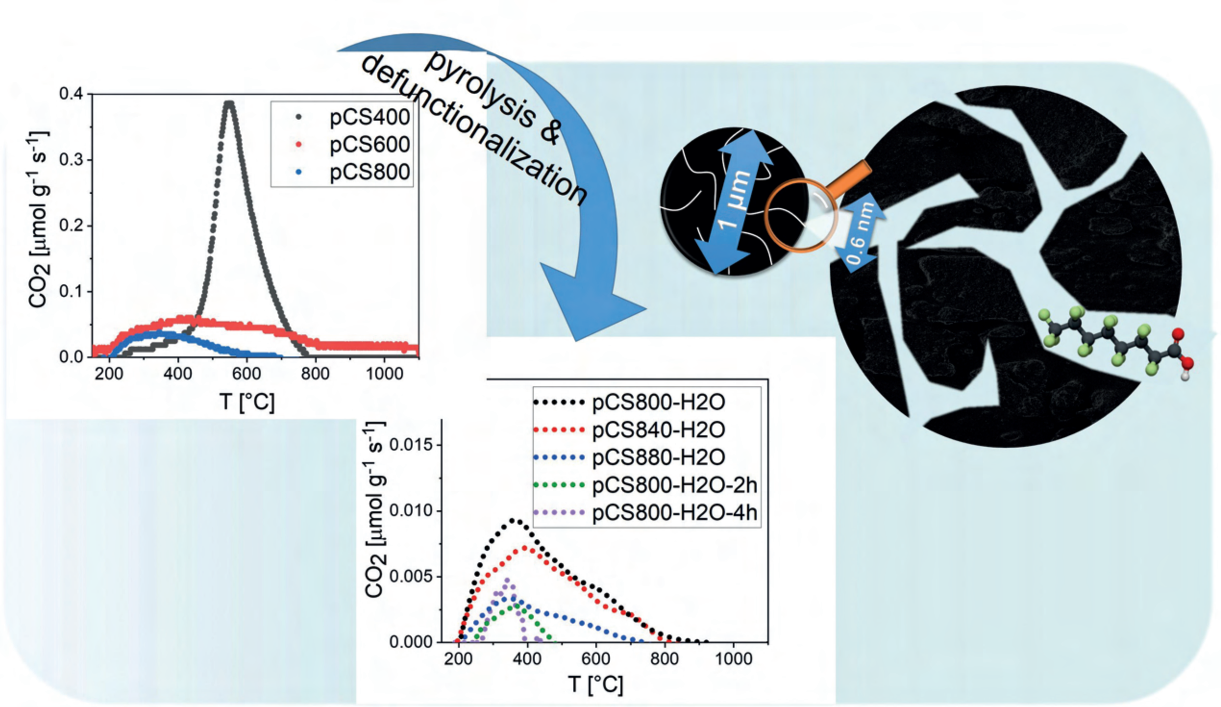

Figure 2 Effect of temperature (400–880 °C), holding time (1–4 h) and dosage of H_2O into the N_2 atmosphere during pyrolysis on the TPD-derived CO_2 content of pyrolyzed CS (pCS) and schematic illustration of the adsorption of PFOA within micropores; “pCS800-H2O-4h” is referred to as “aCS” in the text.

The fine-tuning of the microporous system of the aCS was achieved with average pore diameters of 0.5 to 0.7 nm depending on the pyrolysis atmosphere, treatment time and temperature. The addition of 3 vol.-% steam to the N_2-atmosphere during pyrolysis not only led to a slight increase in mean pore diameter but also to a further de-functionalized surface of the aCS (s. Figure 2). Due to the de-functionalization in combination with tuning the mean pore diameter according to the molecular diameter of the PFOA molecule, the synthesized aCS exhibited high single-point sorption coefficients up to $K_{\mathrm{D,PFOA}} = 10^{6.5}$ L kg^{-1} at equilibrium concentrations of about 20 µg L^{-1} PFOA. It is concluded that the developed synthesis parameters can be adjusted further depending on specific pollutants’ needs. However, the spontaneous ageing of the de-functionalized surface in air and water could not be fully prevented. The ageing of the aCS surface after storage in water under abundant oxygen conditions over one month significantly decreased the adsorption affinity towards PFOA. Nevertheless, the aCS synthesized under 3 vol.-% H_2O/N_2 at 800 °C exhibited equally stable surface properties as aCS treated in 10 vol.-% H_2/N_2 at 900 °C. It was concluded that the applied steam activation process stabilized the de-functionalized aCS surface comparable to hydrogen treatment as opposed to sole high-temperature treatment in pure N_2 which left a rather reactive surface prone to ageing. Therefore, molecular hydrogen and water are appropriate reagents to saturate/deactivate most of the reactive surface sites. While, in this case, the very narrow pore size had a beneficial effect on the affinity towards PFOA, the time for reaching the adsorption equilibrium was rather long due to the slow pore diffusion process in the nanopores. Based on the findings in this work, it is estimated that pore diameters can be increased with higher steam dosages and treatment temperatures. It is also possible to enhance mesoporosity of the material by 'harsh' chemical activation. However, this likely has a detrimental effect on the particle morphology and dispersibility of aCS. Further studies should investigate, how the adsorption behavior of challenging pollutants like PFOA is influenced in the presence of co-contaminants, *e.g.* natural organic matter (NOM).

(IV) Is it possible to generate a functional iron-carbon composite with the desired morphology within a one-pot synthesis based on HTC?

The screening of possible Fe and C precursors for HTC led to the conclusion that specific interactions between carbon precursors and metal ions are needed for the generation of mechanically stable Fe/C composites with the desired colloidal properties (s. Figure 3). Finally, a novel synthesis route based on ferrous gluconate proved as most promising due to the complexation of Fe^{2+} by gluconate.

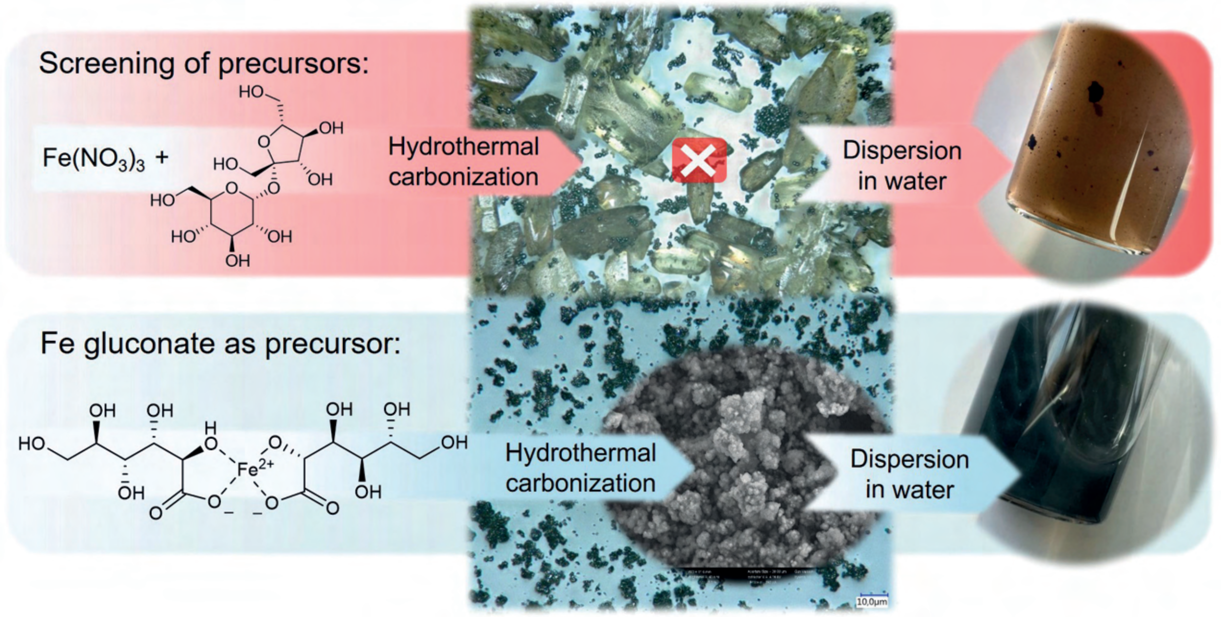

Figure 3 Effect of Fe and C precursors on particle morphologies and aqueous dispersibility.

(V) Do the morphology and speciation of the composite after carbothermal reduction allow the reductive dechlorination of chlorinated hydrocarbons in water?

It was shown for the first time that the morphology of the hydrothermally synthesized and carbothermally reduced colloidal Fe/C composite enables reductive dechlorination with specific activities (normalized to the concentration of zero-valent iron (ZVI) equivalents) that are comparable to nanoscale ZVI. *SSA*s of the composites of 140–280 $m^2\ g^{-1}$ and their mesoporous character suggest a carbonaceous phase with a well-pronounced porosity, ensuring the accessibility of the reactive ZVI surface. XRD and XPS analyses revealed that, besides pristine Fe^0, also Fe_3C was present in the material which was suspected to additionally generate reactive species (e^- and H^*) known to conduct reductive dechlorination. Furthermore, graphitic structures were observed that might facilitate the transfer of reactive species, likely electrons. Further investigations should also take into account the functional groups on the carbonaceous surface which can mediate redox processes. They may act as shuttle for reactive species [4, 5].

(VI) What is the gain in selectivity towards fully dechlorinated products achievable by palladization of the composite?

The reactive ZVI equivalents (Fe^0 and Fe_3C) within the composites were accessible as demonstrated by relatively fast reductive dechlorination. Therefore, also a facile palladization procedure by impregnation of Fe/C with Pd^{2+} and reduction to Pd on the ZVI surface was effective. The resulting Pd/Fe/C composites exhibit drastically higher reaction rates and higher selectivities towards fully dechlorinated products such as methane. The comparison with various other palladized materials showed lower selectivities of Pd/Fe/C to dichloromethane (DCM) and higher selectivities to ethane, even without external feed of H_2. A gap in mass balance was observed after summing up the volatile products methane, ethane, DCM and monochloromethane which points to the generation of longer-chain products. High extents of dechlorination of CF were verified by chloride analysis after the complete CF conversion.

4 Conclusion and Outlook

It was demonstrated that the bottom-up synthesis of finely powdered CS and aCS with particle sizes of about 1 µm as well as a colloidal Fe/C composite in the size range of 2–50 µm is possible *via* HTC and subsequent pyrolysis. The hydrothermally generated particles were optimized regarding their application by adjusting various process parameters. However, the hydrothermal synthesis of micrometer-sized particles with controllable diameters comes with the inevitable tradeoff of small mass yields. This diminishes the overall sustainable, facile and resource-efficient character of HTC processes. Nevertheless, it is shown within this work that mass yields for the desired particles can be optimized within certain boundaries. Consequently, the process parameters derived here can be seen as a basis for future studies in which the mass yield and material properties can be further optimized with regard to various applications. Besides water remediation, the use of aCS might also be possible in electrochemical applications. Moreover, alternative substrates, *e.g.* regional waste streams, can be explored in order to further improve the sustainability of the synthesis.

References

[1] M. Sørengard, D.B. Kleja, L. Ahrens, *Stabilization of per- and polyfluoroalkyl substances (PFASs) with colloidal activated carbon (PlumeStop®) as a function of soil clay and organic matter content*, J. Environ. Manage. 249 (2019).

[2] K. Mackenzie, S. Bleyl, F.-D. Kopinke, H. Doose, J. Bruns, *Carbo-Iron as improvement of the nanoiron technology: from laboratory design to the field test*, Sci. Total Environm. 563–564 (2016) 641–648.

[3] N. Saeidi, F.-D. Kopinke, A. Georgi, *What is specific in adsorption of perfluoroalkyl acids on carbon materials?*, Chemosphere 273 (2021) 128520.

[4] M. Vogel, F.-D. Kopinke, K. Mackenzie, *Acceleration of microiron-based dechlorination in water by contact with fibrous activated carbon*, Sci. Total Environm. 660 (2019) 1274–1282.

[5] H.J. Amezquita-Garcia, E. Razo-Flores, F.J. Cervantes, J.R. Rangel-Mendez, *Activated carbon fibers as redox mediators for the increased reduction of nitroaromatics*, Carbon 55 (2013) 276–284.

Helmholtz Centre for
Environmental Research – UFZ
Permoserstraße 15
04318 Leipzig I Germany
www.ufz.de